66–2972

RHYNE, James Jennings, 1938–

MAGNETOSTRICTION OF DYSPROSIUM, ERBIUM, AND TERBIUM SINGLE CRYSTALS.

Iowa State University of Science and Technology
Ph.D., 1965
Physics, solid state

University Microfilms, Inc., Ann Arbor, Michigan

MAGNETOSTRICTION OF DYSPROSIUM, ERBIUM, AND TERBIUM SINGLE CRYSTALS

by

James Jennings Rhyne

A Dissertation Submitted to the

Graduate Faculty in Partial Fulfillment of

The Requirements for the Degree of

DOCTOR OF PHILOSOPHY

Major Subject: Physics

Approved:

Signature was redacted for privacy.

In Charge of Major Work

Signature was redacted for privacy.

Head of Major Department

Signature was redacted for privacy.

Dean of Graduate College

Iowa State University
Of Science and Technology
Ames, Iowa

1965

TABLE OF CONTENTS

	page
I. INTRODUCTION	1
A. Rare Earths and Magnetostriction	1
B. Early Magnetostriction Work	2
C. Other Rare Earth Magnetostriction Experiments	5
II. PROPERTIES OF THE RARE EARTHS	6
A. General Properties	6
B. Magnetic Interactions in the Rare Earths	6
C. Neutron Diffraction and Magnetization Results on the Rare Earths	10
III. EXPERIMENTAL METHOD AND APPARATUS	15
A. Methods of Strain Measurement	15
B. Strain Gages	16
C. Strain Gage Measurements and Calibration	18
D. Helium Dewar	24
E. Temperature Control Apparatus	28
F. Rotating Sample Holder Assembly	34
G. Sample Mounting	36
H. Temperature Measurement	37
I. Magnet Equipment	38
IV. SPECIMENS FOR MAGNETOSTRICTION MEASUREMENTS	41
A. Specimen Geometry	41

page

B. Crystal Preparation 42

C. Specimen Preparation and Alignment 44

D. Specimen Purity 45

V. MAGNETOSTRICTION OF A FERROMAGNET 47

A. Phenomenological Theory 47

B. Callen Theory of Magnetostriction 50

C. Mason's Expression for the Magnetostriction 53

D. Approximation Valid for Dy and Tb Below the Néel Temperature 55

VI. EXCHANGE MAGNETOSTRICTION IN A HELICAL ANTIFERROMAGNET 59

VII. MEASUREMENTS OF THE MAGNETOSTRICTION CONSTANTS 67

A. Anisotropic Magnetostriction Constants A and C 67

B. Isotropic Constants D and G 76

VIII. ANISOTROPY ENERGY 95

A. General Remarks 95

B. Anisotropy Constants of Dy and Tb Calculated from Magnetostriction Data 96

IX. Tb AND Dy ISOTHERMAL MAGNETOSTRICTION 101

A. Ferromagnetic and Antiferromagnetic Results for Dy and Tb 101

B. Critical Fields in Dy from a-c Plane Field Rotation Measurements 108

C. Paramagnetic Magnetostriction 111

D. Forced Magnetostriction 114

page

X. MAGNETOSTRICTION OF ERBIUM 119

A. Isothermal Measurements in Erbium 119

B. Erbium Field Rotation Measurements 130

C. Temperature Dependence of Er Strain 137

XI. BIBLIOGRAPHY 142

XII. ACKNOWLEDGEMENTS 147

XIII. APPENDIX 149

A. Errors in Strain Gage Measurements 149

B. Errors in the Magnetostriction Constants A and C of Dy and Tb Produced by the Magnetic Anisotropy 150

C. Tabulation of Experimental Data 151

I. INTRODUCTION

A. Rare Earths and Magnetostriction

The development of methods for obtaining pure rare earth metals at the Ames Laboratory has led to an extensive research program directed toward an understanding of the basic physical properties of these materials. Much of this work up to 1960 is summarized by Spedding and Daane (60) based primarily on polycrystalline measurements.

The heavy rare earths exhibit strong magnetic effects accompanied in most cases by large magnetocrystalline anisotropies. Interest in studying these properties and their effect on the galvanomagnetic properties has necessitated and stimulated work in producing single crystals of the elements at the Ames Laboratory. Belov et al. (5) have reviewed some of the results of these single crystal studies.

Recently, considerable interest has been shown in the magneto-elastic properties of the rare earths. These phenomena are a direct manifestation of the interaction between the magnetic exchange and anisotropy energies and the elastic energy. They are thus a way of studying the interatomic forces. It is hoped that this investigation of the magnetostriction of dysprosium, erbium and terbium will provide some insight into the magneto-elastic interactions in these metals.

The magnetostriction of a material is a change in physical dimension

resulting from a change in the direction or magnitude of the magnetization. This change may be the result of a spontaneous ordering or the result of an applied field.

A strain dependent total magnetic energy is the essential requisite for such a distortion. The observed magnetostriction will then accompany changes in the magnetization whenever the dilatation results in a reduction of the total energy.

Magnetostrains are normally small; $\frac{\Delta \ell}{\ell}$ is on the order of 10^{-5} for the transition elements Fe, Co, and Ni. In the rare earths however, due to the large anisotropy energies, the strains are larger by almost two orders of magnitude. The apparent record magnetostriction of 0.96 per cent for an elemental material was observed in this study on dysprosium at 20°K.

B. Early Magnetostriction Work

The mere observation of magnetostriction is not new; its accurate measurement and interpretation is new. The observation dates back to 1842 when Joule first observed the expansion of an iron bar when magnetized. He determined that in small fields the expansion took place along the direction of the magnetization and was accompanied by a transverse contraction which maintained the volume constant. Later work showed that the expansion becomes a contraction in larger fields due to the effects of domain rotations. Joule's result was really quite an

achievement sixty-five years before the Weiss theory of ferromagnetism. Much of the later work showed much less insight.

The early studies of magnetostriction generally suffered from three main deficiencies. Two of these were the lack of measurements on single crystals (Co was measured only in 1954 (10)) and the lack of measurements below room temperature. Both of these make theoretical interpretation difficult, since a good theory must involve anisotropy and temperature dependent effects. By far the most serious defect, however, was the use of the demagnetized state as a zero reference state for the strain measurement. The strain in such a state is a function of the magnetic history. The domain configuration and, hence, the demagnetized strain, is not closely reproducible when the crystal is cooled through its ordering temperature, or when the applied field is removed. The futility of using the demagnetized state as a reference is illustrated in Figure 1, which shows the results of five sequential determinations of the magnetostriction in Dy at 79°K as a function of field applied along the easy magnetic direction. The data for the first and fifth curves were obtained after annealing the crystal above its Néel temperature. The other curves were obtained after conditioning the specimen in a 30 kilogauss field applied in the directions given in the figure. In each case, after the conditioning field was applied, the crystal was allowed to attain strain equilibrium in zero field before the magnetostriction

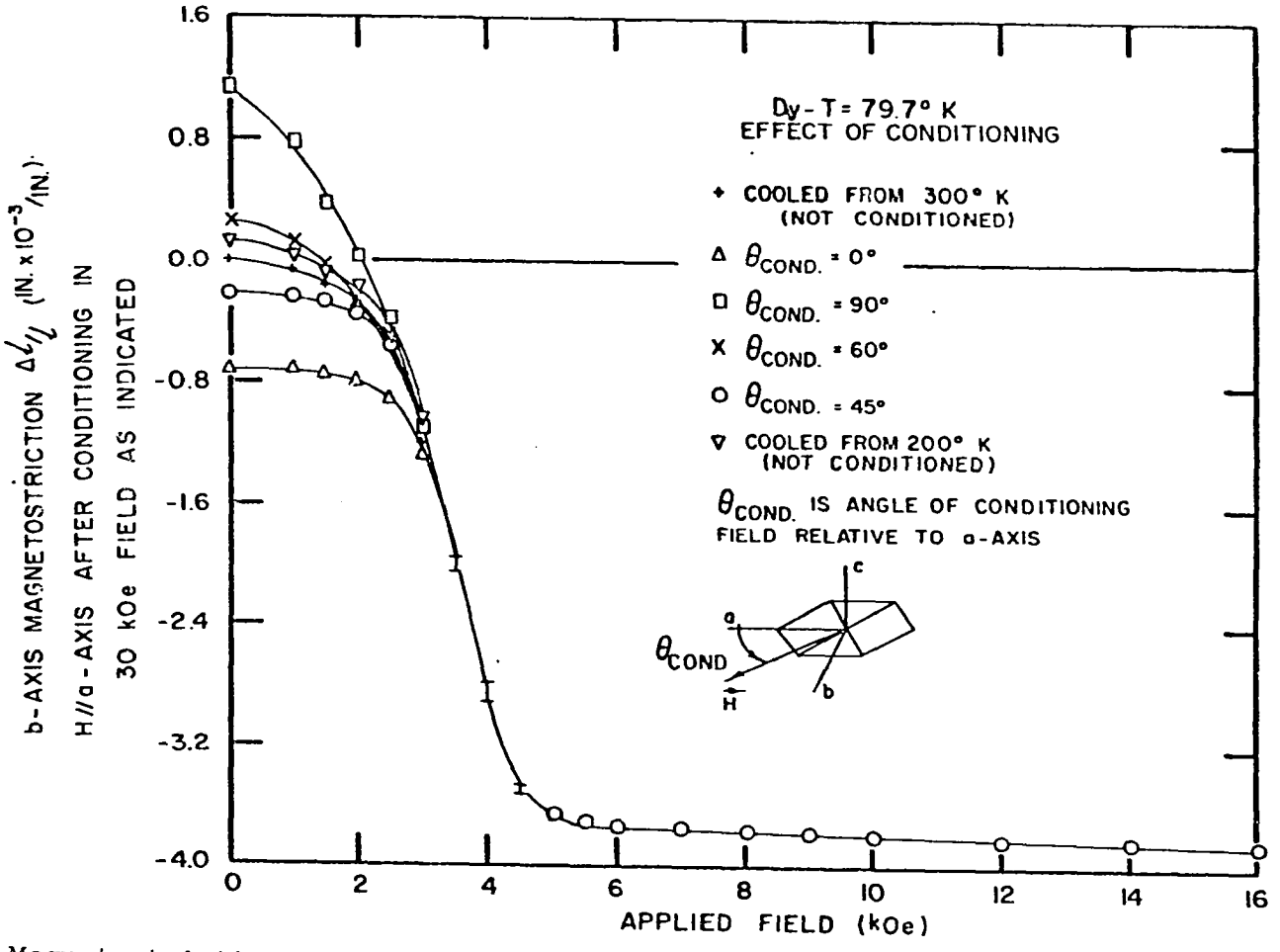

Figure 1. Magnetostriction of dysprosium as a function of field applied along the easy magnetic direction. The curves give the strains which result after pre-conditioning the specimen as indicated.

data were taken. The "demagnetized" strain and low field values of the various curves are observed to be quite variable, emphasizing the errors inherent in obtaining quantitative values from such measurements. It is to be noted, however, that the saturated strain in each case is identical, and thus magnetostriction measurements made between different saturated states are quite valid. This has been the procedure for most of the recent investigations.

C. Other Rare Earth Magnetostriction Experiments

Most of the original magnetostriction work on the rare earths was done on polycrystals in Russia and England. Polycrystalline dyprosium was studied by Belov et al. (6) and by Lee and Alperts (44). Polycrystalline terbium measurements were made by Nikitin (55), gadolinium by Corner and Hutchinson (18) and Belov et al. (6), and holmium by Nikitin (55).

In addition to the work on Dy, Tb, and Er reported in this dissertation and elsewhere (56, 45), single crystal magnetostriction of Ho (45) and Gd (2) has been measured by Alstad while at this laboratory. Bozorth and Wakiyama (11, 12) have also reported the magnetostriction of Gd single crystals. Clark et al. (16, 17) measured the magnetostriction of Dy concurrently with the author's study.

II. PROPERTIES OF THE RARE EARTHS

A. General Properties

The atomic structure of the heavy rare earths is characterized by three conduction electrons in mixed 5d and 6s bands. The 4f shell is being filled as one progresses across the series from Gd (atomic number 64) to Lu (atomic number 71). In view of the uniform number of conduction electrons, and crystal parameters of the series (61) the transport properties would be expected to be almost identical for these elements. This is not realized, however, due to an interaction between the conduction electrons and the 4f electrons which is also responsible for the magnetic properties.

B. Magnetic Interactions in the Rare Earths

The rare earths exhibit exceedingly strong magnetic interactions leading to an observed magnetic moment as high as 10.6 Bohr magnetons per atom in Dy. This is somewhat surprising when one considers that the value of the direct magnetic exchange integral between the deeply buried 4f electrons is essentially zero. In contrast to the direct exchange in the transition elements, rare earth magnetism finds its explanation in an indirect exchange interaction known as the Ruderman-Kittel-Kasuya-Yosida (RKKY) interaction named after the principal contributors to the theory. The fundamental postulate is the existence of an exchange interaction

between the localized 4f ion with effective spin $\vec{S}_n$ (given by $(g-1)\vec{J}_n$) and a conduction electron of spin $\vec{s}$ in momentum state $\vec{k}$. In the interaction the conduction electron is scattered into momentum state $\vec{k}'$. The Hamiltonian for this exchange has the form

$$H = - \Gamma_n (\vec{k}\ \vec{k}') \vec{s}_k \cdot \vec{S}_n , \qquad (1)$$

where $\Gamma_n (\vec{k}\vec{k}')$ is a direct exchange integral between the localized ionic wave function and the conduction electron wave function. The result of the interaction is a polarization of the conduction electron medium with a consequent small increase in the net observed magnetic moment of the crystal.

The energy and wave functions resulting from a Hamiltonian of the above type have been calculated to second order by Ruderman and Kittel (57).

Experimentally it is found that, in addition to normal ferromagnetism, some of the rare earths exhibit a helical antiferromagnetic state over a limited temperature range. In such a state, the atomic magnetic moments are aligned ferromagnetically in each hexagonal layer. However, the direction of alignment changes by an interlayer turn angle α from one layer to the next. The overall picture is one of the magnetic moment following a helical path progressing upward through the crystal along the c axis as shown in Figure 2. The net moment of the crystal is thus zero as required for an antiferromagnet.

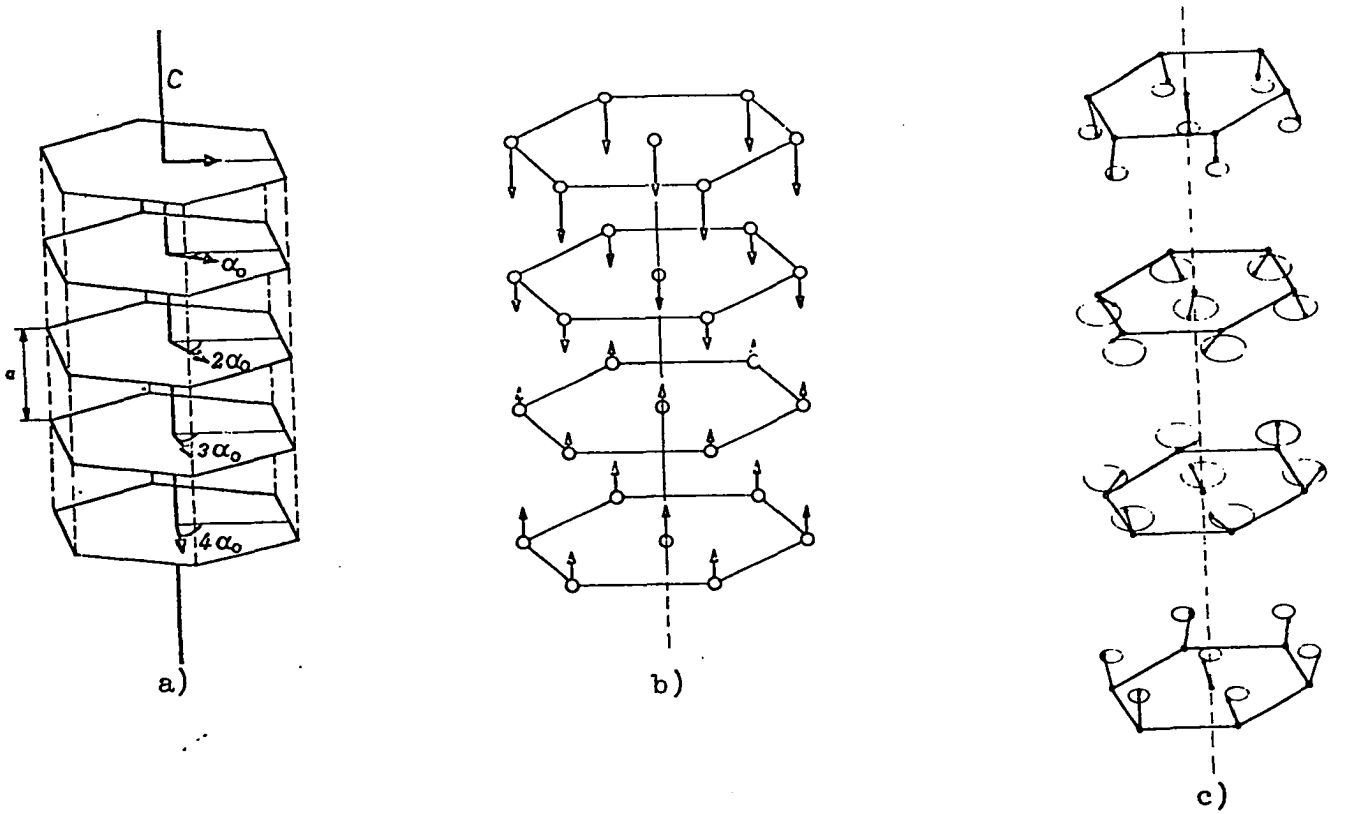

Figure 2. Antiferromagnetic states of the rare earths.
a) The helical magnetic state in the absence of anisotropy and external field.
b) and c) Two possible moment configurations in the modulated moment region of Er.

Ruderman and Kittel have shown that the helical magnetic states in the rare earths can be explained by postulating a ferromagnetic intralayer exchange energy and an interlayer exchange integral that is positive for interactions between nearest neighbor hexagonal layers and negative for interactions between second nearest neighbor layers. This interaction function, dependent on the distance r between two atoms is:

$$J = J_o \frac{\sin x - x \cos x}{x^4}, \quad x = \frac{r}{r_o}, \tag{2}$$

r_o is a constant on the order of an atomic distance. For an appropriate layer spacing, a, this function gives $J\left(\frac{a}{r_o}\right) \equiv J_1 > 0$ and $J\left(\frac{2a}{r}\right) \equiv J_2 < 0$ as required by the RKKY theory. A refined calculation by Herpin (32) gives the following result for the exchange energy in the helical states:

$$E_{ex} = - M_s^2 (J_1 \cos \alpha + J_2 \cos 2\alpha) \tag{3}$$

where M_s is the magnetic moment per atom and J_1, J_2 are the above interlayer exchange functions. The angle α is the interlayer turn angle. By minimizing the energy $\frac{\partial E_{ex}}{\partial \alpha} = 0$, the stable helical angle is found to be:

$$\cos \alpha_o = - \frac{J_1}{4J_2}. \tag{4}$$

If $|J_2| < \frac{1}{4} J_1$ then the second nearest layer exchange is too small to sustain the helical state and α_o becomes zero producing ferromagnetism.

The mechanism of the actual transition from antiferromagnetism to ferromagnetism is somewhat obscure. Yosida and Miwa (69, 70) have postulated an explanation in terms of different temperature dependences of

the second, fourth, and six order anisotropy energies. For example, in Dy they attribute the stability of the helical state to the strong axial second and fourth order anisotropy holding the intralayer magnetic moments in the basal plane. On cooling, a rapid increase in the basal plane (six fold) anisotropy causes the helical structure to be destroyed in favor of the ferromagnetic state of lower energy. It is to be noted, though, that the temperature dependence of the turn angle calculated by Yosida and Miwa is not in good agreement with the observed neutron diffraction results (37).

Additional calculations and extensions of the theory of helical spin structions have been made by many workers including Kasuya (35), DeGennes and Friedel (21), Enz (24), Elliott (22, 23), and Nagamiya (51).

The rare earth magnetic interactions described above represent the situation for zero applied field. On application of an external field, the helical state is radically distorted and eventually collapses into a ferromagnetic configuration as the applied field energy overcomes the "J_2" interlayer exchange energy. These results are described in the section on magnetostriction of a helical antiferromagnet.

C. Neutron Diffraction and Magnetization Results on the Rare Earths

The techniques of neutron diffraction, applied to the rare earths principally by Koehler (37) and associates at Oak Ridge, have yielded considerable insight into the various magnetic phases in these metals.

The qualitative results of studies on Tb (39), Dy (66), Ho (38), and Er (13) are shown in Figure 3.

1. Terbium and dysprosium

Terbium and dysprosium both exhibit the same ordered phases, helical antiferromagnetic and ferromagnetic. The range of stability of the helical state in Tb is quite restricted compared to Dy, and applied fields of less than one kOe will produce a transition to the ferro state. The respective Néel temperatures (para to antiferro transition) of Tb and Dy are 230°K and 179°K, and the Curie temperatures (antiferro to ferro transition) are 221°K and 87°K.

The interlayer turn angle of Tb varies from 20.5° at the Néel temperature to 18° at the Curie temperature. Below the Curie temperature, the b$(10\bar{1}0)$ axis is the easy magnetic direction as established by the work of Hegland et al. (31). They found the value of atomic moment extrapolated to T= 0°K and infinite field to be 9.34 Bohr magnetons, slightly larger than the nine Bohr magnetons expected for a tripositive ion ignoring effects of conduction electron polarization.

The turn angle of Dy exhibits an almost linear decrease with temperature from 43.5° at 179°K down to about 130°K where it departs from linearity. At approximately 95°K it reaches a value of 26.5° and remains constant to the Curie temperature and then drops discontinuously to zero. Magnetization studies of Behrendt et al. (4) give a saturation moment

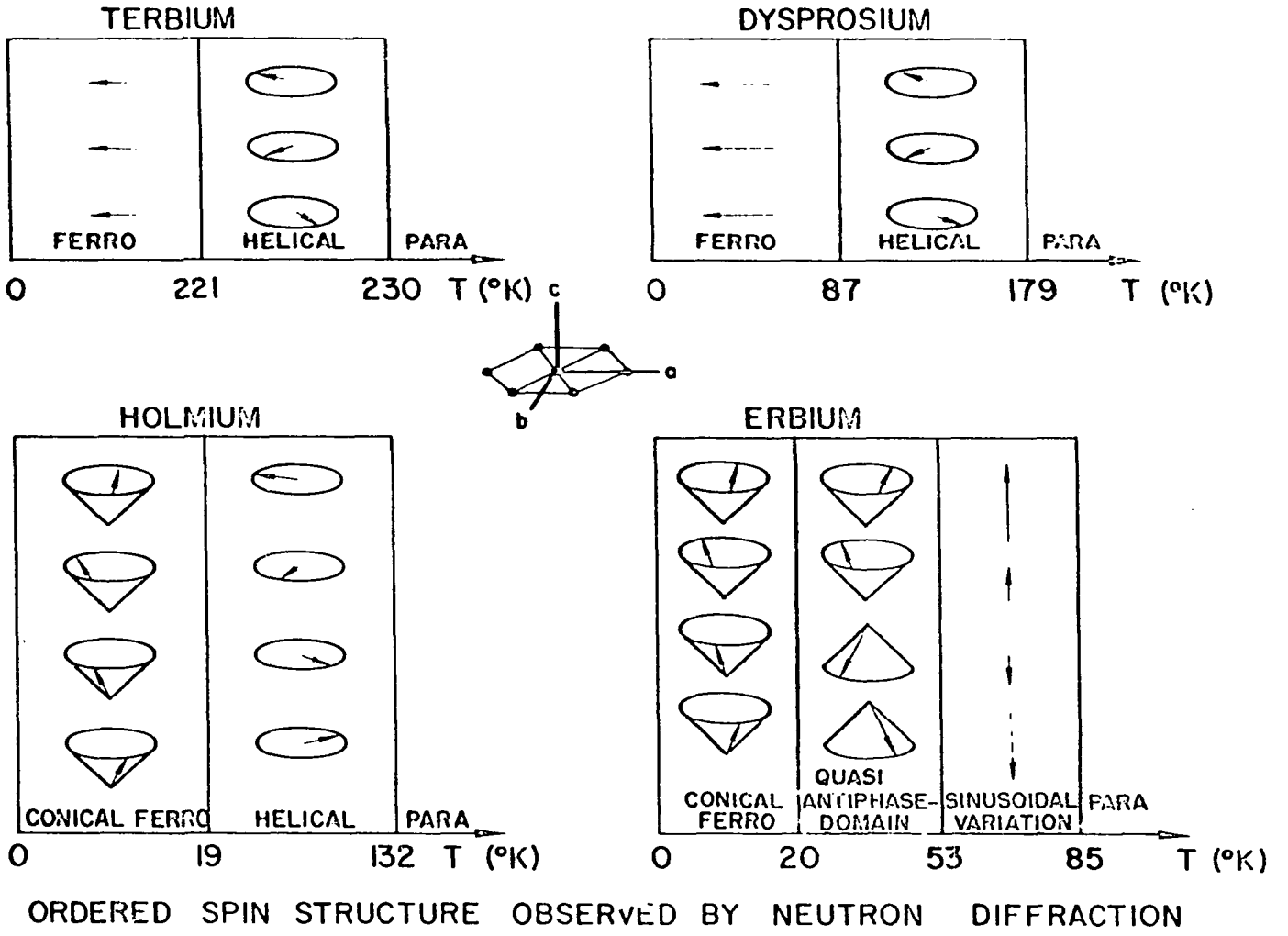

Figure 3. Magnetic states of the rare earths as determined from neutron diffraction results.

value of 10.2 Bohr magnetons per atom. The a($11\bar{2}0$) axis is the easy basal plane direction. The critical fields required to destroy the helical state range from zero at the Curie temperature to over 10 kOe above 160°K.

2. Erbium

Erbium exhibits a rather more complicated magnetic structure consisting of three distinct ordered states. At 85°K Er goes from a paramagnetic state into a state in which the c component of the magnetic moment is observed to oscillate in magnitude in progressing from one hexagonal layer to another. The period of this oscillation is seven layers. The basal plane component (if any) is completely disordered. This situation leads to two possible models for the state as shown in Figure 2. The first is one in which the atomic moments all point in the c-axis direction and their magnitudes are modulated layerwise in a sinusoidal manner. The second explanation assumes that the atomic moments remain constant in magnitude and lie along the generators of cones whose apex angles are modulated sinusoidally. A completely random distribution of the moments over the surface generators of the cones would account for the net disordered basal plane component. At about 53°K the basal plane components of the Er moment are observed to order into a helical configuration. The sinusoidal c-axis component modulation changes to more of a square wave modulation with a period of eight layers.

The result, termed a "quasi-antiphase-domain", is shown in Figure 3. At 20°K (17.5°K is indicated from this study) all the c-axis components swtich to one direction, while the basal plane ordering is essentially undisturbed. The result is a conical ferromagnetic state with the easy magnetic direction being the generators of the cones. The basal plane component of the moment as observed by neutron diffraction is 4.1 μ_B and the c-axis component is 7.2 μ_B corresponding to a cone angle of 30° in zero applied field. Application of a magnetic field drastically alters the magnetic states of Er as is discussed in the section of Er results. Magnetic moment studies below 18 kOe on Er single crystals were made by Green et al. (29).

3. Holmium

Holmium again exhibits only two ordered states--helical antiferromagnetism from 132°K to 19°K and conical ferromagnetism below 19°K. The turn angle varies linearly from 50° at T_n to 36° at 35°K and finally goes to 30° below 18°K and remains fixed. Below 19°K a helical basal plane moment of 9.5 μ_B and a c-axis component of 2.0 μ_B is observed by neutron diffraction.

III. EXPERIMENTAL METHOD AND APPARATUS

A. Methods of Strain Measurement

The measurement of magnetostrictive strains in the rare earths presented several unique problems. Depending upon the applied field and the temperature, linear strains ranging from below $\frac{\Delta \ell}{\ell} = 1 \times 10^{-6}$ up to $\frac{\Delta \ell}{\ell} = 1 \times 10^{-2}$ were encountered. In order to resolve the fine structure present in some measurements, a sensitivity of $\frac{\Delta \ell}{\ell} = 1 \times 10^{-6}$ had to be maintained throughout the entire 10^4 range of strain. This required a highly sensitive and wide range strain detection system, one which was also capable of giving reliable results at temperatures from 350°K to 1.3°K.

Some of the techniques useful in thermal expansion work were not suitable for magnetostriction work. Interferrometric instruments are complicated, difficult to calibrate over a wide temperature range, have relatively slow response time, and do not allow a sample geometry that is appropriate for use in a transverse magnetic field. Capacitive methods in which dilitations of the sample produce changes in capacitance of a capacitor attached to the sample are quite suitable, especially for small dilitations, but require elaborate instrumentation and noise shielding. Similar problems would be expected in a mutual inductance or variable differential transformer method, and, in addition, there would be an unfavorable sample orientation difficulty.

B. Strain Gages

Electrical resistance strain gages first used for magnetostriction measurements in Ni by Goldman (28) have proved quite successful. These gages are made by various manufactures for stress analysis and consist of a thin ($1\text{-}2\times10^{-8}$ inch) metal foil electrical resistance element (nominally 100-200 ohms) embedded in a paper, epoxy, or bakelite carrier. The package is attached to the specimen with a suitable cement. The gage element thus follows any distortion of the sample. From measurements of the fractional change in resistance of the gage, the linear strain along the gage axis may be obtained by the relation

$$\frac{\Delta \ell}{\ell} = \frac{1}{G(T)} \frac{\Delta R_g}{R_g} . \qquad (5)$$

G is a temperature dependent proportionality constant known as the gage factor. The design of the gage elements is such that sensitivity to strains transverse to the gage axis is several orders of magnitude below that along the axis.

In collaboration with J. K. Alstad (1) several of the available strain gage and cement combinations were evaluated. Considerable effort was required to find a suitable combination for the strain and temperature extremes encountered. Initially, the best gage found was the Budd Company type C9-624 epoxy-phenolic backed gage (active area 1/8"x 1/8") made of Budd alloy (similar to nichrome with small additions to improve temperature

stability). The cement used was Budd GA-5 cured for one hour at 100°C followed by a post cure of five hours at 70°C. Pressure was applied to the bond area through pads of silicone and sponge rubber compressed by a small bar clamp. Measurements on Tb were done entirely with this gage using lot number J1-ACC-1. Isothermal strain versus field data on Dy and c-axis isofield runs were also made with the 624 gages from lot number J1-AC1-1. No change in gage characteristics was noted between lot numbers. In late 1963, a new cryogenic design gage (S-421) was introduced by Budd made of nichrome V with an improved epoxy backing. These gages had improved strain accuracy and less variation of the gage factor with temperature. Tests on this type of gage down to liquid He temperature by Kaufman (36) showed good consistency of the gage factor for both tension and compression loading. The gage response was found to be quite linear with strain to 1% strain, after which some non-linearity was apparent. Tests were conducted to 1.2% strain without gage or adhesive failure at 20°K. The strain drift observed at 1.2% strain was 210 and 60 micro-inches/inch in a two hour period for the two gages tested. Negligible gage hysteresis was observed by Kaufman in loading and unloading strains.

The Budd series S-421 gages were used in this investigation for all measurements on erbium and for rotation and isofield (except c axis) measurements on Dy. The lot number used was N2-AJJ11.

C. Strain Gage Measurements and Calibration

Crystal strains were obtained from measurements of fractional changes in resistance of the gages by use of Equation 5. The quantity $\frac{\Delta R_g}{R_g}$ was obtained by using a sensitive shunt-type Wheatstone bridge as shown in Figure 4. Two strain gages were used in opposite arms of the bridge: an active gage (R_a in the figure) bonded to the specimen, and a reference or "dummy" gage (R_d in the figure) bonded to a 2 mm thick disk of fused quartz and placed in the same temperature and magnetic field environment as the specimen gage. This arrangement effectively cancelled out effects of temperature variation of the gage resistance and most of the residual magnetoresistance (see below). The data were not corrected for the thermal expansion of the quartz which is about $0.25 \times 10^{-6}/{}^{o}K$, almost two orders of magnitude smaller than the measured magnetostriction effects. A current of 3.5 ma was used in each gage. The initial bridge balance was obtained by varying the combination of precision fixed and variable decade resistors R_4 in the diagram. All subsequent measurements were taken with the bridge in a balanced configuration by adjusting the five-dial decade resistor R_2. The null was sensed by Leeds and Northrup D.C. Null Detector Model 9834. The fractional change in gage resistance at balance was given by

$$\frac{\Delta R_a}{(R_a)_o} = C \frac{R_1}{(R_2)_o} \left[\frac{\Delta R_2}{\Delta R_2 + R_1 + (R_2)_o}\right] \qquad (6)$$

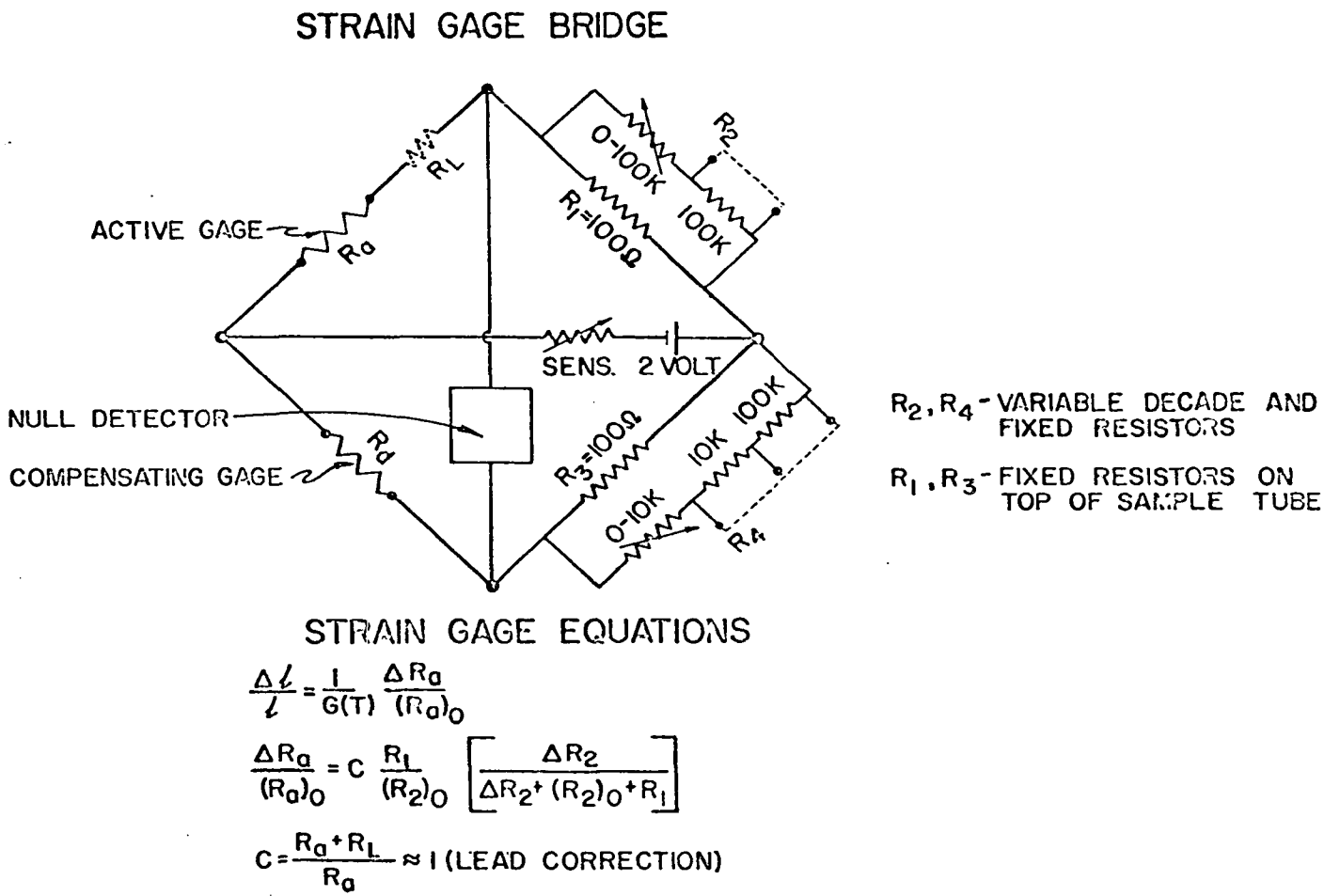

Figure 4. Strain gage bridge circuit and associated equations for calculating linear strains.

where the subscript zero refers to the initial or reference values. C is a correction for the "dead" resistance in the gage leads $C = \frac{R_a + R_L}{R_a} \approx 1.006$ (For R_L = 1.5 ohms and R_a = 260 ohms). The advantage of making all measurements in a balanced configuration is apparent from Equation 6: the gage resistance R_a and its temperature dependence need not be accurately known, as it enters the equations only as a small correction effect. The sensitivity of the bridge was 0.6 micro-ohms/ohm/scale division, corresponding to a strain at room temperature of 0.3 micro-inches/inch/scale division. Bridge resistors R_1 and R_3 were counter-wound on the same form and placed in an enclosure atop the sample holder assembly (see Figure 8) to reduce lead lengths and minimize thermal drifts.

The temperature dependence of the gage factor (see Equation 5) was obtained by use of a cantilever beam strain gage calibration device manufactured by Cryresco. This device, shown in Figure 5, is similar to one described by McClintock (49) which provides a uniform strain in an aluminum beam independent of temperature. Two active strain gages were mounted on the beam, one in compression, and one in tension. Room temperature values of the gage factor supplied by the manufacturer were used to calibrate the device. Strains of -230., +239.; -465.,+481.; -696.,+722. were obtained from the three steps of the wedge block. These values were in fair agreement with those supplied with the calibrator. The temperature of the calibrator assembly could be varied

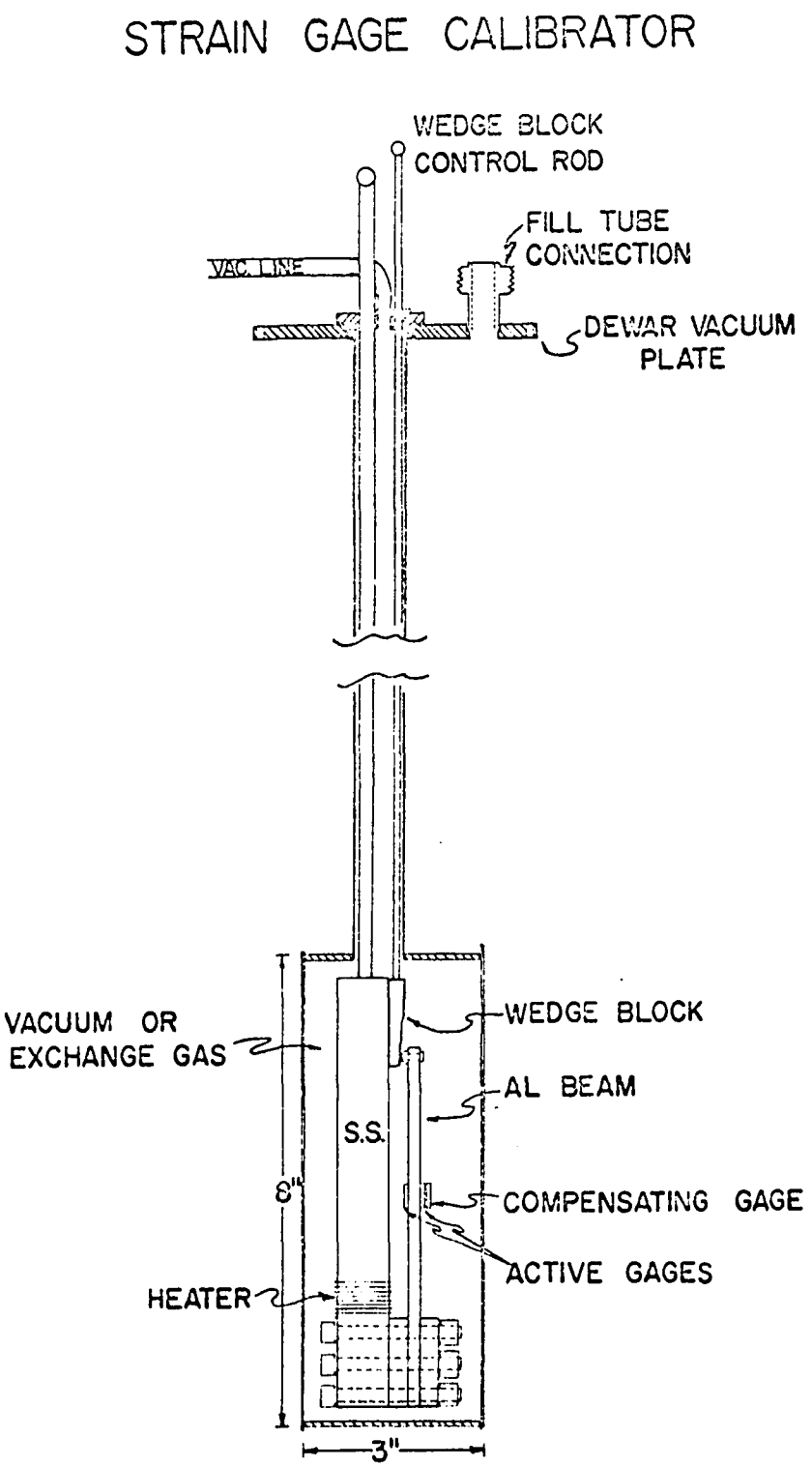

Figure 5. Calibrator and vacuum chamber used to obtain temperature dependence of gage factor.

by placing it in a dewar and alternatively using exchange gas in the enclosing can or evacuating the region and using a heater wound on the calibrator block. Using the known beam strains of the calibrator, the gage factor was computed at a given temperature from Equations 5 and 6. The result is shown in Figure 6 for both the series C9-624 and S-421 gages. Data shown for the C9-624 gages are for a gage in contraction only. The obvious superiority of the small gage factor temperature dependence in the S-421 gages is apparent. Considerable uncertainity is attached to the C9-624 gage factors below 20°K, possibly due to magnetic ordering. The solid lines are the result of a least squares computer fit of the data. For fitting purposes, the temperature range was broken down into three regions for the C9-624 gages and into two regions for the S-421 gages. For strain data taken as a function of temperature, the value of G used in Equation 5 was found by averaging:

$$\bar{G} = \frac{\int_{T_{ref}}^{T} G(T)\, dT}{T - T_{ref}} , \qquad (7)$$

where T_{ref} is the reference temperature (usually 300°K) and T the measurement temperature. G(T) is the polynomial fit of the gage factor data just described. As can be seen from the figure, $\bar{G}$ departs significantly from the simple straight line average in some temperature regions.

The accuracy of the strain gage measurement procedure was checked

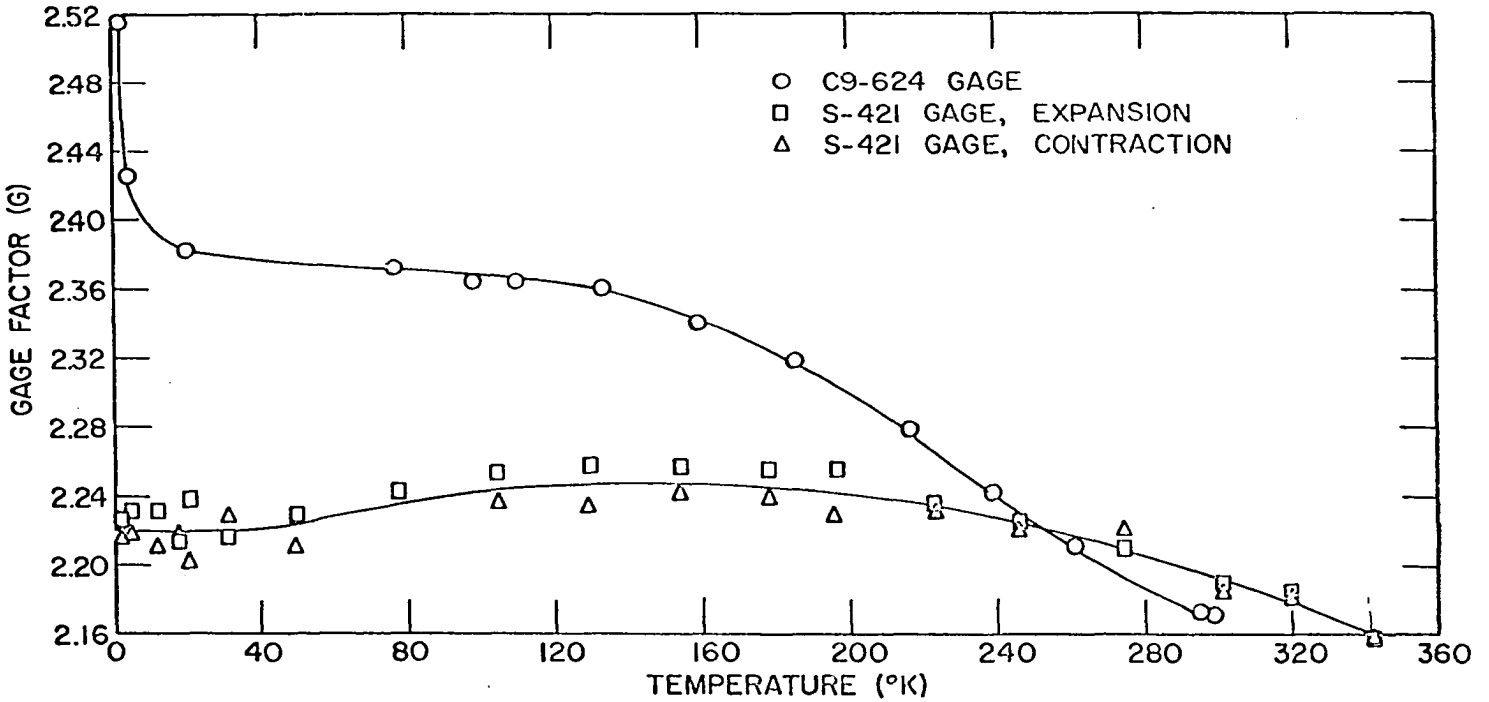

Figure 6. Gage factor as a function of temperature for Budd type C9-624 and type S-421 strain gages. Results are shown for both positive and negative strains applied to the type S-421 gages.

by mounting a gage on a high purity annealed copper disk and measuring the Cu thermal expansion from 300°K to 77°K or 4°K and comparing the data to that of Beenakker and Swenson (3). The results of several runs using different dummy gages showed errors ranging from less than two to about five per cent in the thermal expansion obtained by the strain gage method. The more accurate results were obtained with the S-421 gages. The surface of the quartz disk holding the dummy gage occasionally cracked abruptly during the taking of magnetostriction data necessitating a new quartz disk and gage. A copper thermal expansion run was made on almost every new dummy gage to check its accuracy. The non-magnetostrictive copper sample also provided a convenient method for determining the residual magnetoresistance of the strain gage package. Tests were made of the pseudo-strain introduced by the application of a 30 kOe field and of the rotation of this field about the gage axis in the plane of the gage. The results are shown in Table 1. Essentially no magnetoresistance was found above 20°K and negligible angle dependence of the apparent strain was observed. The S-421 gages show a slightly smaller over-all magnetoresistance effect.

D. Helium Dewar

The nitrogen-shielded helium dewar used for these measurements was similar to one used by Strandburg (63), and is shown in Figure 7. No liquid was present in the tail section, heat transfer being accomplished

Table 1. Pseudo-strain resulting from differential magnetoresistance of gages

S-421 Gages				C9-624 Gages			
Temperature	θ^a	H	Pseudo-strain	Temperature	θ^a	H	Pseudo-strain
°K	degrees	kOe	μ in./in.	°K	degrees		μ in./in.
79.0	0.	0.	0.0	78.9	0.	0.	0.0
	0.	30.	0.0		0.	30.	0.0
	60.	30.	0.0		30.	30.	-1.1
	90.	30.	0.0		60.	30.	-1.1
	90.	0.	0.0		90.	30.	-1.1
					180.	30.	-1.1
48.5	0.	0.	0.0		0.	30.	-1.1
	0.	30.	0.0		0.	0.	-1.1
	60.	30.	0.0				
	90.	30.	0.0	42.7	0.	0.	0.0
	90.	0.	0.0		0.	30.	0.0
					30.	30.	0.0
19.8	90.	0.	0.0		60.	30.	0.0
	90.	30.	0.0		90.	30.	0.0
	60.	30.	0.7		0.	30.	0.0
	0.	30.	0.0		0.	0.	-1.2
	0.	0.	0.0				
				15.8	0.	0.	0.0
10.5	90.	0.	0.0		0.	30.	8.4
	90.	30.	3.0		30.	30.	8.4
	60.	30.	3.0		60.	30.	8.4
	0.	30.	3.0		90.	30.	8.4
	0.	0.	0.0		0.	0.	8.4
6.3	90.	0.	0.0	4.4	0.	0.	0.0
	90.	30.	11.9		0.	30.	33.0
	60.	30.	11.9		30.	30.	33.0
	0.	30.	11.9		60.	30.	33.0
	0.	0.	0.0		90.	30.	34.2
					180.	30.	34.2

[a]Angle of applied field relative to gage axis.

Table 1 (Continued)

Temperature °K	θ degrees	H kOe	Pseudo-strain μ in./in.	Temperature °K	θ degrees	H	Pseudo-strain μ in./in.
4.6	90.	0.	0.0		0.	30.	34.2
	90.	30.	22.3		0.	0.	-1.2
	60.	30.	22.3				
	0.	30.	22.3				
	0.	0.	0.7				
3.7	90.	0.	0.0				
	90.	30.	27.5				
	60.	30.	27.5				
	0.	30.	26.8				
	0.	0.	0.0				

by high purity copper shields connected to the reservoirs at liquid He and liquid N_2 temperatures. This construction saves one metal wall in the tail. Quick changes of cryogenic liquids could be accomplished by use of a transfer tube without the need for boiling residual liquid out of the tail.

The outer diameter of the tail was 1.5 inches, with an inner working dimension of 0.936 inches. Over-all diameter of the dewar was 6.5 inches. All joints were silver soldered except those which need be broken to take the dewar apart.

Inner and outer dewar vacuum chambers were separately pumped to allow pre-cooling of the inner dewar from the outer N_2 liquid by admitting

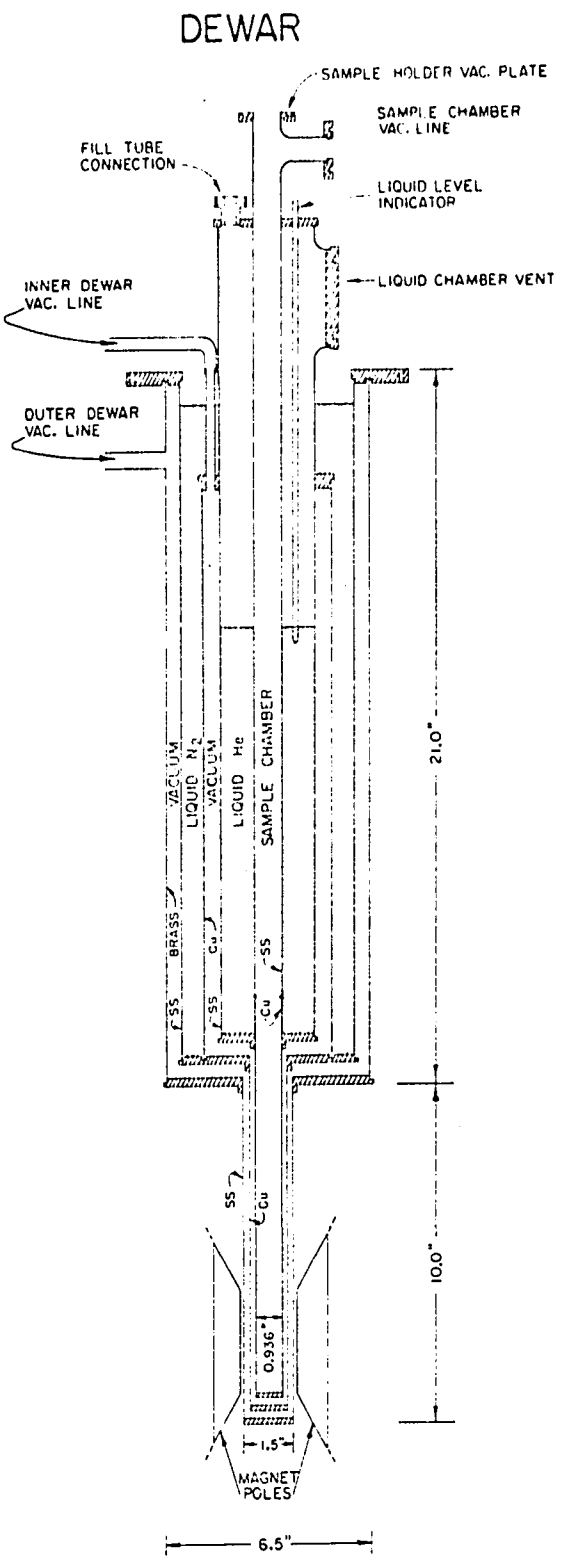

Figure 7. Helium dewar used in this investigation. No liquid was contained in the tail section. Heat transfer was through copper shields at liquid He and N_2 temperatures.

N_2 gas into the vacuum chamber. A N_2 level indicator and automatic fill device were included. Provision was made for pumping on the liquid in the inner dewar. Capacity of the inner dewar was slightly over one liter of liquid. Except when liquid He was used, the vacuum chambers were pumped continuously with an oil diffusion pump. With He the inner vacuum chamber was isolated. No charcoal trap was used.

E. Temperature Control Apparatus

Isothermal and rotation magnetostriction measurements required control of sample temperature to $\pm$ 0.1°K for up to 20 minutes from He bath to above room temperature. Similar control problems have been encountered in other magnetic measurements at this laboratory, and a fairly standard design temperature control system has evolved. This general plan was adopted for the construction of the present apparatus, some of the details of which are shown in Figure 8. The sample support tube was enclosed by a 3/4" tube of which the bottom $8\frac{1}{4}$ inches were made of electrolytic copper and the remainder were of No. 321 stainless steel. The copper cylinder was thermally isolated except for a pair of phosphor bronze spring contacts located about three inches from the copper-stainless steel junction which made contact with the He bath temperature wall of the dewar. Heat generated by a 124 ohm No. 35 manganin wire heater on the copper cylinder was slowly dissipated to the liquid through the three inch stainless steel "heat leak" path, providing thermal grounding for

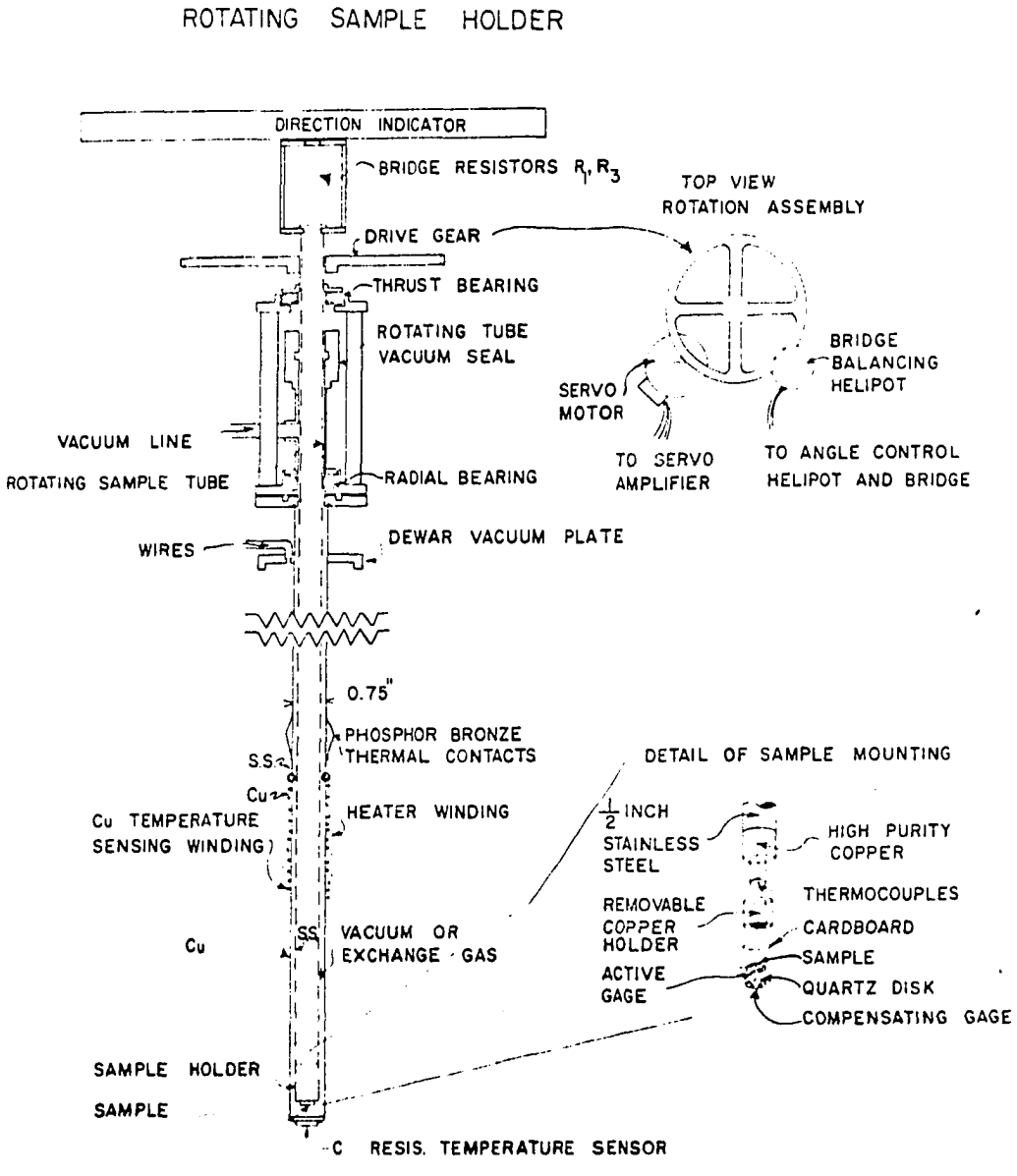

Figure 8. Rotating sample holder used for angle dependent magnetostriction measurements. Outer coaxial tube contains resistance thermometers and heater used for temperature control.

the enclosure. For rapid cool-down, 10-500 microns of He exchange gas were admitted to the vacuum chamber between the dewar bath temperature wall and the copper-stainless steel tube. The sample support tube was centered by teflon spacing washers and thermal contact provided to the surrounding copper can by He exchange gas at a pressure of about five inches of Hg. Thermostatic control of the heater was provided by a 156 ohm No. 40 Cu wire resistance sensing element wound beneath and coaxially with the heater, and by a 57 ohm Allen Bradley carbon resistor fastened to the bottom of the copper can. Both heater and copper resistance elements were wound bifilarly to reduce pickup from the magnetic field and ac interaction. Lead wires to room temperature were of No. 26 manganin. The copper (used above 30°K) and carbon (used below 30°K) resistance thermometers were part of a temperature control bridge shown in Figure 9. Desired operating temperatures were selected using helipots R_5 (for carbon element) or R_6 (for copper elements). The bridge error signal was fed to a modified dc Brown Chopper amplifier shown in Figure 10. The low level dc error signal from the bridge was chopped and amplified to operate a thyratron tube and plate relay to control the heater in either on-off pulses or in a "max-min" mode. The dc heater current was provided and could be varied by the power supply shown in Figure 11. In addition to the automatic control, this supply allowed separate manual operation of the heater and had provision for applying

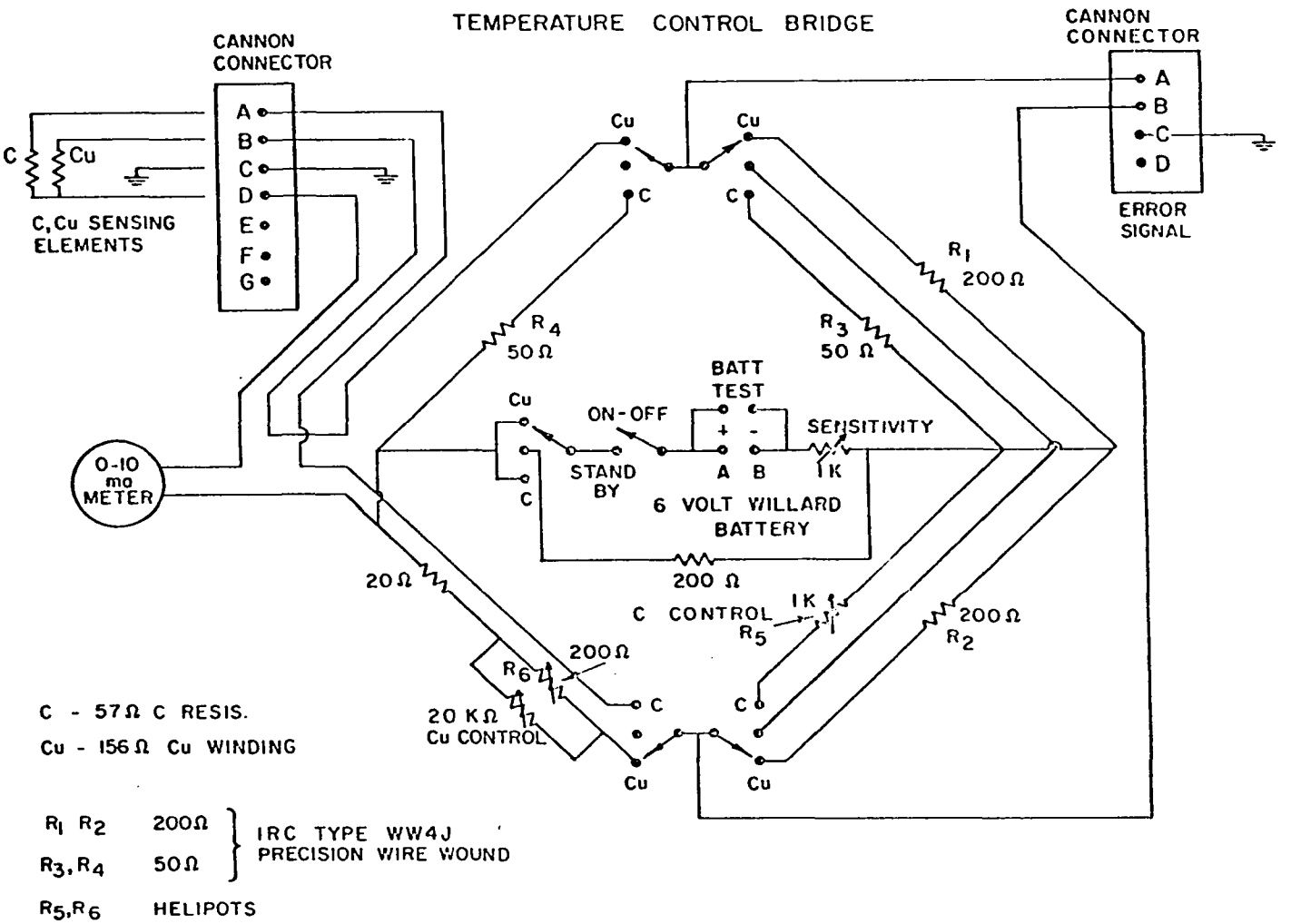

Figure 9. Bridge used in conjunction with resistance thermometers shown in Figure 8 for temperature control.

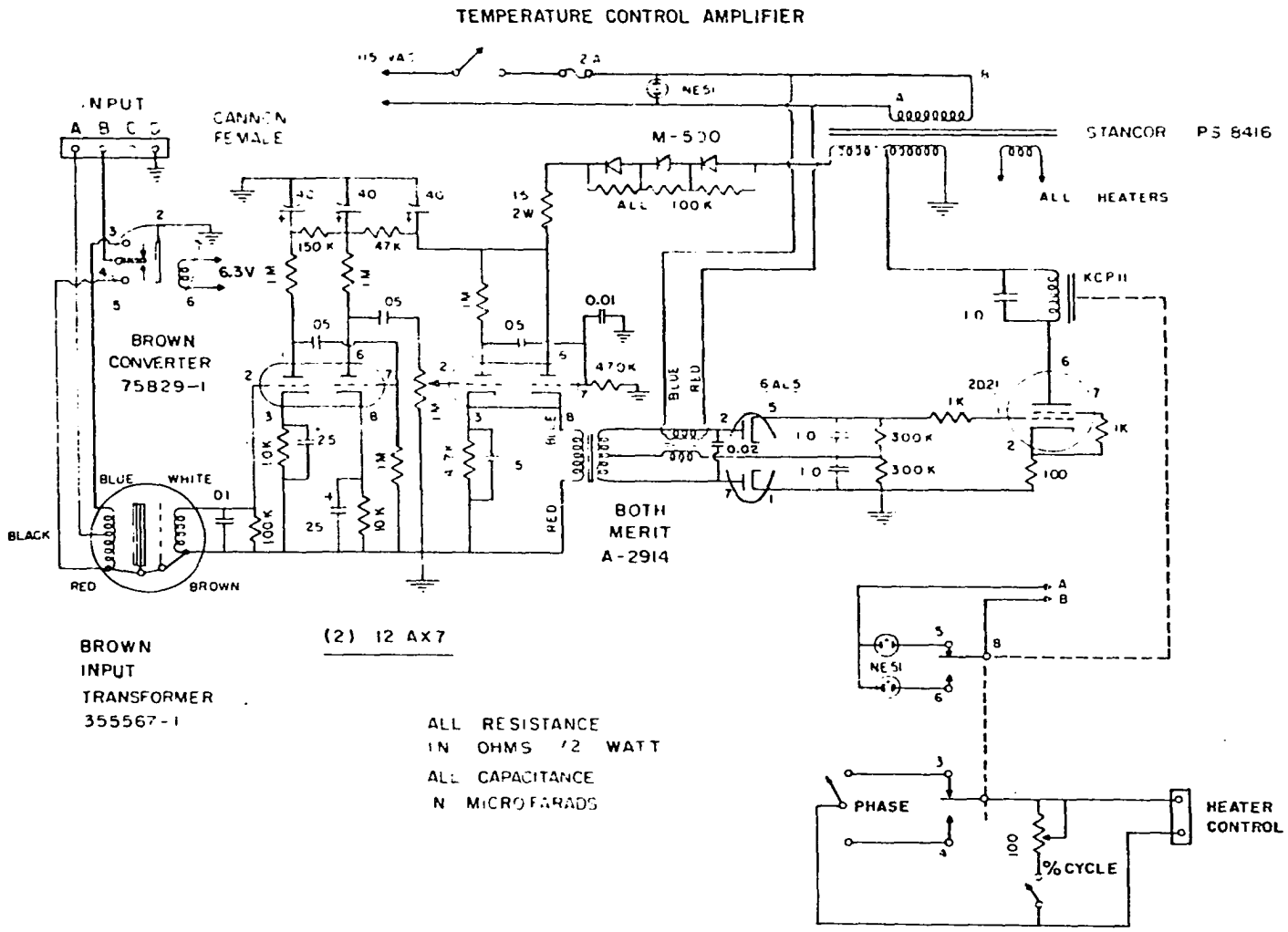

Figure 10. Servo amplifier used to amplify error signal from temperature control bridge shown in Figure 9. Amplifier output controls heater power supply shown in Figure 11.

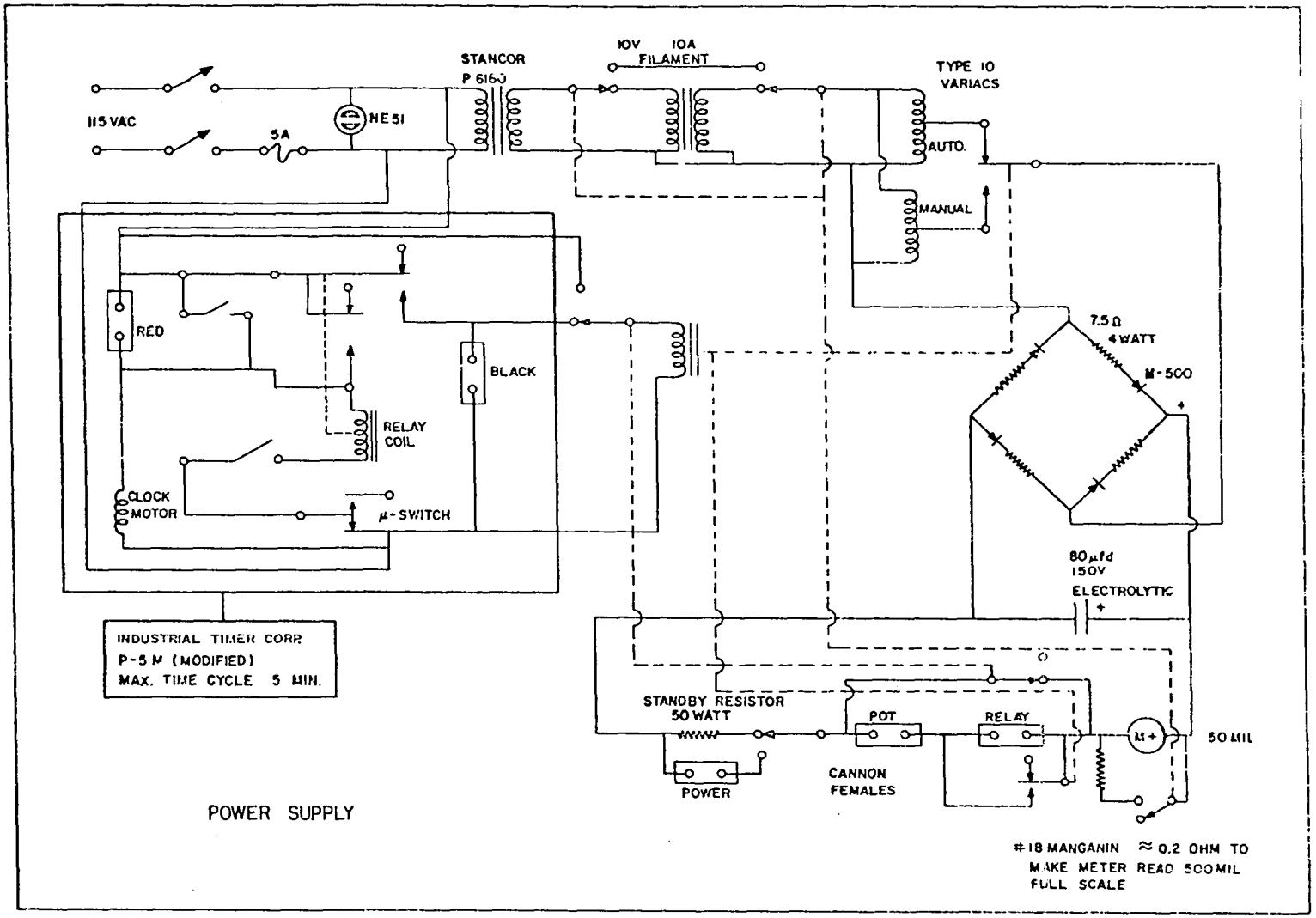

Figure 11. Heater power supply for temperature control apparatus.

a timed heat pulse of up to five minutes duration at a different heater current level. This facilitated rapid change in temperature with return to automatic operation at the completion of the high heat pulse. Using this temperature control apparatus, $\pm$ .1 degree control could be achieved within about twenty minutes from He temperature to about 200°K. At higher temperatures a somewhat longer period was required for stabilization. The appropriate cryogenic liquid (or solid) was used in the inner dewar depending on the temperature range to be covered.

F. Rotating Sample Holder Assembly

In order to obtain the anisotropic magnetostriction constants, it was necessary to rotate the magnetic field relative to the crystal axes. This was accomplished in the magnetostriction experiments by making a servo-controlled rotating sample holder. The major mechanical details are shown in Figure 8. The stainless steel sample support tube passed through a pair of ball bearings and a Cenco glass tube connector which provided a good vacuum seal and at the same time permitted relatively free rotation of the tube. The sample assembly was turned by a six inch diameter brass spur gear attached to the upper end of the sample tube and driven by Brown No. 76750-3 20 rpm servo-motor in a 12:1 gear reduction. A ten turn helipot was driven from the same six inch gear in a 12:1 gear ratio. This helipot formed part of the bridge shown in Figure 12. The servo-amplifier which sensed the bridge error signal was

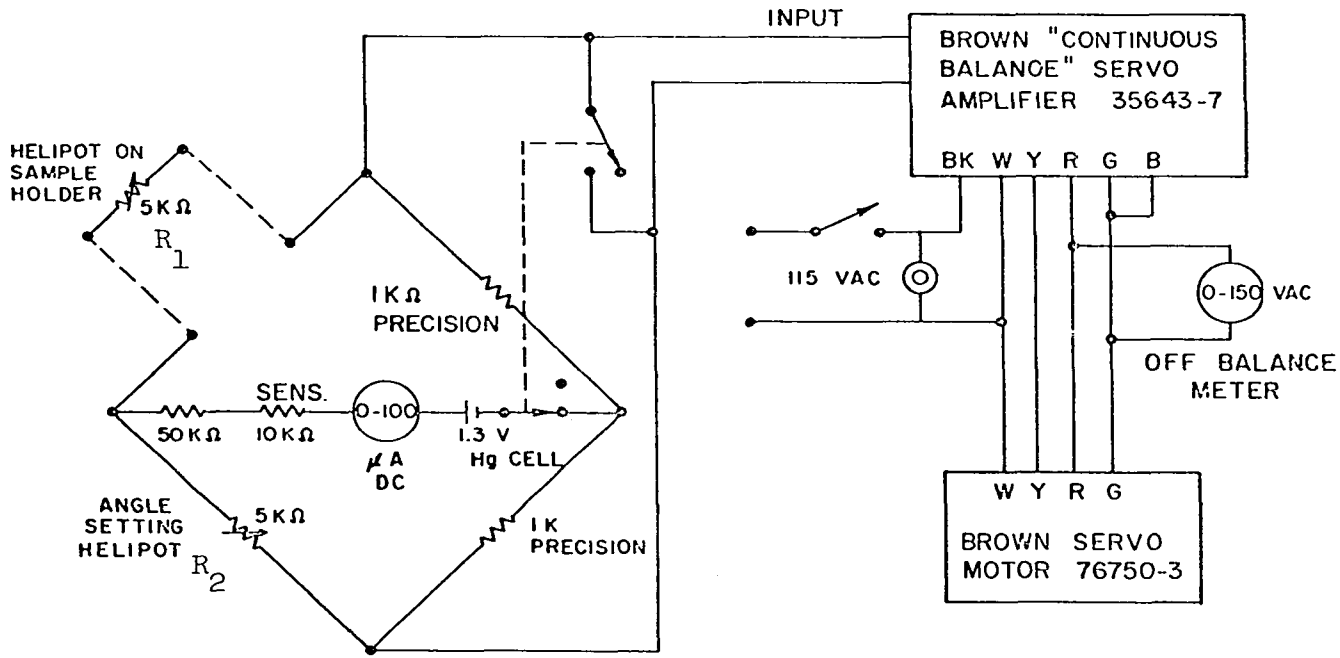

ROTATING SAMPLE HOLDER ELECTRONICS

Figure 12. Rotating sample holder control bridge and electronics.

a Brown type 356413-7. Helipot R_2 was calibrated in angle (degrees) of rotation. When the desired angle of rotation was set on R_2 the bridge was unbalanced, and the servo-amplifier and motor rotated the six inch gear atop the sample holder. This gear was directly linked to helipot R_1 which in turn brought the bridge back into a new balance and stopped the rotation. The assembly easily responded to angle changes as small as 0.3 degrees which corresponded to one division on the angle setting helipot. Electrical leads to the strain gages and thermocouples were brought out through a glass vacuum seal at the top of the sample tube.

G. Sample Mounting

The lower end of the rotating sample tube contained a removable copper sample mount as shown in the detail of Figure 8. The sample disk carrying the active strain gage was affixed to this mount which also supported the quartz disk and dummy gage. Considerable time was spent in trying methods of fastening the sample disk to the mount which would be flexible and not restrain the dilatation of the sample, and at the same time be resistant to failure from the high torques on the disk produced by the magnetic anisotropy. Several combinations of spacer materials and glues of the cellulose acetate type and also General Electric 7031 varnish were tried with little success at resisting the torques especially at low temperature. It was then decided to try Budd GA-5 epoxy which is designed to allow considerable strain. The sample

was cemented to a cardboard spacer using a thin strip of epoxy under about one-half of the sample. The cardboard was, in turn, fastened to the copper sample mount with GA-5 epoxy. A measurement of the thermal expansion of a copper disk 2 mm thick mounted in this fashion showed that negligible strain errors were induced by the mounting; however, some adverse effects were noted on a sample slightly less than 0.8 mm thick. Rare earth samples were thus generally prepared about 1.5-2 mm in thickness. It was possible to loosen the GA-5 epoxy bond to the sample and also the strain gage by soaking for 24-72 hours in DuPont dimethyl formamide, a reducing agent. This allowed the sample and gage to be removed without grinding off the epoxy bond.

II. Temperature Measurement

Temperature of the sample was determined by thermocouples located in the copper tip of the sample support tube. A copper constantan thermocouple was used above 20°K and a AuFe versus Cu thermocouple below 20°K. The calibration of the AuFe wire was performed by Finnemore et al. (26) of this laboratory. Individual thermocouples prepared from the same roll of thermocouple wire are found to differ by several microvolts, presumably due to nonhomogeneous distributions of impurities in the wires. Due to the "dry-tail" design of the dewar, it was not possible to renormalize the calibration at bath temperature for each run. From a series of tests made over a period of time by immersing the sample tube directly in the cryogenic liquid storage dewars, a set of values was obtained for the emf

of the thermocouples at N_2, H_2, and He temperatures. The accepted calibration tables for constantan and for AuFe were divided into regions (five for constantan, four for Au-Fe), and the points in each region were fit to cubic equations by least squares. Some care was taken in picking the region boundaries and the amount of overlap of each region to produce a smooth change in slope of the fitted curve. The deviations in emf of the experimental thermocouple at He, H_2, N_2 and ice bath (zero deviation) temperatures were fit to a second order polynomial. This error curve was then added algebraically to the calibration data polynomials, and a thermocouple table listing the emf for each tenth degree Kelvin was prepared on the computer.

Thermocouple junctions in the ice bath were made with soft solder and those at the sample were made by spot welding (constantan) and beading (Au-Fe). Thermocouple emf was measured with a Rubicon K2 potentiometer and Honeywell galvanometer. Absolute accuracy of the temperature data is estimated to be $\pm$ 0.5°K and the relative accuracy of the data is about 0.1°K over the range 4°K to 300°K.

I. Magnet Equipment

The principal electromagnet used in this study was a fifteen inch Harvey Wells L-158 with an accompanying 22 kilowatt HS-200 solid state power supply. The magnet was equipped with Hyperco-35 tapered pole caps with a final diameter of three inches and a gap of 1.6 inches.

The maximum field attainable was 30.7 kOe. Calibration was done with a Rawson Type 501 0.1% rotating coil gaussmeter checked against a NMR spectrometer in fields up to 26 kOe.

The Harvey Wells magnet was capable of rotation, and this was used for initial line-up of the field; subsequent sample rotations during the experiment were accomplished with the rotating sample holder previously described.

Residual fields in the magnet gap varied from 35 to 75 gauss depending on the method and rate of demagnetization. A small constant current power supply was connected in parallel opposition to the HS-200 supply and used to reverse the magnet current and reduce the field to zero in the gap. This required a reverse current of approximately 0.2 to 0.3 amperes. Null field within $\pm$ 0.5 gauss was sensed by a Bell Hall-effect element type BH-206 placed in the gap. The output of the element was amplified by a Bell design two-transistor difference amplifier and displayed on a zero-center 25 microampere meter. As a precaution, the amplifier output was also used to drive a thyratron tube and relay circuit which automatically disconnected the small reverse current supply from the magnet when the main supply was turned up.

All magnetostriction measurements on Tb, Er, and Dy were made on the equipment described in this chapter except the magnetostrain versus applied field measurements in Dy which were made on the apparatus built and

described by Alstad (1) utilizing an A.D. Little electromagnet with a maximum field of 25.8 kOe.

IV. SPECIMENS FOR MAGNETOSTRICTION MEASUREMENTS

A. Specimen Geometry

As mentioned earlier, single crystal specimens are necessary for magnetic studies on the rare earths in order to directly observe the effects of anisotropy. The single crystals were grown and aligned by the methods described in the following section.

Ideally, ellipsoidal samples would be desirable in order to have a uniform internal demagnetizing field. In practice however, this is a difficult geometry to obtain or work with, and as a result, disk shaped samples were used to approximate an oblate ellipsoid. Diameter to thickness ratios ranged from 11.6:1 to 5.4:1 which represent a compromise between ideal ellipsoidal geometry and a sample sufficiently thin to be distorted by the strain gage and mounting.

Table 2 lists the dimensions of the disk shaped samples of Tb, Er, and Dy prepared for this investigation. For Tb and Dy the two sample planes prepared were the basal plane and the plane containing the c axis and the easy basal plane magnetic direction. For Er three samples were prepared. The approximate demagnetizing fields for the specimens, assuming that they were oblate ellipsoids (9), are also given in Table 2. The demagnetizing field was found from $H_{demag} = 4\pi N\rho\sigma$ where N is the demagnetizing constant, ρ is the density, and σ is the magnetic

Table 2. Sizes and approximate demagnetizing fields for disk-shaped magnetostriction specimens

Code[a]	Diameter (in.)	Thickness (in.)	H_{demag} (gauss)
Dy a-b	0.245	0.035	10.2σ
Dy a-c	0.350	0.030	6.5σ
Er a-b	0.365	0.037	8.1σ
Er a-c	0.383	0.071	13.3σ
Er b-c	0.367	0.065	12.9σ
Tb a-b	0.368	0.088	14.9σ
Tb b-c	0.370	0.070	12.4σ

[a]Letters following element name indicate axes in the plane of disk--a ($11\bar{2}0$), b($10\bar{1}0$), c(0001).

moment per gram. The maximum demagnetizing field for these specimens is about six kilogauss.

B. Crystal Preparation

The rare earth metal used in this investigation was produced at the Ames Laboratory by use of an ion exchange process for the separation of the rare earth compounds (62) and a reduction process for the preparation of the pure metal from the fluoride. The single crystal specimens were grown from arc-melted buttons of pure metal by a thermal-strain-anneal method described by Nigh (53, 54). The high strains induced by the

arc-melting process were removed by annealing the metal button in a temperature gradient of about 25°C/cm in a series of 50°C temperature steps. These were started about 200°K below the melting or crystal structure transition temperature, and ended about 15-50 degrees below the above temperatures. The crystal was annealed 8-10 hours at each step. A post anneal of 8-10 hours in a constant temperature zone at the highest temperature was followed by a slow cool-down. In the furnace the metal button was not in contact with a crucible, but was supported by a tungsten bail to minimize contamination. Grain boundaries were clearly visible in the annealed crystals due to thermal etching. Crystals produced by this method did not have predictable or uniform size and orientation, thus it was often necessary to re-arc-melt the button or obtain new material and repeat the process. A button was not generally arc-melted more than three times to minimize impurity contamination--principally oxygen. In general, if crystal growth was successful, the resulting crystals were of good quality and were of the same orientation throughout the thickness of the buttons. Laue X-ray pictures taken at various points on the face gave uniformly good single crystal patterns with virtually no twinning from surface platelets or twisting of the axis direction. One exception occurred in the first basal plane sample of Tb which was prepared. This specimen apparently contained a small inclusion of a different crystal orientation which was not visible and

did not show on X-ray pictures. This defect had the effect of increasing the magnetic hardness of the dominant b-axis direction in the sample. This phenomenon became more pronounced with repeated thermal cycling. All data taken with this crystal were marked and are not included in this dissertation. A new basal plane Tb sample was prepared and is the one reported on here.

C. Specimen Preparation and Alignment

Appropriately oriented crystals were selected from the button and aligned by use of Laue back reflection X-ray pictures (30). The disk shaped single crystal specimens were cut from the button by use of a Servomet electro-spark cutter which produced a relatively strain free cut. In this process the X-ray goniometer was mounted on the spark cutter eliminating the errors inherent in demounting the crystals. After cutting, the crystals were etched in a solution of 60% nitric and 40% acetic acid and re-X-rayed. Final alignment, if needed, was accomplished by light grinding using fine carborundum paper. The prepared crystals were oriented by X-ray and scribed in the principal axis directions using a height gage and scribing accessory.

Strain gages were aligned with the crystal axis scribe marks and mounted under a microscope. Alignment of the gage axis with the magnetic field in basal plane samples was accomplished by exploiting the symmetry of the magnetostrain effect as the field was rotated about the easy

magnetic axis. For specimens with the hard c-axis direction in the plane, a visual alignment process was used employing two plumb bobs and an alignment bar fixed to the sample holder. For the basal plane samples total alignment error between crystal axis, gage and magnetic field directions is estimated to be $\pm$ 1°. Due to the less precise visual alignment, the error expected with the c-axis samples is about $\pm$ 2°. The larger field alignment errors in the Tb and Dy c-axis samples do not affect the data significantly as the magnetization is strongly constrained to the basal plane direction by the magnetic anisotropy. The angle error thus changes only the applied field component and not the magnitization.

D. Specimen Purity

Samples used in this work were obtained from the best metal available at the Ames Laboratory in 1963-4. Residual pieces of the metal immediately surrounding the crystal disks were analyzed for impurities at the Laboratory. A semi-quantitative spectrographic analysis was performed as well as a quantitative vacuum fusion analysis for dissolved gas impurities. The results of the analyses are presented in Table 3 and indicate an over-all purity of the specimens of better than 99.8%, except for the Tb which contained Ta amounting to 0.2-0.4% and O_2 amounting to 0.1%. No impurity analysis was made on the Er basal plane sample.

Table 3. Analysis of impurities in rare earth specimens. Impurities given in percent

Impurity	Spectrographic Analysis Sample Code						Dissolved Gas	Vacuum Fusion Analysis Sample Code					
	Dy		Er		Tb			Dy		Er		Tb	
	a-b	a-c	a-c	b-c	a-b	b-c		a-b	a-c	a-c	b-c	a-b	b-c
Al	~.01	~.01	<.0035	<.0035	.006	.0035	O_2	.0340	.0326	.0545	.0420	.1215	.1040
Ca	<.003	<.003	~.0015	<.0015	.006	.003	H_2	.0024	.0022	.0029	.0033	.0012	.0004
Co	-	-	-	-	-	-	N_2	.0025	.0022	.0011	.0052	.0218	.0100
Cr	<.003	<.003	.0080	.0060	<.006	<.006							
Cu	X	X	-	-	<.002	<.002							
Fe	~.02	~.02	.01	.003	.006	.0115							
Mg	<.007	<.007	.002	<.001	<.0016	<.0016							
Mn	-	-	-	-	-	-							
Mo	-	-	TX	TX	-	-							
Ni	~.01	~.01	.02	.004	.0055	<.0020							
Pb	-	-	-	-	-	-							
Si	<.002	<.002	.03	.005	.004	.004							
Ta	~.04	~.04	<.03	<.03	~.23	~.42							
Ti	-	-	-	-	-	-							
V	-	-	-	-	-	-							
W	TX	TX	<.03	<.03	-	-							
Y	<.001	<.001	<.001	<.001	~.05	<.01							
Dy,Er	<.005	<.005	<.01	<.01	<.01	<.01							
Eu	-	-	-	-	-	-							
Gd	<.02	<.02	-	-	<.02	~.1							
Ho	~.1	~.1	<.005	<.005	-	-							
Nd	-	-	-	-	-	-							
Pr	-	-	-	-	-	-							
Tb	<.1	<.1	-	-									
Tm	-	-	<.001	<.001	-	-							
Yb	X	X	<.005	<.005	-	-							

SYMBOL MEANING

-	Element not detected
<	Less than
X	Interference
T	Trace

V. MAGNETOSTRICTION OF A FERROMAGNET

A. Phenomenological Theory

The magnetostriction of a material arises as a result of an interaction between the total magnetic energy and the elastic energy. The observed distortions will occur if their result is a lowering of the total energy of the crystal.

The total magnetic energy of a material consists of three contributions--the exchange energy, the anisotropy energy, and the demagnetizing energy. The fundamental postulate of magnetostriction is that at least one of these must be a function of the state of strain of the crystal (i.e. of the interatomic distances). If there is no strain dependent magnetic energy, there will be no magnetostriction.

The strain dependence of the demagnetizing energy, known as the form effect, arises from the variation of the demagnetizing factor with changes in the geometry of the specimen. Normally, the contribution from this source is relatively small and is neglected (64).

The exchange energy (or indirect exchange energy) is a function only of the relative orientation and magnitude of the magnetic electron spins. Since this is generally not altered by application or rotation of a magnetic field, the strain dependence of the exchange energy is largely neglected in magnetostriction calculations (an important

exception to this statement occurs in the rare earths as is discussed later).

The remaining magnetic energy, the anisotropy energy, is thus the key contribution in most magnetostriction studies. To produce a magnetostriction, there must be an anisotropy energy, E_K, and it must be dependent on the strains, S_{ij}, viz.:

$$E_K = E_K^o + \frac{\partial E_K}{\partial S_{ij}} S_{ij} + \frac{1}{2} \frac{\partial^2 E_K}{\partial S_{ij} \partial S_{kl}} S_{ij} S_{kl} \qquad (8)$$

in phenomenological form. The first term is the undistorted anisotropy energy, the second a coupling term between the anisotropy and elastic energies (normally referred to as the magneto-elastic coupling energy), and the third term, known as the morphic energy, represents contribution to the total energy arising from the distortion of the crystal symmetry. The morphic term is again small and normally neglected.

The formal calculation of the expression for the magnetostriction of a hexagonal ferromagnet was done originally by Bitter (8) with independent calculations and later refinements by Mason (47, 48), Birss (7), Lee (43), and Callen and Callen (14, 15). The general procedure most have followed involves writing a magneto-elastic Hamiltonian consisting of the following terms

$$H = H_{el} + H_k^o + H_{ME} + H_R \qquad (9)$$

where H_{el} is the elastic energy, H_k^o is the undistorted anisotropy

energy, H_{ME} is the magneto-elastic coupling energy, and H_R is the morphic energy, if included.

The lowest order anisotropy energy expression which is consistent with hexagonal symmetry has the form $k_2 \sin^2\theta + k_4 \sin^4\theta + \sin^6\theta (k_6 + k_6^6 \cos 6\phi)$. The coefficients k_2, k_4, (k_6 and k_6^6) are made up respectively of the components of the second, fourth, and sixth rank anisotropy energy tensors K_{mn}, K_{mnop}, and K_{mnopqr}. The angle θ is measured from the c axis toward the basal plane, and ϕ is an angle in the basal plane measured from the easy magnetic axis. Similarly, the equivalent magneto-elastic coupling coefficients are made up of fourth and sixth rank tensor components, M_{ijmn} and N_{ijklmn}. Odd rank tensors are absent since the lattice possesses a center of symmetry. Thus, up to sixth rank contributions, the total magneto-elastic energy may be written:

$$\begin{aligned} H = {} & C_{ijkl} S_{ij} S_{kl} + K_{mn} \alpha_m \alpha_n + K_{mnop} \alpha_m \alpha_n \alpha_o \alpha_p \\ & + K_{mnopqr} \alpha_m \alpha_n \alpha_o \alpha_p \alpha_q \alpha_r + M_{ijmn} \alpha_i \alpha_j S_{mn} \\ & + N_{ijklmn} \alpha_i \alpha_j \alpha_k \alpha_l S_{mn} + R_{ijklno} \alpha_i \alpha_j S_{kl} S_{no} \end{aligned} \tag{10}$$

where C_{ijkl} are the elastic constants, S_{ij} are the strains, α_i are direction cosines of the magnetization, and R_{ijklno} are the morphic energy terms. The program followed by most authors is to evaluate the tensor components of Equation 10 in the symmetry group of the hexagonal lattice, 6m2, 6mm, 62, and 6/mmm. This result is then minimized with

respect to the strains and transformed back to Cartesian coordinates to obtain the equilibrium magnetostriction lattice strains. A slightly different approach was followed by Mason (48) which involves using the elastic enthalpy $H_1 = U - T_{ij}S_{ij}$ as the fundamental quantity. This is a function of the stresses T_{ij}, intensity of magnetization and the entropy. After expansion of the tensor form, the equilibrium strains are found from $S_{ij} = -\frac{\partial H_1}{\partial T_{ij}}$

B. Callen Theory of Magnetostriction

Callen and Callen (14, 15) have developed a very elegant expression for the magneto-elastic interaction energy using group theory. They considered two types of interactions namely, interactions of a single ion (e.g. a 4f in the rare earths) with its surrounding charge environment and interactions between pairs of ions. The single ion terms describe the effects of the anisotropy energy while the two ion terms are necessary to evaluate the exchange energy and dipole-dipole energy. As basis functions they used polynomials of the spin components of an ion "f" for the one ion terms, and polynomials in the product spaces of ions "f and g" for the two ion terms. These polynomials designated $K_i^{\mu\ell}(S_f)$ and $K_i^{\mu\ell}(S_f, S_g)$ transform as the basis functions of the μ'th irreducible representation of the symmetry group (6m2, 6mm, 62, 6/mmm). The ℓ labels the order of the polynomial, and describes the magnetic symmetry represented (i.e. $\ell = 0$ corresponds to spherical symmetry, $\ell = 2$ to

cylindrical symmetry, and $\ell = 4$ and $\ell = 6$ to hexagonal symmetry). The one interaction Hamiltonian containing one ion and two ion magneto-elastic coupling coefficients $B_j^{\mu\ell}$ and $D_j^{\mu\ell}$ and irreducible strains $\epsilon_i^{\mu j}$ has the form

$$H_{me} = - \sum_{\mu j} \sum_{\ell} B_j^{\mu\ell} \sum_i \epsilon_i^{\mu j} \sum_f K_i^{\mu\ell}(S_f) + \sum_{\mu j} \sum_{\ell j} \epsilon_i^{\mu j} \sum_{f,g} D_j^{\mu\ell}(f,g)\, K_i^{\mu\ell}(S_f,S_g). \quad (11)$$

They have expanded this Hamiltonian up to order $\ell = 4$, calculated the free energy by a perturbation method, minimized the result with respect to the hexagonal strains, and transformed the equilibrium strains back to Cartesian symmetry.

The linear dilatation $\Delta\ell/\ell$ in a direction characterized by direction cosines $\beta_x\beta_y\beta_z$ may be derived from the equilibrium tensor strains S_{ij} by the following method: Consider lattice coordinates X_i distorted from their equilibrium values X_{io} by the strains S_{ij}. Then: $X_i = X_{io} + S_{ij}X_{jo}$ (assuming summation over repeated indicies). The direction cosine $\beta_i = X_{io}/r_o$ where r_o is the radial distance of the lattice point; thus:

$$X_i = r_o(\beta_i + S_{ij}\beta_j)$$

squaring and adding

$$r^2 = r_o^2(1 + 2S_{ij}\beta_i\beta_j)$$

or

$$r^2 - r_o^2 \approx 2r_o(r-r_o) = 2r_o^2 S_{ij}\beta_i\beta_j$$

therefore the linear strain

$$\frac{\Delta\ell}{\ell} = \frac{r-r_o}{r_o} = S_{ij}\beta_i\beta_j \,. \quad (12)$$

From the equilibrium strains and the above relation, the following expression was obtained by the Callens[1] for the magnetostriction of a hexagonal ferromagnet correct to fourth order in the magnetization direction cosines α; (Complete specification of hexagonal magnetostriction requires terms to $\ell = 6$ which results in a 19 constant expression.)

$$\frac{\Delta\ell}{\ell} = [\lambda_1^{\alpha,0} + \lambda_1^{\alpha,2}(\alpha_z^2 - \tfrac{1}{3}) + \lambda_1^{\alpha,4}(\alpha_z^4 - 6(\alpha_z^2 - \tfrac{1}{3}) - \tfrac{1}{5})](\beta_x^2 + \beta_y^2)$$

$$+ [\lambda_2^{\alpha,0} + \lambda_2^{\alpha,2}(\alpha_z^2 - \tfrac{1}{3}) + \lambda_2^{\alpha,4}(\alpha_z^4 - 6(\alpha_z^2 - \tfrac{1}{3}) - \tfrac{1}{5})]\beta_z^2$$

$$+\tfrac{1}{2}[\lambda^{\gamma,2} + \lambda_1^{\gamma,4}(\alpha_z^2 - \tfrac{1}{7})][(\alpha_x\beta_x - \alpha_y\beta_y)^2 - (\alpha_x\beta_y - \alpha_y\beta_x)^2]$$

$$+ \lambda^{\gamma,4}[\tfrac{1}{2}(\beta_x^2 - \beta_y^2)(\alpha_x^4 - 6\alpha_x^2\alpha_y^2 + \alpha_y^4) + 4\beta_x\beta_y\alpha_x\alpha_y(\alpha_y^2 - \alpha_x^2)]$$

$$+ 2[\lambda^{\epsilon,2} + \lambda^{\epsilon,4}(\alpha_z^2 - \tfrac{3}{7})][\alpha_x\beta_x + \alpha_y\beta_y]\alpha_z\beta_z \qquad (13)$$

The coordinate system used here is orthogonal with the x axis along the a($11\bar{2}0$) crystal axis, the y axis along the b($10\bar{1}0$) direction, and the z axis along the c(0001) crystal axis. This expression contains eleven magnetostriction constants λ, which are functions of the elastic constants c_{ij}, the one and two magneto-elastic coupling coefficients (except $\lambda_1^{\alpha,0}$ and $\lambda_2^{\alpha,0}$ which describe the exchange energy and thus contain only two ion terms) and expectation values of the spin operators.

---

[1]Callen, E. R., U.S. Naval Ordnance Laboratory, Silver Spring, Maryland. The fourth order magnetostriction terms. Private Communication. 1965.

These functions are given in reference 17 and only the form of $\lambda^{\gamma,2}$ will be given here as an example:

$$\lambda^{\gamma,2} = -\frac{B^{\alpha,2}}{c_{11}-c_{12}} < (S_f^{\xi})^2 - \frac{1}{3} S(S+1) >$$

$$+ \sum_{f,g} D^{\alpha,2}(f,g) < S_f^{\xi} S_g^{\xi} - \frac{1}{3} S_f \cdot S_g > \qquad (14)$$

The superscripts 0,2,4 denote ℓ, the order of the spin symmetry polynomials K appearing in the Hamiltonian and correspond to the order of the magnetization direction cosines in the coefficient of the magnetostriction constant. The superscripts α, γ, and ϵ denote the strain representation as shown in Figure 13. The α modes are a symmetry preserving stretching of a direction or directions (e.g. in cylindrical symmetry ($\ell = 2$), $\lambda_1^{\alpha,2}$ expands the basal plane diameter, $\lambda_2^{\alpha,2}$ expands the c axis). The γ modes correspond to a distortion of the basal plane from hexagonal to orthorhombic symmetry (from a circle to an ellipse in the second order $\ell = 2$), and the ϵ mode describes a shearing of the planes perpendicular to the c axis.

C. Mason's Expression for the Magnetostriction

At the start of this investigation, the above expression derived by Callen and Callen was not available and the interpretation used was that due to Mason (47). His expression for the magnetostriction of a hexagonal ferromagnet derived from the elastic enthalpy is:

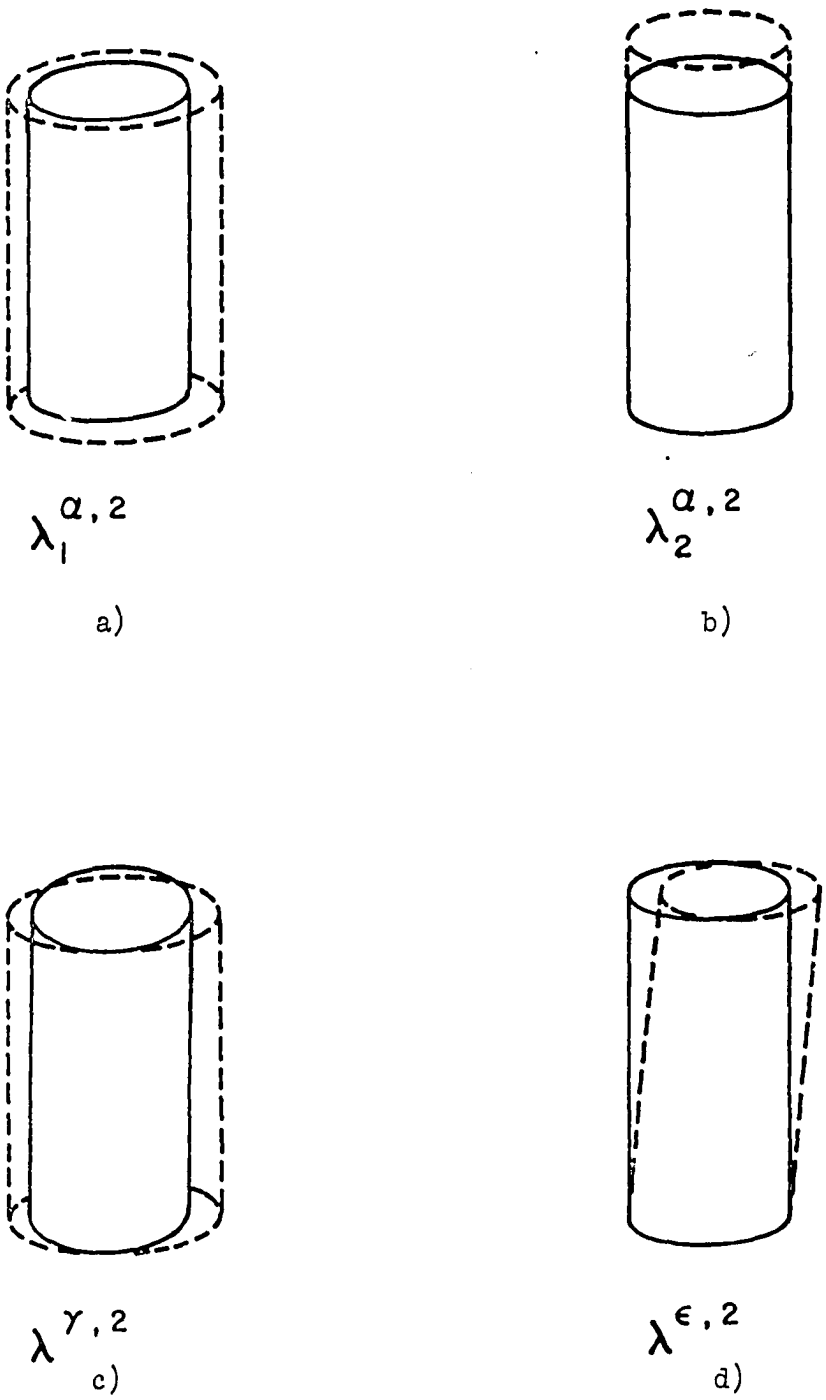

Figure 13. Magnetostrictive strain modes for a hexagonal crystal in the second order approximation. Modes (a) and (b) are symmetry preserving dilatations; (c) and (d) are distortion and shearing modes.

$$\frac{\Delta \ell}{\ell} = A\,[2\alpha_x\alpha_y\beta_x + (\alpha_x^2 - \alpha_y^2)\,\beta_y]^2 + B\,\alpha_z^2\,[(\alpha_x\beta_x + \alpha_y\beta_y)^2$$

$$- (\alpha_x\beta_y - \alpha_y\beta_x)^2] + C\,[(\alpha_x\beta_x + \alpha_y\beta_y)^2 - (\alpha_x\beta_y - \alpha_y\beta_x)^2]$$

$$+ D\,(1 - \alpha_z^2)(1 - \beta_z^2) + E\,\alpha_z^2\,\beta_z^2\,(1 - \alpha_z^2) + F\,\alpha_z^2\,(1 - \alpha_z^2)$$

$$+ G\,\beta_z^2\,(1 - \alpha_z^2) + H\,\alpha_z\beta_z\,(\alpha_z\beta_x + \alpha_y\beta_y) + I\,\alpha_z^2\beta_z$$

$$(\alpha_x\beta_x + \alpha_y\beta_y) + J\alpha_z^2\,(1 - \beta_z^2) + K\,\alpha_z^2\,\beta_z^2 \qquad (15)$$

This equation was originally derived for Co which has the z axis as the direction of spontaneous magnetization. Since Tb and Dy have an easy direction in the basal plane, it is necessary to retain the J and K terms which were dropped by Mason in his expression for Co. The eleven magnetostriction constants, A through K, are expressible in terms of the components of the magnetostriction energy tensors and the saturation magnetization (see Mason (48)). Mason's expression describes the magnetostriction to the same degree of symmetry as the Callen equation; however, the physical representation of the strain modes is not as apparent in Mason's expression since it is not derived directly by group theory.

D. Approximation Valid for Dy and Tb Below the Neel Temperature

In the antiferromagnetic and ferromagnetic temperature range, Dy and Tb possess quite large axial magnetic anisotropy energies constraining the magnetization to the basal plane. Flippen (27) has shown that fields

considerably in excess of normal laboratory fields would be necessary to produce significant rotation of the moment out of the basal plane (estimated to be of order 10^6 gauss). It is then not unrealistic to assume $\alpha_z = 0$ in the above magnetostriction expression. This assumption reduces Mason's eleven constant equation to one containing only four constants:

$$\left.\frac{\Delta \ell}{\ell}\right|_{\alpha_z=0} = A\,[2\alpha_x\alpha_y\beta_x + (\alpha_x^2 - \beta_y^2)\,\beta_y]^2$$
$$+C\,[(\alpha_x\beta_x + \alpha_y\beta_y)^2 - (\alpha_x\beta_y - \alpha_y\beta_x)^2]$$
$$+D\,(\beta_x^2 + \beta_y^2) + G\beta_z^2 \qquad (16)$$

An immediate comparison can be made between this simplified equation and Callen's form which for $\alpha_z = 0$ becomes:

$$\left.\frac{\Delta \ell}{\ell}\right|_{\alpha_z = 0} = [\lambda_1^{\alpha,0} - \tfrac{1}{3}\lambda_1^{\alpha,2} + \tfrac{9}{5}\lambda_1^{\alpha,4}]\,(\beta_x^2 + \beta_y^2)$$
$$+ [\lambda_2^{\alpha,0} - \tfrac{1}{3}\lambda_2^{\alpha,2} + \tfrac{9}{5}\lambda_2^{\alpha,4}]\,\beta_z^2$$
$$+ \tfrac{1}{2}[\lambda_2^{\gamma,2} - \tfrac{1}{7}\lambda_1^{\gamma,4}]\,[(\alpha_x\beta_x + \alpha_y\beta_y)^2 - (\alpha_x\beta_y - \alpha_y\beta_x)^2]$$
$$+ \lambda_2^{\gamma,4}\,[\tfrac{1}{2}(\beta_x^2 - \beta_y^2)(\alpha_x^4 - 6\alpha_x^2\alpha_y^2 + \alpha_y^4)$$
$$+ 4\beta_x\beta_y\alpha_x\alpha_y\,(\alpha_y^2 - \alpha_x^2)] \qquad (17)$$

It is thus apparent that the inseparable combinations in the first two brackets may be identified directly with D and G in Mason's formulation. The constants in the third bracket are equivalent to C. (The fourth

order correction $\frac{1}{7}\lambda_1^{\gamma,4}$ is apparently small and will be neglected as shown later.) The form of the α,β polynomial multiplying $\lambda_2^{\gamma,4}$ is not of the same form as that multiplying A in Mason's expression, although it can be obtained by antisymmetrizing Mason's polynomial. The result of this is merely a shift in the zero or reference level for the measurement of A. The relations between the two sets of constants are then:

$$\begin{aligned} A &= -\lambda_2^{\gamma,4} + A_{Sym.} \\ C &= \tfrac{1}{2}\left(\lambda^{\gamma,2} - \frac{1}{7}\lambda_1^{\gamma,4}\right) \\ D &= \lambda_1^{\alpha,0} - \frac{1}{3}\lambda_1^{\alpha,2} + \frac{9}{5}\lambda_1^{\alpha,4} \\ G &= \lambda_2^{\alpha,0} - \frac{1}{3}\lambda_2^{\alpha,2} + \frac{9}{5}\lambda_2^{\alpha,4} \quad . \end{aligned} \tag{18}$$

Equation 16 was chosen as the working expression for this investigation. The constants A, C, D, G appearing in the expression have been determined for Dy and Tb by methods discussed in a later section. The A is the only constant characteristic of hexagonal symmetry, the others correspond to cylindrical symmetry. D and G represent, respectively, an isotropic dilatation of the basal plane and a dilatation of the c-axis direction. C corresponds to a distortion of an assumed circular basal plane into an ellipse and A corresponds to a higher order distortion of hexagonal symmetry into orthorhombic symmetry. Note that the shearing ϵ strains of Equation 13 cannot be measured unless the magnetic moment

can be aligned out of the basal plane toward the c axis.

Equation 16 cannot be applied to magnetostriction in Er due to the high magnetic anisotropy as is discussed later.

VI. EXCHANGE MAGNETOSTRICTION IN A HELICAL ANTIFERROMAGNET

An examination of Equation 16 for the magnetostriction of a hexagonal ferromagnet indicates that no c-axis dilatation is expected from changes in the basal plane magnetization. This is seen by setting $\beta_2 = 1$, $\beta_1 = \beta_2 = 0$ in which case $\frac{\Delta \ell}{\ell} = G$. No dependence on the magnetic moment direction remains, thus the magnetostriction between any two measurement states will be zero. This is confirmed (except for small domain induced strains) in the experimental results on Dy and Tb in a later section.

In a helical antiferromagnet the situation is quite different and the field induced and spontaneous transitions to ferromagnetism are both accompanied by large c-axis magnetostriction. The origin of the anomalous behavior lies in the strain dependence of the exchange energy. The exchange energy is a function of the magnitude and angle between the spins. In a normal ferromagnet or antiferromagnet this angle remains fixed at zero or 180°. The process of magnetization, being one of domain rotation and expansion, does not alter the exchange integral (an exception occurs near the Curie temperature where the field induced enhancement of the saturation magnetization may be appreciable). Hence the strain dependence of the exchange energy is not manifested in an isothermal measurement on such a material.

In a helical antiferromagnet the situation is different, as the angle between the spins in neighboring hexagonal layers can be changed

drastically by the application of a field, as shown for progressively higher fields in Figure 14. H_k is the critical field required to perturb the helical structure and H_o is the field required for complete ferromagnetic alignment. The effects of the strain dependence of the exchange energy thus becomes apparent in a helical antiferromagnet. E. W. Lee (42) has calculated the expected results using the work of Yoshimori (67), Enz (25), Herpin et al. (33), and Nagamiya et al. (52) on the behavior of a helical spin structure in the presence of an applied field.

A brief review of Lee's results follow. The derivation applies only to high temperatures where the basal plane anisotropy energy is sufficiently small that the helical state is not distorted in zero applied field (e.g. Dy above 130°K). If the two exchange integrals J_1, J_2 appearing in Equation 3 are assumed to be strain dependent, the sum of the elastic and exchange energy may be represented as

$$E_m = \frac{1}{2} \frac{(c-c_o)^2}{c_o^2} E - M_S^2 \left[J_1(0) + \frac{dJ_1}{dc} (c-c_o) \right] \cos \theta$$
$$- M_S^2 \left[J_2(0) + \frac{dJ_2}{dc} (c-c_o) \right] \cos 2\theta \qquad (19)$$

where c_o is the equilibrium interlayer separation for $\theta = \pi/2$. E is a combination of elastic constants appropriate to the c-axis direction, $J(0)$ is the value of J for $c = c_o$ and M is the saturation magnetization. Minimizing this with respect to the c-axis dilatation, $\partial E/\partial c = 0$ gives

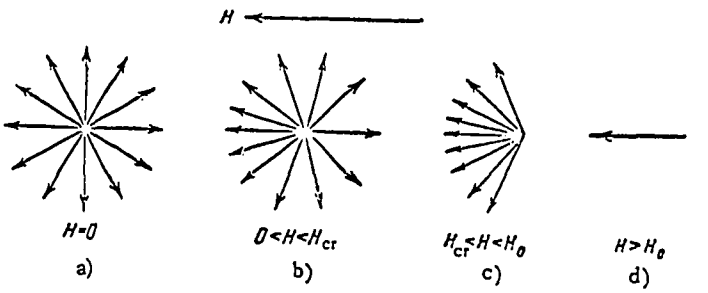

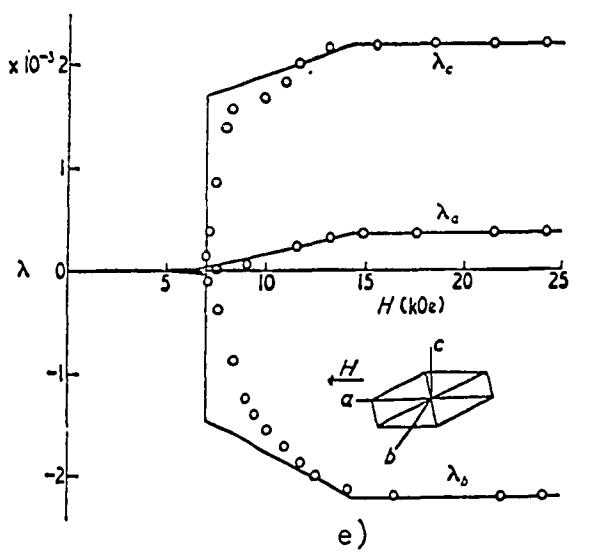

Figure 14. Field induced magnetic transitions in Dy.
a)- d) Helical magnetic states of Dy under the influence of progressively higher external fields.
e) Experimental data and theoretical fit for the magnetostriction of Dy at 144°K.

$$\frac{\Delta \ell}{\ell}\Big|_c = \frac{cM_s^2}{E}\left(\frac{dJ_1}{dc}\cos\theta + \frac{dJ_2}{dc}\cos 2\theta\right) \tag{20}$$

In the absence of an external field, $\theta = \alpha_o$, the equilibrium turn angle. In the presence of a filed θ varies from layer to layer due to the perturbed helical structure.

The strain can be calculated by introducing an appropriate average of the turn angles over the layers of the crystal.

$$\frac{\Delta \ell}{\ell}\Big|_c = \frac{cM_s^2}{E}\left[\frac{dJ_1}{dc} < \cos(\theta_n - \theta_{n-1}) >_{av} + \frac{dJ_2}{dc} < \cos(\theta_n - \theta_{n-2}) >\right] \tag{21}$$

Enz (25) and others have shown that the turn angles in the presence of a field may be found by solving the variational problem

$$\delta \int E_{ex} - M_s H \cos\theta(z)\, dz = 0 \tag{22}$$

where the exchange energy of the n'th layer is

$$E_{ex} = -M_s^2 [J_1 \cos(\theta_n - \theta_{n-1}) + J_2 \cos(\theta_n - \theta_{n-2})] . \tag{23}$$

The solution for all field strengths has not been found, but low and high field limits are available. In low fields $H < H_{critical}$ the helix is only slightly perturbed and the turn angle of the nth layer is represented by $\theta_n = n\alpha_o + \epsilon_n + \theta'$ where (24)

$$\epsilon_n = A_1 \sin(n\alpha_o + \theta') + A_2 \sin 2(n\alpha_o + \theta')$$

and A_1 and A_2 are functions of J_1, J_2, H, M_s, and α_o (42, 52). The angle θ' in the above equation is not significant and is dropped by Lee.

The low field average of θ_n is then found to be $\cos \theta_n = -\frac{1}{2} A_1$ and the average over-all layers of the crystal is

$$\begin{aligned} \langle \cos (\theta_n - \theta_{n-1}) \rangle_{av} &= \cos \alpha_o \left[1 - \tfrac{1}{2} A_1^2 (1 - \cos \alpha_o)\right] \\ \langle \cos (\theta_n - \theta_{n-2}) \rangle_{av} &= \cos 2\alpha_o \left[1 - \tfrac{1}{2} A_1^2 (1 - \cos 2\alpha_o)\right] \end{aligned} \tag{25}$$

A_1 is proportional to H_{appl} and is thus zero in the initial state.

The resulting low field c-axis strain found from substituting the above averages in Equation 21 and subtracting the initial strain is:

$$\left.\frac{\Delta \ell}{\ell}\right|_{c_{ex}}^{\text{low field}} = -\tfrac{1}{2} \lambda_{cs} A_1^2 \tag{26}$$

where

$$\lambda_{cs} = \frac{cM_s^2}{2E} \left[\frac{dJ_1}{dc} \cos \alpha_o (1 - \cos \alpha_o) + \frac{dJ_2}{dc} \cos 2\alpha_o (1 - \cos 2\alpha_o)\right].$$

This low field magnetostriction was found to be quite small in Dy. However, at higher fields, a discontinuity in the magnetization of the helical structure occurs at a critical field H_k given by

$$H_k = -2M_s J_2 (1 - \cos 2\alpha_o)^2 \tag{27}$$

with large magnetostriction resulting. In the absence of a basal plane anisotropy energy complete ferromagnetic saturation is achieved in a field $H_o = 2H_k$. In a highly anisotropic material such as Dy (below 100°K) the critical field expression is modified somewhat:

$$H_k = -2M_s J_2 (1 - \cos 2\alpha_o)^2 - K_6^6 - E_m \tag{28}$$

where K_6^6 is the basal plane anisotropy energy and E_m is the magnetostrictive energy. In such a material saturation is reached essentially

at H_k since the total energy above H_k is abruptly lowered by E_m for magnetization in the hard directions and by $E_m + K_6^6$ for magnetizations in the easy directions. Above 130°K in Dy, and in the helical state of Tb, K_6^6 and E_m are small and for values of H between H_{cr} and $2H_{cr}$ the turn angle is found to have an oscillatory behavior about the field direction. The moment of the nth layer makes an angle θ_n with the field given by (Enz (25))

$$\theta_n = B_1 \sin k z_n \qquad \text{(z is the coordinate along the c axis).} \tag{29}$$

B_1^2 as given by Enz is:

$$B_1^2 = \frac{4}{3} \left[\left(\frac{c_o}{\alpha_o}\right)^2 \left(\frac{-M_s c_o^4 J_2}{H}\right)^{\frac{1}{2}} - 1 \right] \tag{30}$$

and $k^4 = - H/M_s \left(\frac{c_o}{\alpha_o}\right)^4 J_2$.

The average of $\cos \theta_n$ over all layers is then:

$$\langle \cos \theta_n \rangle_{av} = 1 - \tfrac{1}{4} B_1^2 . \tag{31}$$

Substitution of the result into Equation 21 gives after subtraction of the initial strain,

$$\left.\frac{\Delta \ell}{\ell}\right|_{c_{ex}}^{\text{high field}} = \lambda_{cs} \left(1 - \tfrac{1}{2} B_1^2\right) \tag{32}$$

where

$$\lambda_{cs} = \frac{c M_s^2}{E} \left[\frac{dJ_1}{dc} \cos \alpha_o \left(1 - \cos \alpha_o\right) + \frac{dJ_2}{dc} \cos 2\alpha_o \left(1 - \cos 2\alpha_o\right) \right] .$$

The significant result is that in both low and high field limits a

c-axis magnetostriction occurs in a helical antiferromagnet in contrast to the behavior of a normal ferromagnetic or antiferromagnetic material. Experimentally (see Dy results) this c-axis strain is also accompanied by a large basal plane strain, although this cannot be deduced from the theoretical arguments presented above. Lee has assumed that the basal plane strain may be represented by

$$\frac{\Delta \ell}{\ell}\Big|_{b,p} = \rho \frac{\Delta \ell}{\ell}\Big|_{c} \tag{33}$$

where ρ is the magnetic equivalent of the Poisson ratio. The resulting over-all strain produced by the combination of the anisotropic magnetostriction discussed in the previous section and the exchange magnetostriction presented here may be represented (e.g. for H along the a axis):

$$\begin{aligned} &\text{a-axis strain} && \frac{\Delta \ell}{\ell}\Big|_{a}^{a} = C - \rho \frac{\Delta \ell}{\ell}\Big|_{c_{ex}} \\ &\text{b-axis strain} && \frac{\Delta \ell}{\ell}\Big|_{b}^{a} = -C - \rho \frac{\Delta \ell}{\ell}\Big|_{c_{ex}} \\ &\text{c-axis strain} && \frac{\Delta \ell}{\ell}\Big|_{c}^{a} = \frac{\Delta \ell}{\ell}\Big|_{c_{ex}} \end{aligned} \tag{34}$$

C is the second order anisotropic magnetostriction constant and $\frac{\Delta \ell}{\ell}\Big|_{c_{ex}}$ is the c-axis exchange magnetostriction. Lee has calculated the theoretical helical magnetostriction curve for Dy using the above expressions and the exchange magnetostriction results outlined in this section. He has compared the results to this author's experimental data

on the field dependence of the magnetostriction of Dy at 144°K (45) corrected for the forced magnetostriction and demagnetizing fields. The results are shown in Figure 14. The value of C used was 1.3×10^{-3}, of λ_{cs} was 2.2×10^{-3} and of ρ was 0.43.

VII. MEASUREMENTS OF THE MAGNETOSTRICTION CONSTANTS

Equation 16 represents the magnetostriction of a hexagonal ferromagnet under the assumption that the magnetic moment is constrained to the basal plane. Strictly speaking it pertains only to a single domain; hence, if bulk measurements are to be made, the crystal must be magnetically saturated. Only under this constant moment condition may the constants be unambiguously determined.

A. Anisotropic Magnetostriction Constants A and C

The constants A and C may be determined as follows: a basal plane sample is rotated in a saturating field applied parallel to the sample plane, and the linear strain along the a or b axis is measured as a function of the angle between the magnetization and the easy magnetic axis direction.

The following equations are obtained for the a- and b-axis strains from Equation 16:

a axis $(\beta_x = 1, \beta_y = \beta_z = 0)$: $\left[\frac{\Delta \ell}{\ell}\right]_a = A(4\alpha_x^2\alpha_y^2) + C(\alpha_x^2-\alpha_y^2) + D$ (35a)

b axis $(\beta_x = 0, \beta_y = 1, \beta_z = 0)$: $\left[\frac{\Delta \ell}{\ell}\right]_b = A(\alpha_x^2-\alpha_y^2)^2 + C(\alpha_y^2-\alpha_x^2) + D$ (35b)

1. Dysprosium

The a axis of dysprosium is the easy magnetic axis and is thus taken as the reference state. The a- and b-axis strains with the magnetization

in this direction ($\alpha_x = 1$, $\alpha_y = 0$) are:

$$\text{a axis:} \quad \left[\frac{\Delta\ell}{\ell}\right]_a^a = C + D \tag{36a}$$

$$\text{b axis:} \quad \left[\frac{\Delta\ell}{\ell}\right]_b^a = A - C + D \tag{36b}$$

In this notation the superscript indicates the magnetization direction and the subscript the measuring or gage direction.

The a- and b-axis strains between the above reference state and any other state where the magnetic moment makes an angle θ_a with the a axis may be written ($\alpha_x = \cos\theta_a$, $\alpha_y = \sin\theta_a$):

$$\text{a axis:} \quad \left[\frac{\Delta\ell}{\ell}\right]_a^{\theta_a} - \left[\frac{\Delta\ell}{\ell}\right]_a^{\theta_a=0} = \left[\frac{\Delta\ell}{\ell}\right]_a^{\theta'_a} = A \sin^2 2\theta'_a - 2C \sin^2 \theta'_a \tag{37a}$$

$$\text{b axis:} \quad \left[\frac{\Delta\ell}{\ell}\right]_b^{\theta_a} - \left[\frac{\Delta\ell}{\ell}\right]_b^{\theta_a=0} = \left[\frac{\Delta\ell}{\ell}\right]_b^{\theta'_a} = -A \sin^2 2\theta'_a + 2C \sin^2 \theta'_a \tag{37b}$$

Here θ' indicates the strain of the reference state has been subtracted.

2. Terbium

The b axis of Terbium is the easy magnetic axis and the reference strains with the magnetic moment along the b axis ($\alpha_x = 0$, $\alpha_y = 1$) are:

$$\text{a axis:} \quad \left.\frac{\Delta\ell}{\ell}\right|_a^b = - C + D \tag{38a}$$

$$\text{b axis:} \quad \left.\frac{\Delta\ell}{\ell}\right|_b^b = + A + C + D \tag{38b}$$

The a- and b- axis strains between this reference state and any other state where the magnetization makes an angle θ_b with the b axis may be written ($\alpha_x = \sin\theta_b$, $\alpha_y = \cos\theta_b$):

$$\text{a axis:}\quad \left[\frac{\Delta\ell}{\ell}\right]_a^{\theta_b} - \left[\frac{\Delta\ell}{\ell}\right]_a^{\theta_b=0} \equiv \left[\frac{\Delta\ell}{\ell}\right]_a^{\theta'_b} = A \sin^2 2\theta'_b + 2C \sin^2 \theta'_b \qquad (39a)$$

$$\text{b axis:}\quad \left[\frac{\Delta\ell}{\ell}\right]_b^{\theta_b} - \left[\frac{\Delta\ell}{\ell}\right]_b^{\theta_b=0} \equiv \left[\frac{\Delta\ell}{\ell}\right]_a^{\theta'_b} = -A \sin^2 2\theta'_b - 2C \sin^2 \theta \qquad (39b)$$

Equations 37 and 39 form the basic equations for the determination of the constants A and C in dysprosium and terbium respectively. The procedure followed in this investigation was to measure the a- or b-axis strains at $\theta = 60^\circ$ (adjoining easy axis) and at $\theta = 90^\circ$ where respectively:

Dysprosium	Terbium
$\left[\frac{\Delta\ell}{\ell}\right]_{a,b}^{\theta'_a=60^\circ} = \frac{3}{4}\left[\mp A \mp 2C\right]$	$\left[\frac{\Delta\ell}{\ell}\right]_{a,b}^{\theta'_b=60^\circ} = \pm\frac{3}{4}\left[A + 2C\right]$
$\left[\frac{\Delta\ell}{\ell}\right]_{a,b}^{\theta'_a=90^\circ} = \mp 2C$	$\left[\frac{\Delta\ell}{\ell}\right]_{a,b}^{\theta'_b=90^\circ} = \pm 2C$

(40)

The upper sign is for the a-axis strain measurement, the lower for the b-axis measurement. From these relations and the 60° and 90° strains, A and C were calculated.

As stated above, the fourth order constant A is the only one characteristic of hexagonal symmetry. The importance of using at least a fourth order theory in Tb and Dy as opposed to the second order theory used with Co (10) and Gd (2,11) is illustrated in Figure 15. The experimental data for the b-axis strain versus angle of the 30 kOe applied field in the basal plane of Tb at 99.9°K are shown (data points and solid curve). This can be compared to the results of the fourth order theory (dash line) fitted at $\theta'_b = 60^\circ$ and 90°; and to the results

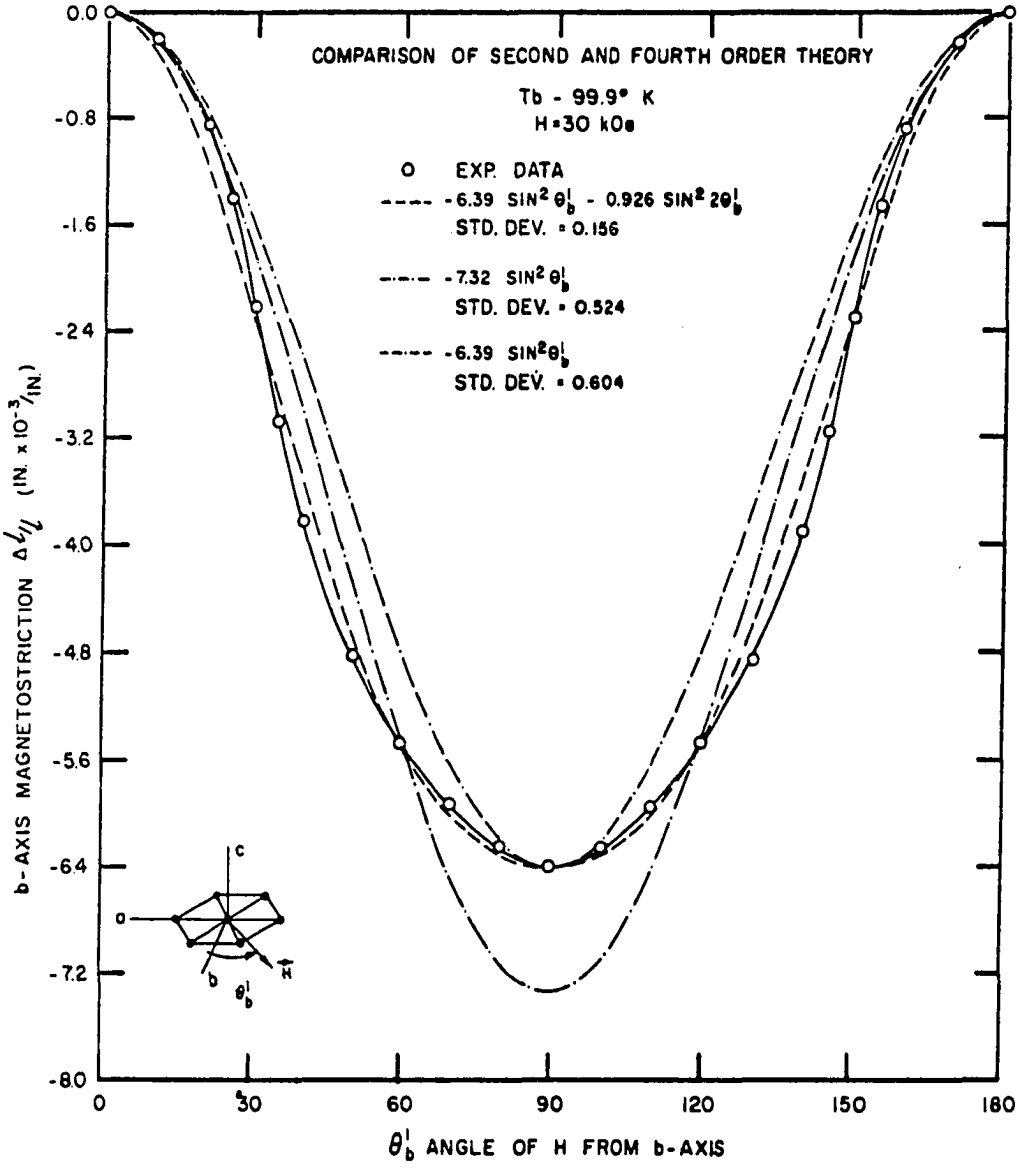

Figure 15. Comparison of second and fourth order theoretical fit to the field rotation magnetostriction data of Tb at 99.9°K.

of a second order theory ($-2C \sin^2 \theta'_b$) fitted at $\theta'_b = 60^\circ$ (dash-dot line) and at $\theta'_b = 90^\circ$ (dash-dash-dot line). The standard deviations of the various curves from the data points are indicated. From this, it is readily apparent that the inclusion of fourth order term $A \sin^2 2\theta$ improves the fit considerably.

Figures 16 and 17 show representative curves of the a- and b-axis strains versus angle θ'_a of applied field relative to the a axis in the basal plane of Dy. The result of the fourth order theory fit are also shown for three temperatures. Similar data for Tb are shown in Figures 18 and 19 for the a- and b-axis strain versus applied field angle θ'_b relative to the b axis.

Considerable "squaring off" of the experimental rotation curves is evident at temperatures well below the Curie temperature, especially in dysprosium. This is due to the large six fold basal plane anisotropy which prevents the magnetic moment from closely aligning with the magnetic field applied in hard magnetic direction. Indeed, in Dy at very low temperatures the magnetization remains essentially along the easy axis as the magnetic field angle θ changes from 0° to 30°, and then abruptly jumps to the next easy axis and remains there as θ goes from 30° to 90°, etc. The result is the sharp change in strain observed at 30° and 150°, with only a small variation for intermediate angles. The magnetostriction Equations 37 and 39 involve the angle of the magnetic moment, and the

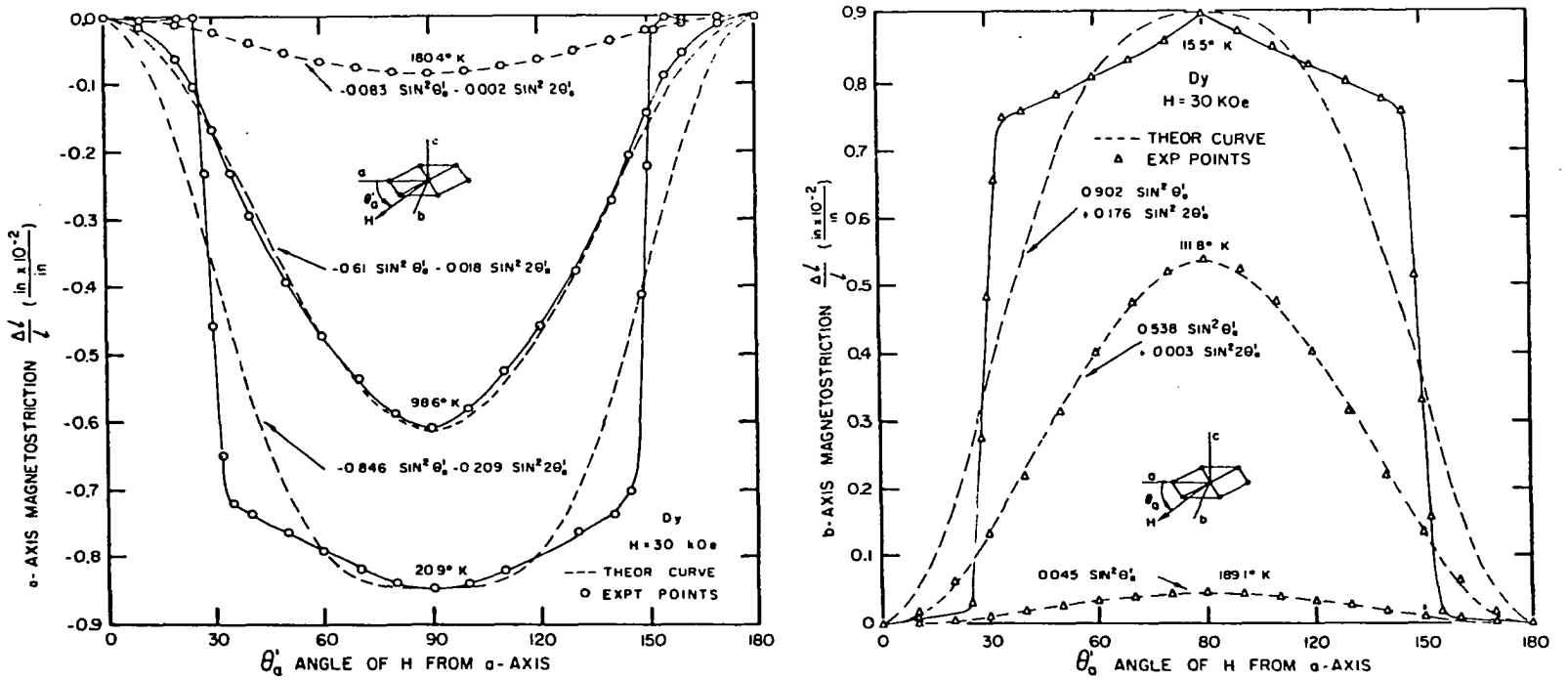

Figure 16. Dy a- and b-axis magnetostriction as a function of applied field angle, θ'_a, relative to the a axis. The 30 kOe field was applied in the basal plane. The dash curve shows the result of the fourth order theoretical fit.

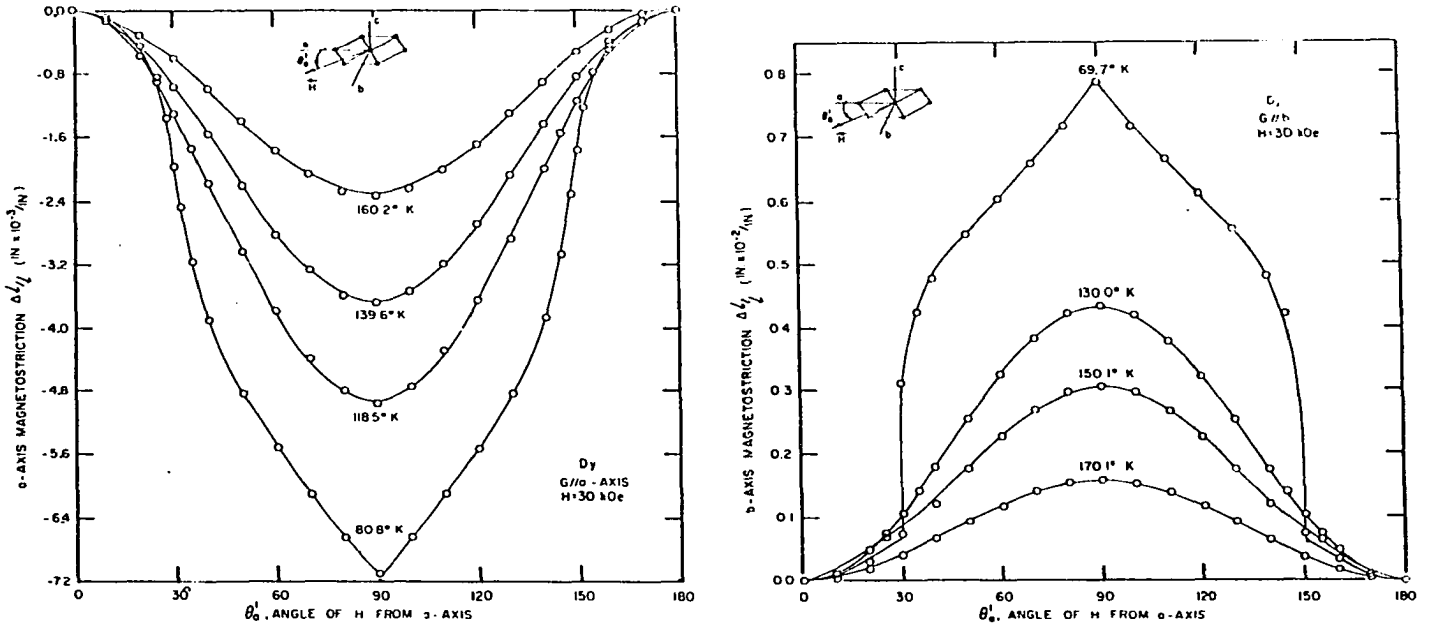

Figure 17. Dy a- and b-axis magnetostriction as a function of applied field angle, θ'_a, relative to the a axis. The 30 kOe field was applied in the basal plane.

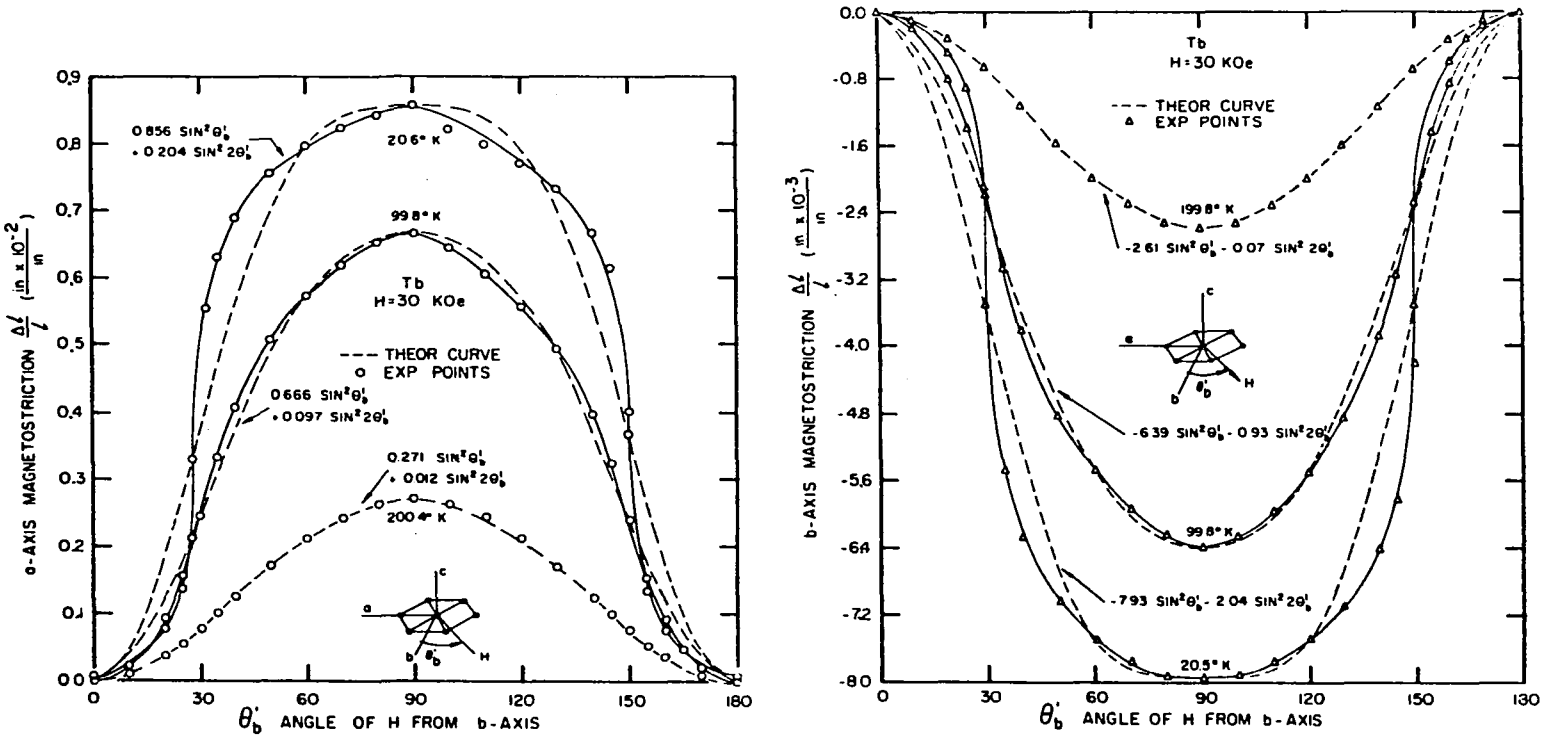

Figure 18. Tb a- and b-axis magnetostriction as a function of applied field angle, θ'_b, relative to b axis. The 30 kOe field was applied in the basal plane. The dash curve shows the result of the fourth theoretical fit.

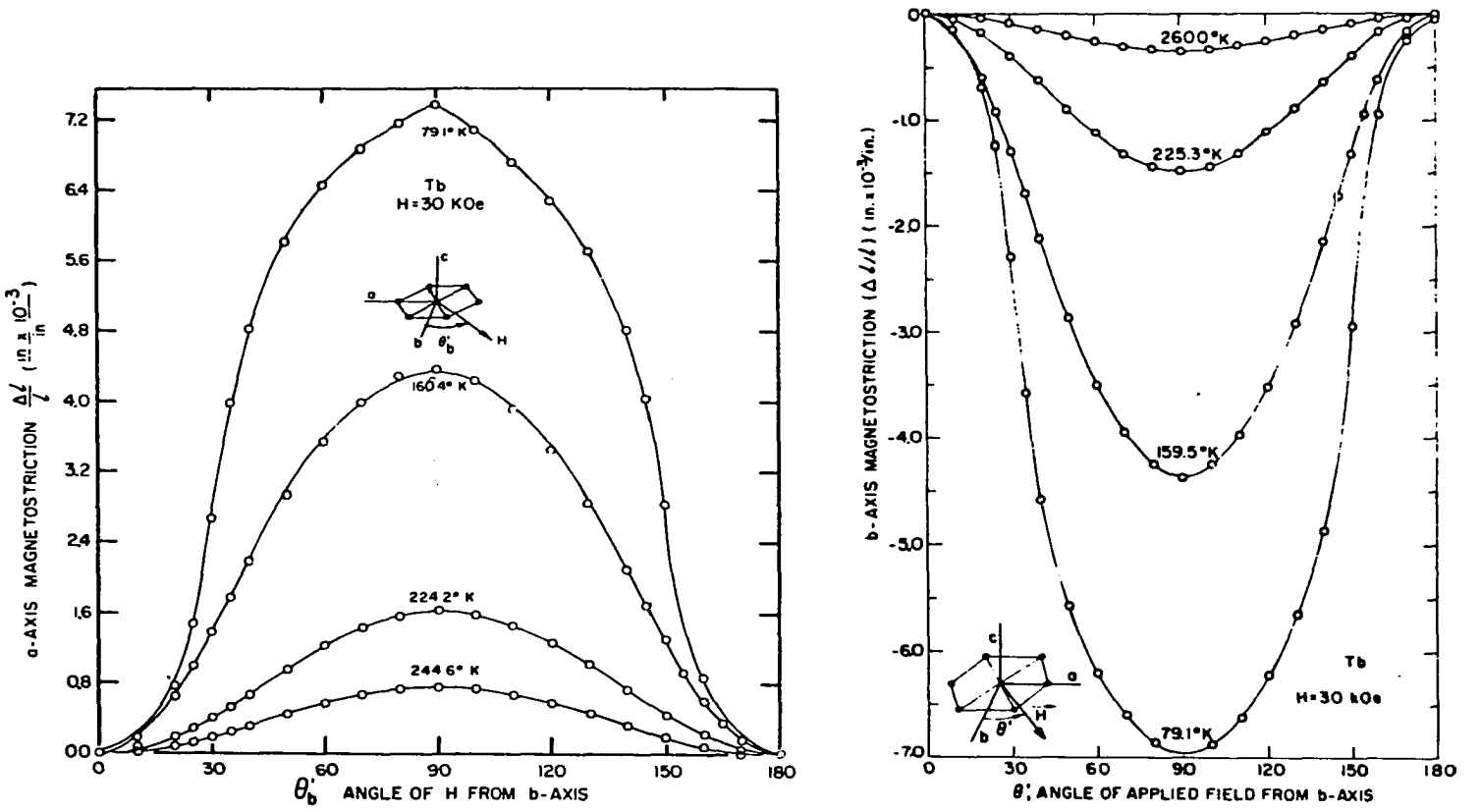

Figure 19. Tb a- and b-axis magnetostriction as a function of applied field angle, θ_b', relative to the b axis. The 30 kOe field was applied in the basal plane.

substitution of the applied field angle can produce errors in the determination of the constants A and C at low temperatures principally in Dy. These effects are considered in a later section.

B. Isotropic Constants D and G

The remaining magnetostriction constants D and G are not dependent upon the magnetic field direction in the basal plane. These constants were determined by measuring the strain as a function of temperature in a saturating applied field and subtracting the thermal expansion extrapolated from above the Néel temperature. The difference is the magnetostriction contribution. It is to be noted that the thermal expansion cannot be measured below the Néel temperature as here the magnetostrain is the dominant effect and cannot be isolated from the thermal strain. Measurements of the strain below the Curie temperature in the absence of an applied field are subject to the same hysteresis effects and lack of reproducibility mentioned in the introduction with respect to the demagnetized state. Hence the need to extrapolate the expected thermal expansion from the paramagnetic region.

1. Extrapolation of the thermal expansion

This extrapolation of the thermal strain was done by measuring the linear thermal expansion coefficients for the a, b, and c axes in a limited zone around 300°K (350°K for Tb) and using the Grüneisen expression

$$\frac{\partial V}{\partial T} = K\gamma C_v(T) \qquad (41)$$

to obtain the lower temperature dependence of these expansion coefficients. C_v is the specific heat from the Debye theory and K and γ are, respectively, the isothermal compressibility and the Grüneisen constant, both of which were assumed independent of temperature. The Grüneisen relation is actually a bulk relationship and its application to single crystal properties is dubious. To test this and the other assumptions, the method was applied to Er shown in Figure 20, whose thermal expansion exhibits normal behavior down to 85°K, its first magnetic transition temperature. The procedure was as follows: From the measured thermal expansion coefficients α at the reference temperature, 300°K, the relation

$$\frac{\Delta \ell}{\ell}(T) = \int_{T_{ref}}^{T} \alpha(t)\, dT = \frac{\alpha(T_{ref})}{C_v(T_{ref})} \int_{T_{ref}}^{T} C_v(T) dT \qquad (42)$$

was used to evaluate the linear strain as a function of temperature. The calculated results are compared to the experimental data in the figure. The Debye specific heat tables of Landolt and Bornstein (41) were fitted to least squares polynomials using several regions, and these polynomials were used in the calculation of the integral. The Debye temperature, obtained from sound velocity measurements (61), of Er is 192°K, of Tb is 175°K, and of Dy is 182°K.

As the figure for Er shows, this extrapolation method is far from exact. The justification for its use lies in the fact that the errors involved are only a few per cent of the total effect and are within the

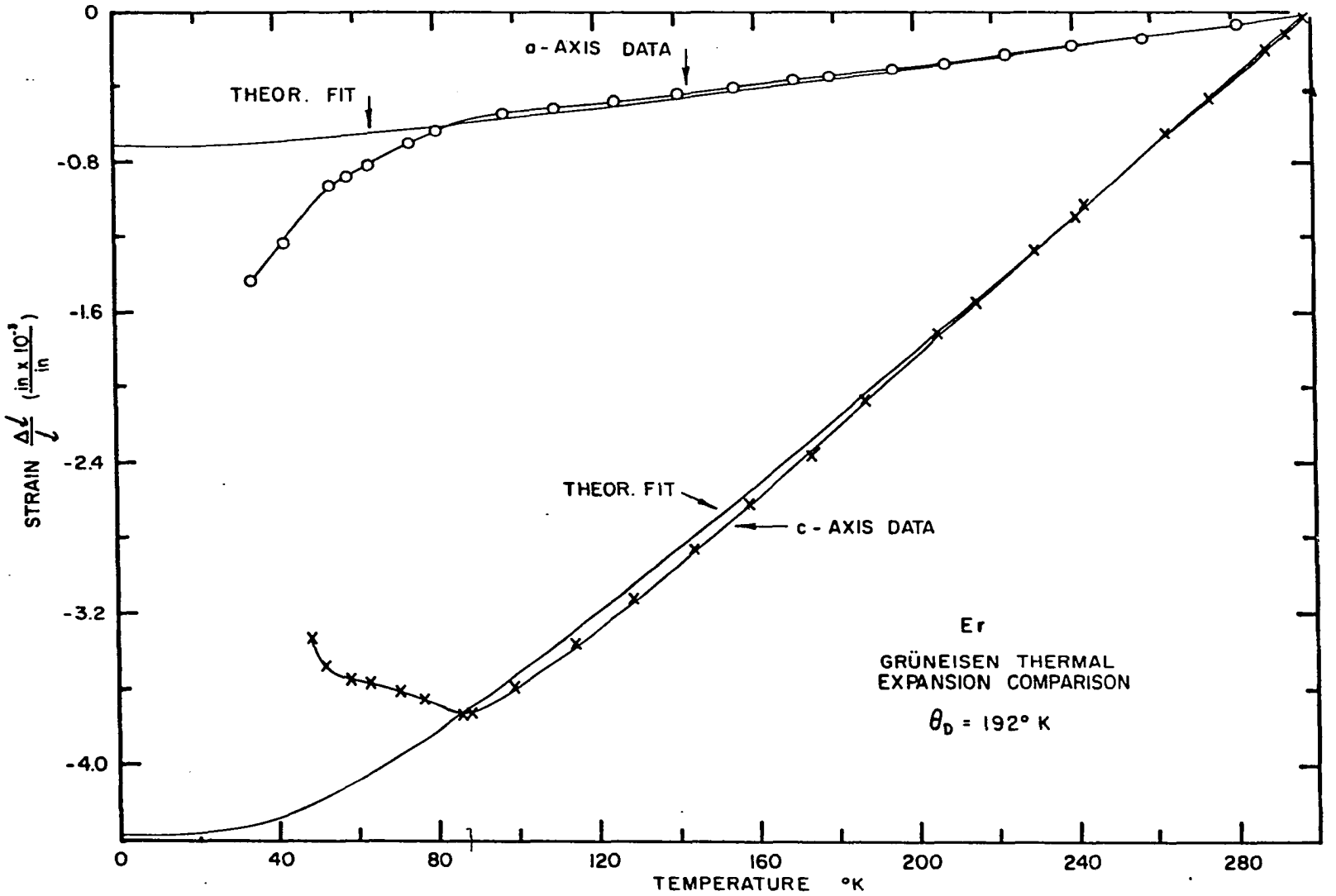

Figure 20. Comparison of thermal expansion fit using Grüneisen relation to experimental data in Er.

limits of other experimental errors.

2. Determination of constants D and G from strain versus temperature measurements

a. Results for dysprosium The easy magnetic direction of Dy is the a axis. It is thus appropriate to apply a saturating field in this direction and measure the strains in the a-, b-, and c-axis direction. With the field along the a axis ($\alpha_x = 1$, $\alpha_y = 0$) Equation 16 becomes:

$$\frac{\Delta \ell}{\ell}\Big|^{a} = A\beta_y^2 + C\,[\beta_x^2 - \beta_y^2] + D(1 - \beta_z^2) + G\beta_z^2 \,.$$

The strains found by subtraction of the extrapolated thermal expansion from the a-, b-, and c-axis strains measured in an applied field satisfy the following relations:

a axis ($\beta_x = 1$, $\beta_y = \beta_z = 0$): $\left[\frac{\Delta \ell}{\ell}\right]_a^a - \left[\frac{\Delta \ell}{\ell}\right]_a^o = C + D$ (43a)

b axis ($\beta_x = 0$, $\beta_y = 1$, $\beta_z = 0$): $\left[\frac{\Delta \ell}{\ell}\right]_b^a - \left[\frac{\Delta \ell}{\ell}\right]_b^o = A - C + D$ (43b)

c axis ($\beta_x = \beta_y = 0$, $\beta_z = 1$): $\left[\frac{\Delta \ell}{\ell}\right]_c^a - \left[\frac{\Delta \ell}{\ell}\right]_c^o = G$ (43c)

Here the superscripts indicate the field direction and the subscripts the measurement direction. From Equation 43a and the values of C obtained from rotation measurements, the constant D was calculated. Equation 43c provided the remaining constant G directly. It should be remarked that it is not possible to obtain all four constants by linear strain measurements as outlined above with the magnetic moment remaining in the easy direction. This is seen by assuming a fourth measuring direction

with cosines u, v, w and inspecting the determinant of the coefficients of A, C, D, and G from Equations 43a, 43b, and 43c and the fourth direction equation. This determinant is seen to be zero. The constant A which represents departures from cylindrical symmetry in the magnetoelastic energy cannot be isolated unless the magnetic moment is rotated out of the easy magnetic direction. This resolves some of the discrepancies between the results presented here and those obtained by Darnell (19) in the absence of an applied field.

Figure 21 shows the temperature dependence of the a-, b-, and c-axis strains in both zero field and in a 30 kOe field applied along the a axis of Dy. In a field the c axis is observed to expand with decreasing temperature in the (zero field) antiferromagnetic range as discussed above while showing a saturation effect with a decreasing strain at lower temperatures characteristic of the thermal expansion. This is in accord with the negligible c-axis magnetostriction expected well below the Curie temperature for a magnetic moment constrained to the basal plane. The b-axis magnetostrain exhibits a large contraction with decreasing temperatures amounting to 0.8 per cent at 20°K after subtracting an extrapolated value of the thermal expansion. The a-axis magnetostriction reverses slope just below the Néel temperature. This is presumably due to the change in interlayer exchange energy resulting from the variation in the helical turn angle.

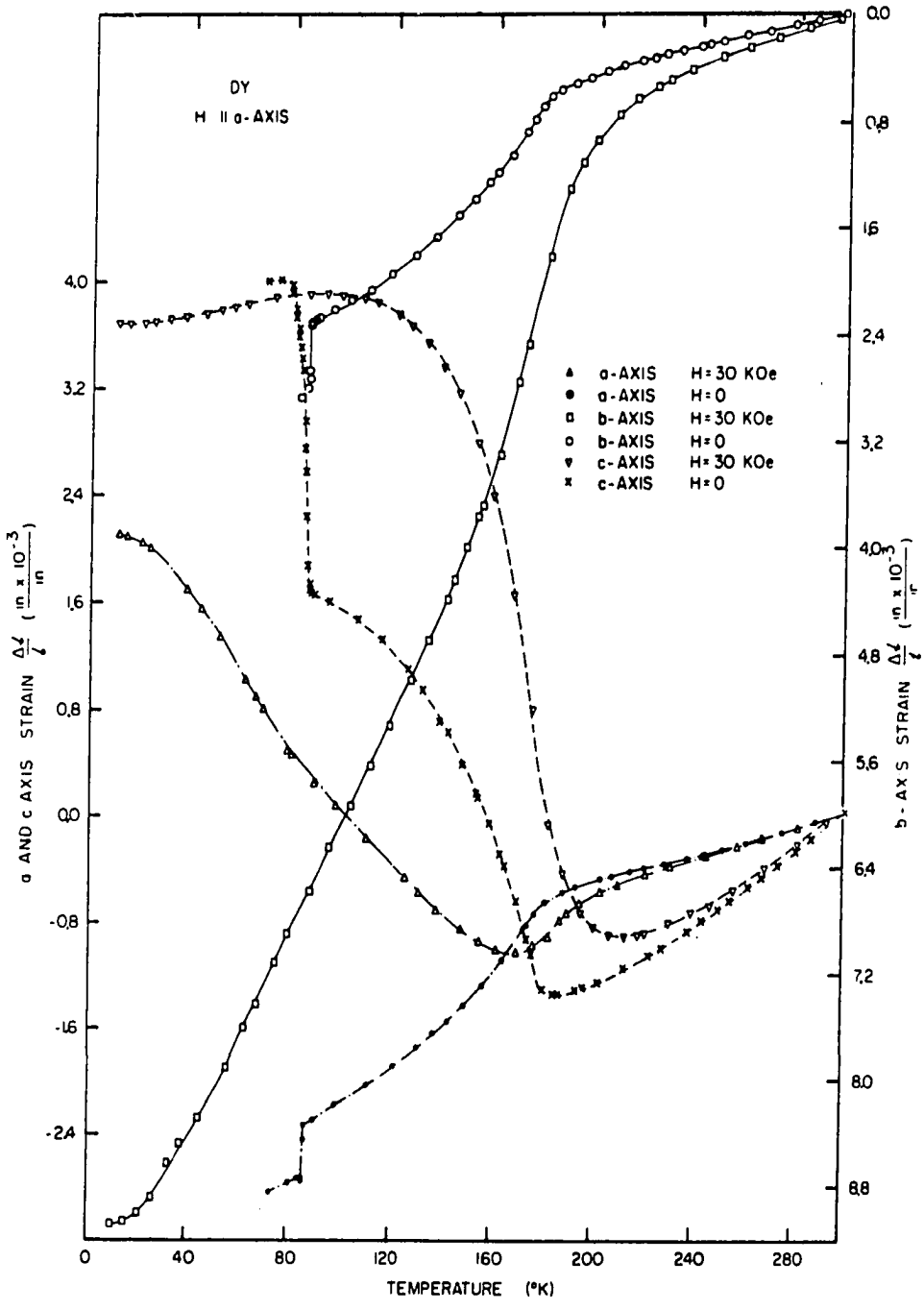

Figure 21. The a-, b-, and c-axis strain of Dy as a function of temperature in zero field and in a 30 kOe field applied along the a axis. The large discontinuities in the zero field curves at 85°K are the result of an orthorhombic distortion of the lattice at the ordering temperature.

The zero applied field strain curves are observed to have discontinuities at the Curie temperature, 87°K. This is an agreement with the change in crystal structure from hexagonal to orthorhombic at the ordering temperature as observed by Darnell (19) in X-ray studies on Dy. His results indicate a contraction, $\Delta\ell/\ell = -4.52\times10^{-3}$, in the b axis with a correspondingly smaller expansion, $\Delta\ell/\ell = 2.79\times10^{-3}$, of the a axis in the unit cell. In the macroscopic average results reported here, the a axis was also observed to contract due to the component of the large contraction along the adjoining b axis. The zero field measurements were not continued below 80°K due to hysteresis effects encountered below the Curie temperature as mentioned above.

Thermal hysteresis amounting to several degrees was noted in the 87°K transition temperature both in these zero field strain measurements and in measurements of the resitivity (34) and other transport properties. The antiferro-ferromagnetic transition always occurs at a lower temperature in cooling runs than in warming runs. A possible explanation lies in the effect of the large orthorhombic distortion on the anisotropy energy. As the crystal is cooled, the rapidly increasing basal plane anisotropy overcomes the helical exchange energy at the ferromagnetic transition temperature, producing the observed distortion.

Once in the ferromagnetic state, the anisotropy field is changed to one characteristic of the orthorhombic cell instead of the original

hexagonal cell. This means that the reverse (ferro to antiferro) transition can take place at a different temperature due to the new energy balance. The result in Dy is that, on warming the specimen, the orthorhombic anisotropy energy maintains the ferromagnetic alignment against the exchange forces to a higher temperature than is possible in the reverse process.

Figure 22 shows the temperature dependence of the constants A, C, D, and G. C was obtained from the rotation measurements as described and D and G were obtained by subtracting from the magnetostriction curves of Figure 21 the extrapolation of the linear region of the thermal expansion curve from far above the Néel temperature. The constants as shown apply to a 30 kOe applied field. No attempt was made to extrapolate values of the constants to zero applied field (or more properly, zero internal field) for two reasons: first, some error is inherent in the values of C at low temperatures due to the unknown discrepancy between the angles of the magnetization and applied magnetic field, and second, extrapolation to zero of the field dependence of C would produce an unrealistically large correction due to the lack of saturation. The differences between the values of C obtained from a- and b-axis measurements shown in the figure are ascribed to nonlinear behavior of the strain gages at low temperatures and strains approaching $\pm$ 1%.

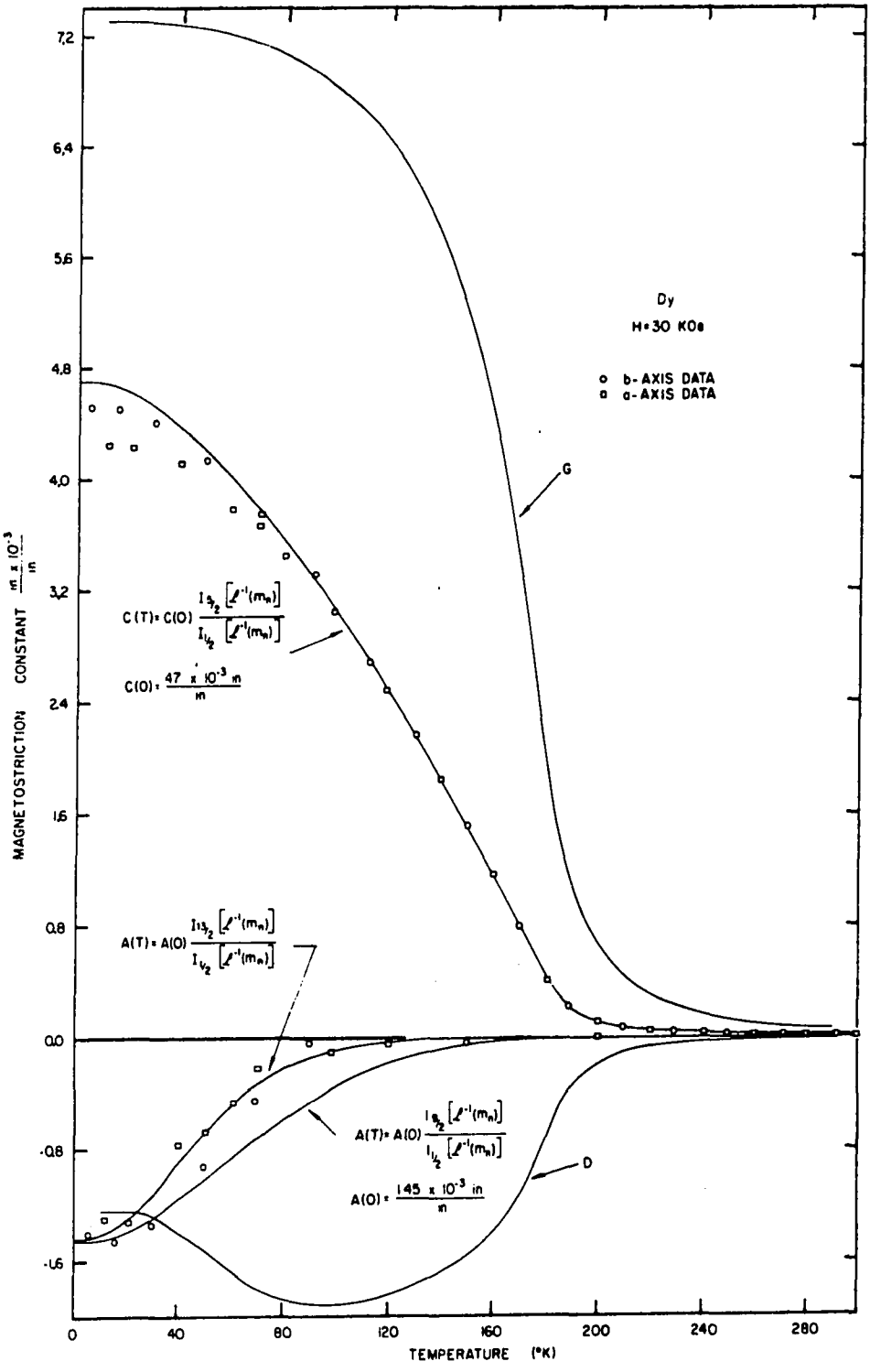

Figure 22. Magnetostriction constants A, C, D, and G of Dy at 30 kOe applied field. The theoretical expressions for the anisotropic constants A and C are shown along with the experimental data obtained from the a- and b-axis field rotation measurements.

The solid line relationships shown for C and A are the result of a theory by Callen and Callen (14, 15) which relates the magnetostriction constants to the magnetic moment. Using the one ion term in the internal field Hamiltonian exhibited in Equation 11 they have found that the temperature dependence of the related magnetostriction constant is represented by

$$\frac{\Delta \ell}{\ell}(T) = \frac{\Delta \ell}{\ell}(T=0)\,\frac{I_{\ell+\frac{1}{2}}\left[L^{-1}(M_n)\right]}{I_{\frac{1}{2}}\left[L^{-1}(M_n)\right]} \qquad (44)$$

where I is a modified Bessel function of the first kind, L^{-1} is the inverse of the Langevin function and $M_n = \frac{M(T)}{M(T=0)}$ is the reduced magnetization. The subscript ℓ again denotes the degree of the symmetry polynomial in the Hamiltonian and corresponds to the degree of the magnetization direction cosines appearing in the magnetostriction expression. The magnetostriction constant C represents terms of second degree ($\ell = 2$), while the constant A represents terms of fourth degree ($\ell = 4$). Using the Dy magnetic moment data of Behrendt (4) and Jew (34), the Langevin function was inverted using an iterative procedure on the Iowa State IBM 7074 computer and the ratio of the Bessel functions calculated from their closed form expressions. The curve calculated for $C(T) = C(T=0)\, I_{\frac{5}{2}}(L^{-1}(M_n))/I_{\frac{1}{2}}(L^{-1}(M_n))$ using $C(T=0) = 4.7\times10^{-3}$ is shown in Figure 22.

The data points for the constant A in the figure were obtained from Equations 37a,b using the experimental strains measured at $\theta = 60^{\circ}$ and the values of C taken from the above theoretical curve. Use of the experimental values of C directly for calculating A produced unrealistically large values due to the angle errors resulting from the high basal plane anisotropy mentioned above. In general, values of A shown in the figure should be viewed only qualitatively due to the uncertainties in the data. Theoretical curves are shown for A derived from Bessel functions of order 9/2 ($\ell = 4$) and order 13/2 ($\ell = 6$). The temperature dependence of A should be represented by the 9/2 order Bessel function; however, as shown, the agreement is actually better with the 13/2 order function. This anomaly could be the result of a significant sixth order constant admixed with the fourth order term, or it could be merely the result of inaccurate data. In terbium, which is described in the next subsection, the basal plane anisotropy is much lower and the constant A clearly follows the 9/2 order Bessel function relation.

Values of D and G shown in the figure are not affected by basal plane anisotropy and may be considered correct within stated experimental error. G shows that the c axis expands rapidly in the antiferromagnetic range before reaching saturation near the Curie temperature. The isotropic dilatation of the basal plane described by D shows a contraction down to the Curie temperature with a subsequent expansion for lower temperatures.

This is presumably a result of the change in the exchange forces in going from the zero field antiferromagnetic state into the spontaneously ordered ferromagnetic state.

Figure 23 shows the b-axis strain of Dy with a 26 kOe field applied along the b axis. As shown in the next paragraph, the fourth order expression for this strain after subtraction of the thermal contribution is:

$$[\frac{\Delta\ell}{\ell}]^b_b - [\frac{\Delta\ell}{\ell}]^o_b = A + C + D$$

Thus, to second order (A=0), this curve should be identical to the a-axis magnetostrain curve of Figure 21 (cf. Equation 43a). The radical departure below 75°K is a consequence of the fourth order correction constant A and also of a regression of the moment from the b-axis direction into the adjoining a-axis directions as a consequence of the rapidly increasing anisotropy energy.

b. Results for terbium The b axis of Tb is the easy magnetic direction. Equation 16 gives the following result for the strain with the magnetization along the b axis ($\alpha_x = 0$, $\alpha_y = 1$):

$$[\frac{\Delta\ell}{\ell}]^b = A\beta_y^2 + C[\beta_y^2 - \beta_x^2] + D(1-\beta_z^2) + G\beta_z^2 \qquad (45)$$

The strains found by subtraction of the extrapolated thermal expansion from the a-, b-, and c-axis magnetostrain curves satisfy the following relations:

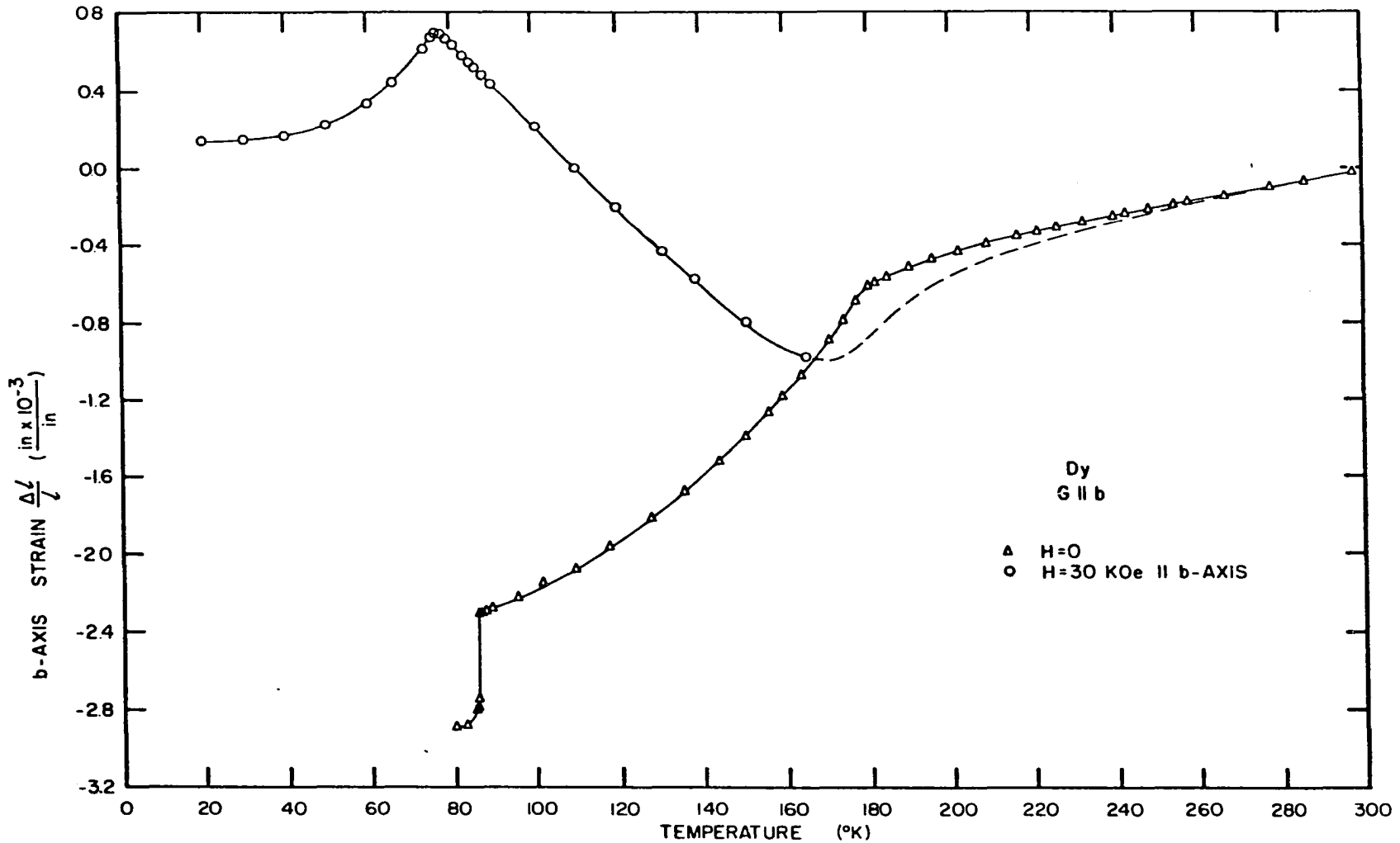

Figure 23. The b-axis strain of Dy as a function of temperature in zero field and in a 30 kOe field applied along the b axis. The effect of the large basal plane anisotropy is evident below 75°K.

$$\text{a axis } (\beta_x = 1,\ \beta_y = \beta_z = 0)\ \left[\frac{\Delta\ell}{\ell}\right]_a^b - \left[\frac{\Delta\ell}{\ell}\right]_a^o = -C + D \qquad (46a)$$

$$\text{b axis } (\beta_x = 0,\ \beta_y = 1,\ \beta_z = 0)\ \left[\frac{\Delta\ell}{\ell}\right]_b^b - \left[\frac{\Delta\ell}{\ell}\right]_b^o = A + C + D \qquad (46b$$

$$\text{c axis } (\beta_x = \beta_y = 0,\ \beta_z = 1)\ \left[\frac{\Delta\ell}{\ell}\right]_c^b - \left[\frac{\Delta\ell}{\ell}\right]_c^o = G \qquad (46c)$$

From Equation 46a and the values of C obtained in the rotation measurements, D was calculated. Equation 46c provided G directly.

Figure 24 shows the temperature dependence of the a-, b-, and c-axis strains in both zero field and in a 30 kOe field applied along the b axis of Tb. The exchange interaction giving rise to the helical antiferromagnetic structure of Tb is much weaker than in Dy. The spiral structure appears only above 221°K and is stable over only a 9 degree range in zero field. Thus the c-axis strain shown in Figure 24 is much smaller than in Dy. The a- and b-axis behavior in an applied field is essentially opposite to that in Dy as expected, although the magnetostrain of the b axis does not reverse sign as does the a axis in Dy. This is probably due to the restricted variation in the interlayer turn angle ranging from 20.5° at 230°K to 18° at 220°K (39). As a result of the smaller change in exchange energy at the Curie temperature, the spontaneous orthorhombic distortion is almost unobservable except in the a axis. This effect amounting to about 80 μ inches/inch is shown in the inset of the figure. The transition is not as sharp as in Dy but is smeared out over a two degree range about 221°K.

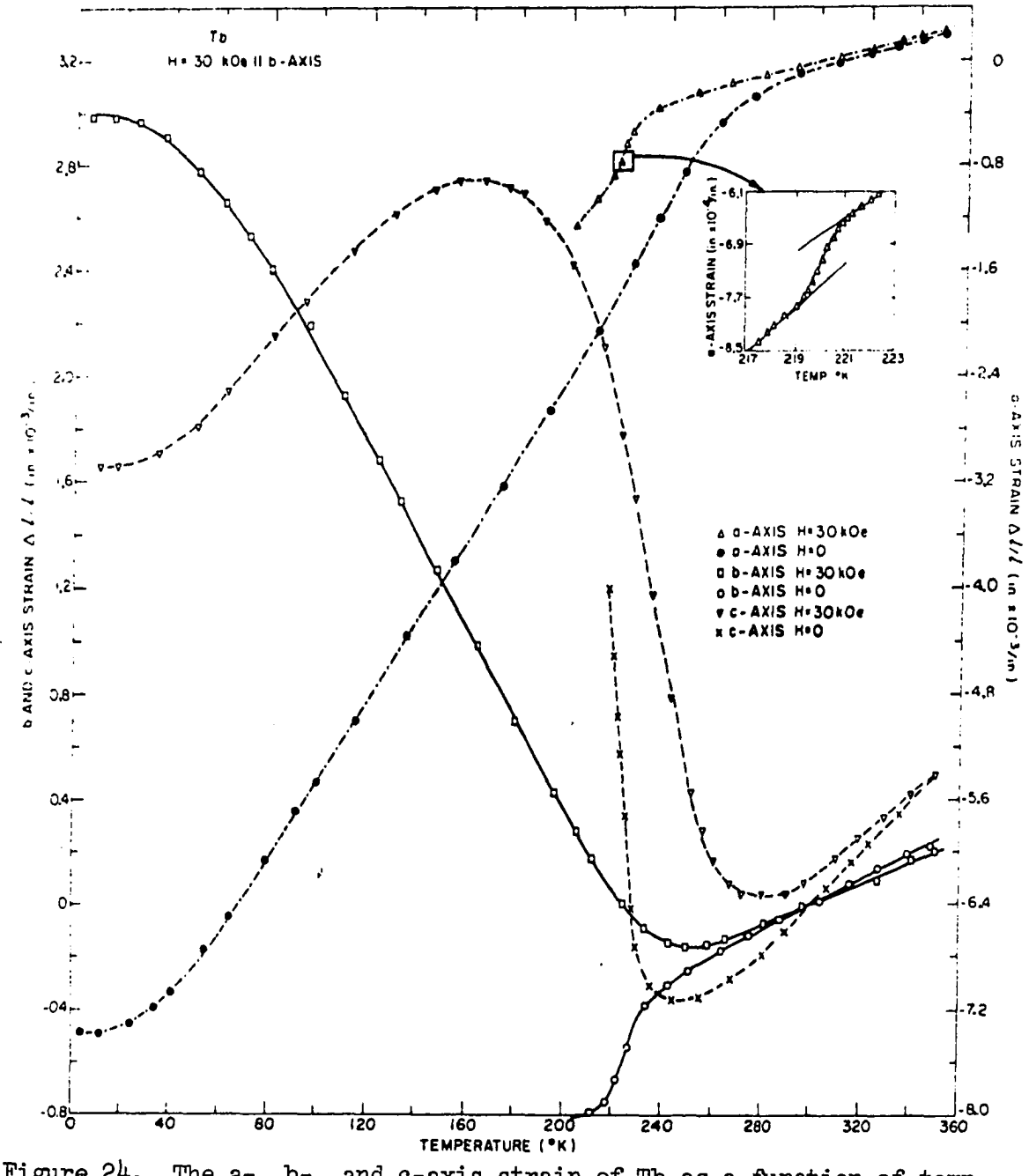

Figure 24. The a-, b-, and c-axis strain of Tb as a function of temperature in zero field and in a 30 kOe field applied along the b axis. The inset shows the anomalous slope change of the a-axis zero-field strain at 220°K. This corresponds to a structure change from hexagonal to orthorhombic at the ordering temperature.

Figure 25 shows the temperature dependence of the constants A, C, D, and G for Tb. In Tb C and A were both obtained directly from the experimental rotation data (e.g. Figure 18). C was determined from the $\theta = 90^{\circ}$ strain and A from the $\theta = 60^{\circ}$ strain and the value of C in accordance with Equations 39a,b. This direct determination of A was possible because of the much lower basal plane anisotropy in Tb than in Dy. Constants D and G were obtained from Equations 46a,c and the values of C.

The theoretical curve for the temperature dependence of the constants A and C according to the Callen one ion theory is also shown in the figure. The magnetic moment data of Hegland (31) were used. It should be noted that the constant C actually consists of two terms:

$$2C = \lambda^{\gamma,2} - \frac{1}{7}\lambda_2^{\gamma,4} \tag{47}$$

From the fit of C to $I_{\frac{5}{2}}(L^{-1}(M_n))^2/I_{\frac{1}{2}}(L^{-1}(M_n))$ (i.e. $\ell = 2$) it can be concluded that the $\ell = 4$ term $\frac{1}{7}\lambda_2^{\gamma,4}$ is negligible in Tb. The fourth order term A shows the $I_{\frac{9}{2}}(L^{-1}(M_n))/I_{\frac{1}{2}}(L^{-1}(M_n))$ behavior as expected. The closeness of the theoretical fit to the constants A and C shows that the one ion interaction in the Callen theory is sufficient to describe the behavior in Tb. This means that the anisotropy energy (represented by the one ion terms) is the dominant basal plane magnetostriction mechanism as postulated earlier.

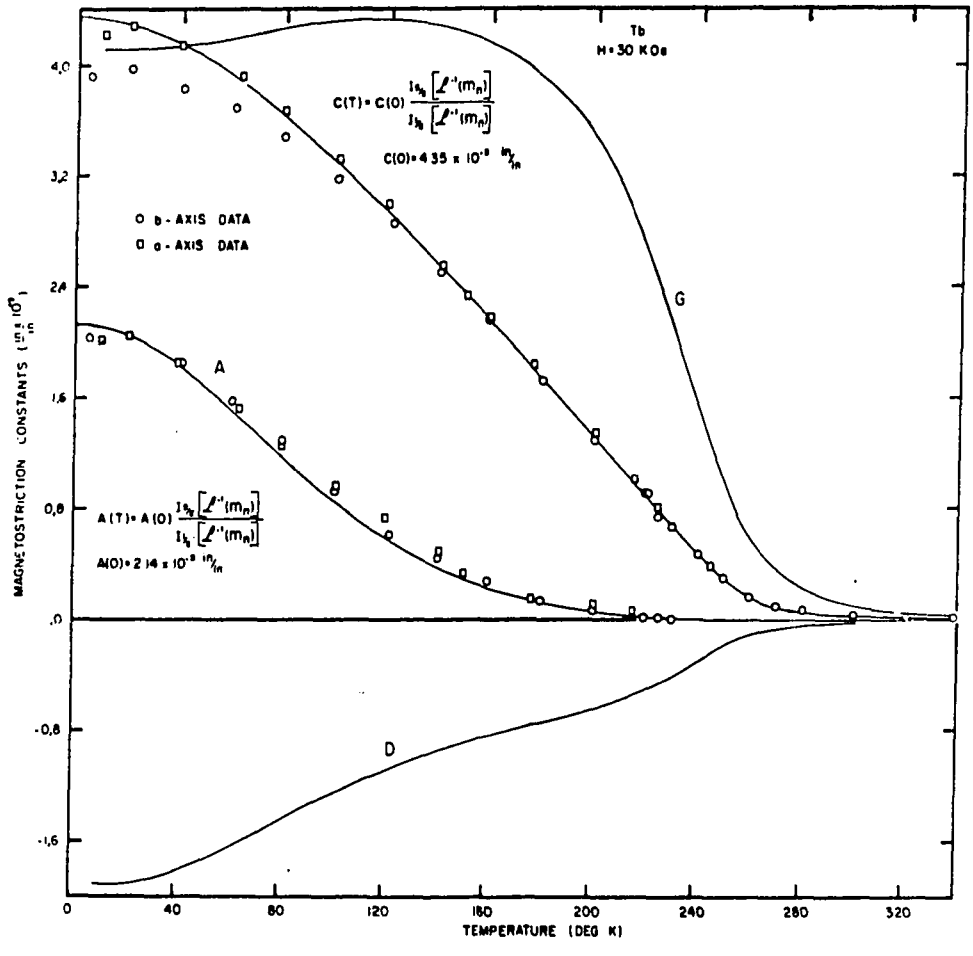

Figure 25. Magnetostriction constants, A, C, D, and G, of Tb at 30 kOe applied field. The theoretical expressions for the temperature dependence of the anisotropic constants A and C are shown along the experimental data obtained from the a- and b-axis field rotation measurements.

The values of the constants shown in Figure 25 apply to a 30 kOe magnetic field. Figure 26 shows the values of the constants A_o, C_o, D_o, and G_o extrapolated to zero applied field. The constants D_o and G_o were corrected to zero field by use of the a- and c-axis forced magnetostriction data (discussed in a later section) while A_o and C_o were obtained by direct measurement of the field dependence of C and A+2C. Above 240°K, the forced magnetostriction correction becomes large and difficult to evaluate; hence, there is some uncertainty in the values of D_o and G_o in this region.

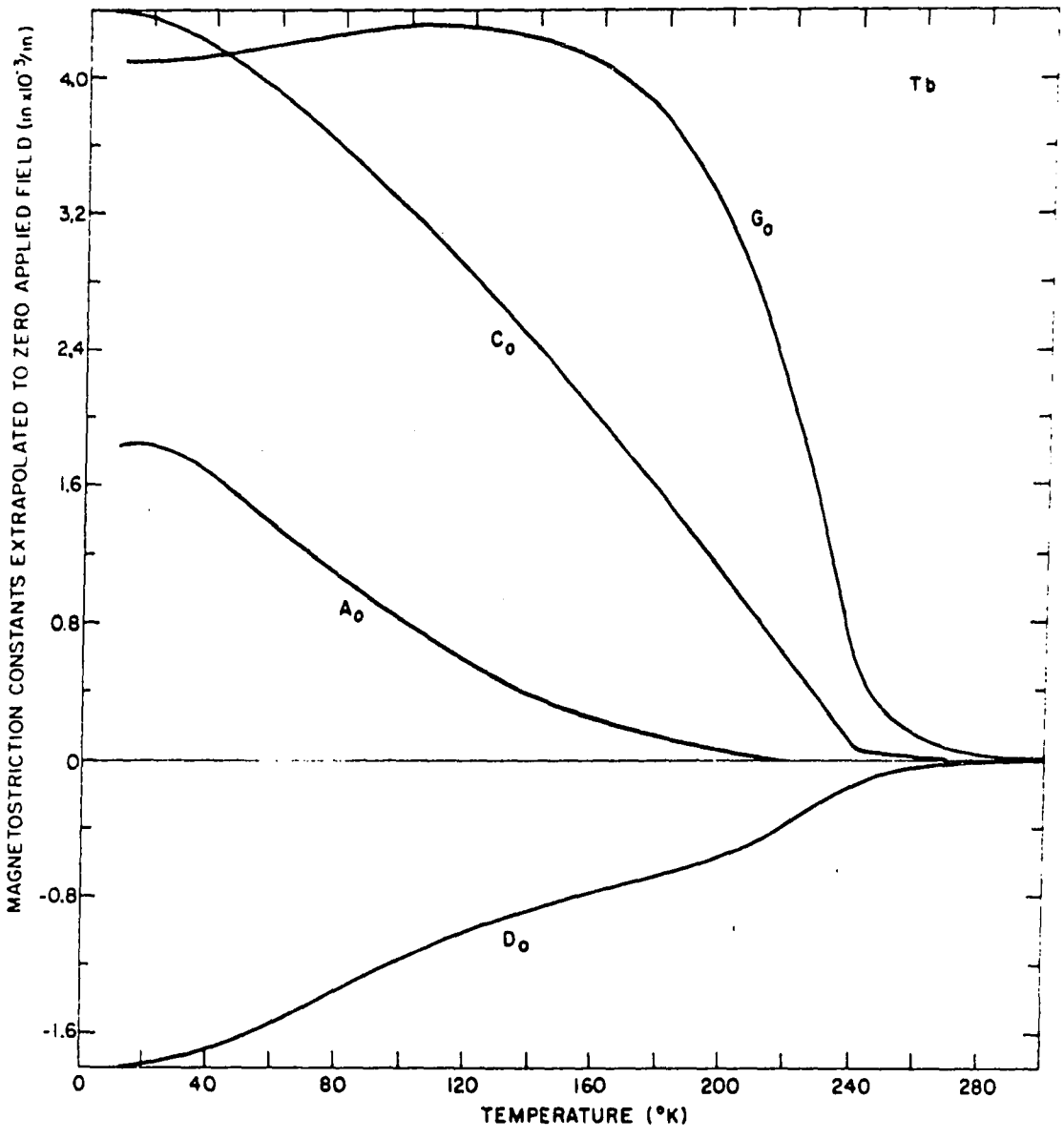

Figure 26. Tb magnetostriction constants A_o, C_o, D_o and G_o. The subscript indicates the values have been extrapolated to zero applied field.

VIII. ANISOTROPY ENERGY

A. General Remarks

The magnetic anisotropy energy of a hexagonal ferromagnet can be written in the following form due to Miwa and Yosida (50):

$$H_{anis} = V_2^o + V_4^o + V_6^o + V_6^6 \tag{48}$$

The first four terms describe the axial anisotropy tending to align the spins either parallel to the c axis, perpendicular to the c axis, or on a cone about the c axis. The last term describes the anisotropy of the basal plane (six fold anisotropy). Treating the atomic spins classically, the functional form of the anisotropy may be written:

$$H_{anis}(\theta,\phi) = K_2 Y_2^o(\theta,\phi) + K_4 Y_4^o(\theta,\phi) + K_6 Y_6^o(\theta,\phi) + K_6^6 Y_6^6(\theta,\phi) \tag{49}$$

where the Y^m are spherical harmonics, and the K's are the anisotropy constants. Theta and ϕ are the spin angles measured from the c and a axes respectively. The relative signs, magnitudes, and temperature dependences of the constants determine the stable zero field magnetic states in the rare earths. Negative values of K_2, K_4, and K_6 favor spin alignment along the c axis, positive values correspond to basal plane alignment. Mixed signs in these constants produce the intermediate (cone, etc.) states such as in Er. From calculations of the

effects of the crystalline field at the tri-positive ion sites, Miwa and Yosida deduced the signs for the rare earth anisotropy constants in Table 4.

Table 4. Signs of anisotropy constants in the heavy rare earths

	Tb	Dy	Ho	Er	Tm
K_2	+	+	+	-	-
K_4	-	+	+	-	-
K_6	-	+	-	+	-
K_6^6	+	-	+	-	+

B. Anisotropy Constants of Dy and Tb Calculated from Magnetostriction Data

As indicated previously, departures of the experimental basal plane rotation magnetostriction from the fourth order theoretical curves are due largely to the six fold anisotropy in Tb and Dy. This anisotropy prevents the magnetization from following the field applied in hard magnetic directions. For $30^\circ < \theta' < 60^\circ$ the magnetization leads the field, and the measured strain is larger than that predicted by the theory. For $60^\circ < \theta' < 90^\circ$ the magnetization lags behind the field direction, and the measured strain is lower than the theoretical strain. At $\theta = 0^\circ$ and 60° the magnetization and field are aligned in the easy direction.

The total angle dependent magnetic energy consists of two parts--the six fold anisotropy energy and the internal magnetic energy:

$$E_m = -MH \cos(\theta - \phi) - K_6^6 \cos 6\phi$$

where ϕ is the angle of the magnetization relative to the easy magnetic direction. Minimization of this energy with respect to the magnetization angle ϕ gives the equilibrium configuration:

$$\frac{\partial E_m}{\partial \phi} = 0 = -MH \sin(\theta - \phi) + 6K_6^6 \sin 6\phi \qquad (50)$$

The quantity θ-ϕ represents the degree of misalignment of the magnetic moment and field. Equation 50 also provides a method for calculation of the anisotropy constant K_6^6 if the angles θ and ϕ are known. These angles were obtained from the rotation magnetostriction data of Dy and Tb by forcing the experimental data to fit the prediction of the fourth order theory as follows:

The fourth order rotation theory (Equations 37 and 39) predicts a strain dependence of the form,

$$\frac{\Delta \ell}{\ell} = \mp A \sin^2 2\phi \pm 2C \sin^2\phi, \qquad (51)$$

where ϕ is the magnetization angle relative to the easy magnetic direction. Knowing the values of the magnetostriction constants A and C and the measured strains for $\theta = 40^\circ$, 50°, 70°, and 80° (θ = applied field angle), it was possible to solve Equation 51 for the corresponding magnetization

angles which would produce the observed strains. These angles ϕ together with the field angles θ when substituted into Equation 50 provided values of K_6^6. The region $40^\circ < \theta < 80^\circ$ was chosen since it is in this region that the strain deviations due to the anisotropy are most pronounced. The values of C used were from the experimental data except in regions of high anisotropy where the values were obtained from the theoretical curve of Figures 22 and 24. From values of C and the strain at $\theta = 60^\circ$, A was calculated. It should be mentioned that the anisotropy does not seriously affect the experimental values of C due to the small first derivative of the dominant $\sin^2\theta$ in the vicinity of $\theta = 90^\circ$ (see appendix). Figure 27 shows the anisotropy constants of Dy and Tb obtained by this method. The experimental points represent an average of the values obtained at the four field angles $\theta = 40^\circ$, 50°, 70°, and 80°. The accuracy of the values is not expected to be better than $\pm$ 25 per cent, especially in Tb due to the smallness of the effect.

The solid line represents the theoretical dependence of K_6^6 on the 21st power of the magnetic moment predicted by the Zener (71) theory. This theory predicts the temperature dependence of the anisotropy constants through the relationship $K(T) \cong [M(T)]^{n(n+1)/2}$ where n=6 for a six fold axis.

Liu, Behrendt, Legvold and Good (46) have calculated the anisotropy

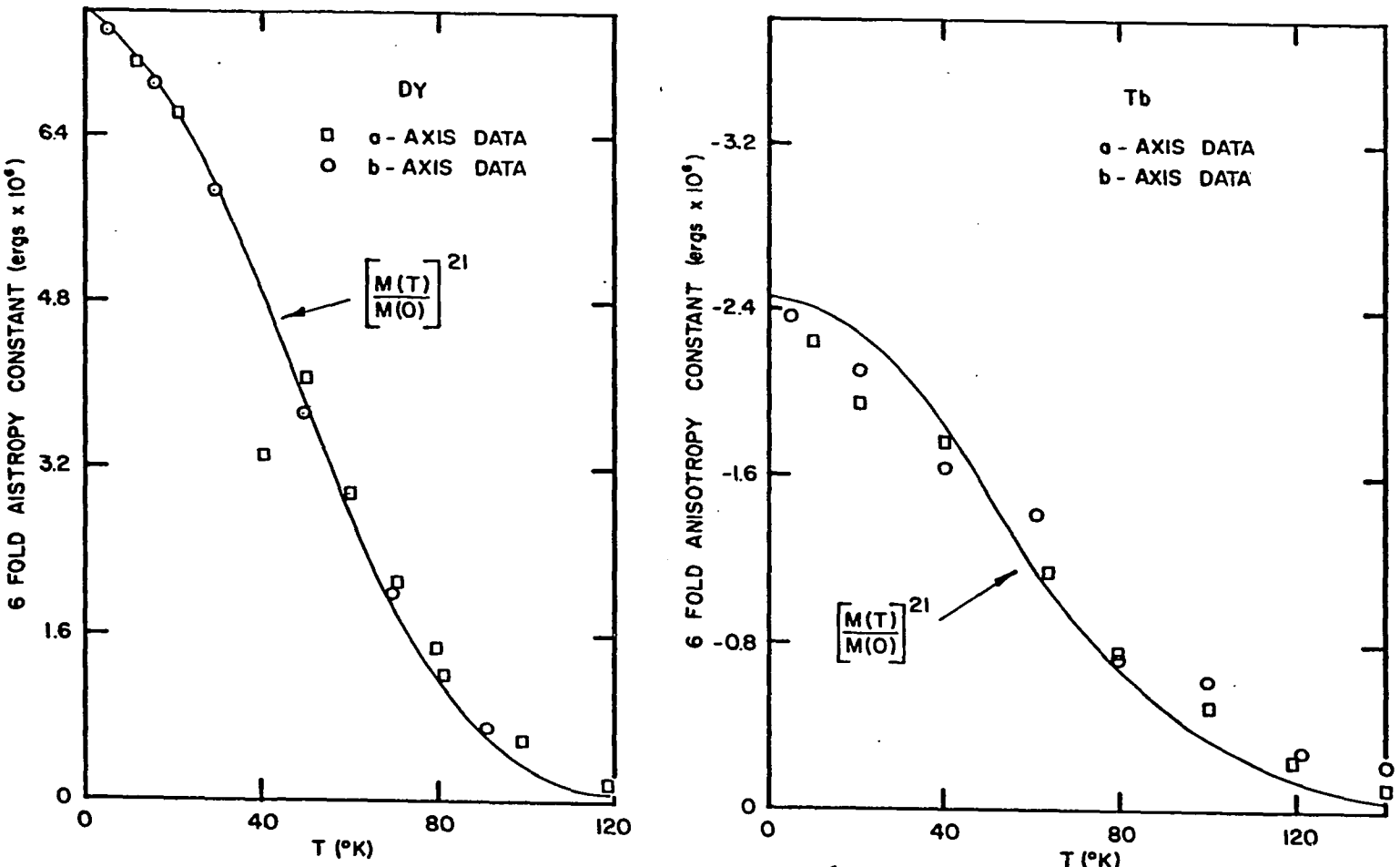

Figure 27. Basal plane magnetic anisotropy constant, K_6^6, for Dy and Tb as determined from rotation magnetostriction data.

constants of Dy from the single crystal magnetization data. Their method, which is less susceptible to experimental error, gave values of K_6^6 somewhat smaller than those found in the present study. Their value of K(T=0) was 5.24×10^6 ergs/cm^3 compared to 7.6×10^6 ergs/cm^3 found from this calculation.

IX. Tb AND Dy ISOTHERMAL MAGNETOSTRICTION

Measurement of the magnetostrain as a function of applied field in a ferromagnet below saturation is a classic but virtually fruitless study. As mentioned in the introduction, quantitative results require a knowledge of the domain structure at each stage in the magnetization process. Semi-quantitative results can be obtained for the magnetostriction constants by averaging Equation 16 over a hypothetical "ideal demagnetized state" (e.g. assuming an equal distribution of domains along each of the six equivalent a-axis directions in Dy). In reality, however, this ideal state is seldom realized and variations up to 20 or 30 per cent in the demagnetized strain are encountered depending on the magnetic history as demonstrated in Figure 1.

A. Ferromagnetic and Antiferromagnetic Results for Dy and Tb

Measurements of magnetostrain versus applied field were made on Dy, Tb, and Er. These gave information on the forced magnetostriction (discussed later) and on the required critical fields and strains resulting from collapse of the spiral antiferromagnetic states of the metals.

The measurements reported here were made with the magnetic field along the respective easy magnetic directions. Measurements were principally confined to this case due to the lack of magnetic saturation with the applied field in other directions.

The results for Dy and Tb are shown in Figures 28-32. Er is discussed in a later section. Figures 28 and 29 show the a-, b-, and c-axis strains in the ferro- and antiferromagnetic regions of Dy as a function of applied field along the a (easy) axis. Qualitatively, the crystal is observed to expand in the direction of the magnetization and to contract in the transverse basal plane direction. The strains are larger for the lower temperatures as a result of the increased anisotropy energy. The c-axis strain is quite small below the Curie temperature (87°K) as was shown previously from Equation 16 for the case of a magnetic moment constrained to the basal plane. In the helical antiferromagnetic range ($87^{\circ}K < T < 178^{\circ}K$) the c axis exhibits a large positive strain as discussed in the section on magnetostriction of a helical antiferromagnet. In this temperature range the strains of all three axes are observed to exhibit almost zero strain up to a critical field characteristic of the exchange energy producing the helical state. Above this field the helix is collapsed and ferromagnetic alignment takes place along the applied field direction.

The situation is similar for Tb as shown in Figures 30-32. Here the field was applied along the b-axis (easy) direction and the a-, b-, and c-axis strains were measured. Similar behavior to Dy is noted below the Curie temperature ($220^{\circ}K$), with the a and b axis interchanged.

The antiferromagnetic state of Tb is much weaker than in Dy and an

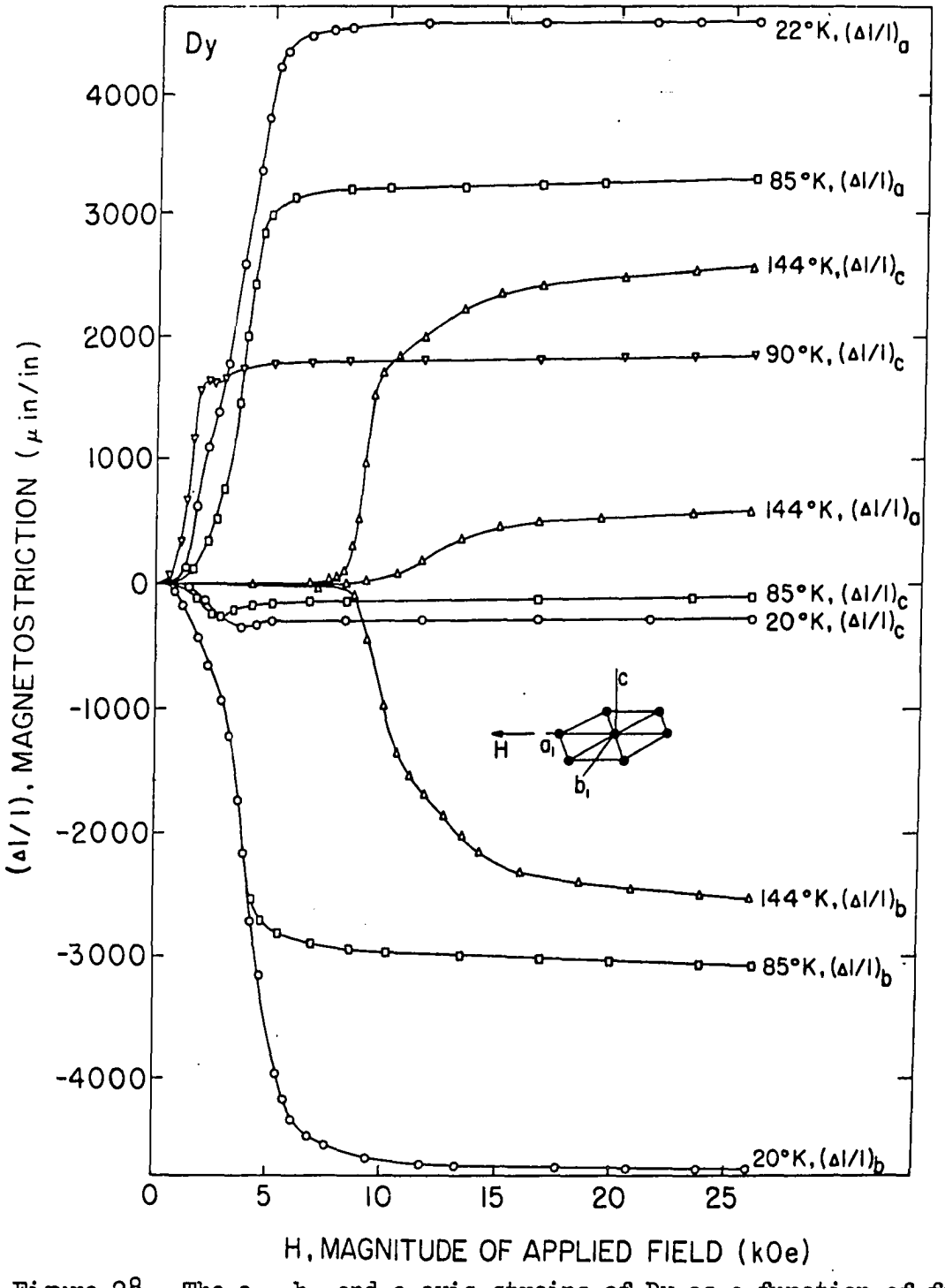

Figure 28. The a-, b- and c-axis strains of Dy as a function of field applied along the a axis. Curves are shown for both ferromagnetic and antiferromagnetic temperature regions. The subscript indicates the strain gage direction.

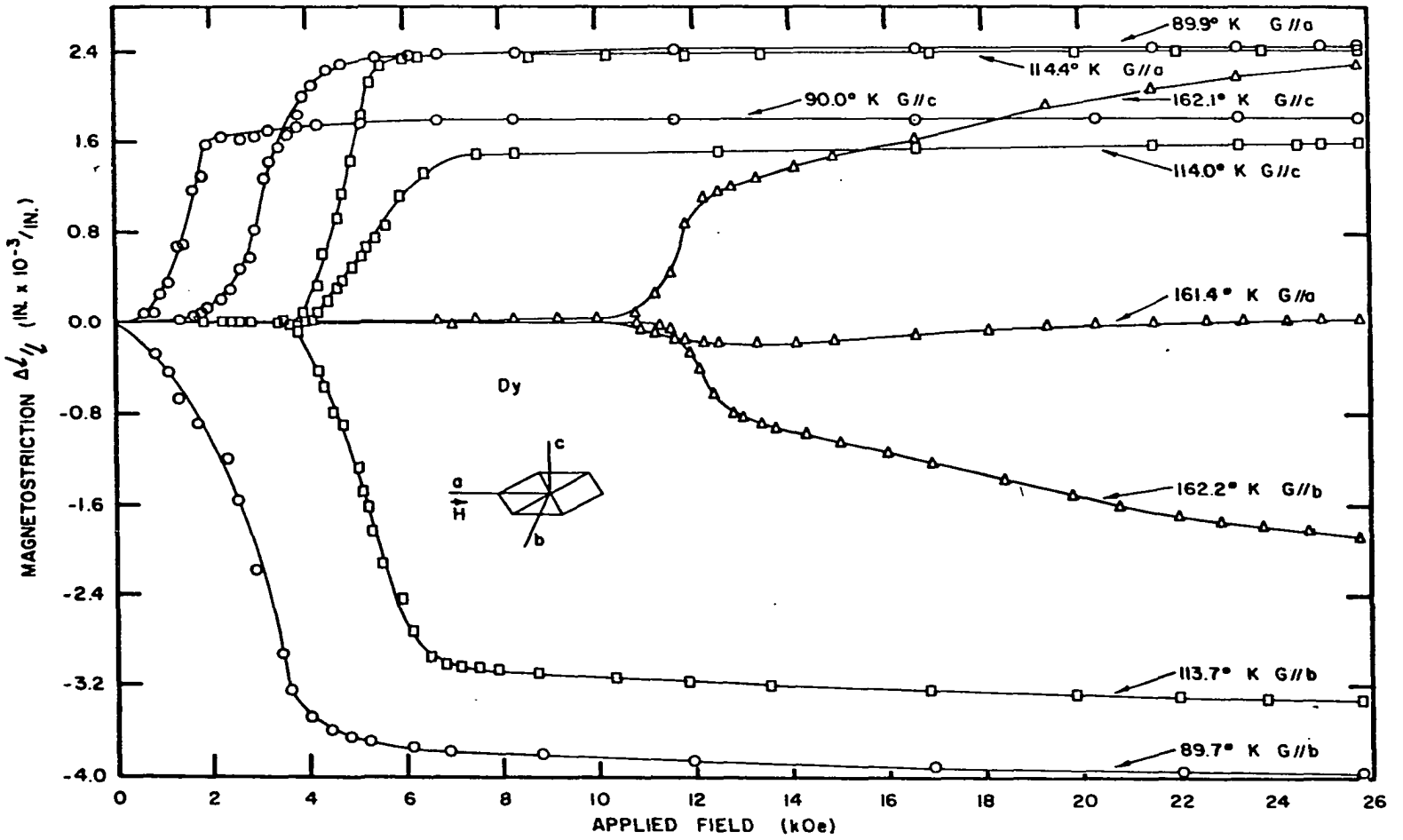

Figure 29. Magnetostriction of Dy as a function of field applied along the a axis. The curves shown are in the antiferromagnetic temperature range.

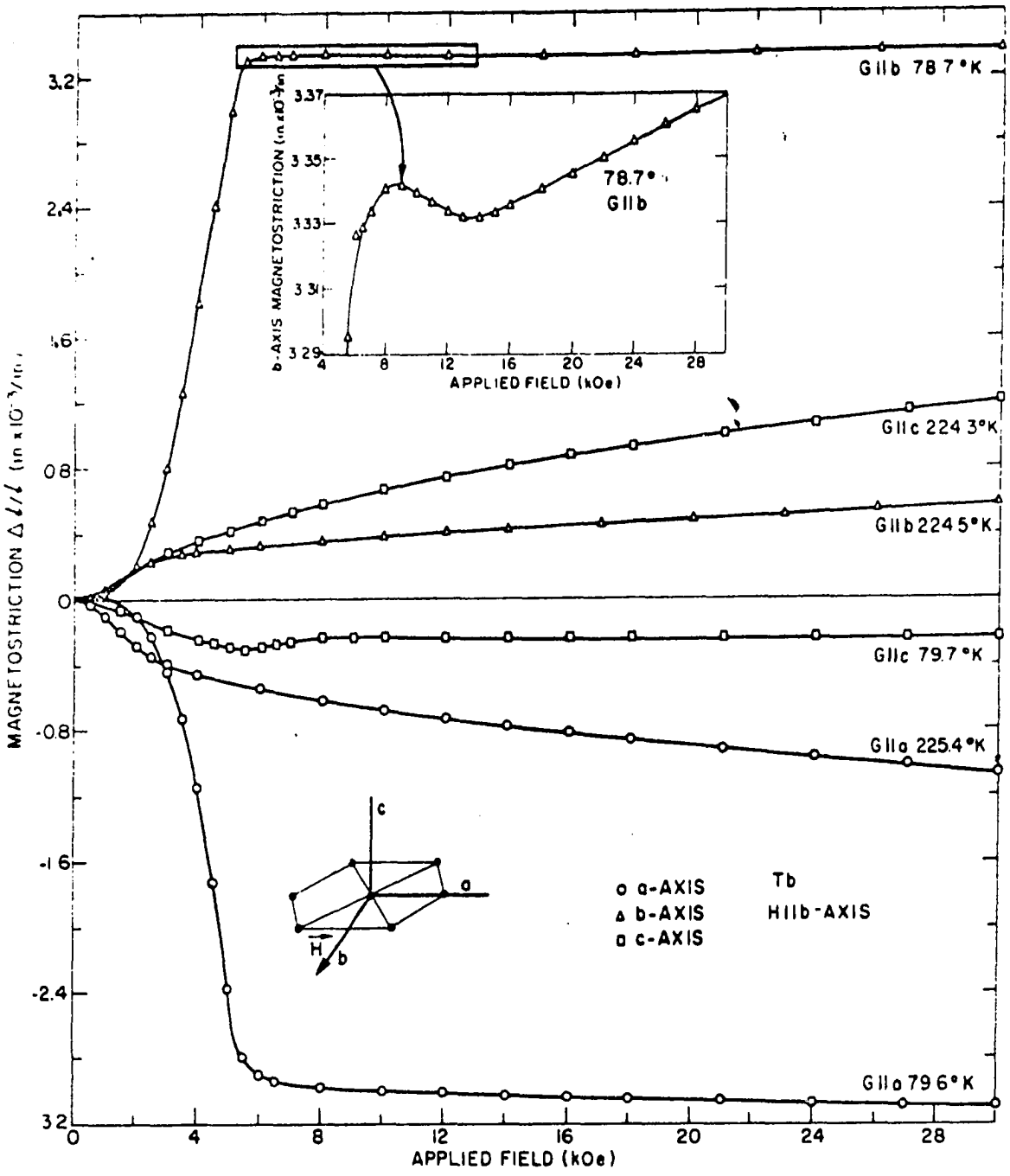

Figure 30. The a-, b-, and c-axis strains of Tb as a function of field magnitude applied along the b direction. Curves in the ferromagnetic and antiferromagnetic temperature range are given. The inset shows the forced magnetostriction above saturation. G indicates the strain gage direction.

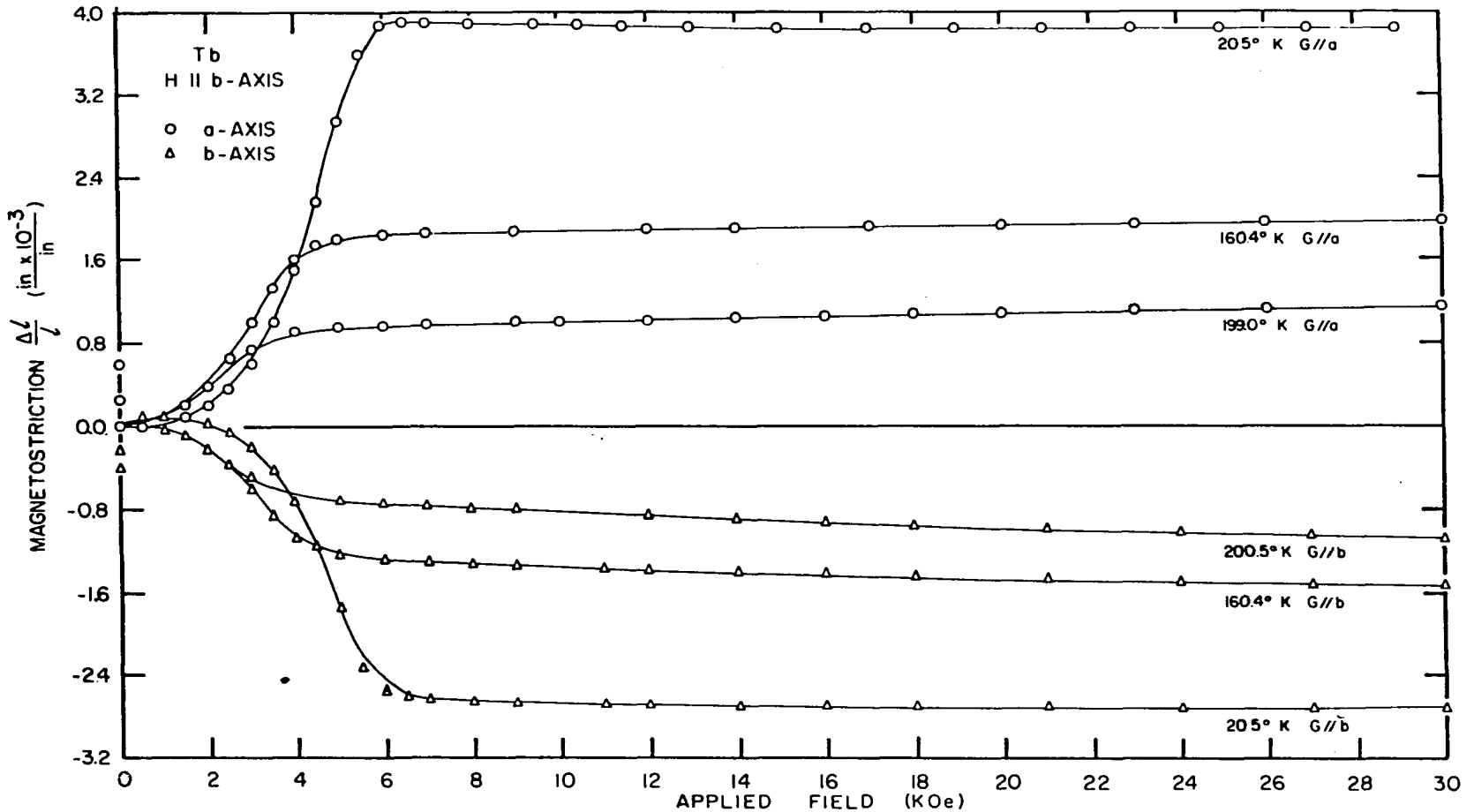

Figure 31. Basal plane magnetostriction of Tb as a function of field applied along the easy b-axis direction. The curves shown are in the ferromagnetic temperature range. G indicates the strain gage direction.

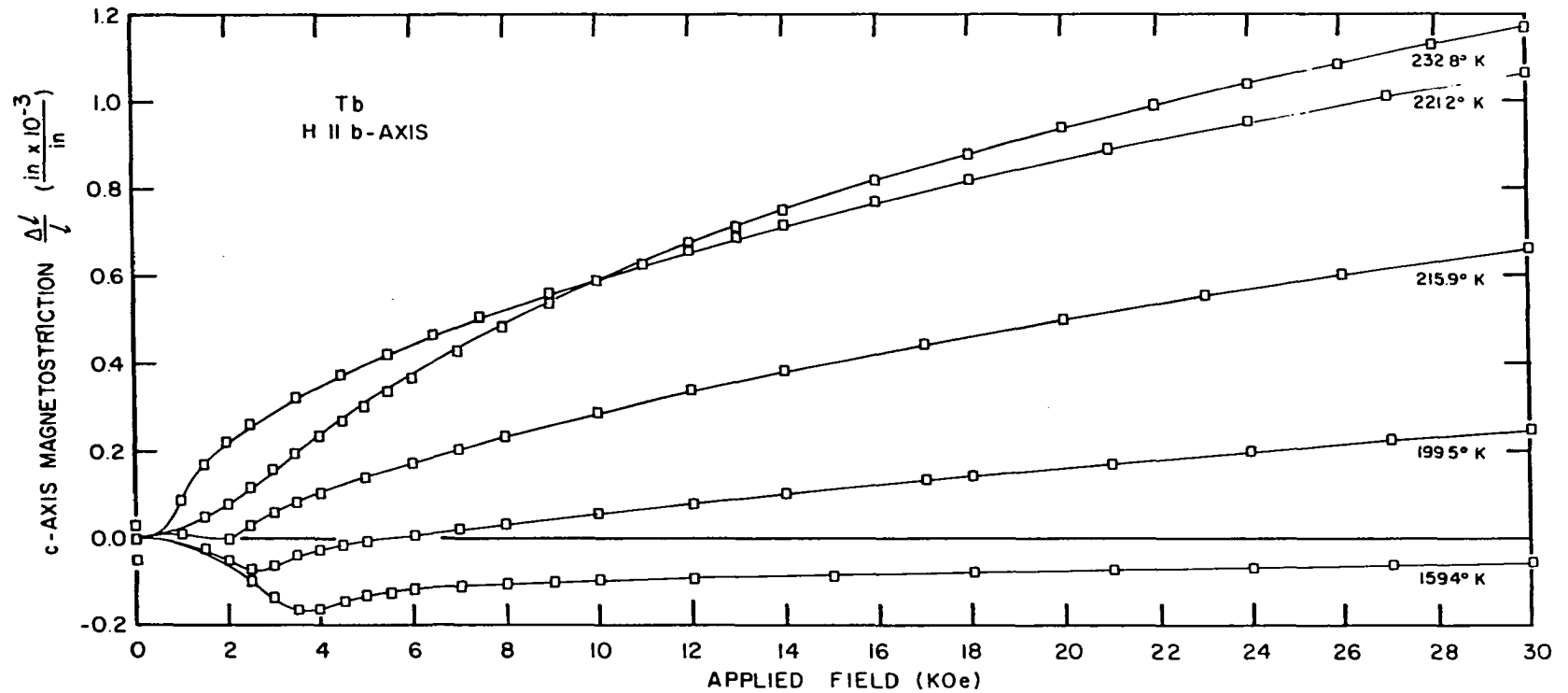

Figure 32. The c-axis magnetostriction of Tb as a function of field applied along the easy b-axis direction. The 221°K curve is in the antiferromagnetic temperature range. In contrast to Dy, fields less than 1 kOe are sufficient to remove the helical state. The 232°K curve is in the paramagnetic range. The remainder of the curves are in the ferromagnetic region.

applied field of less than one kOe will overcome the exchange field. As expected, the c-axis strain accompanying the breakdown of the helical state is relatively small as shown in the 224°K curve.

An anomalous change in slope of the strain at the onset of technical saturation was observed, principally in the b- and c-axis curves. This effect, shown in the inset of the figure, is attributed to the rotation of domains across hard magnetic directions in the magnetization process, giving rise to the extra observed strain. The b-axis anomaly is largest at the lower temperatures and vanishes above 140°K.

The finite slope of the ferromagnetic magnetostriction curves below saturation is due to the demagnetizing field effect. The large values of magnetic moment (350 emu/gm. in Dy at 4°K) produces a maximum demagnetizing field in the specimens used of about 5.9 kilogauss.

B. Critical Fields in Dy from a-c Plane Field Rotation Measurements

Curves are given in Figure 33 for the c-axis magnetostriction of Dy as a function of the angle of the applied field in the a-c plane. The angle γ_a of the 26 kOe field was referenced to the a axis. As shown below, these curves provide an alternate determination of the critical fields required to overcome the helical exchange energy and produce ferromagnetic alignment.

In the antiferromagnetic temperature region, applied fields whose

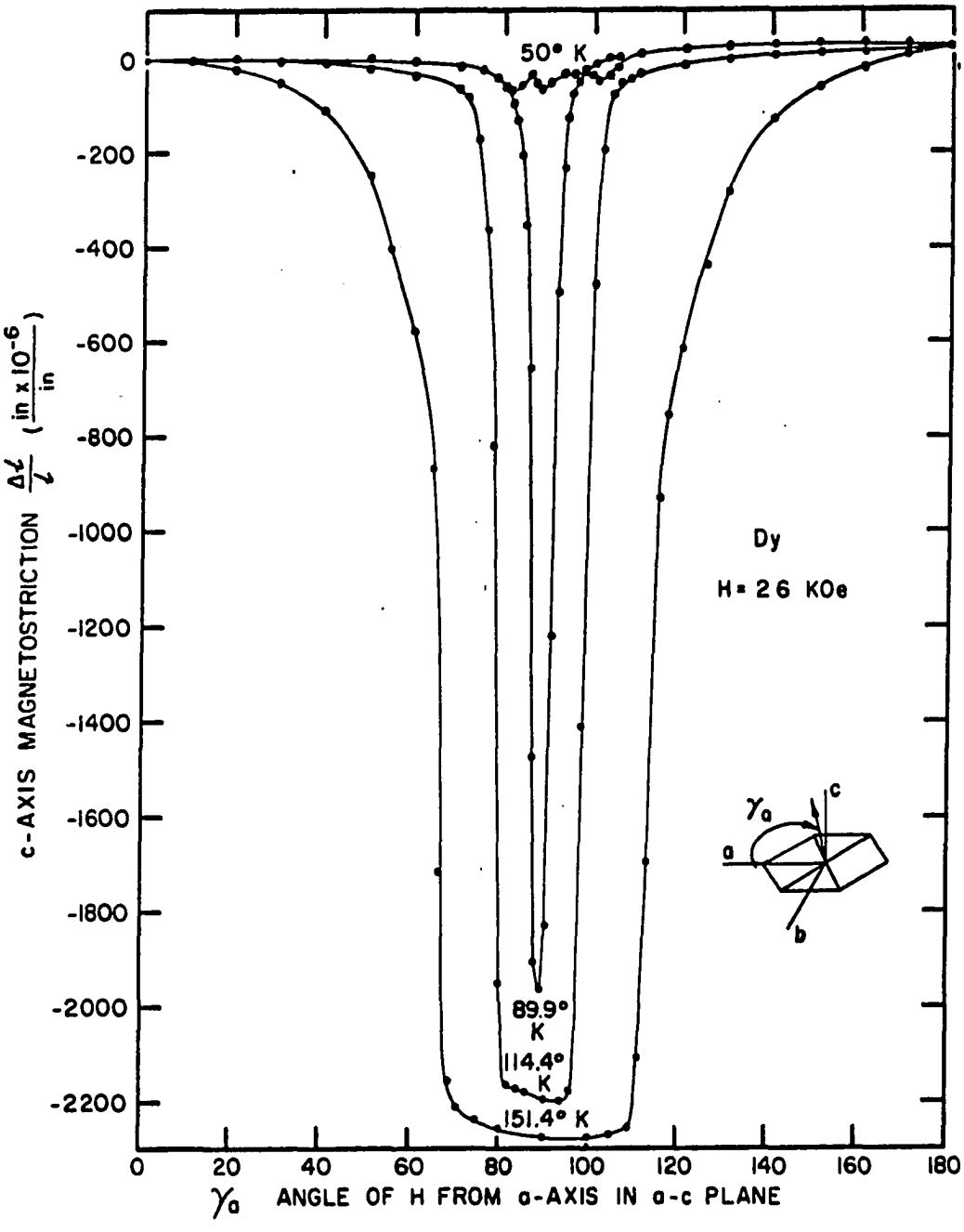

Figure 33. Dy c-axis magnetostriction as a function of applied field angle relative to the a axis. The 26 kOe field was applied in the a-c plane. The broadening of the curves at higher temperatures indicates the larger basal plane field component required to maintain the ferromagnetic state.

a-axis component is greater than the critical fields shown in Figures 28 and 29 will produce a spontaneous transition to ferromagnetic alignment of the moment along the a axis. This effect is the origin of the abrupt changes in c-axis strain evidenced in Figure 33. The a-axis component of the field is $H_a = 26 \cos \gamma_a$. The strain discontinuity occurs at a field

$$H_{cr} = 26 \cos \gamma_{ac} \tag{52}$$

where γ_{ac} is the critical angle of Figure 33. Values of the critical field calculated from this expression agree rather closely with those found from the linear magnetostriction curves as shown in Table 5. This fact again indicates that the axial magnetic anisotropy of Dy is sufficient to prevent appreciable rotation of the moment out of the basal plane by the 26 kOe field even in this temperature range.

Table 5. Comparison of calculated and observed values of the critical fields in dysprosium

T ^{o}K	H_{cr}^{a} kOe	H_{cr}^{b} kOe
89.9	0.45 ± .3	0.5 ± .2
114.4	4.5 ± .3	4.2 ± .2
151.4	9.7 ± .4	9.2 ± .5

[a] H_{cr} from Equation 52.

[b] H_{cr} from linear magnetostriction curves.

C. Paramagnetic Magnetostriction

In the paramagnetic region ($T > 230^{\circ}K$ in Tb and $T > 179^{\circ}K$ in Dy) the magnetostriction is proportional to the square of the applied field as follows:

From thermodynamics $dU = Tds - PdV + HdM$

$$\therefore \quad -\frac{\partial V}{\partial H_{ext}}\Big|_M = \frac{\partial M}{\partial P}\Big|_V \tag{53}$$

To first order $M = VI = V\chi H$, therefore, integrating

$$\Delta V = -\int \frac{\partial}{\partial P}(V\chi H)\, dH \tag{54}$$

For a paramagnetic substance the susceptibility χ is not a function of the magnetization ($\chi \neq \chi(M,H)$). Neglecting the pressure dependence of χ and introducing the compressibility $K = \frac{1}{V}\frac{\partial V}{\partial P}$ we have

$$\frac{\Delta V}{V} = \omega = \chi K \int H dH = \chi K \frac{H^2}{2} \tag{55}$$

Assuming the linear magnetostriction to be proportional to this, the desired result is obtained.

Figures 34 and 35 show the linear magnetostriction of Dy and Tb plotted as a function of the square of the applied field. The curves are observed to be quite linear except at $240^{\circ}K$ in Tb which shows slight curvature. This is probably the result of the breakdown of the assumption $\chi \neq \chi(H,M)$ due to spin corrolation. In principal in the paramagnetic range it is possible to obtain values for all of the magnetostriction

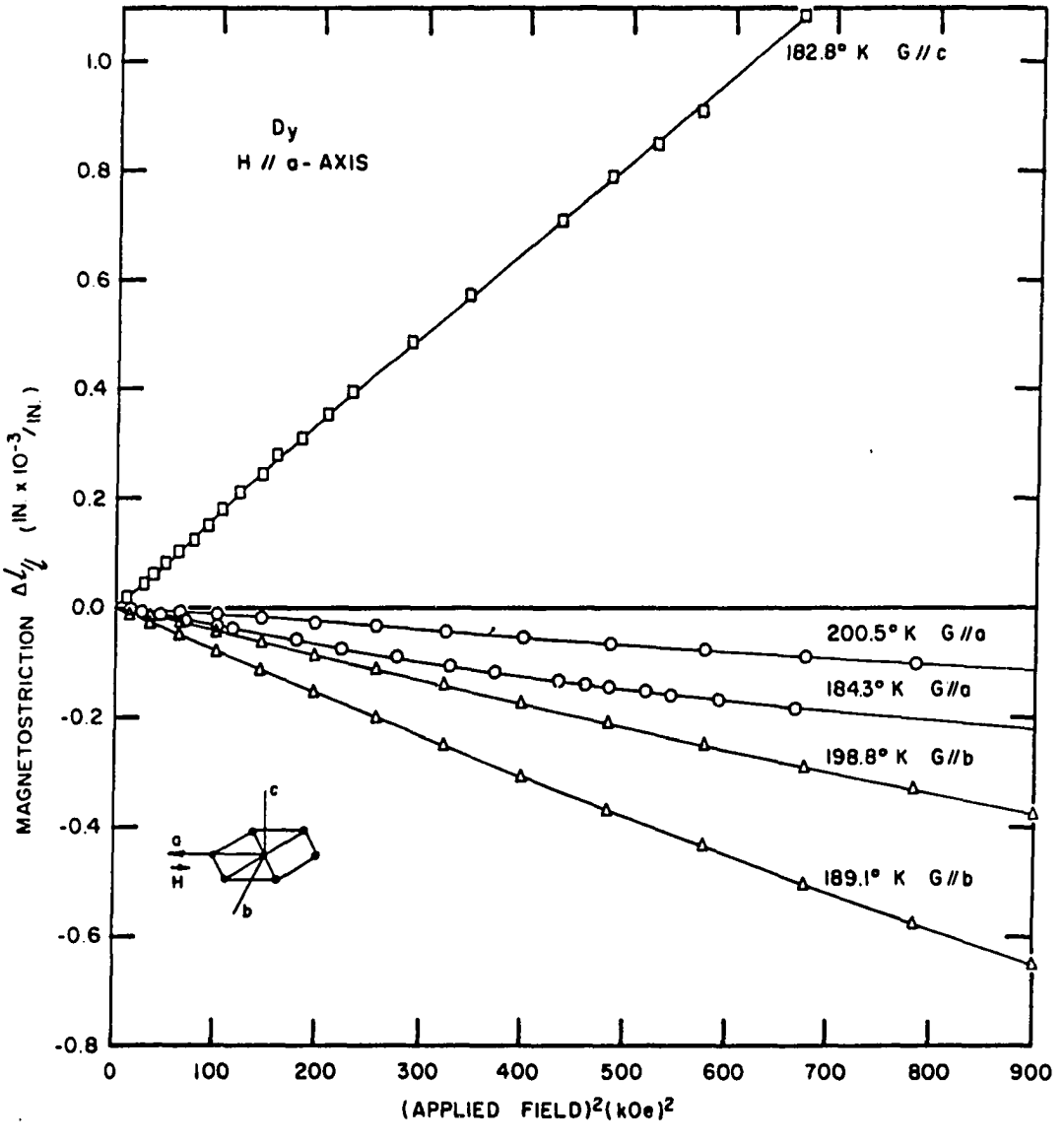

Figure 34. Dy a-, b-, and c-axis strain as a function of H^2 applied along the a axis in the paramagnetic region. G indicates the strain gage direction.

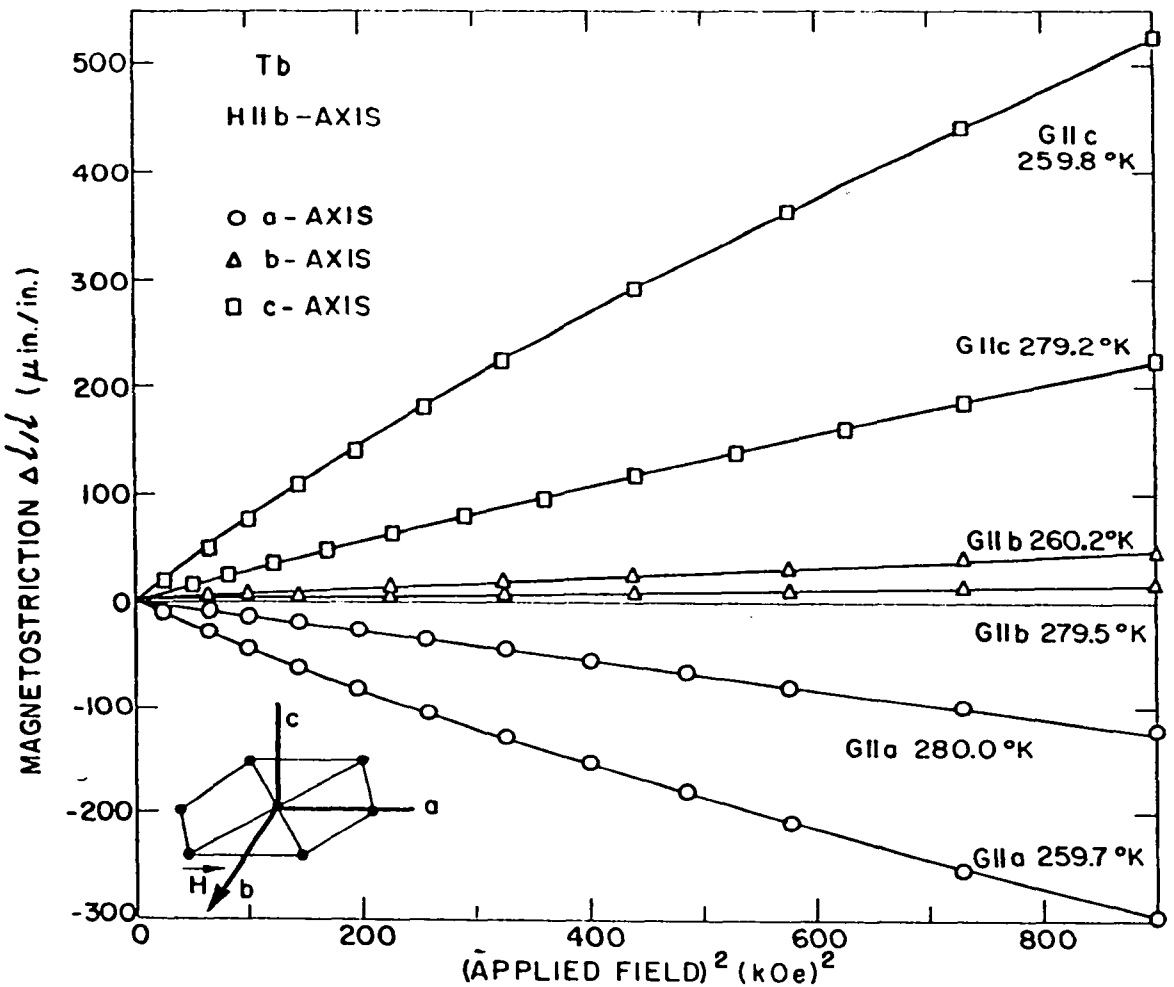

Figure 35. Tb a-, b-, and c-axis strain as a function of H^2 applied along the b direction in the paramagnetic region. Some ordering is indicated at 260° by the slight curvature at the higher fields. G indicates the strain gage direction.

constants appearing in Equation 13 since the anisotropy energy no longer constrains the moment to the basal plane. In reality, however, values so measured are highly field dependent and are difficult to obtain at constant value of magnetic moment as required by the theory. Due to these complications, no attempt was made to measure additional magnetostriction constants in the paramagnetic range.

D. Forced Magnetostriction

In the region above technical saturation, magnetostriction curves exhibit a small field dependence known as the forced magnetostriction. This is a volume effect arising chiefly from the field induced change in the magnetization above saturation. Starting with the Maxwell relation

$$\left(\frac{\partial V}{\partial H_{ext}}\right)_P = - \frac{\partial M}{\partial P}\Big|_{H_{ext}}, \tag{56}$$

and assuming a linear volume dependence of the magnetization, it can be shown (42) that the volume magnetostriction $\omega = \Delta V/V$ is given by:

$$\omega = \tfrac{1}{2}\frac{NI^2}{K} - \frac{1}{V_o}\int_o^{H_s} \frac{\partial}{\partial P}(VI)dH - \frac{I_s^o H_s \upsilon}{K} + \frac{I_s^o \upsilon}{K}(H_{ext} - NI_s) \tag{57}$$

Here $M = VI$ is the magnetic moment, N the demagnetizing constant, K the compressibility, I_s^o and H_s the undistorted saturation magnetization and field, I_s and H_{ext} the values of the magnetization and applied field above saturation, and υ is a constant describing the volume dependence of I_s^o. The first term in the expression is the dominant low field term

proportional to the square of the magnetization. It saturates when $I = I_s$. The second and third terms depend on the saturating field and not on the applied field. Their origin lies in the rotation of domains in the sample below saturation. The final term is the true volume forced magnetostriction and is linear in the applied field. As shown here the term is magnetically isotropic; however, Sato (58) has shown that in general the crystal anisotropy is field dependent, and this gives rise to an anisotropic forced magnetostriction.

Figures 36 and 37 show the forced magnetostriction of the a, b, and c axis of Dy and Tb as found from the high field slopes of the strain versus field curves. The values quoted for temperatures near the Néel temperature cannot be literally ascribed to forced magnetostriction as complete magnetic saturation cannot be obtained in the applied fields used here. The values given in this region were field dependent and were used only for correcting the magnetostriction constants to zero applied field. Points close to and above the Neel temperature were obtained from the slopes of strain versus H^2 plots.

Equation 55 gives a clue to the effect of pressure on the magnetization. As an example, combining the values of the a-, b-, and c-axis forced magnetostriction of Tb at 80° to obtain $\frac{\partial(\Delta V/V)}{\partial H} = \frac{\partial \omega}{\partial H} = -\frac{1}{V}\frac{\partial M}{\partial P}$ it is found that $\frac{\partial \omega}{\partial H}$ is negative indicating an increase in pressure will increase the magnetization. At $200^\circ K$, due to the large positive

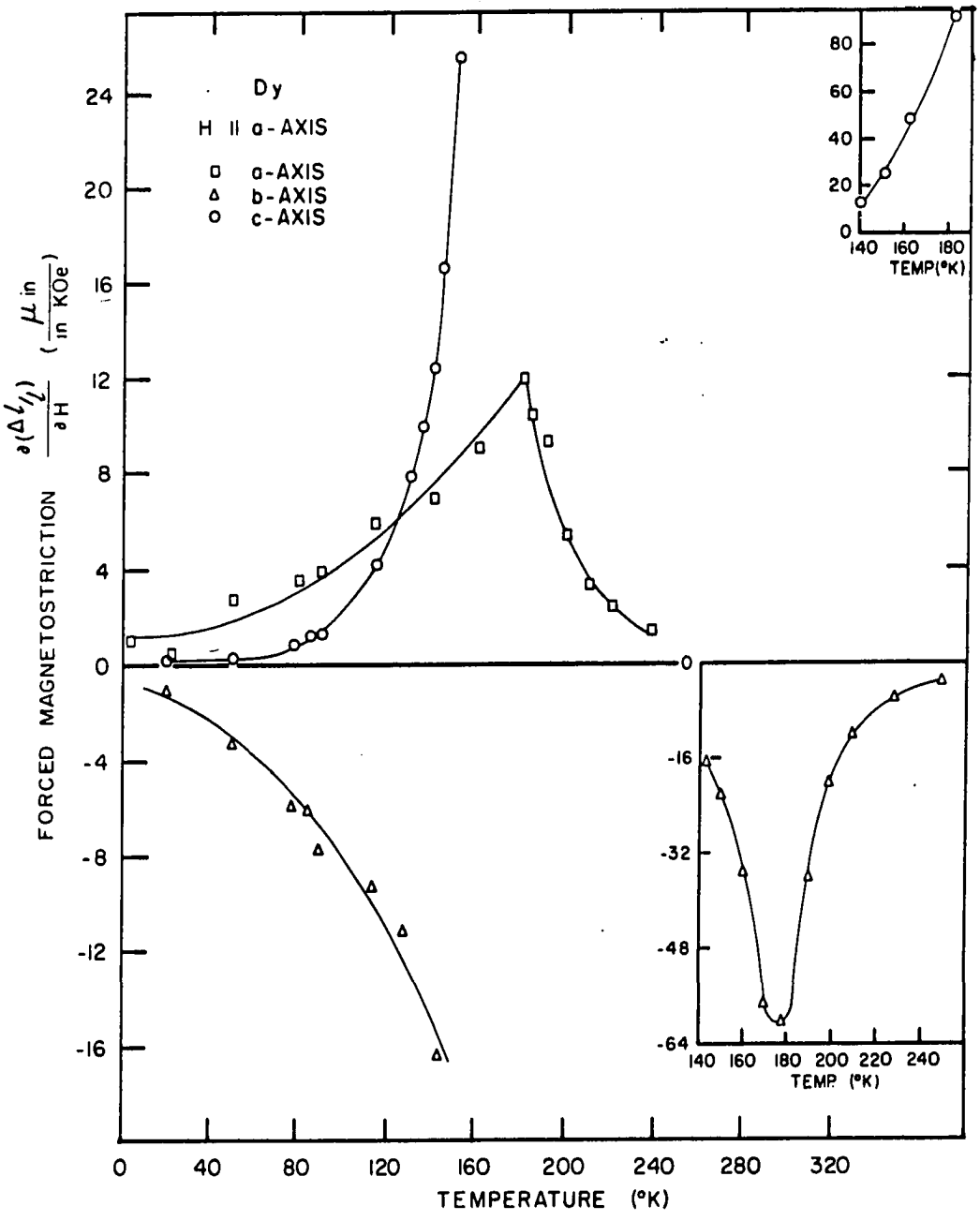

Figure 36. Forced magnetostriction of Dy in the a-, b-, and c-axis directions. The data points are the slopes of the high field region of the isothermal mangetostriction curves. The field was applied along the a axis. Values near the Néel temperature are field dependent and do not represent true saturation forced magnetostriction.

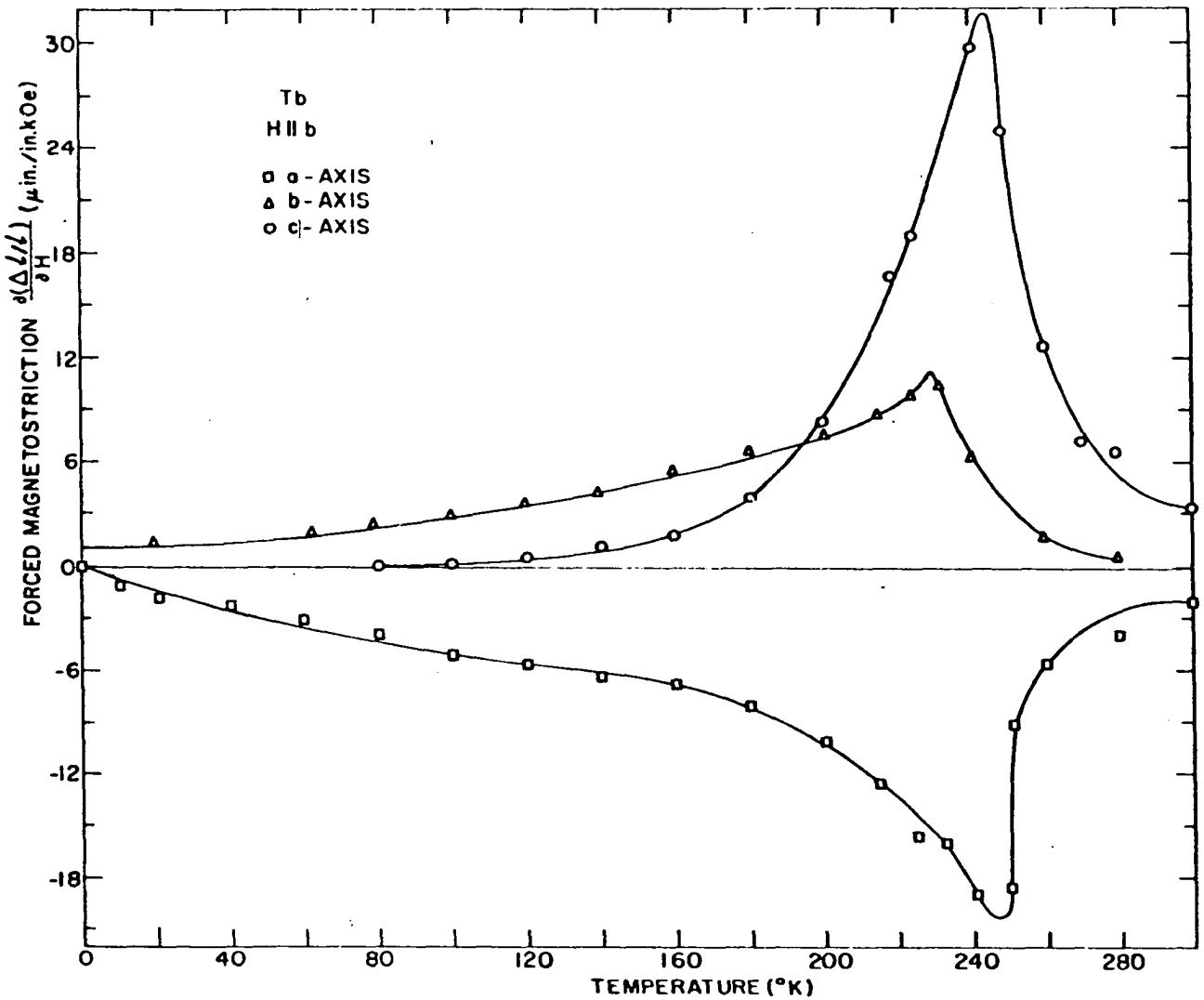

Figure 37. Forced magnetostriction of Tb in the a-, b-, and c-axis directions. The data points are the slopes of the high field region of the isothermal magnetostriction curves. The field was applied along the b direction.

contribution from the c axis, $\frac{\partial \omega}{\partial H}$ is positive indicating an increase in pressure lowers the magnetization.

The pressure dependence of the Curie temperature can be obtained from the forced volume magnetostriction under the assumptions of a theory by Kornetzki (40). He assumed that the change in saturation magnetization was the result of the volume dependence of the exchange integral or molecular field constant. In doing so it was possible to relate the pressure dependence of the Curie temperature to the volume magnetostriction by assuming $M_s = f(T/T_c)$ with T_c a function of volume. The exact functional form of f was not critical in his calculation. The result derived by Kornetzki for the pressure dependence of the Curie temperature is

$$\frac{1}{T_c}\frac{\partial T_c}{\partial P} = \frac{1}{T}\quad\frac{\partial \omega/\partial H}{(\partial M_s/\partial T)_P - 3\alpha K\,\partial \omega/\partial H}\quad , \tag{58}$$

where α is the thermal expansion, K is the compressibility, and the other quantities are the same as used previously. This theory and its assumptions have several inherent deficiencies which are discussed by Sato (58) who also gives details of some later work on the subject.

X. MAGNETOSTRICTION OF ERBIUM

The four magnetic states of erbium which are stable in zero applied field have been described previously. The application of a field produces striking distortions of these phases as is described in the next subsection. The nature of these distortions is quite different from that encountered in the helical phases of Dy due to the anisotropy energy.

In Er large negative values of the second and fourth order anisotropy constants (see Table 4) favor magnetic alignment along the c axis. A positive value of the sixth order constant K_6 produces a small basal plane component also (cone configurations). From these considerations the c axis is generally considered to be the easy magnetic direction.

A. Isothermal Measurements in Erbium

The a- and c-axis strains in Er as a function of field magnitude applied along the c axis are shown in Figure 38. The b-axis strain is essentially collinear with the a axis on this scale. Curves are shown for both the sinusoidal c-component region ($53^\circ < T < 85^\circ$) and quasi-antiphase-domain ($18^\circ < T < 53^\circ$) regions of Er. It was mentioned earlier that this type of measurement in ferromagnets is highly non-reproducible due to random domain effects. This objection does not exist in Er since the zero field state is a unique and reproducible magnetic configuration. The large strains shown in the figure at 20°, 29°, and 47° result from

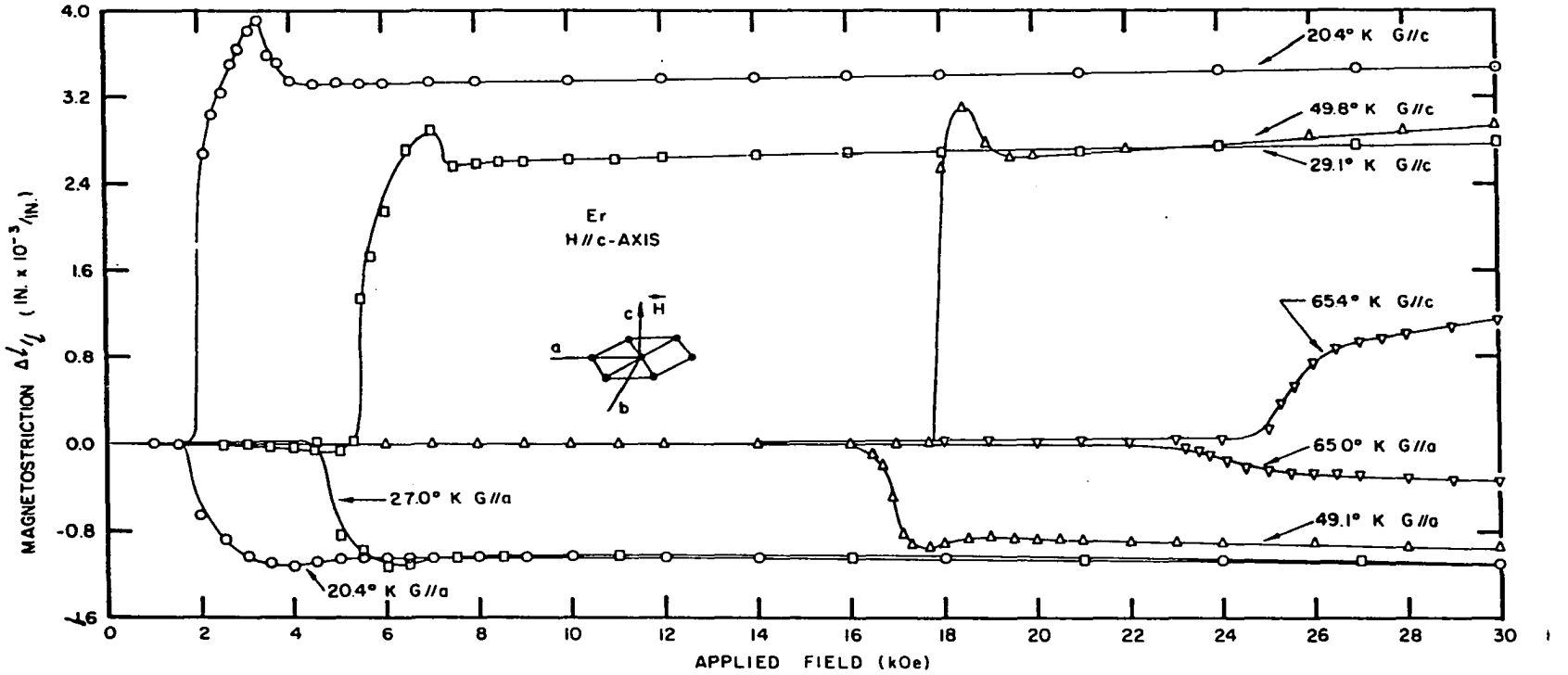

Figure 38. Magnetostriction of Er as a function of field applied along the c axis. Temperatures below 53°K correspond to the quasi-antiphase-domain structure in zero external field. The 65°K curves are in the modulated moment phase. G indicates the strain gage direction.

the destruction of the intermediate magnetic phase in favor of ferromagnetic alignment along the c axis. Actually, complete alignment of the moment along the c axis is probably not accomplished due to the magnetic anisotropy. The quasi-antiphase-domain is spontaneously destroyed by the anisotropy energy at 18°K in favor of conical ferromagnetism. At higher temperatures, increasingly higher critical applied fields are required to effect the transition as shown in the figure. At 64°K the strain produced above the critical field presumbly arises from a field induced modification of the sinusoidal c-component structure in opposition to the exchange field. Below 18°K application of a c-axis field produced very small strains due to the extremely high axial magnetic anisotropy as shown in Figure 39. Very little modification of the zero field conical state is apparently produced by the c-axis field. This is also confirmed by the magnetic moment work of Green (29). He measured a c-axis moment at 18 kOe of 7.9 μ_B which is close to the zero field neutron diffraction result (13) at 7.2 μ_B (ignoring conduction electron polarization).

Application of a field along a basal plane direction below 18°K produced the striking effect shown in Figure 40. Negligible strain (corresponding to no modification of the magnetic structure) was observed up to about 18.5 kOe at which point a fairly large strain was observed in all three axes. This critical field of approximately 18.5 kOe is independent of temperature within experimental accuracy from 15°K

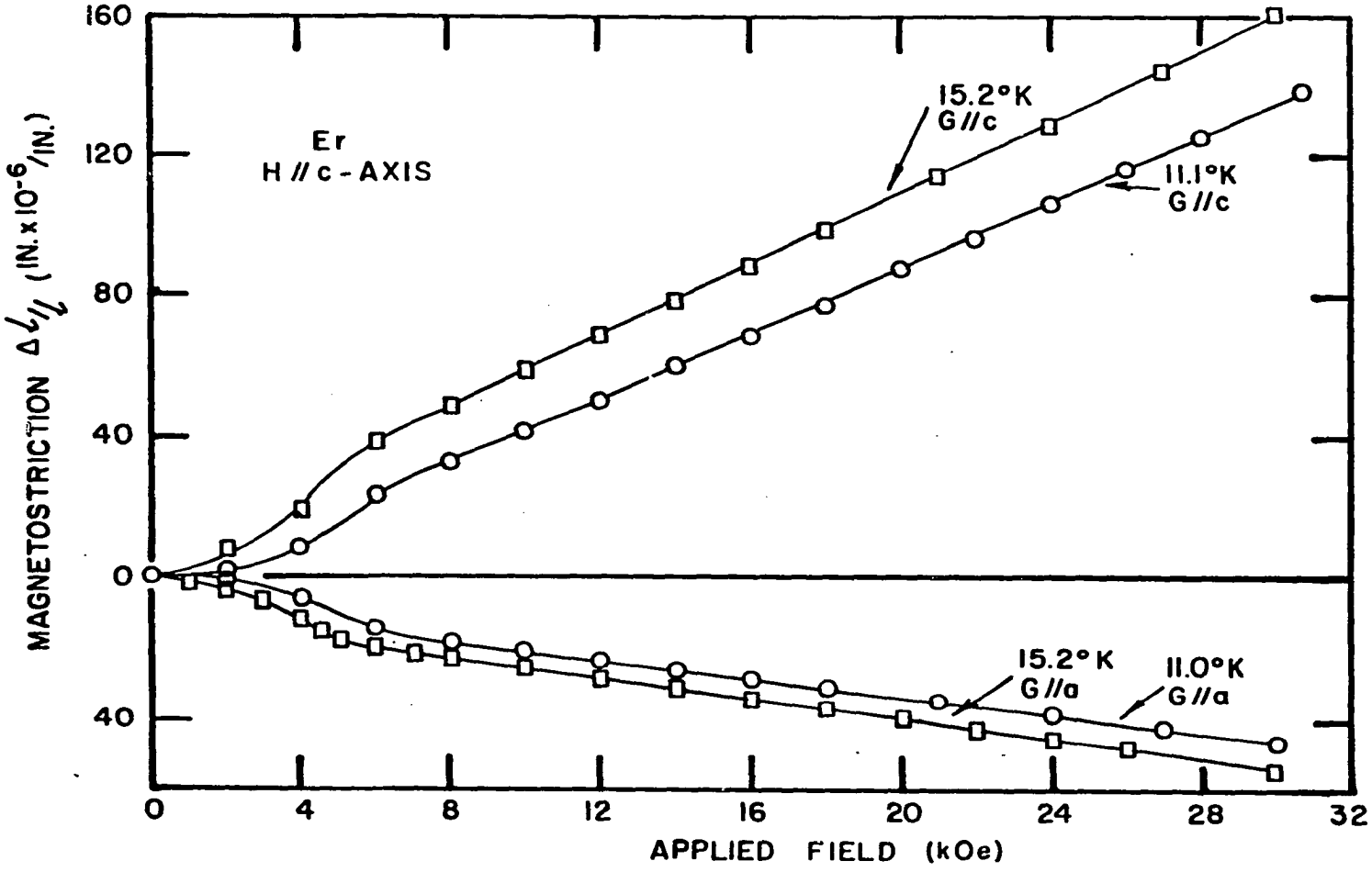

Figure 39. Magnetostriction of Er as a function of applied field in the conical ferromagnetic region. The field was applied along the c axis.

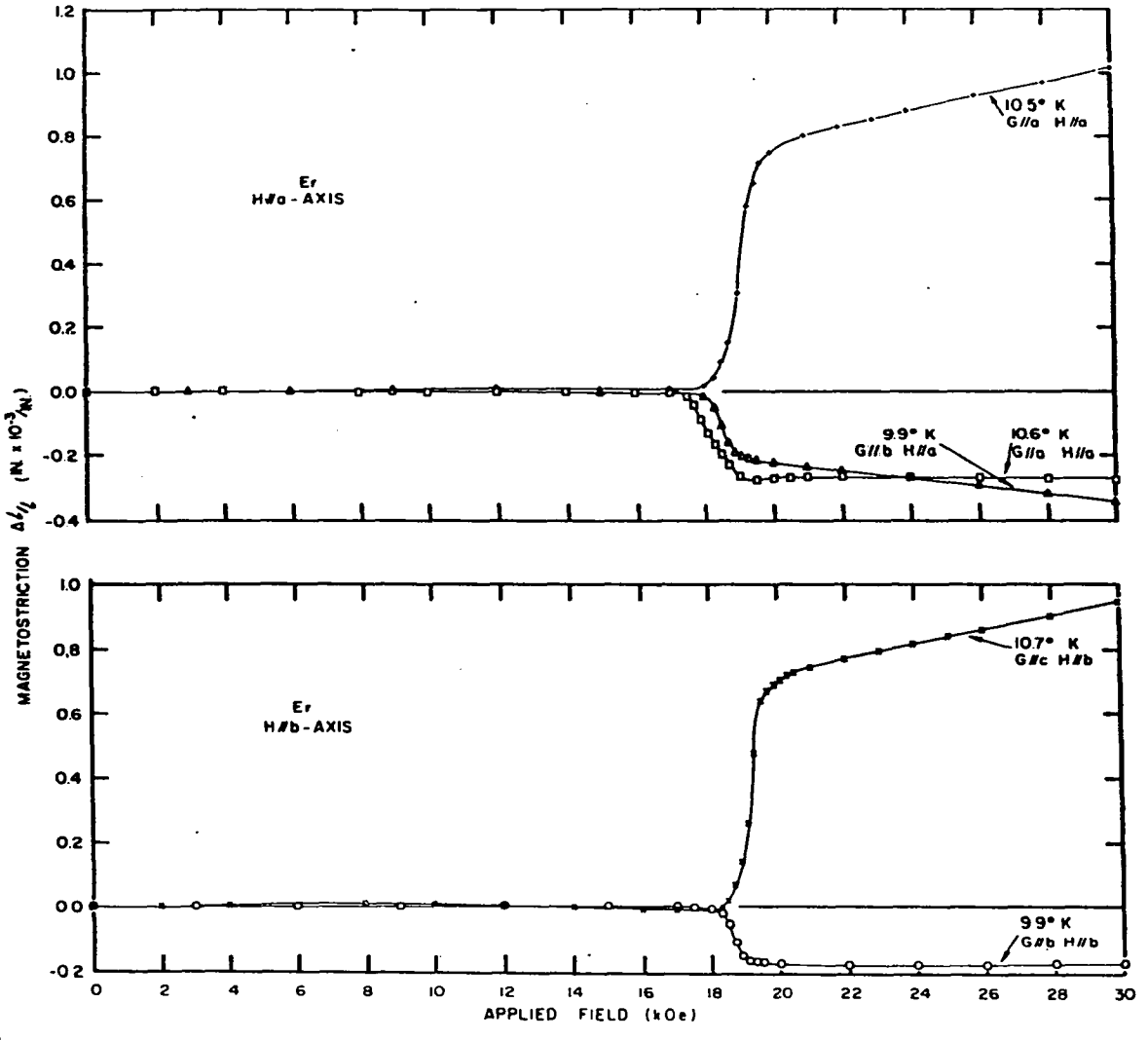

Figure 40. Magnetostriction of Er as a function of applied field in the conical ferromagnetic temperature range. The field was applied along the a axis in the upper figure and along the b axis in the lower figure.

down to 4.2°K. Only small temperature variations in strain magnitude were observed. The prominent features of this effect are the essentially isotropic contraction of the basal plane and expansion of the c axis which results from application of the field along either the a or b axis. This indicates the magnetostrain is dominated by the change in the exchange energy terms and not by the six fold anisotropy energy in contrast to Dy and Tb. Basal plane strain measurements made perpendicular to the field direction exhibited larger strain variations above the "knee" of the curve than those made parallel to the field directions as shown in the figure.

Flippen (27) has measured the magnetic moment of an a-axis Er crystal in static fields up to 56 kOe. He found a value of 3.8 Bohr magnetons/ion along the field direction. This is somewhat lower than the value of 4.1 μ_B found by Cable et al. (13) by neutron diffraction for the basal plane component in zero applied field. This observation, together with the larger variation of the magnetostrain measured perpendicular to the field direction mentioned above, lead to the postulate shown in Figure 41 about the effect of an applied field on the Er magnetic structure. It is conjectured that the application of a basal plane field above about 18 kOe partially overcomes the exchange field and breaks the conical magnetic moment distribution (a) down into a "fan-like" configuration (b) about the field direction. The relatively larger variation of magnetostrain

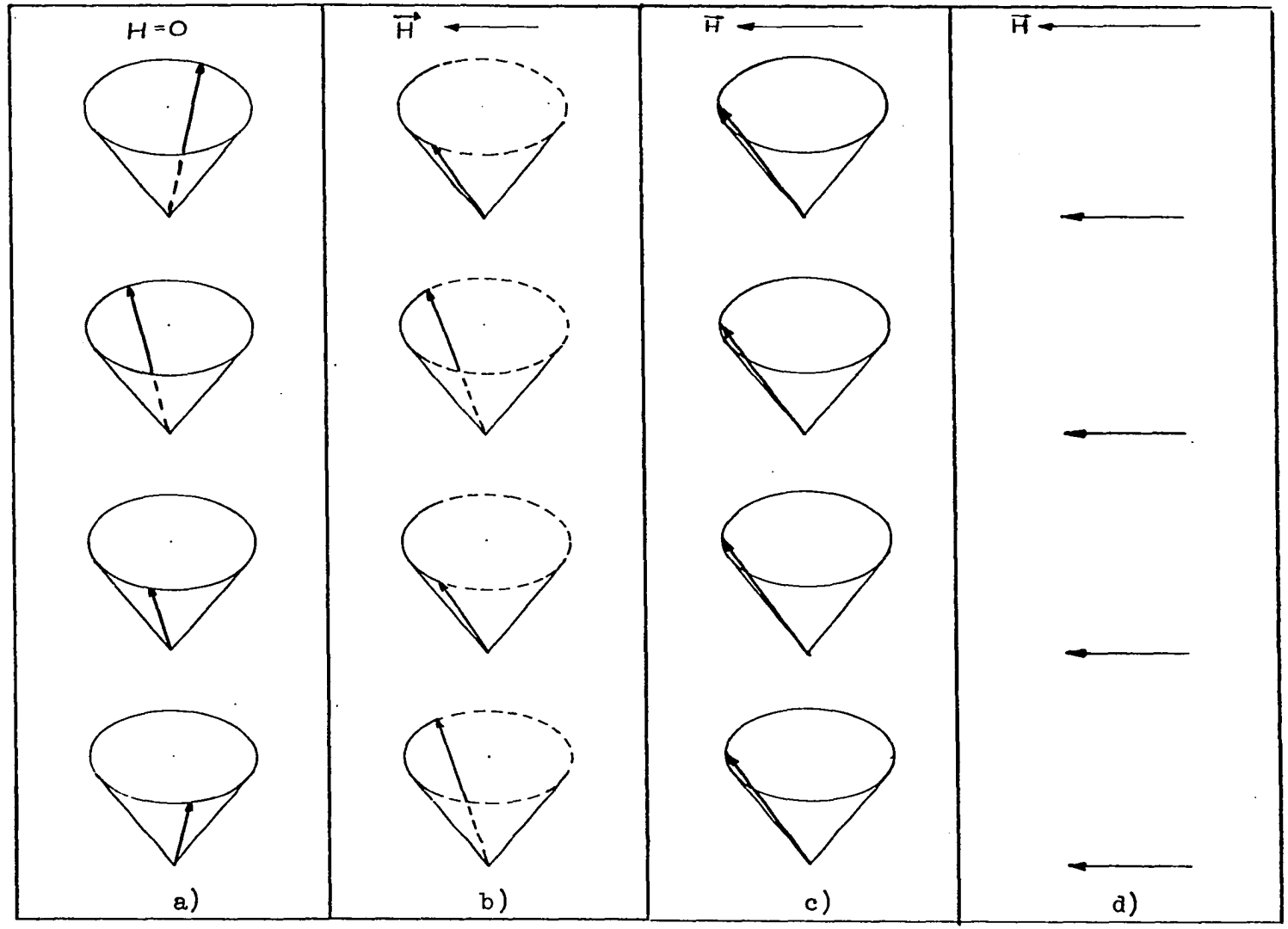

Figure 41. Influence of progressively larger magnetic fields applied in the basal plane of Er below 20°K.

perpendicular to the field direction suggests that the spread of the fan may be smoothly decreased by increased fields in opposition to the exchange force. At fields higher than present measurements extend, the fan may disappear in favor of ferromagnetic alignment in the plane containing the c axis and the applied field direction (c). Conceivably this could also be accompanied by some modification in the apex angle of the cone in opposition to the large axial anisotropy energy. Eventually fields large enough to overcome the anisotropy would produce ferromagnetic alignment in the basal plane along the field direction (d).

The magnetostriction resulting from application of a basal plane field is shown in Figures 42 and 43 in the quasi-antiphase-domain region. The figures indicate considerable modification of the magnetic state is induced by the field. An initial expansion is observed along the field direction accompanied by a transverse contraction. This initial behavior is proportional to H^2 indicating no ordering has occurred. A reversal in slope occurs at higher fields. From Figure 43 the parallel magnetostrictions along either the a or b axis are seen to be equivalent after correcting for the difference in measurement temperature.

The results of the magnetostriction measurements in the sinusoidal c-component temperature range are shown in Figure 44. The strain is proportional to the square of the applied field, showing that no change in the state of magnetic order is produced by the application of a

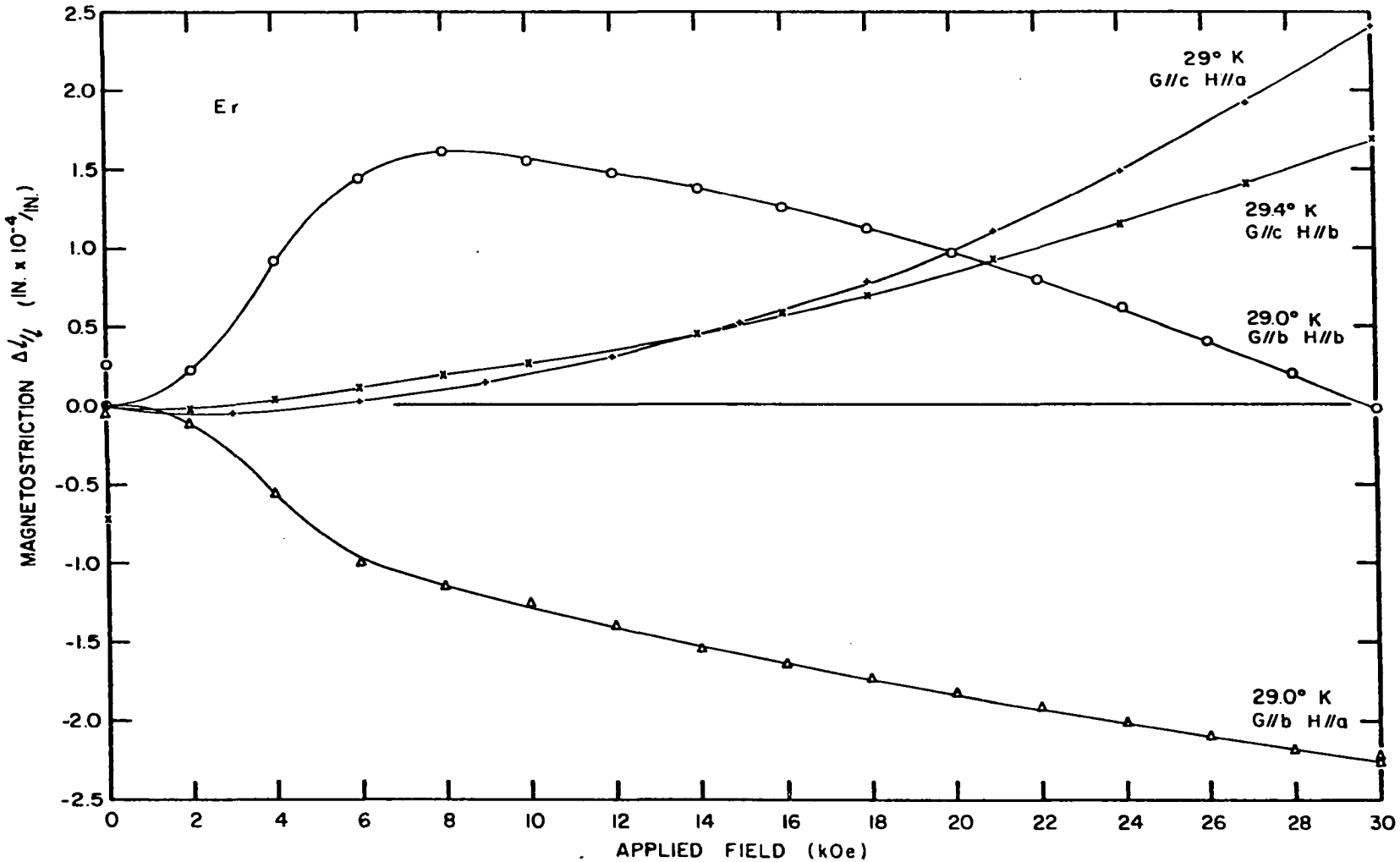

Figure 42. Magnetostriction of Er as a function of applied field in the quasi-antiphase-domain temperature region. The field was applied in the basal plane.

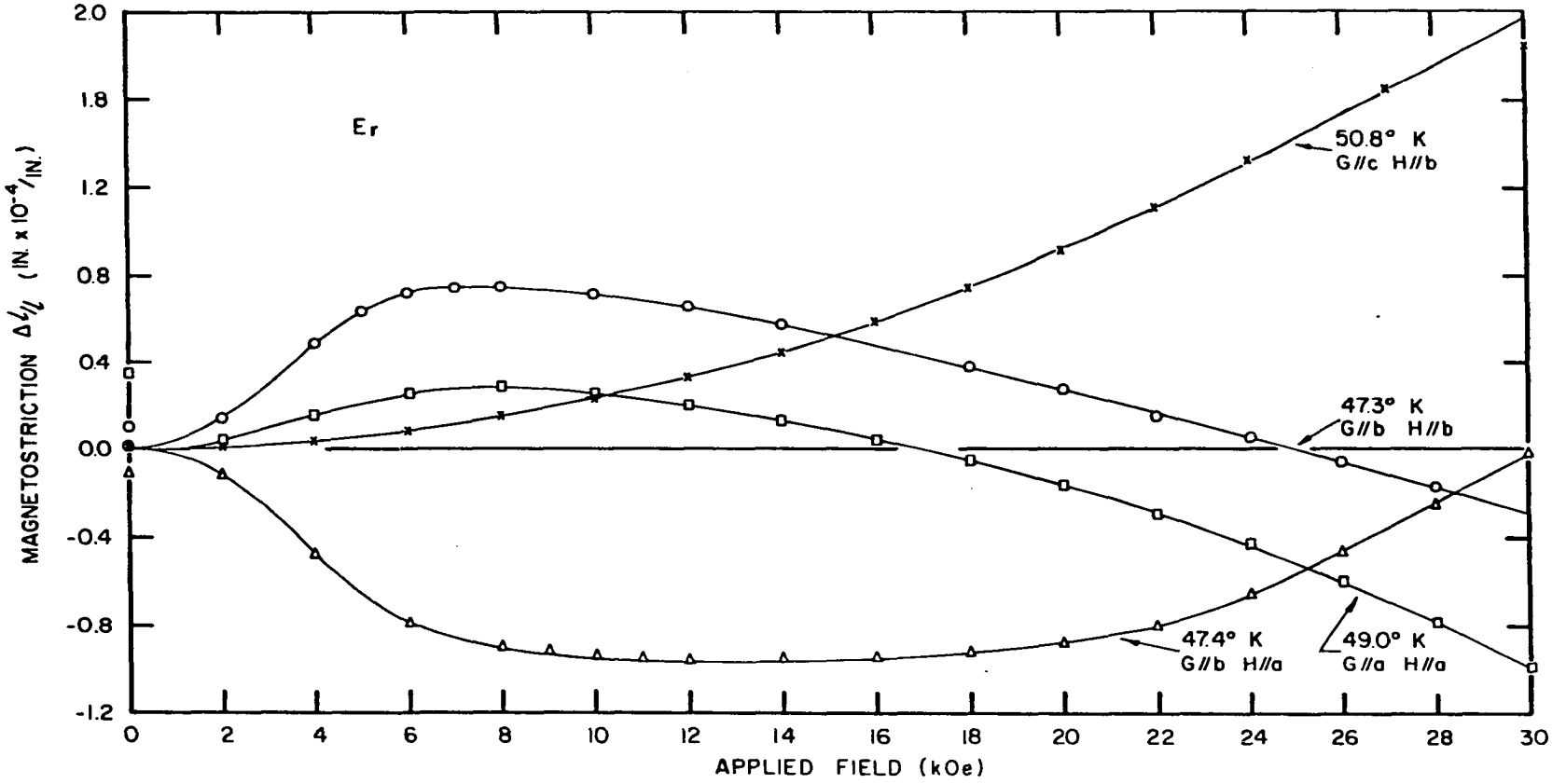

Figure 43. Magnetostriction of Er as a function of applied field in the quasi-antiphase-domain temperature range. The field was applied in the basal plane.

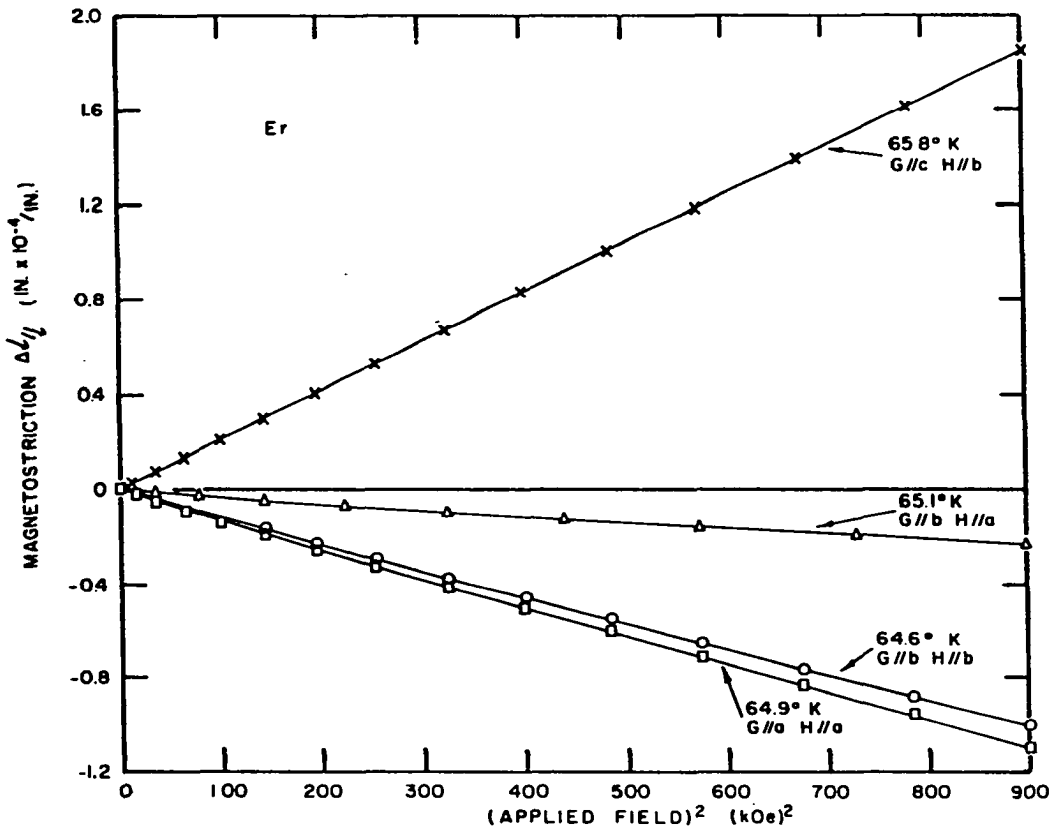

Figure 44. Magnetostriction of Er as a function of H^2 applied in the basal plane. The curves shown are in the modulated moment temperature range. G indicates the strain gage direction.

field in the basal plane at this temperature.

In the paramagnetic temperature range ($T > 85^{\circ}K$), the magnetostriction is again proportional to H^2 as shown in Figure 45 for the field applied along the c axis. Similar H^2 dependence was obtained for the magnetic field along the b axis.

B. Erbium Field Rotation Measurements

1. Constants--second order theory

As is indicated later in this section, the basal plane (six fold) anisotropy of Er is sufficiently small that a second order theory is sufficient to describe the magnetostriction. Retaining only terms up through second order ($\ell = 0$ and 2) the magnetostriction expression (Equation 13) becomes:

$$\frac{\Delta\ell}{\ell} = [\lambda_1^{\alpha,0} + \lambda_1^{\alpha,2}(\alpha_z^2 - \tfrac{1}{3})](\beta_x^2 + \beta_y^2) + [\lambda_2^{\alpha,0} + \lambda_2^{\alpha,2}(\alpha_z^2 - \tfrac{1}{3})]\beta_z^2$$

$$+ \tfrac{1}{2}\lambda^{\gamma,2}[(\alpha_x\beta_x + \alpha_y\beta_y)^2 - (\alpha_x\beta_y - \alpha_y\beta_x)^2]$$

$$+ 2\lambda^{\epsilon,2}(\beta_x\alpha_x + \beta_y\alpha_y)\beta_z\alpha_z \qquad (59)$$

This expression corresponds to cylindrical symmetry.

In rotation measurements on Er at low temperatures with the field applied in the basal plane, the magnetization will be constrained by the anisotropy energy to move on the surface of a cone of half apex angle ϕ. If the angle of the applied field (or of the projection of the magnetic

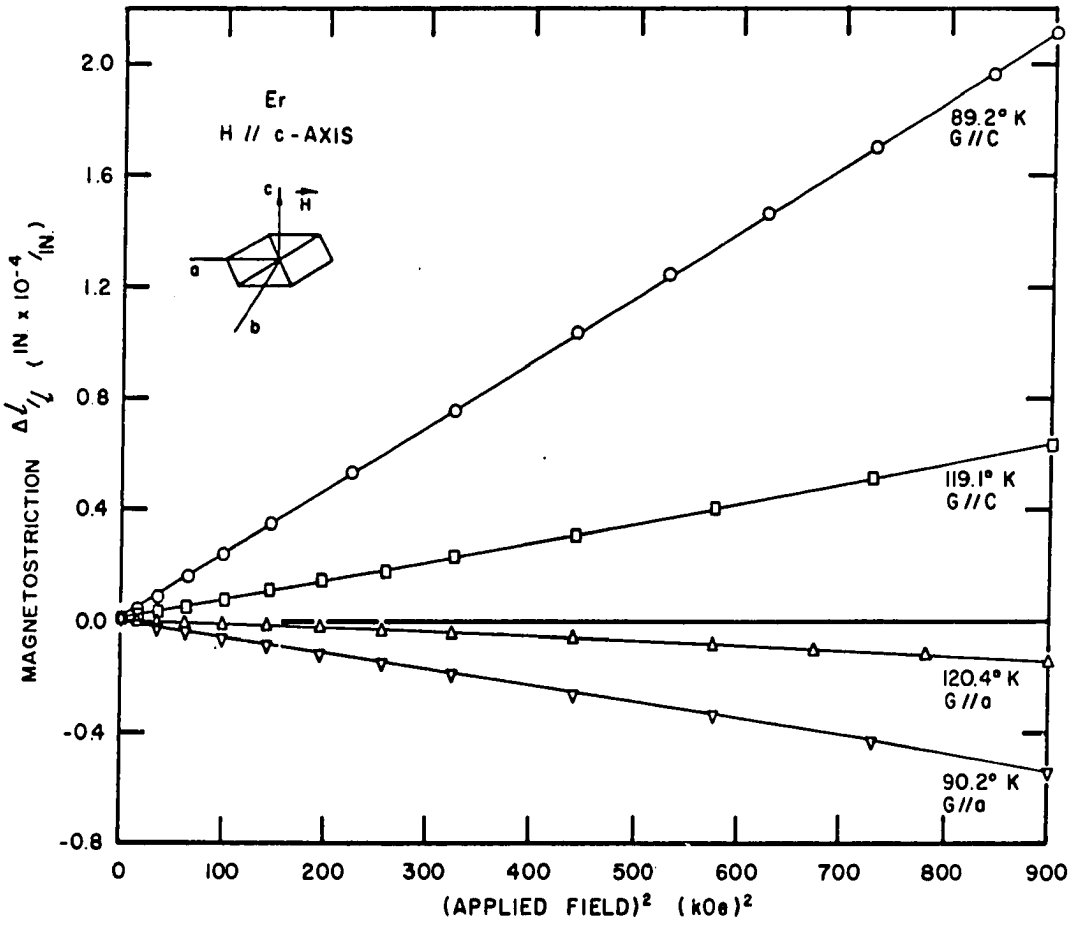

Figure 45. Magnetostriction of Er in the paramagnetic temperature range as a function of the square of the applied field. G refers to the strain gage direction. The field was applied along the c axis.

moment on the basal plane) relative to the a axis is θ_a, then the angle dependence of the anisotropic constant $\lambda^{\gamma,2}$ can be written,

$$\tfrac{1}{2}\lambda^{\gamma,2}\sin^2\phi\,[(\beta_x\cos\theta_a+\beta_y\sin\theta_a)^2 - (\beta_x\sin\theta_a-\beta_y\cos\theta_a)^2]\,. \qquad (60)$$

On subtracting the reference strain in the state $\theta = 0^\circ$, the second order expression for the rotation magnetostriction appropriate to Er becomes:

$$\frac{\Delta\ell}{\ell}\Big|_{a,b}^{\theta'_a} = \mp\,\lambda^{\gamma,2}\sin^2\phi\,\sin^2\theta'_a = \mp\,2C\,\sin^2\phi\,\sin^2\theta'_a \qquad (61)$$

The $\mp$ signs pertain to the a- and b-axis strains respectively. The constant C may thus be calculated in the conical magnetic states if the cone angle is known.

Below 19°K the neutron diffraction results indicate a c-axis component of the moment of 7.2 μ_B and a basal plane component of 4.1 μ_B. This corresponds to a cone angle $\phi = 30^\circ$. In a 56 kOe applied field, Flippen (27) measured an a-axis moment of 3.8 μ_B. Thus, within experimental uncertainty, one can assert that the cone angle is not changed by a-axis fields of this magnitude.

2. Field rotation results

The results of the measurement of the b-axis strain versus angle θ'_a in Er at 15°K and 4.6°K in a 30 kOe field are shown in Figure 46. The reasonably close fit to the $\sin^2\theta$ curve indicates a small six fold

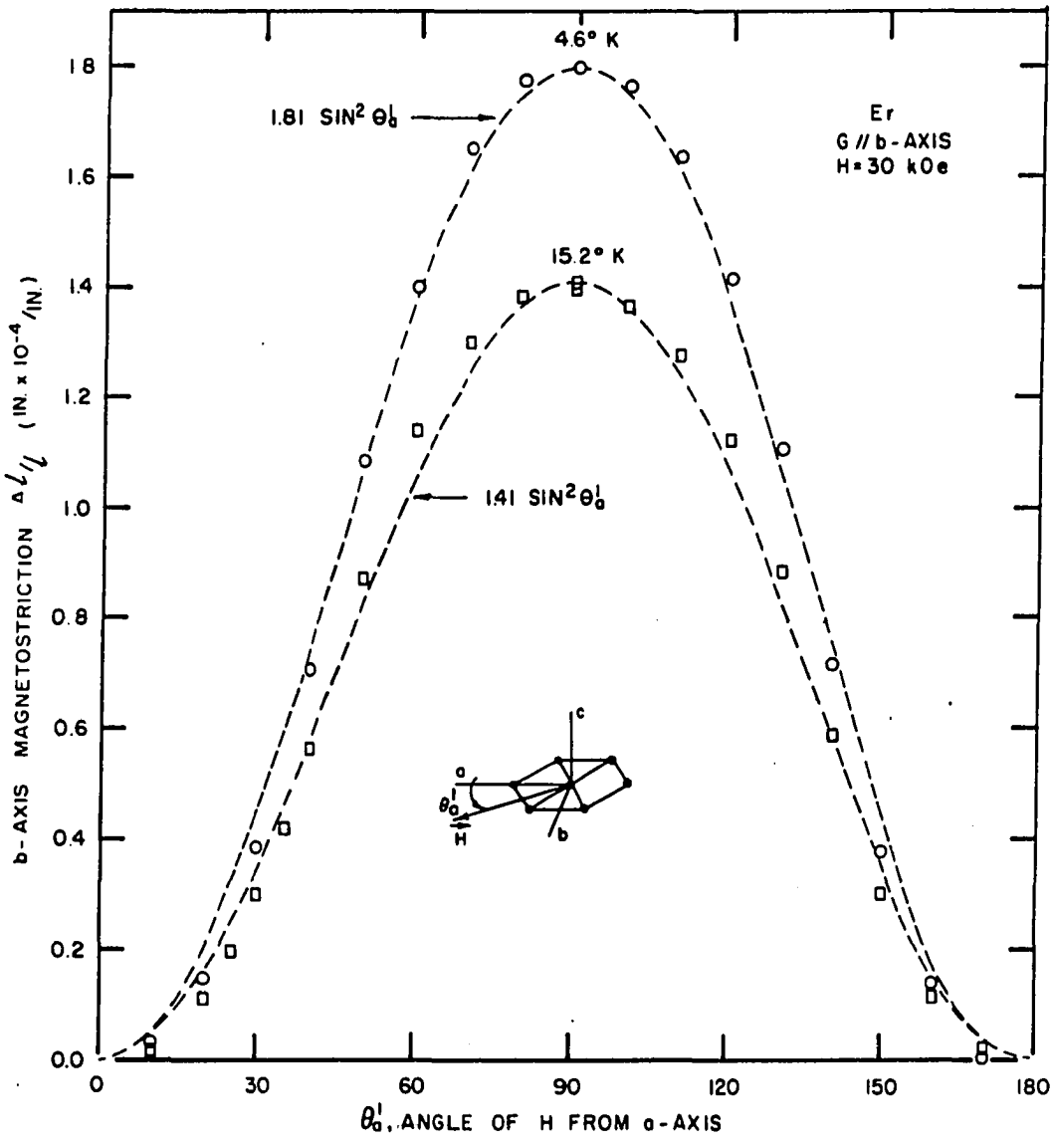

Figure 46. Second order theoretical fit and experimental results for the b-axis magnetostriction of Er as a function of the angle of the applied field relative to the a axis. The 30 kOe field was applied in the basal plane. The zero external field state is one of conical ferromagnetism at these temperatures.

anisotropy. From these measurements and assuming $\phi = 30^{\circ}$, a value C = 362 micro-inches/inch is obtained at $4.6^{\circ}K$ and a value C = 282 micro-inches/inch at $15.2^{\circ}K$.

Figure 47 shows the magnetostrain versus applied field angle in the quasi-antiphase-domain temperature range. In the temperature range shown, the strain magnitude and signare a function of field strength as seen from the $47^{\circ}K$ curves here or from the isothermal data of Figures 42 and 43. Due to the lack of knowledge about the exact details of the field-induced modifications of the quasi-antiphase-domain structure values of the constant C cannot be precisely calculated. If the moment remains in a conical configuration, then the $\theta'_a = 90^{\circ}$ strain is proportional to C. Under this assumption, C becomes negative at higher fields in the $47^{\circ}K$ measurements. The results of rotation measurements in the modulated moment region above the $53^{\circ}K$ transition and in the paramagnetic range above $85^{\circ}K$ are shown in Figure 48. The values of C above $53^{\circ}K$ are consistently negative and exhibit an H^2 field dependence.

3. Theoretical value of C at $T=0^{\circ}K$

From these data and the a-axis magnetic moment data of Green (29), the anticipated value of the constant C at T=0 may be calculated using the Callen theory (Equation 44 with $\ell = 2$). The value of the magnetic moment at T = 0 was taken to be the theoretical value of 300 emu/gm. A value of C(T=0) = -2600 micro-inches/inch was calculated by the

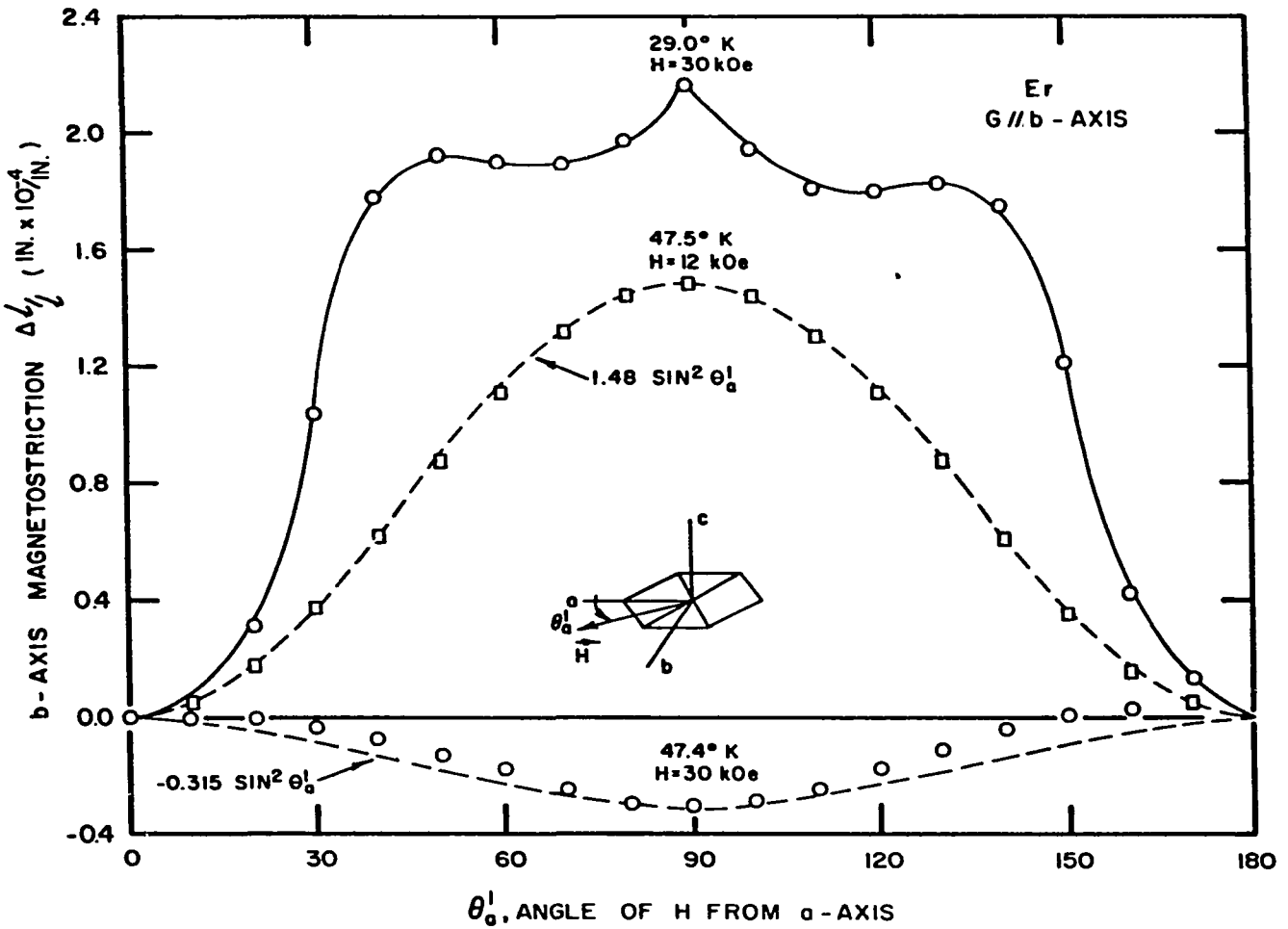

Figure 47. The b-axis magnetostriction of Er as a function of applied angle relative to the a axis. The field was applied in the basal plane. Note the opposite signs of the 47°K curves at the two fields shown. These temperatures correspond to the quasi-antiphase-domain structure in zero applied field.

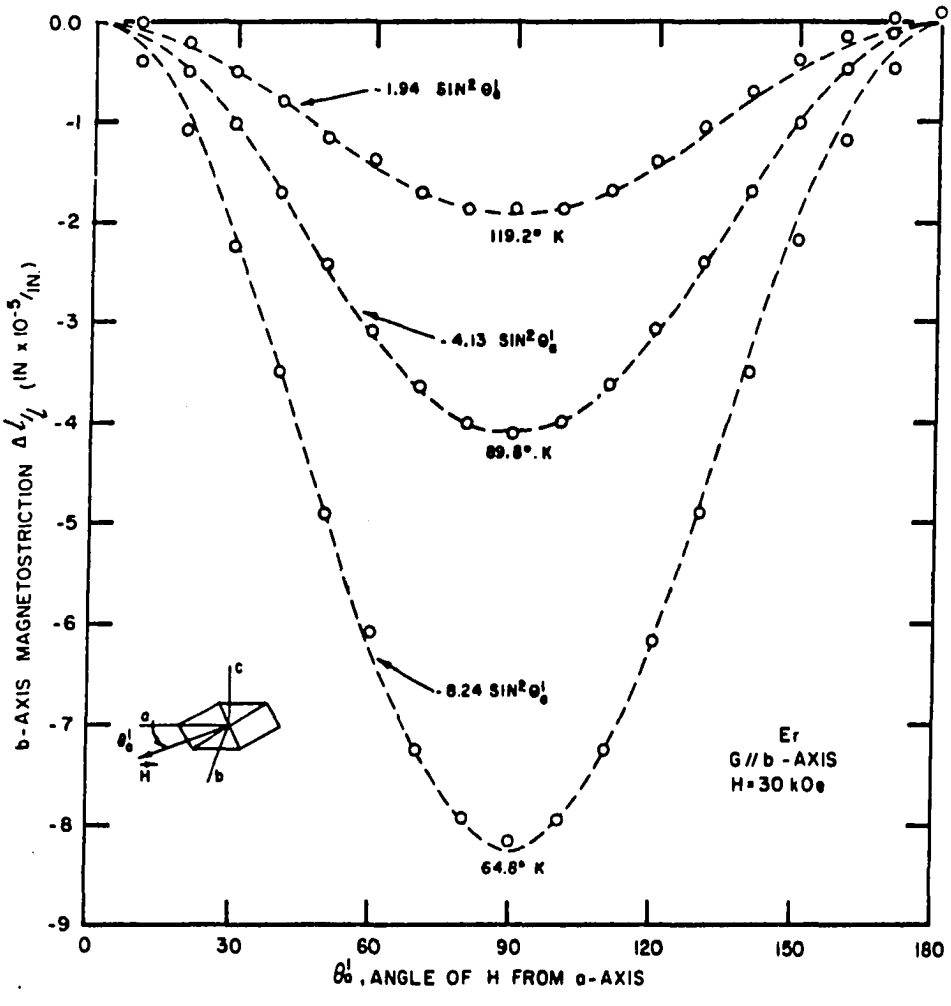

Figure 48. Second order theoretical fit and experimental results for the b-axis magnetostriction of Er as a function of applied field angle relative to the a axis. The 30 kOe field was applied in the basal plane. At 64.8°K in zero external field Er has the modulated moment magnetic state. At the other temperatures Er is paramagnetic.

method using the data shown in Figure 48.

Tsuya, Clark and Bozorth (65) have calculated the one ion magnetoelastic coupling coefficients in the rare earths considering the effects of the distortion of the crystal field by the nearest neighbor positive ions and the field arising from the strained charge distribution of the conduction electrons. Their theory predicts negative values for the constant C in Er due to the prolate form of the 4f electron charge cloud in contrast to the oblate nature of the distribution in Dy, Tb, and Ho which gives rise to a positive magnetostriction. The positive values of C found in Er at low temperatures are thus not in accord with this theory. The discrepancy may be due to a large contribution from the exchange energy which is not properly accounted for by the one ion terms used in the theory of Tsuya et al.

C. Temperature Dependence of Er Strain

Figure 49 shows the temperature dependence of the a-, b-, and c-axis strains as a function of temperature. Curves are shown for zero field and for a 30 kOe field applied along the c axis. The a- and c-axis curves also show the strain resulting from application of a 30 kOe field along the a axis. The zero field curves show inflection points at about 55° and 85°K corresponding to changes in the states of magnetic order. The similarity between the a- and b-axis curves again demonstrates the essential absence of basal plane anisotropy in Er. At

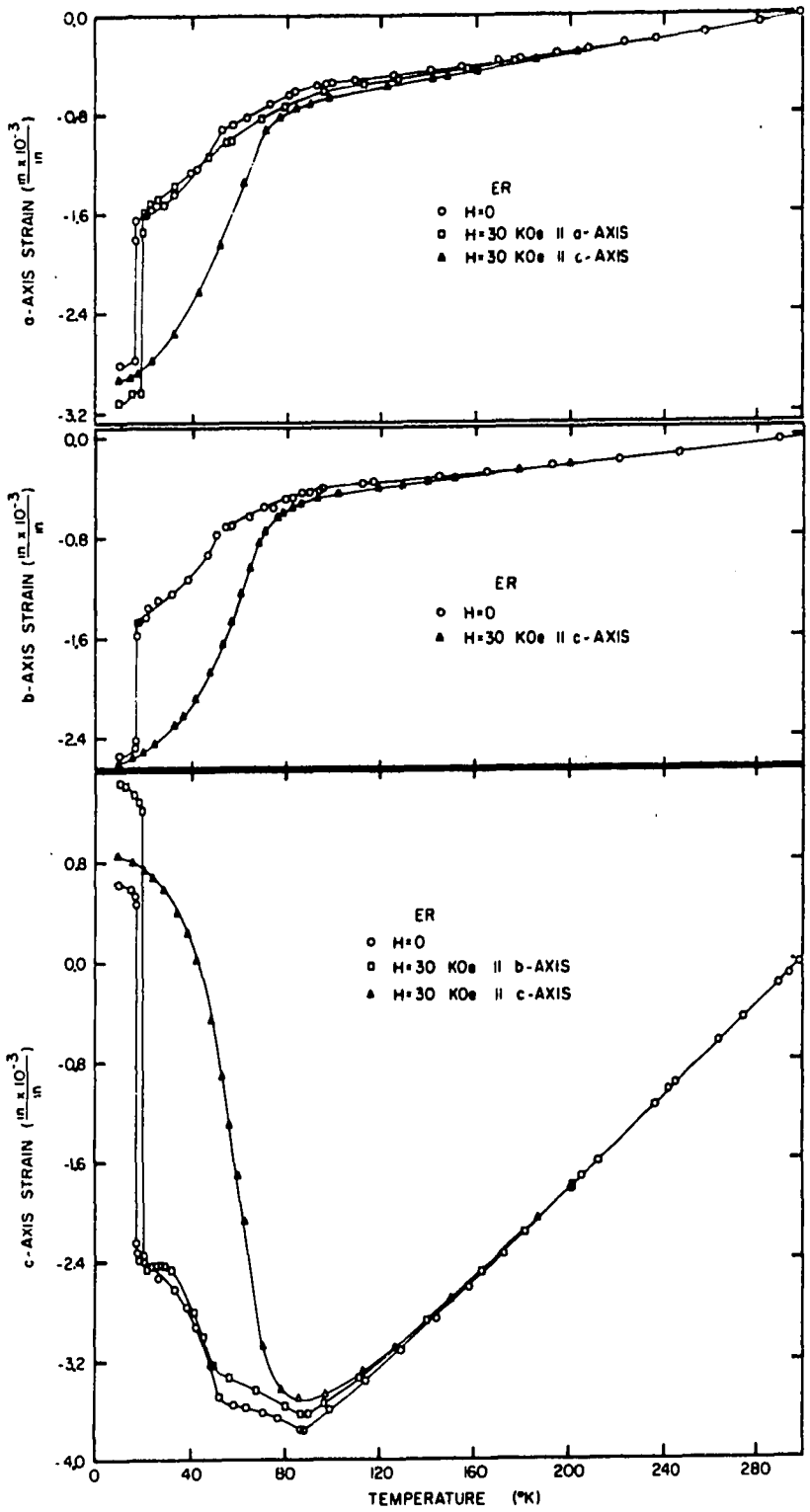

Figure 49. The a-, b-, and c-axis strain of Er as a function of temperature in zero field and in a 30 kOe field applied along the c axis. Results are also given for the a- and c-axis strain with the field applied in the basal plane.

the lowest transition temperature, large discontinuities are observed in the zero field strain corresponding to the large change in exchange energy as the axial anisotropy annihilates the quasi-antiphase-domain in favor of the conical ferromagnetic structure. As opposed to Dy and Tb, this change is not accompanied by an orthorhombic distortion of the hexagonal lattice as shown from the X-ray studies of Darnell (20). The conical ferromagnetic transition occurs spontaneously at 17.5°K and can be induced by a 30 kOe field applied in the basal plane at 20°K. It is noted that from 20°K to 17.5°K two states are stable in a field--the fan-ferro state formed by application of the field in the basal plane and c-axis conical ferromagnetic alignment produced by the c-axis field. This situation, resulting from a metastable anisotropy energy near the spontaneous transition, is shown in Figure 50.

As indicated above, the cone angle is not significantly modified by the application of a 30 kOe c-axis field below 18°K. Figure 49 shows that the strain measured in a c-axis field is a continuous function of the temperature across the 20°K transition. This lends support to the earlier statement that at 20°K there is no discontinuous change from conical ferromagnetism to c-axis ferromagnetic alignment. Presumably a conical structure is stable in a field well into the quasi-antiphase-domain region.

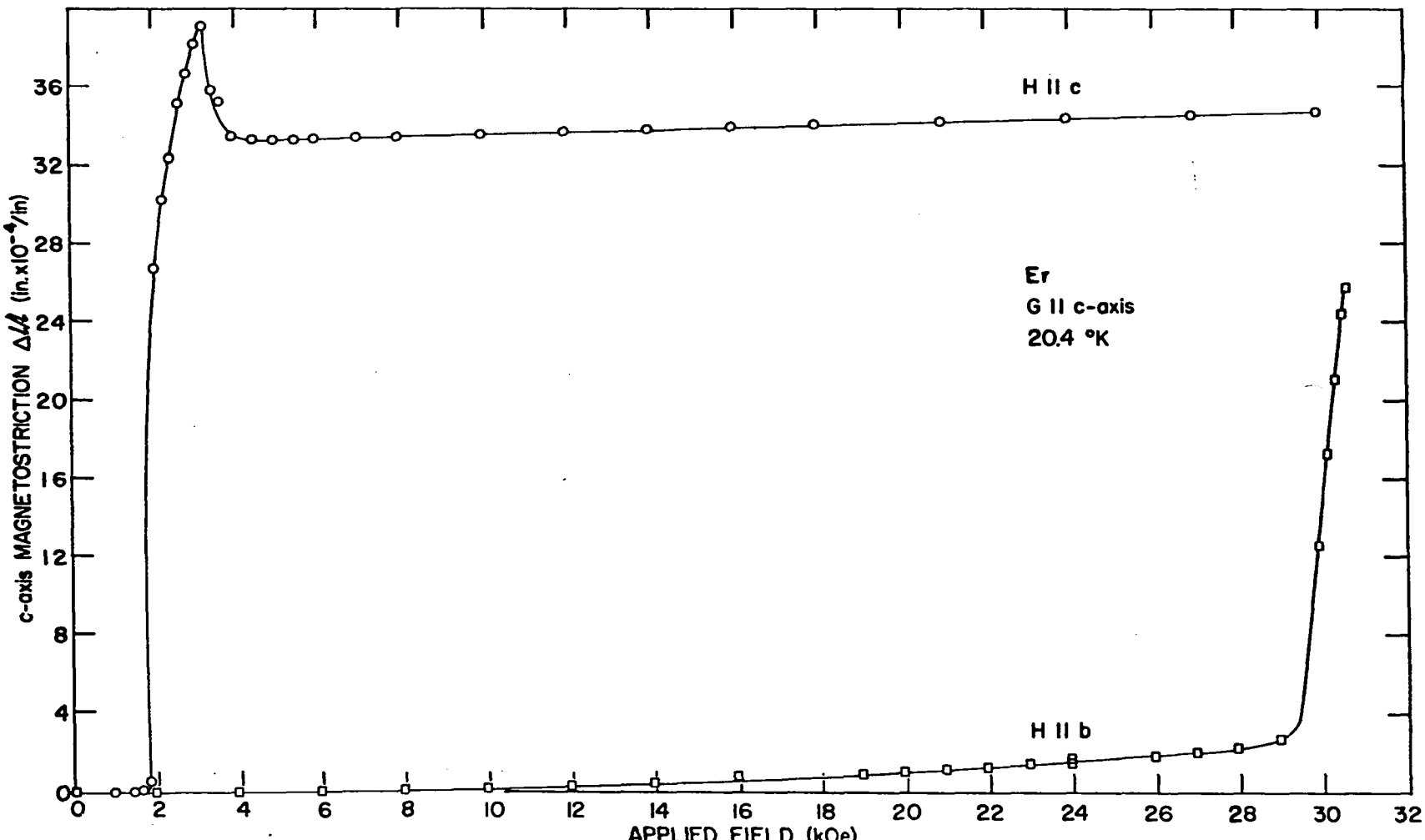

Figure 50. Metastable nature of the magnetic states of Er at 20°K. The 30 kOe field provides energy sufficient to remove the quasi-antiphase-domain state when applied along the c axis, or to produce the fan-ferromagnetic phase when applied in the basal plane.

No attempt was made to calculate the remaining constants in Equation 59 due to uncertainties about the nature of the field induced magnetic states. As is seen from the results presented here, the effect of a magnetic field on the magnetic structure of Er is quite pronounced. Neutron diffraction experiments performed in high fields (> 50 kilogauss) should provide considerable insight into the exact nature of these field induced modifications.

XI. BIBLIOGRAPHY

1. Alstad, J., The magnetostriction of gadolinium and holmium single crystals, unpublished Ph.D. thesis, Ames, Iowa, Library, Iowa State University of Science and Technology, 1963.

2. Alstad, J. and S. Legvold, J. Appl. Phys., 35, 1752 (1964).

3. Beenakker, J.J.M. and C. A. Swenson, Rev. Sci. Instrum., 26, 1204 (1955).

4. Behrendt, D. R., S. Legvold and F. H. Spedding, Phys. Rev., 109, 1544 (1958).

5. Belov, K. P., R. Z. Levitin and S. A. Nikitin, Soviet Physics Uspekhi, 7, 179 (1964).

6. Belov, K. P., R. Z. Levitin, S. A. Nikitin and A. V. Ped'ko, Soviet Physics-JETP, 13, 1096 (1961).

7. Birss, R. R., Advances in Physics 8, 252 (1959).

8. Bitter, F., Introduction to ferromagnetism, New York, McGraw-Hill Book Company, 1937.

9. Bozorth, R. M., Ferromagnetism, New York, D. Van Nostrand, Inc., 1951.

10. Bozorth, R. M., Phys. Rev., 96, 311 (1954).

11. Bozorth, R. M. and T. Wakiyama, J. Phys. Soc. Japan, 17, 1669 (1962).

12. Bozorth, R. M. and T. Wakiyama, J. Phys. Soc. Japan, 18, 97 (1963).

13. Cable, J. W., E. O. Wollan, W. C. Koehler and M. K. Wilkinson, J. Appl. Phys., 32, 49S (1961).

14. Callen, E. R. and H. B. Callen, Phys. Rev., 129, 578 (1963).

15. Callen, E. R., A. E. Clark, B. F. DeSavage and W. Coleman, Phys. Rev., 130, 1735 (1963).

16. Clark, A. E., R. M. Bozorth and B. F. DeSavage, Phys. Letters 5, 100 (1963).

17. Clark, A. E., B. F. DeSavage and R. M. Bozorth, Phys. Rev., 138, A216 (1965).

18. Corner, W. D. and F. Hutchinson, Proc. of the Royal Society, 75, 781 (1960).

19. Darnell, F. J., Phys. Rev., 132, 128 (1963).

20. Darnell, F. J., Phys. Rev., 132 1098 (1963).

21. deGennes, P. G. and J. Friedel, J. Phys. Chem. Solids, 4, 71 (1958).

22. Elliott, J., J. Phys. Soc. Japan, 17, Suppl. B1, 1 (1962).

23. Elliott, J., Phys. Rev., 124, 346 (1961).

24. Enz, U., J. Appl. Phys., 32S, 22 (1961).

25. Enz, U., Physica, 26, 698 (1960).

26. Finnemore, D. K., J. E. Ostenson and T. F. Stromberg, U.S. Atomic Energy Commission Report IS-1046 [Iowa State Univ. of Science and Technology, Ames. Inst. for Atomic Research] (1964).

27. Flippen, R. B., J. Appl. Phys., 7, 2026 (1963).

28. Goldman, J. E. and R. Smoluchowski, Phys. Rev., 75, 140 (1949).

29. Green, R. W., S. Legvold and F. H. Spedding, Phys. Rev., 122, 827 (1961).

30. Greninger, A. B., Trans. Am. Inst. Mining, Met. Engrs., 117, 61 (1963).

31. Hegland, D. E., S. Legvold and F. H. Spedding, Phys. Rev., 131, 158 (1963).

32. Herpin, A., J. Phys. Radium, 23, 453 (1962).

33. Herpin, A., P. Meriel and J. Villain, C. R. Acad. Sci., Paris, 249, 1334 (1959).

34. Jew, T. T., Magnetic anisotropy in dysprosium single crystals, Unpublished M.S. thesis, Ames, Iowa, Library, Iowa State University of Science and Technology, 1963.

35. Kasuya, T., Prog. Theoret. Phys. (Kyoto), 16, 45 (1956).

36. Kaufman, A., Investigation of strain gages for use at cryogenic temperatures, unpublished paper, Society for Experimental Stress Analysis Spring Meeting, Seattle, Washington, 1963, Cleveland, Ohio, Library, National Aeronautics and Space Administration, 1963.

37. Koehler, W. C., J. Appl. Phys., 36, 1078 (1965).

38. Koehler, W. C., J. W. Cable, E. O. Wollan and M. K. Wilkinson, J. Phys. Soc. Japan, 17, Suppl. B3, 32 (1962).

39. Koehler, W. C., H. R. Child, E. O. Wollan and J. W. Cable, J. Appl. Phys., 34, 1335 (1963).

40. Kornetzki, M., Z. Physik, 98, 289 (1935).

41. Landolt, H. H. and R. Bornstein, Landolt-Bornstein Zahlenwerte und Funktionen aus Physik, Chemie, Astronomie, Geophysik und Tecknik, Berlin, Verlag J. Springer, 1923.

42. Lee, E. W., Proc. Phys. Soc. (London), 84, 693 (1964).

43. Lee, E. W., Rept. on Prog. in Phys., 18, 184 (1955).

44. Lee, E. W. and L. Alperts, Proc. Phys. Soc. (London), 79, 997 (1962).

45. Legvold, S., J. Alstad and J. Rhyne, Phys. Rev. Letters, 10, 509 (1963).

46. Liu, S. H., D. R. Behrendt, S. Legvold and R. H. Good, Jr., Phys. Rev., 116, 1464 (1959).

47. Mason, W. P., Phys. Rev., 96, 302 (1954).

48. Mason, W. P. and J. A. Lewis, Phys. Rev., 94, 1439 (1954).

49. McClintock, R. M., Rev. Sci. Instrum., 30, 715 (1959).

50. Miwa, H. and K. Yosida, Prog. Theoret. Phys. (Kyoto), 26, 693 (1961).

51. Nagamiya, T., J. Appl. Phys., 33, 1029S (1962).

52. Nagamiya, T., K. Nagata and Y. Kitano, Prog. Theoret. Phys. (Kyoto), 27, 1253 (1962).

53. High, H. E., J. Appl. Phys., 34, 3323 (1963).

54. Nigh, H. E., Magnetization and electrical resistivity of gadolinium single crystals, unpublished Ph.D. thesis, Ames, Iowa, Library, Iowa State University of Science and Technology, 1963.

55. Nikitin, S. A., Soviet Physics-JETP, 16, 21 (1963).

56. Rhyne, J. J. and S. Legvold, Phys. Rev., 138, A507 (1965).

57. Ruderman, M. A. and C. Kittel, Phys. Rev., 96, 99 (1954).

58. Sato, H., Phys. Rev., 109, 802 (1958).

59. Spedding, F. H. and A. H. Daane, J. Metals, 6, 504 (1954).

60. Spedding, F. H. and A. H. Daane, Met. Rev., 5, 297 (1960).

61. Spedding, F. H., S. Legvold, A. H. Daane and L. D. Jennings, Prog. in Low Temp. Phys., 2, 368 (1957).

62. Spedding, F. H. and J. E. Powell, J. Metals, 6, 1131 (1954).

63. Strandburg, D. L., Electrical and magnetic properties of holmium single crystals, unpublished Ph.D. thesis, Ames, Iowa, Library, Iowa State University of Science and Technology, 1961.

64. Strauss, H. E., J. Appl. Phys., 30, 698 (1959).

65. Tsuya, N., A. E. Clark and R. M. Bozorth, Magnetostriction in heavy rare earth metals, unpublished paper, American Physical Society April Meeting, Washington, D.C., 1965, Silver Spring, Maryland, Library, Naval Ordnance Laboratory, 1964.

66. Wilkinson, M. K., W. C. Koehler, E. O. Wollan and J. W. Cable, J. Appl. Phys., 32, 48S (1961).

67. Yoshimori, A., J. Phys. Soc. Japan, 14, 807 (1959).

68. Yosida, K., Phys. Rev., 106, 893 (1957).

69. Yosida, K. and H. Miwa, J. Appl. Phys., 32, 8S (1961).

70. Yosida, K. and H. Miwa, Prog. Theoret. Phys. (Kyoto), 26, 693 (1961).

71. Zener, C., Phys. Rev., 96, 1335 (1954).

XII. ACKNOWLEDGEMENTS

The author wishes to express sincere appreciation to Dr. Sam Legvold, for suggesting this problem and for his advice and assistance throughout the investigation in the dual capacity of group leader and friend.

The assistance of Dr. J. K. Alstad who developed many of the experimental techniques used for magnetostriction measurements is gratefully acknowledged.

Special credit is extended to Mr. P. Palmer and Mr. B. J. Beaudry for the preparation of the rare earth metal; to the Ames Laboratory graphics department for the preparation of the figures and to the maintenance department for help in installation of the Harvey Wells magnet system; and to Mr. W. Sylvester and Mr. R. Brown for aid in constructing the experimental apparatus.

It is a pleasure to acknowledge the help of many of the author's Ames Laboratory colleagues: Dr. L. R. Sill for growing the single crystals and for many helpful discussions; Mr. G. McClellan and Mr. E. T. Rodine for performing the strain gage calibrations; Mr. T. Erskine, Mr. M. Knotek and Mr. B. Carpenter for aid in constructing equipment for the magnet system and for preparation of graphs and data calculations.

Dr. A. E. Clark, Dr. E. R. Callen, Mr. H. H. Sample, Mr. T. F. Stromberg, Mr. R. S. Lee, and others are thanked for numerous helpful discussions.

Certainly not least was the assistance of the author's wife, Marilyn, for many suggestions in the writing of the computer programs, for her help in preparation of the manuscript, and for her encouragement during this investigation.

XIII. APPENDIX

A. Errors in Strain Gage Measurements

The absolute errors inherent in the magnetostriction measurements are difficult to calculate due to the rather large number of unknown parameters. These include the reliability of the strain gage bond to both dummy quartz disk and sample, variation in the linearity of strain between individual gages, etc.

The systematic errors in the strain gage measurement are dominated by the variability of the strain gage factor. The manufacturer asserts that the gage factor remains constant from gage to gage within $\pm$ 0.5 per cent. From the calibration performed, the temperature variation of the gage factor was known within about $\pm$ 1.0 per cent. On the basis of copper thermal expansion comparison measurements and other reproducibility checks, the over-all accuracy of the strain gage measurements is estimated to be five per cent for isothermal measurements and about ten per cent for measurements as a function of temperature. It should be pointed out that the relative accuracy and precision of the strain measurement is considerably better than indicated by these values. Relative strains as small as 0.5 micro-inch/inch can be reliably measured throughout the 10^4 gross strain range.

B. Errors in the Magnetostriction Constants A and C of Dy and Tb Produced by the Magnetic Anisotropy

The effect of the six fold magnetic anisotropy in Tb and Dy is to prevent the magnetization from aligning with the field applied in hard magnetic directions.

In the determination of the constant C from the expression $\frac{\Delta \ell}{\ell} = \mp A \sin^2 2\theta \pm 2C \sin^2\theta$ the strain measured at an applied field angle of $\theta = 90^\circ$ was used. Correctly this should be the strain measured when the magnetization angle $\phi = 90^\circ$. This number is not obtainable at low temperatures due to the anisotropy. It should be pointed out that errors in C due to this misalignment are not as serious as might at first appear, due to the small value of the first derivative of the dominant $\sin^2\theta$ term in the neighborhood of $\theta = 90^\circ$.

The degree of misalignment between the magnetization and applied field for $\theta = 90^\circ$ may be calculated from the equilibrium expression for the angular dependent magnetic energy, Equation 50:

$$0 = M_s H \sin (90^\circ - \phi_o) - 6K_6^6 \sin 6\phi_o . \qquad (50)$$

Using the values of the saturation magnetization M_s, approximate internal field H, and values of K_6^6 found previously, this equation was solved for the magnetization angle ϕ_o corresponding to a field angle $\theta = 90^\circ$ using an iteration technique on the computer. Values of ϕ_o were evaluated for several temperatures in Dy and Tb.

The effect of the misalignment on the constants A and C was calculated from the fourth order rotation expression above and the measured strains at $\theta = 60^\circ$ and $\theta = 90^\circ$. The equations obtained for the corrected values of C and A are: (algebraic signs of A and C chosen correspond to a-axis strains with θ, ϕ relative to the b-axis)

$$C_{cor} = \frac{\frac{\Delta\ell}{\ell}\Big|_{\theta=90^\circ} - \frac{4}{3}\frac{\Delta\ell}{\ell}\Big|_{\theta=60^\circ} \sin^2 2\phi_o}{2\,(\sin^2\phi_o - \sin^2 2\phi_o)} \tag{62}$$

and

$$A_{cor} = \frac{4}{3}\frac{\Delta\ell}{\ell}\Big|_{\theta=60^\circ} - 2C_{cor}. \tag{63}$$

Values of the magnetization angle ϕ_o for an applied field angle $\theta = 90^\circ$ in Dy and Tb at low temperatures are given in Table 6 along with the experimental and corrected values of C and A found by this method. It is noted that the errors encountered in Tb are negligible above 20°K. In Dy the effect of the anisotropy is more severe as shown.

C. Tabulation of Experimental Data

Magnetostriction data appearing in this thesis are tabulated in the following figures. All strains $\Delta\ell/\ell$ are given in units of (inches x 10^{-6}/ inch); applied fields, H, in kOe; applied field angles, θ, in degrees; and temperatures T, in degrees Kelvin. Due to the precision of the strain measurement, data are given to the nearest micro-inch/inch; however, for large strains, these numbers must be considered in light of the over-all

Table 6. Effect of six fold anisotropy on the experimental values of the magnetostriction constants C and A

Dy

T °K	ϕ^a degrees	ϕ^b degrees	C^b_{exp} μ in/in	C^b_{cor} μ in/in	% Error in C_{exp}	A^b_{exp} μ in/in	A^b_{cor} μ in/in	% Error in A_{exp}
11.5	70.4	67.4	4249.	4498.	5.5	-2148.	-1651.	30.1
20.9	71.0	68.0	4232.	4472.	5.3	-2086.	-1606.	29.9
59.3	89.4	78.3	3794.	3834.	1.1	-1566.	-1485.	5.5
69.7	90.0	89.5	3926.	3926.	0.	-193.	-193.	0.3

Tb

T °K	ϕ^b degrees	C_{exp} μ in/in	C_{cor} μ in/in	% Error in C_{exp}	A_{exp} μ in/in	A_{cor} μ in/in	% Error in A_{exp}
5.3	78.6	3936.	3937.	0.0	2042.	2041.	0.0
10.2	78.6	4254.	4270.	0.4	2034.	2001.	1.6
20.5	79.1	3966.	3967.	0.0	2044.	2042.	0.1
39.5	89.5	4157.	4157.	0.0	1858.	1858.	0.0

[a]Magnetization angle ϕ obtained from the anisotropy constants of Liu et al. (46). Applied field angle $\theta = 90^\circ$.

[b]Magnetization angle ϕ obtained from the anisotropy constants found from the magnetostriction data of this study.

accuracies discussed above. Dysprosium data are given in Figures 51 through 56, erbium data in Figures 57 through 62, and terbium data in Figures 63 through 69. Table 7 gives the magnetic field dependence of the constants A and C for Tb.

Dy-- STRAIN VERSUS TEMPERATURE
H APPLIED ALONG a-AXIS
EXCEPT * APPLIED ALONG b-AXIS

a-Axis H=0		a-Axis H=30		b-Axis H=0		b-Axis H=30		b-Axis H=26*		c-Axis H=0		c-Axis H=30	
T	Δt/ℓ	T	Δt/ℓ	T	Δt/ℓ	T	Δt/ℓ	T	Δt/ℓ	T	Δt/ℓ	T	Δt/ℓ
297.0	-15.	302.7	15.	304.2	15.	295.4	-20.	164.8	-973.	299.3	-10.	255.7	-650.
296.1	-22.	302.7	9.	297.7	-8.	295.4	-46.	150.6	-794.	287.3	-189.	255.7	-575.
289.0	-58.	290.7	-56.	286.2	-54.	282.9	-114.	138.4	-573.	273.8	-388.	246.7	-680.
283.6	-90.	281.8	-104.	277.6	-87.	270.1	-190.	130.6	-432.	262.2	-553.	218.4	-904.
275.0	-133.	267.7	-183.	266.7	-131.	259.1	-258.	119.8	-200.	250.4	-719.	206.7	-893.
268.4	-169.	257.3	-243.	257.7	-166.	247.9	-333.	110.0	9.	237.9	-885.	200.8	-835.
261.5	-208.	244.9	-317.	254.4	-181.	235.9	-420.	100.6	219.	227.6	-1009.	195.7	-727.
251.6	-259.	230.8	-388.	248.1	-205.	227.5	-493.	90.0	437.	202.6	-1265.	188.3	-432.
243.9	-296.	221.1	-439.	242.5	-228.	214.7	-636.	88.6	456.	196.3	-1309.	181.9	69.
243.0	-304.	202.8	-578.	239.5	-240.	222.4	-546.	87.6	485.	192.7	-1329.	175.4	798.
237.5	-326.	195.2	-657.	232.2	-271.	207.7	-741.	86.0	524.	186.5	-1349.	167.9	1660.
234.7	-340.	187.1	-785.	225.8	-300.	198.3	-941.	84.6	549.	184.5	-1349.	159.4	2393.
228.1	-369.	152.3	-916.	220.9	-324.	192.8	-1117.	83.1	585.	182.5	-1341.	153.2	2804.
220.3	-400.	167.2	-1040.	216.1	-347.	188.0	-1327.	80.7	642.	176.0	-1047.	145.4	3170.
214.9	-422.	209.3	-533.	208.8	-386.	180.3	-1832.	77.8	694.	169.6	-645.	139.5	3373.
207.4	-463.	190.0	-743.	202.0	-426.	172.5	-2476.	76.8	694.	163.4	-296.	133.1	3555.
202.8	-484.	179.5	-938.	195.5	-469.	169.0	-2764.	80.7	636.	159.0	-63.	126.7	3683.
193.4	-543.	176.3	-985.	190.0	-510.	161.4	-3314.	79.2	671.	153.9	161.	121.7	3755.
188.0	-580.	171.8	-1027.	184.6	-558.	155.1	-3696.	76.9	694.	148.7	378.	112.7	3846.
180.8	-654.	170.0	-1032.	181.7	-589.	144.6	-4247.	75.6	674.	139.2	710.	107.5	3879.
172.7	-866.	162.2	-1016.	180.0	-612.	153.5	-3777.	73.7	615.	126.4	1095.	98.3	3901.
174.3	-827.	155.6	-952.	177.2	-684.	149.2	-4015.	66.4	448.	115.3	1319.	92.8	3912.
177.4	-741.	148.4	-858.	173.9	-783.	141.3	-4393.	60.0	336.	106.1	1461.	86.0	3908.
164.3	-1090.	138.6	-709.	170.5	-883.	134.7	-4688.	50.0	227.	95.1	1596.	79.4	3896.
156.5	-1277.	131.6	-583.	163.8	-1065.	127.6	-4989.	40.0	173.	89.1	1655.		
149.4	-1430.	126.0	-474.	159.3	-1182.	119.0	-5343.	30.0	151.	88.0	1673.	293.7	-90.
142.9	-1549.	110.5	-175.	155.9	-1263.	111.3	-5641.	20.0	146.	87.5	1681.	293.6	-54.
137.5	-1641.	98.3	72.	150.3	-1389.	103.8	-5936.	20.0	-829.	87.2	1678.	281.8	-220.
130.8	-1749.	89.7	242.	144.1	-1516.	95.7	-6256.			87.1	1687.	268.8	-394.
121.5	-1887.	80.8	451.	135.6	-1672.	87.9	-6583.			86.8	1705.	256.1	-556.
111.0	-2029.			127.4	-1811.	80.1	-6897.			86.5	1732.	239.3	-733.
98.4	-2185.	79.3	480.	117.8	-1957.	79.4	-6933.			86.3	1778.	230.5	-808.
89.9	-2285.	69.6	805.	109.4	-2074.	78.7	-6972.			86.0	1859.	221.0	-877.
88.0	-2310.	66.4	894.	101.6	-2144.	74.9	-7119.			85.7	1999.	213.0	-907.
87.0	-2327.	62.4	1016.	95.5	-2216.	67.4	-7426.			85.4	2232.	79.7	3954.
86.7	-2338.	59.5	1103.	89.4	-2272.	62.7	-7610.			85.0	2570.	82.2	3959.
86.5	-2420.	51.8	1339.	88.0	-2289.	55.0	-7913.			84.7	2743.	67.4	3887.
86.1	-2732.			87.0	-2300.	52.4	-8004.			84.4	2952.	60.8	3873.
85.8	-2773.	64.7	950.	86.4	-2296.	44.4	-8285.			84.0	3188.	73.2	3921.
84.6	-2743.	59.3	1131.	86.0	-2736.	38.2	-8479.			83.7	3330.	62.2	3874.
80.4	-2769.	51.2	1379.	85.7	-2782.	32.9	-8628.			83.4	3422.	55.3	3844.
73.1	-2835.	45.0	1554.	85.5	-2798.	26.4	-8897.			83.0	3492.	47.8	3770.
71.8	-2712.	39.5	1687.	83.0	-2872.	20.4	-9000.			82.4	3585.		
68.6	-2685.	30.9	1888.	80.3	-2884.	14.3	-9067.			82.0	3643.	61.2	3830.
64.2	-2716.	24.2	2001.			10.0	-9084.			81.5	3727.	56.4	3810.
61.0	-2738.	20.9	2038.	200.9	-390.					81.0	3785.	51.0	3788.
		14.6	2086.	188.9	-490.					80.5	3834.	45.0	3765.
		11.1	2100.	168.2	-911.					80.0	3898.	37.8	3737.
				155.8	-1219.					78.9	3967.	31.7	3718.
				137.0	-1594.					77.8	3996.	24.7	3702.
				111.5	-1987.					75.3	4004.	20.5	3696.
				90.5	-2247.					69.5	3998.	14.4	3687.
				88.0	-2281.					65.0	3989.	10.1	3690.
				87.0	-2300.					60.5	3949.	10.1	3538.
				86.6	-2310.					260.2	-537.		
				86.3	-2319.								
				86.0	-2660.					301.0	20.		
				85.8	-2688.					281.4	-273.		
				85.5	-2638.					267.3	-475.		
				83.2	-2665.					254.8	-650.		
				81.3	-2685.					243.7	-800.		
				73.1	-2748.					222.7	-1060.		
				64.0	-2842.					212.8	-1163.		
				61.4	-2860.					196.5	-1301.		
				293.1	103.					180.7	-1315.		
										174.4	-939.		
										165.0	-781.		
										154.7	133.		
										142.7	619.		
										132.1	940.		
										119.9	1248.		
										108.0	1441.		
										295.2	-48.		

Figure 51. Dy a-, b-, and c-axis strain (in x 10^{-6}/in) as a function of temperature. The horizontal lines separate data runs.

Dy-- a-AXIS STRAIN VERSUS FIELD APPLIED ALONG a-AXIS

T = 22.1		T = 49.8		T = 79.8		T = 85.0		T = 89.9		T = 114.4		T = 144.0		T = 152.0	
H	Δℓ/ℓ	H	Δℓ/ℓ	H	Δℓ/ℓ	H	Δℓ/ℓ	H	Δℓ/ℓ	H	Δℓ/ℓ	H	Δℓ/ℓ	H	Δℓ/ℓ
0.0	-4.	0.0	0.	0.0	-264.	0.0	-162.	0.0	14.	0.0	0.	0.0	0.	0.0	2.
0.0	359.	1.6	883.	0.0	0.	0.0	0.	0.0	0.	1.8	4.	0.0	0.	0.0	0.
0.6	375.	1.8	885.	0.9	119.	0.9	56.	0.8	-12.	2.2	6.	6.7	-6.	0.9	-1.
0.9	402.	2.1	970.	1.4	255.	1.6	121.	0.9	-13.	2.4	7.	8.3	-6.	1.8	-3.
1.3	489.	2.4	1092.	1.8	436.	1.9	227.	1.3	14.	2.6	7.	9.2	17.	2.6	-4.
1.4	735.	2.8	1327.	1.9	602.	2.2	341.	1.6	37.	2.8	9.	10.0	56.	3.1	-5.
1.6	846.	3.1	1524.	2.1	716.	2.6	523.	1.8	92.	3.4	11.	10.5	78.	3.8	-5.
1.8	977.	3.4	1941.	2.2	813.	2.9	751.	1.9	130.	3.9	17.	11.6	183.	4.2	-2.
1.9	1188.	3.8	2378.	2.4	978.	3.2	1170.	2.1	205.	4.1	20.	12.5	273.	4.6	-4.
2.1	1244.	3.9	2934.	2.6	1097.	3.6	1455.	2.2	204.	4.2	86.	13.3	393.	6.7	0.
2.2	1455.	4.2	3044.	2.8	1231.	3.9	2151.	2.4	294.	4.4	192.	14.9	464.	10.0	-27.
2.4	1570.	4.5	3352.	2.9	1328.	4.2	2418.	2.6	469.	4.6	301.	16.6	501.	10.3	-56.
2.6	1739.	4.9	3511.	3.1	1440.	4.6	2819.	2.8	576.	4.7	368.	19.3	525.	11.2	-70.
2.8	1847.	5.2	3593.	3.2	1564.	4.9	2974.	2.9	827.	4.9	492.	20.3	540.	11.6	-76.
2.9	2047.	5.9	3652.	3.4	1628.	5.2	3028.	3.1	1280.	5.1	587.	23.3	551.	12.0	-71.
3.1	2133.	6.7	3684.	3.6	1800.	5.6	3094.	3.2	1420.	5.2	660.	25.8	568.	12.3	-63.
3.2	2354.	8.3	3710.	3.8	2057.	5.9	3119.	3.4	1556.	5.4	744.	25.8	566.	12.6	-46.
3.4	2412.	11.6	3724.	3.9	2297.	8.3	3182.	3.6	1665.	5.6	865.	25.8	568.	13.3	-11.
3.6	2614.	16.6	3733.	4.1	2452.	10.0	3196.	3.8	1837.	5.9	1118.	0.0	-12.	14.1	33.
3.8	2932.	20.3	3744.	4.2	2555.	13.3	3211.	3.9	2006.	6.4	1331.	0.0	-11.	14.9	75.
3.9	3156.	23.3	3751.	4.4	2624.	16.6	3223.	4.1	2112.	7.5	1484.			15.7	118.
4.1	3266.	25.8	3759.	4.7	2711.	23.3	3242.	4.4	2237.	8.3	1494.			16.6	153.
4.2	3602.	0.0	939.	5.1	2741.	25.0	3261.	4.7	2292.	12.5	1524.			17.4	190.
4.4	3698.			5.9	2795.	25.8	3277.	5.4	2336.	16.6	1549.			18.1	222.
4.6	3926.			6.7	2814.	0.0	394.	6.1	2357.	21.5	1576.			18.8	239.
4.7	4126.			8.3	2837.	0.0	370.	6.7	2372.	23.3	1584.			19.8	252.
4.9	4286.			11.6	2856.			8.3	2392.	24.5	1589.			21.5	263.
5.1	4421.			16.6	2871.			11.6	2412.	25.0	1592.			23.3	272.
5.2	4563.			21.5	2890.			16.6	2430.	25.8	1597.			25.8	289.
5.4	4647.			23.3	2897.			21.5	2449.					25.8	290.
5.6	4681.			25.0	2902.			23.3	2456.					25.8	294.
5.7	4716.			25.8	2905.			25.0	2462.					0.0	-3.
5.9	4748.			0.0	886.			25.8	2469.						
6.1	4767.							0.0	-31.						
6.2	4786.														
6.4	4806.														
6.6	4814.														
6.7	4824.														
7.1	4839.														
7.5	4856.														
8.3	4870.														
11.6	4873.														
16.6	4894.														
21.5	4891.														
23.3	4892.														
25.8	4892.														
0.0	1518.														

T = 161.4		T = 184.3		T = 200.5		T = 210.0	
H	Δℓ/ℓ	H	Δℓ/ℓ	H	Δℓ/ℓ	H	Δℓ/ℓ
0.0	0.	0.0	0.	0.0	0.	0.0	0.
3.4	2.	0.0	0.	2.0	-1.	2.0	-1.
6.7	-1.	3.4	-4.	4.0	-2.	4.0	-2.
10.8	-11.	5.1	-9.	6.0	-5.	6.0	-3.
11.3	-31.	6.7	-16.	8.0	-9.	8.0	-6.
11.5	-57.	8.3	-25.	10.0	-15.	10.0	-9.
11.6	-119.	10.0	-35.	12.0	-20.	12.0	-13.
11.8	-147.	10.8	-41.	14.0	-28.	14.0	-17.
12.2	-167.	13.3	-60.	16.0	-35.	16.0	-22.
12.5	-174.	14.9	-75.	18.0	-44.	18.0	-28.
13.3	-179.	16.6	-90.	20.0	-55.	20.0	-35.
14.1	-171.	18.1	-105.	22.0	-65.	22.0	-41.
14.9	-154.	19.3	-118.	24.0	-76.	24.0	-49.
16.6	-109.	20.9	-135.	26.0	-89.	26.0	-57.
18.1	-64.	21.5	-141.	28.0	-101.	28.0	-65.
19.3	-28.	22.0	-146.	30.0	-114.	30.0	-74.
20.3	-5.	22.8	-153.	0.0	-1.	0.0	0.
21.5	17.	23.3	-159.				
22.6	26.	24.3	-169.				
23.4	29.	25.8	-185.				
24.3	34.	25.8	-187.				
25.0	36.	0.0	-5.				
25.8	42.	0.0	-5.				

Figure 52. Dy a-axis strain (in x 10^{-6}/in) versus field, H, applied along the a axis of the a-b plane specimen.

Dy-- b-AXIS STRAIN VERSUS FIELD APPLIED ALONG a-AXIS

T = 20.0		T = 50.0		T = 77.5		T = 85.1		T = 89.7		T = 113.7		T = 143.9		T = 150.2	
H	Δℓ/ℓ	H	Δℓ/ℓ	H	Δℓ/ℓ	H	Δℓ/ℓ	H	Δℓ/ℓ	H	Δℓ/ℓ	H	Δℓ/ℓ	H	Δℓ/ℓ
0.2	0.	0.2	0.	0.2	0.	0.2	0.	0.0	0.	0.0	0.	0.0	0.	0.0	0.
0.5	-15.	0.9	-1.	0.5	-84.	0.3	-68.	0.8	-277.	3.6	-27.	3.6	-11.	2.0	-3.
0.9	-51.	1.5	-19.	1.0	-149.	1.2	-169.	1.1	-448.	3.8	-80.	4.2	-20.	4.0	-12.
1.2	-148.	1.7	-41.	1.1	-243.	1.5	-319.	1.3	-670.	4.2	-432.	7.1	-37.	6.0	-26.
1.5	-292.	2.0	-95.	1.5	-379.	1.9	-491.	1.7	-895.	4.3	-579.	8.6	-99.	8.0	-47.
1.9	-435.	2.3	-191.	2.0	-561.	2.3	-745.	2.3	-1205.	4.5	-790.	9.0	-241.	10.0	-577.
2.3	-651.	2.7	-371.	2.3	-750.	2.5	-951.	2.5	-1570.	4.7	-910.	9.3	-452.	12.0	-1426.
2.6	-745.	3.1	-590.	2.5	-929.	2.9	-1147.	2.9	-2174.	5.0	-1276.	9.6	-671.	14.0	-1752.
2.9	-918.	3.4	-910.	3.0	-1165.	3.3	-1391.	3.4	-2920.	5.1	-1486.	10.0	-983.	16.0	-2045.
3.3	-1202.	3.7	-1346.	3.2	-1342.	3.6	-1730.	3.6	-3237.	5.2	-1624.	10.2	-1114.	18.0	-2230.
3.7	-1660.	4.1	-1837.	3.6	-1641.	4.0	-2172.	4.0	-3479.	5.3	-1848.	10.6	-1361.	20.0	-2303.
4.1	-2331.	4.5	-2319.	4.0	-2193.	4.3	-2541.	4.4	-3598.	5.5	-2127.	10.8	-1445.	22.0	-2354.
4.2	-2696.	4.8	-2709.	4.2	-2578.	4.7	-2718.	4.8	-3658.	5.9	-2443.	11.2	-1530.	24.0	-2399.
4.7	-3129.	5.2	-3038.	4.7	-2864.	5.0	-2783.	5.2	-3701.	6.1	-2734.	11.5	-1604.	26.0	-2439.
5.1	-3578.	5.5	-3186.	5.1	-2987.	5.5	-2832.	6.1	-3749.	6.5	-2954.	11.8	-1680.	28.0	-2475.
5.5	-3935.	5.9	-3278.	5.5	-3055.	5.7	-2852.	6.9	-3775.	6.8	-3016.	12.2	-1762.	30.0	-2509.
5.8	-4155.	6.3	-3329.	5.7	-3083.	6.1	-2873.	8.8	-3812.	7.1	-3040.	12.6	-1863.	0.0	-19.
6.1	-4312.	6.6	-3368.	6.2	-3116.	6.9	-2908.	11.9	-3853.	7.5	-3052.	13.5	-2026.		
6.5	-4398.	7.1	-3404.	6.5	-3131.	7.9	-2933.	16.9	-3899.	7.9	-3064.	14.3	-2153.		
6.9	-4446.	7.8	-3450.	7.0	-3155.	8.6	-2950.	22.0	-3937.	8.7	-3093.	15.1	-2256.		
7.2	-4494.	8.6	-3483.	7.9	-3181.	10.2	-2975.	23.8	-4026.	10.3	-3136.	16.0	-2314.		
7.6	-4523.	9.5	-3508.	8.6	-3201.	11.9	-2994.	25.8	-4044.	11.8	-3165.	17.0	-2351.		
7.8	-4542.	10.2	-3526.	10.2	-3228.	13.5	-3009.	25.8	-3944.	13.5	-3191.	18.5	-2398.		
8.8	-4594.	11.8	-3549.	11.9	-3245.	16.9	-3037.	0.0	-121.	16.8	-3231.	19.8	-2428.		
9.4	-4624.	13.4	-3563.	13.5	-3259.	19.9	-3058.	25.8	-3959.	19.8	-3263.	20.8	-2447.		
10.2	-4646.	16.9	-3581.	16.9	-3284.	22.0	-3071.	0.0	-117.	22.0	-3285.	22.0	-2470.		
11.8	-4676.	19.9	-3592.	19.9	-3302.	23.8	-3083.			23.8	-3300.	23.8	-2501.		
13.3	-4693.	22.0	-3599.	22.0	-3313.	26.0	-3102.			25.8	-3323.	25.8	-2541.		
17.7	-4708.	23.8	-3605.	23.8	-3324.	25.8	-3101.			25.8	-3249.	25.8	-2555.		
20.8	-4716.	26.0	-3612.	26.0	-3338.	25.8	-3134.			0.0	91.	0.0	-24.		
23.8	-4719.	25.8	-3611.	25.8	-3336.	0.2	-725.								
25.8	-4722.	25.8	-3675.	25.8	-3385.										
26.0	-4722.	0.2	-283.	0.2	-782.										
0.2	-562.			26.0	-3373.										
26.0	-4722.			0.2	-748.										
0.2	-571.														

T = 162.2		T = 189.1		T = 198.8		T = 209.2	
H	Δℓ/ℓ	H	Δℓ/ℓ	H	Δℓ/ℓ	H	Δℓ/ℓ
0.0	0.	0.0	0.	0.0	0.	0.0	0.
3.6	-2.	2.0	-4.	2.0	-2.	2.0	-1.
7.0	-12.	4.0	-13.	4.0	-7.	4.0	-5.
10.9	-57.	6.0	-29.	6.0	-17.	6.0	-10.
11.2	-79.	8.0	-51.	8.0	-29.	8.0	-18.
11.6	-150.	10.0	-80.	10.0	-45.	10.0	-28.
11.9	-268.	12.0	-115.	12.0	-65.	12.0	-39.
12.1	-405.	14.0	-155.	14.0	-87.	14.0	-53.
12.4	-622.	16.0	-202.	16.0	-113.	16.0	-69.
12.8	-798.	18.0	-252.	18.0	-142.	18.0	-86.
13.0	-833.	20.0	-309.	20.0	-175.	20.0	-107.
13.4	-887.	22.0	-371.	22.0	-210.	22.0	-128.
13.7	-923.	24.0	-436.	24.0	-248.	24.0	-151.
14.3	-980.	26.0	-506.	26.0	-289.	26.0	-177.
15.0	-1058.	28.0	-578.	28.0	-333.	28.0	-204.
16.0	-1142.	30.0	-652.	30.0	-378.	30.0	-233.
16.9	-1224.	0.0	1.	0.0	2.	0.0	2.
18.4	-1378.						
19.8	-1513.						
20.8	-1604.						
22.0	-1696.						
22.9	-1741.						
23.8	-1780.						
24.7	-1817.						
25.8	-1871.						
25.8	-1879.						
25.8	-1891.						
0.0	-16.						

Figure 53. Dy b-axis strain (in x 10^{-6}/in) versus field, H, applied along the a axis of the a-b plane specimen.

Dy-- c-AXIS STRAIN VERSUS FIELD APPLIED ALONG a-AXIS

T = 20.0		T = 50.4		T = 77.4		T = 85.0		T = 90.0		T = 114.0		T = 129.6		T = 144.1	
H	Δℓ/ℓ	H	Δℓ/ℓ	H	Δℓ/ℓ	H	Δℓ/ℓ	H	Δℓ/ℓ	H	Δℓ/ℓ	H	Δℓ/ℓ	H	Δℓ/ℓ
0.0	12.	0.0	0.	0.0	22.	0.0	7.	0.0	-55.	0.0	0.	0.0	5.	0.0	-1.
0.0	0.	0.9	7.	0.0	0.	0.0	0.	0.0	0.	3.5	34.	0.0	0.	0.0	0.
0.9	-5.	1.7	28.	0.8	-13.	0.9	-13.	0.6	73.	3.9	91.	3.4	-1.	6.7	2.
1.3	-12.	2.1	-31.	1.1	-28.	1.4	-59.	0.8	82.	4.2	324.	4.4	-1.	7.5	42.
1.4	-21.	2.4	-41.	1.4	-41.	1.8	-117.	0.9	251.	4.3	607.	5.9	34.	7.9	45.
1.8	-69.	2.9	-74.	1.6	-65.	2.1	-187.	1.1	343.	4.6	929.	6.2	165.	8.2	97.
2.1	-127.	3.2	-291.	1.8	-89.	2.4	-240.	1.3	671.	4.7	1145.	6.6	414.	8.5	299.
2.4	-206.	3.5	-360.	1.9	-116.	2.8	-262.	1.4	693.	4.9	1442.	6.9	671.	8.8	517.
2.8	-256.	3.8	-446.	2.1	-143.	3.1	-251.	1.6	1170.	5.1	1842.	7.2	1119.	9.2	972.
3.1	-308.	4.2	-413.	2.2	-169.	3.4	-212.	1.8	1294.	5.3	2124.	7.5	1432.	9.5	1511.
3.4	-327.	4.5	-394.	2.4	-182.	3.8	-183.	1.9	1573.	5.5	2273.	7.9	1841.	9.9	1690.
3.8	-349.	5.3	-366.	2.6	-199.	4.2	-173.	2.2	1643.	6.0	2348.	8.2	1971.	10.2	1756.
4.1	-343.	5.9	-389.	2.8	-207.	5.1	-155.	2.6	1627.	6.3	2350.	8.5	2042.	10.5	1825.
4.4	-323.	7.0	-378.	2.9	-239.	6.7	-144.	2.9	1647.	6.6	2349.	8.9	2109.	10.8	1878.
4.7	-311.	11.8	-361.	3.1	-233.	8.3	-138.	3.2	1697.	8.6	2357.	9.2	2142.	11.6	1989.
5.1	-313.	16.9	-354.	3.2	-214.	16.6	-123.	3.8	1732.	10.2	2366.	9.5	2160.	12.5	2095.
5.9	-302.	22.0	-350.	3.4	-186.	23.3	-115.	4.2	1754.	11.8	2375.	10.0	2188.	13.3	2203.
8.3	-291.	23.8	-350.	3.6	-186.	25.8	-111.	5.1	1772.	13.4	2384.	11.6	2226.	14.1	2286.
11.6	-286.	25.8	-349.	3.8	-172.	0.0	-37.	6.7	1785.	16.9	2400.	13.3	2247.	14.9	2338.
16.6	-280.	0.0	-367.	3.9	-160.			8.3	1792.	19.9	2413.	16.6	2280.	16.6	2394.
21.5	-279.	0.0	0.	4.4	-147.			11.6	1801.	22.0	2421.	19.3	2306.	20.3	2471.
23.3	-279.	3.5	-178.	5.1	-136.			16.6	1810.	23.8	2428.	20.3	2323.	23.3	2520.
25.8	-278.	4.2	-119.	5.9	-130.			20.3	1819.	25.8	2439.	23.3	2336.	25.8	2558.
0.0	-79.	25.8	-355.	6.7	-126.			23.3	1821.	0.0	84.	25.8	2353.	0.0	14.
		0.0	-264.	8.3	-121.			25.8	1825.			0.0	5.	0.0	11.
				10.0	-112.			0.0	57.						
				11.6	-111.										
				16.6	-105.										
				21.5	-101.										
				23.3	-99.										
				25.8	-97.										
				0.0	21.										

T = 151.2		T = 162.1		T = 182.8	
H	Δℓ/ℓ	H	Δℓ/ℓ	H	Δℓ/ℓ
0.0	0.	0.0	-2.	0.0	0.
6.9	33.	0.0	0.	3.4	21.
9.5	71.	6.7	30.	5.3	44.
9.8	134.	7.5	33.	6.1	60.
10.0	397.	8.3	35.	6.9	80.
10.4	815.	9.2	41.	7.8	103.
10.7	1278.	10.0	59.	8.7	123.
11.1	1529.	10.8	92.	9.5	149.
11.4	1605.	11.2	249.	10.2	179.
11.7	1648.	11.5	442.	11.0	208.
12.0	1691.	11.8	877.	11.9	241.
12.5	1769.	12.2	1109.	12.5	275.
13.9	1911.	12.5	1169.	13.4	309.
15.1	2036.	12.8	1211.	14.3	351.
16.9	2200.	13.3	1288.	15.1	395.
19.8	2356.	14.1	1388.	16.9	485.
21.5	2404.	14.9	1475.	18.5	571.
22.5	2428.	16.6	1630.	20.8	708.
23.8	2461.	19.3	1928.	21.9	789.
25.8	2517.	21.5	2102.	22.9	846.
0.0	9.	23.3	2195.	23.8	908.
25.8	2519.	25.8	2306.	25.8	1085.
0.0	13.	0.0	42.	0.0	6.
		0.0	40.		

Figure 54. Dy c-axis strain (in x 10^{-6}/in) versus field, H, applied along the a axis.

Dy-- a-AXIS STRAIN VERSUS ANGLE OF APPLIED FIELD IN a-b PLANE RELATIVE TO a-AXIS

T = 11.5		T = 20.9		T = 40.2		T = 59.3		T = 70.3		T = 80.8		T = 98.6		T = 118.5	
θ	Δℓ/ℓ	θ	Δℓ/ℓ	θ	Δℓ/ℓ	θ	Δℓ/ℓ	θ	Δℓ/ℓ	θ	Δℓ/ℓ	θ	Δℓ/ℓ	θ	Δℓ/ℓ
0.0	0.	0.0	0.	0.0	-534.	0.0	532.	0.0	0.	0.0	0.	0.0	0.	0.0	0.
60.0	-7985.	60.0	-7912.	60.0	-7128.	60.0	-6865.	60.0	-5829.	60.0	-5526.	60.0	-4706.	60.0	-3794.
90.0	-8490.	90.0	-8464.	90.0	-8237.	90.0	-7587.	90.0	-7295.	90.0	-7100.	90.0	-6098.	90.0	-4967.
0.0	-15.	0.0	-0.	0.0	-529.	0.0	511.	0.0	0.	0.0	4.	0.0	18.	0.0	16.
10.0	-30.	10.0	-15.	10.0	-574.	10.0	487.	10.0	-51.	10.0	-77.	10.0	-122.	10.0	-133.
20.0	-44.	20.0	-33.	20.0	-726.	20.0	432.	20.0	-267.	20.0	-417.	20.0	-598.	20.0	-581.
23.0	-31.	25.0	-11.	25.0	-855.	25.0	423.	25.0	-492.	25.0	-849.	25.0	-1045.	25.0	-909.
25.0	-28.	28.0	-2324.	28.0	-2006.	28.0	-1473.	30.0	-2093.	28.0	-1358.	30.0	-1656.	30.0	-1308.
27.0	-1112.	30.0	-4577.	30.0	-4118.	30.0	-3765.	35.0	-3902.	30.0	-1976.	35.0	-2317.	35.0	-1745.
29.0	-3370.	32.0	-6531.	32.0	-5341.	32.0	-5515.	40.0	-4490.	32.0	-2468.	40.0	-2963.	40.0	-2193.
30.0	-4598.	35.0	-7197.	35.0	-5713.	35.0	-5946.	50.0	-5255.	35.0	-3173.	50.0	-3934.	50.0	-3045.
32.0	-6520.	40.0	-7357.	40.0	-6088.	40.0	-6160.	60.0	-5833.	40.0	-3911.	60.0	-4705.	60.0	-3791.
35.0	-7296.	50.0	-7643.	50.0	-6659.	50.0	-6530.	70.0	-6331.	50.0	-4845.	70.0	-5347.	70.0	-4392.
40.0	-7454.	60.0	-7916.	60.0	-7134.	60.0	-6867.	80.0	-6820.	60.0	-5523.	80.0	-5873.	80.0	-4818.
50.0	-7724.	70.0	-8170.	70.0	-7552.	70.0	-7175.	90.0	-7295.	70.0	-6106.	90.0	-6095.	90.0	-4960.
60.0	-7995.	80.0	-8383.	80.0	-7951.	80.0	-7449.	100.0	-6791.	80.0	-6655.	100.0	-5794.	100.0	-4759.
70.0	-8236.	90.0	-8464.	90.0	-8242.	90.0	-7587.	110.0	-6315.	90.0	-7095.	110.0	-5244.	110.0	-4286.
80.0	-8436.	100.0	-8390.	100.0	-7942.	100.0	-7451.	120.0	-5824.	100.0	-6652.	120.0	-4580.	120.0	-3645.
90.0	-8498.	110.0	-8168.	110.0	-7553.	110.0	-7169.	130.0	-5263.	110.0	-6103.	130.0	-3781.	130.0	-2893.
100.0	-8427.	120.0	-7908.	120.0	-7101.	120.0	-6857.	140.0	-4492.	120.0	-5527.	140.0	-2739.	140.0	-2012.
110.0	-8212.	130.0	-7639.	130.0	-6631.	130.0	-6530.	145.0	-3847.	130.0	-4845.	145.0	-2065.	145.0	-1561.
120.0	-7958.	140.0	-7355.	140.0	-6021.	140.0	-6146.	150.0	-1454.	140.0	-3872.	150.0	-1418.	150.0	-1150.
130.0	-7698.	145.0	-7010.	145.0	-5558.	145.0	-5784.	155.0	-479.	145.0	-3077.	155.0	-870.	155.0	-775.
140.0	-7426.	148.0	-4130.	148.0	-3739.	148.0	-3284.	160.0	-267.	148.0	-2319.	160.0	-510.	160.0	-492.
145.0	-7130.	150.0	-2212.	150.0	-1948.	150.0	-1402.	170.0	-54.	150.0	-1777.	170.0	-111.	170.0	-113.
148.0	-4315.	152.0	-183.	152.0	-912.	152.0	331.	180.0	-1.	152.0	-1238.	180.0	-18.	180.0	-12.
150.0	-2277.	155.0	-24.	155.0	-812.	155.0	419.			155.0	-792.				
152.0	-175.	160.0	-44.	160.0	-719.	160.0	426.			160.0	-441.				
155.0	-41.	170.0	-32.	170.0	-596.	170.0	466.			170.0	-125.				
157.0	-55.	180.0	-29.	180.0	-565.	180.0	478.			180.0	-46.				
160.0	-69.														
165.0	-70.														
170.0	-65.														
180.0	-64.														

T = 139.6		T = 160.2		T = 180.4		T = 200.2		T = 220.1		T = 240.5		T = 259.7		T = 280.1	
θ	Δℓ/ℓ	θ	Δℓ/ℓ	θ	Δℓ/ℓ	θ	Δℓ/ℓ	θ	Δℓ/ℓ	θ	Δℓ/ℓ	θ	Δℓ/ℓ	θ	Δℓ/ℓ
0.0	0.	0.0	0.	0.0	0.	0.0	0.	0.0	0.	0.0	0.	0.0	0.	0.0	0.
60.0	-2827.	60.0	-1777.	60.0	-637.	60.0	-177.	60.0	-78.	60.0	-42.	60.0	-27.	60.0	-19.
90.0	-3704.	90.0	-2330.	90.0	-830.	90.0	-230.	90.0	-102.	90.0	-55.	90.0	-36.	90.0	-25.
0.0	12.	0.0	3.	0.0	1.	0.0	1.	0.0	0.	0.0	1.	0.0	1.	0.0	0.
10.0	-114.	10.0	-75.	10.0	-29.	10.0	-7.	10.0	-3.	10.0	-1.	10.0	-0.	10.0	-1.
20.0	-447.	20.0	-292.	20.0	-104.	20.0	-29.	20.0	-13.	20.0	-6.	20.0	-4.	20.0	-3.
30.0	-967.	30.0	-616.	30.0	-218.	30.0	-61.	30.0	-27.	30.0	-14.	30.0	-9.	30.0	-7.
40.0	-1571.	40.0	-993.	40.0	-355.	40.0	-99.	40.0	-44.	40.0	-23.	40.0	-14.	40.0	-11.
50.0	-2219.	50.0	-1401.	50.0	-499.	50.0	-139.	50.0	-62.	50.0	-33.	50.0	-21.	50.0	-15.
60.0	-2869.	60.0	-1780.	60.0	-634.	60.0	-176.	60.0	-78.	60.0	-42.	60.0	-27.	60.0	-19.
70.0	-3383.	70.0	-2092.	70.0	-739.	70.0	-206.	70.0	-91.	70.0	-49.	70.0	-31.	70.0	-23.
80.0	-3600.	80.0	-2276.	80.0	-808.	80.0	-224.	80.0	-99.	80.0	-54.	80.0	-34.	80.0	-25.
90.0	-3689.	90.0	-2334.	90.0	-826.	90.0	-230.	90.0	-102.	90.0	-55.	90.0	-35.	90.0	-25.
100.0	-3549.	100.0	-2245.	100.0	-793.	100.0	-221.	100.0	-98.	100.0	-53.	100.0	-34.	100.0	-24.
110.0	-3193.	110.0	-2020.	110.0	-714.	110.0	-199.	110.0	-88.	110.0	-48.	110.0	-30.	110.0	-22.
120.0	-2687.	120.0	-1697.	120.0	-597.	120.0	-166.	120.0	-74.	120.0	-40.	120.0	-25.	120.0	-18.
130.0	-2085.	130.0	-1311.	130.0	-462.	130.0	-128.	130.0	-57.	130.0	-31.	130.0	-19.	130.0	-14.
140.0	-1447.	140.0	-908.	140.0	-317.	140.0	-89.	140.0	-40.	140.0	-21.	140.0	-13.	140.0	-10.
150.0	-848.	150.0	-534.	150.0	-185.	150.0	-51.	150.0	-23.	150.0	-12.	150.0	-7.	150.0	-6.
160.0	-384.	160.0	-241.	160.0	-81.	160.0	-21.	160.0	-10.	160.0	-4.	160.0	-2.	160.0	-2.
170.0	-93.	170.0	-57.	170.0	-14.	170.0	-2.	170.0	-2.	170.0	0.	170.0	1.	170.0	-0.
180.0	-10.	180.0	-4.	180.0	4.	180.0	2.	180.0	0.	180.0	1.	180.0	2.	180.0	0.
0.0	2.														
60.0	-2807.														
90.0	-3678.														
0.0	3.														

Figure 55. Dy a-axis strain (in x 10^{-6}/in) versus angle of applied field, θ, relative to a axis. The 30 kOe field was applied in the basal plane.

Dy-- b-AXIS STRAIN VERSUS ANGLE OF APPLIED FIELD IN a-b PLANE RELATIVE TO a-AXIS

T =	4.9	T =	15.5	T =	29.6	T =	49.5	T =	69.7	T =	91.2	T =	111.8	T =	130.0
θ	Δℓ/ℓ	θ	Δℓ/ℓ	θ	Δℓ/ℓ	θ	Δℓ/ℓ	θ	Δℓ/ℓ	θ	Δℓ/ℓ	θ	Δℓ/ℓ	θ	Δℓ/ℓ
0.0	0.	0.0	0.	0.0	0.	0.0	0.	0.0	0.	0.0	0.	0.0	0.	0.0	0.
60.0	8096.	60.0	8086.	60.0	7807.	60.0	7005.	60.0	6034.	60.0	4971.	60.0	4012.	60.0	3236.
90.0	9040.	90.0	9019.	90.0	8809.	90.0	8282.	90.0	7846.	90.0	6632.	90.0	5384.	90.0	4345.
0.0	-3.	0.0	7.	0.0	-3.	0.0	-38.	0.0	-12.	0.0	-44.	0.0	-23.	0.0	-6.
10.0	7.	10.0	13.	10.0	13.	10.0	-9.	10.0	51.	60.0	4911.	10.0	100.	10.0	109.
20.0	43.	20.0	53.	20.0	67.	20.0	107.	20.0	320.	90.0	6600.	20.0	541.	20.0	473.
25.0	252.	25.0	295.	25.0	261.	25.0	275.	25.0	671.	0.0	-44.	30.0	1349.	25.0	727.
28.0	2676.	28.0	2751.	28.0	2533.	28.0	2122.	30.0	3100.	10.0	65.	40.0	2315.	30.0	1062.
30.0	4542.	30.0	4827.	30.0	4732.	30.0	3934.	35.0	4225.	20.0	519.	50.0	3207.	35.0	1406.
32.0	6493.	32.0	6558.	32.0	6393.	32.0	5446.	40.0	4751.	25.0	995.	60.0	4002.	40.0	1776.
35.0	7524.	35.0	7497.	35.0	7118.	35.0	5935.	50.0	5456.	28.0	1448.	70.0	4666.	50.0	2530.
40.0	7608.	40.0	7587.	40.0	7239.	40.0	6171.	60.0	6041.	30.0	1762.	80.0	5182.	60.0	3240.
50.0	7845.	50.0	7825.	50.0	7517.	50.0	6592.	70.0	6564.	32.0	2108.	90.0	5383.	70.0	3805.
60.0	8120.	60.0	8093.	60.0	7815.	60.0	6997.	80.0	7140.	35.0	2564.	100.0	5161.	80.0	4207.
70.0	8375.	70.0	8351.	70.0	8091.	70.0	7370.	90.0	7852.	40.0	3181.	110.0	4653.	90.0	4343.
80.0	8638.	80.0	8623.	80.0	8395.	80.0	7764.	100.0	7140.	50.0	4159.	120.0	3987.	100.0	4187.
90.0	9047.	90.0	9023.	90.0	8813.	90.0	8269.	110.0	6634.	60.0	4920.	130.0	3224.	110.0	3778.
100.0	8815.	100.0	8769.	100.0	8529.	100.0	7870.	120.0	6113.	70.0	5584.	140.0	2305.	120.0	3192.
110.0	8582.	110.0	8531.	110.0	8258.	110.0	7515.	130.0	5542.	80.0	6230.	150.0	1317.	130.0	2505.
120.0	8318.	120.0	8268.	120.0	7974.	120.0	7145.	140.0	4786.	90.0	6599.	160.0	552.	140.0	1761.
130.0	8036.	130.0	8000.	130.0	7684.	130.0	6749.	145.0	4201.	100.0	6198.	170.0	110.	145.0	1384.
140.0	7810.	140.0	7758.	140.0	7399.	140.0	6311.	150.0	1805.	110.0	5611.	180.0	-23.	150.0	1042.
145.0	7634.	145.0	7587.	145.0	7229.	145.0	6046.	155.0	625.	120.0	4958.			155.0	726.
148.0	5132.	148.0	5143.	148.0	4982.	150.0	5208.	160.0	334.	130.0	4221.			160.0	473.
150.0	3465.	150.0	3303.	150.0	3172.	155.0	261.	170.0	59.	140.0	3223.			170.0	113.
152.0	1720.	152.0	1564.	152.0	1358.	160.0	133.	180.0	-20.	150.0	1668.			180.0	-4.
155.0	165.	155.0	170.	155.0	177.	170.0	3.			160.0	533.				
160.0	90.	160.0	89.	160.0	96.	180.0	-38.			170.0	77.				
170.0	33.	170.0	33.	170.0	22.					180.0	-49.				
180.0	17.	180.0	13.	180.0	-3.										

T =	150.1	T =	170.1	T =	189.1	T =	209.4	T =	228.3	T =	249.3	T =	270.9	T =	291.5
θ	Δℓ/ℓ	θ	Δℓ/ℓ	θ	Δℓ/ℓ	θ	Δℓ/ℓ	θ	Δℓ/ℓ	θ	Δℓ/ℓ	θ	Δℓ/ℓ	θ	Δℓ/ℓ
0.0	0.	0.0	0.	0.0	0.	0.0	0.	0.0	0.	0.0	0.	0.0	0.	0.0	0.
60.0	2264.	60.0	1182.	60.0	339.	60.0	117.	60.0	60.	60.0	35.	60.0	23.	60.0	16.
90.0	3047.	90.0	1584.	90.0	451.	90.0	155.	90.0	80.	90.0	46.	90.0	31.	90.0	21.
0.0	-7.	0.0	-2.	0.0	1.	0.0	1.	0.0	1.	0.0	0.	0.0	0.	0.0	0.
10.0	78.	10.0	45.	10.0	15.	10.0	6.	10.0	3.	10.0	1.	10.0	1.	10.0	1.
20.0	329.	20.0	179.	20.0	54.	20.0	20.	20.0	10.	20.0	6.	20.0	4.	20.0	3.
30.0	727.	30.0	408.	30.0	115.	30.0	41.	30.0	21.	30.0	12.	30.0	8.	30.0	6.
40.0	1208.	40.0	640.	40.0	187.	40.0	66.	40.0	34.	40.0	19.	40.0	13.	40.0	9.
50.0	1756.	50.0	918.	50.0	266.	50.0	93.	50.0	47.	50.0	27.	50.0	19.	50.0	13.
60.0	2264.	60.0	1179.	60.0	339.	60.0	118.	60.0	60.	60.0	35.	60.0	24.	60.0	16.
70.0	2675.	70.0	1397.	70.0	399.	70.0	139.	70.0	71.	70.0	41.	70.0	27.	70.0	19.
80.0	2957.	80.0	1536.	80.0	438.	80.0	152.	80.0	78.	80.0	45.	80.0	30.	80.0	21.
90.0	3048.	90.0	1584.	90.0	451.	90.0	156.	90.0	80.	90.0	46.	90.0	31.	90.0	21.
100.0	2947.	100.0	1532.	100.0	436.	100.0	151.	100.0	78.	100.0	45.	100.0	30.	100.0	21.
110.0	2660.	110.0	1386.	110.0	395.	110.0	138.	110.0	70.	110.0	41.	110.0	27.	110.0	19.
120.0	2236.	120.0	1165.	120.0	334.	120.0	116.	120.0	59.	120.0	34.	120.0	23.	120.0	16.
130.0	1737.	130.0	911.	130.0	260.	130.0	91.	130.0	46.	130.0	27.	130.0	18.	130.0	12.
140.0	1208.	140.0	634.	140.0	181.	140.0	65.	140.0	33.	140.0	19.	140.0	13.	140.0	9.
150.0	717.	150.0	375.	150.0	109.	150.0	40.	150.0	19.	150.0	11.	150.0	8.	150.0	5.
160.0	331.	160.0	177.	160.0	50.	160.0	19.	160.0	9.	160.0	5.	160.0	4.	160.0	2.
170.0	70.	170.0	41.	170.0	11.	170.0	6.	170.0	2.	170.0	1.	170.0	2.	170.0	1.
180.0	-15.	180.0	-3.	180.0	-1.	180.0	2.	180.0	0.	180.0	-0.	180.0	1.	180.0	0.

Figure 56. Dy b-axis strain (in x 10^{-6}/in) versus angle of applied field, θ, relative to a axis. The 30 kOe field was applied in the basal plane.

Er-- STRAIN VERSUS TEMPERATURE

1 H APPLIED ALONG a-AXIS 2 H APPLIED ALONG b-AXIS 3 H APPLIED ALONG c-AXIS

a-AXIS H=0		$a\text{-AXIS}_1$ H=30		$a\text{-AXIS}_3$ H=30		b-AXIS H=0		$b\text{-AXIS}_3$ H=30		c- AXIS H=0		$c\text{-AXIS}_2$ H=30		$c\text{-AXIS}_3$ H=30	
T	Δℓ/ℓ	T	Δℓ/ℓ	T	Δℓ/ℓ	T	Δℓ/ℓ	T	Δℓ/ℓ	T	Δℓ/ℓ	T	Δℓ/ℓ	T	Δℓ/ℓ
100.2	-550.	200.1	-305.	203.9	-300.	289.6	-30.	201.1	-220.	289.2	-195.	201.8	-1815.	201.3	-1815.
81.3	-638.	200.2	-313.	203.7	-303.	247.5	-139.	201.1	-223.	263.4	-651.	201.8	-1801.	201.4	-1804.
73.8	-710.	176.7	-373.	186.3	-357.	221.0	-190.	179.5	-260.	245.3	-983.	181.5	-2177.	186.9	-2069.
63.3	-833.	156.8	-434.	160.6	-454.	193.8	-234.	166.4	-289.	242.5	-1040.	162.8	-2506.	163.4	-2482.
58.0	-888.	142.8	-459.	148.9	-501.	165.7	-289.	152.8	-321.	212.3	-1608.	139.9	-2892.	150.4	-2715.
53.5	-927.	127.5	-506.	142.7	-515.	145.2	-322.	141.3	-346.	205.7	-1734.	134.2	-2989.	127.0	-3103.
43.5	-1237.	113.5	-546.	124.5	-580.	117.9	-362.	129.9	-373.	173.1	-2363.	111.2	-3340.	113.3	-3291.
34.2	-1438.	96.6	-614.	98.9	-674.	103.3	-371.	120.5	-392.	144.6	-2868.	89.7	-3634.	97.8	-3479.
29.0	-1533.	79.4	-739.	91.0	-720.	96.6	-413.	103.2	-440.	114.3	-3366.	89.9	-3734.	85.0	-3545.
24.2	-1559.			90.9	-668.	95.2	-419.	94.5	-473.	87.8	-3757.			84.7	-3753.
20.5	-1606.	100.3	-550.			90.6	-436.	86.9	-513.	293.8	-120.	96.5	-3635.		
18.5	-1627.	100.3	-647.	99.6	-626.	87.0	-441.	83.3	-540.	298.4	-31.	96.6	-3548.	98.4	-3605.
17.7	-1634.	83.2	-670.	99.7	-660.	85.0	-458.	79.5	-582.	274.3	-464.	88.6	-3614.	98.4	-3682.
17.3	-1639.	70.2	-842.	84.8	-727.	83.0	-479.	79.5	-590.	236.5	-1158.	86.0	-3632.	89.1	-3494.
17.0	-1804.	57.3	-1007.	77.9	-817.	80.2	-513.	76.9	-627.	214.9	-1558.	79.8	-3567.	85.8	-3502.
16.6	-2768.	55.3	-1028.	72.1	-932.	75.0	-558.	72.1	-732.	187.2	-2083.	67.4	-3437.	83.3	-3500.
16.1	-2768.	50.2	-1110.	62.8	-1345.	72.2	-603.	69.4	-827.	157.9	-2625.	56.7	-3342.	78.6	-3439.
15.2	-2782.	47.7	-1142.	53.1	-1842.	65.7	-669.	65.3	-1030.	128.8	-3128.	49.4	-3234.	70.9	-3082.
12.2	-2806.	39.9	-1271.	44.1	-2229.	58.5	-756.	61.8	-1234.	99.0	-3604.	41.4	-2814.	63.1	-2072.
10.3	-2815.	33.7	-1381.	33.4	-2572.	55.0	-789.	57.7	-1450.	201.2	-1828.	40.6	-2758.	60.5	-1709.
		26.2	-1485.	24.1	-2782.	50.1	-904.	53.8	-1639.			32.1	-2465.	57.1	-1304.
298.4	-5.	23.3	-1518.	20.2	-2846.	48.1	-972.	48.8	-1862.	98.4	-3605.	29.2	-2428.	54.2	-914.
280.9	-68.	23.3	-1548.	18.5	-2876.	47.3	-1000.	42.6	-2072.	88.4	-3737.	27.3	-2426.	49.5	-464.
257.3	-147.	22.0	-1562.	15.2	-2907.			37.2	-2217.	86.0	-3752.	25.5	-2441.	43.2	9.
237.7	-199.	21.2	-1571.	13.0	-2922.	97.9	-479.	33.4	-2281.	76.4	-3658.	23.3	-2459.	39.4	241.
223.1	-233.	20.3	-1582.	10.0	-2934.	80.2	-560.	30.6	-2341.	70.2	-3617.	21.3	-2464.	35.0	386.
208.1	-278.	20.1	-1743.	10.0	-2891.	71.7	-639.	24.2	-2513.	63.0	-3584.	20.7	-2432.	34.1	426.
195.2	-307.	19.6	-3036.			64.9	-700.	33.4	-2281.	58.5	-3563.	20.6	-2355.	29.5	583.
179.0	-353.	19.2	-3032.			57.4	-773.	29.0	-2371.	52.2	-3490.	20.0	1212.	25.0	672.
170.2	-370.	18.6	-3024.			55.0	-789.	25.3	-2432.	48.3	-3242.	19.2	1247.	23.3	704.
154.8	-408.	15.2	-3053.			53.0	-819.	20.6	-2506.	42.6	-2929.	18.6	1277.	21.4	737.
141.3	-443.	12.0	-3108.			51.7	-846.	15.9	-2557.	38.5	-2773.	16.7	1337.	20.9	745.
125.4	-480.	10.0	-3112.			47.3	-1006.	14.5	-2568.	33.5	-2625.	15.2	1373.	18.6	777.
110.0	-521.	11.2	-2845.			39.4	-1202.	14.2	-2573.	26.6	-2538.	13.0	1410.	16.7	796.
93.8	-565.					34.0	-1291.	9.9	-2592.	20.2	-2399.	11.0	1433.	14.7	810.
97.4	-557.					32.4	-1315.	9.9	-2551.	18.6	-2389.	10.7	1435.	12.3	819.
83.2	-612.					26.8	-1371.			18.1	-2333.	10.9	602.	10.0	825.
						22.4	-1431.			17.7	-2250.			29.1	586.
						21.2	-1519.			17.4	464.			29.1	-2149.
						21.2	-1524.			17.0	532.				
						20.0	-1532.			16.3	553.				
						18.9	-1539.			15.2	578.				
						18.3	-1543.			13.0	608.				
						17.7	-1545.			11.7	618.				
						17.7	-1594.			10.5	624.				
						17.6	-1657.								
						17.3	-2507.								
						16.9	-2564.								
						16.6	-2571.								
						15.9	-2583.								
						15.3	-2592.								
						13.5	-2612.								
						10.3	-2629.								

Figure 57. Er a-, b-, and c-axis strain (in x 10^{-6}/in) as a function of temperature in zero field and in 30 kOe fields. The horizontal lines separate data runs.

Er-- a-AXIS STRAIN VERSUS FIELD APPLIED ALONG c-AXIS

T = 11.0		T = 15.2		T = 20.4		T = 27.0		T = 49.1		T = 65.0		T = 79.8		T = 90.2	
H	Δℓ/ℓ	H	Δℓ/ℓ	H	Δℓ/ℓ	H	Δℓ/ℓ	H	Δℓ/ℓ	H	Δℓ/ℓ	H	Δℓ/ℓ	H	Δℓ/ℓ
0.0	0.	0.0	0.	0.0	0.	0.0	0.	0.0	0.	0.0	0.	0.0	0.	0.0	0.
2.0	-1.	1.0	-2.	1.0	1.	1.0	2.	2.0	-2.	2.0	0.	2.0	0.	2.0	0.
4.0	-6.	2.0	-4.	1.5	1.	2.0	5.	4.0	-10.	4.0	0.	4.0	0.	4.0	-1.
6.0	-15.	3.0	-7.	2.0	-666.	3.0	6.	6.0	-15.	6.0	-1.	6.0	-1.	6.0	-2.
8.0	-18.	4.0	-12.	2.5	-876.	4.0	6.	8.0	-16.	8.0	-2.	8.0	-1.	8.0	-4.
10.0	-21.	4.5	-15.	3.0	-1028.	4.5	6.	10.0	-16.	10.0	-3.	10.0	-2.	10.0	-6.
12.0	-23.	5.0	-18.	3.5	-1097.	5.0	-841.	12.0	-15.	12.0	-4.	12.0	-2.	12.0	-8.
14.0	-26.	6.0	-20.	4.0	-1119.	5.5	-983.	14.0	-16.	14.0	-6.	14.0	-3.	14.0	-12.
16.0	-28.	7.0	-22.	4.5	-1080.	6.0	-1108.	16.0	-19.	16.0	-9.	16.0	-3.	16.0	-15.
18.0	-31.	8.0	-23.	5.0	-1053.	6.5	-1103.	16.5	-100.	18.0	-12.	18.0	-6.	18.0	-19.
21.0	-35.	10.0	-25.	5.5	-1050.	7.0	-1052.	16.7	-183.	20.0	-15.	20.0	-14.	21.0	-26.
24.0	-39.	12.0	-29.	6.0	-1051.	7.5	-1028.	16.9	-485.	22.0	-20.	22.0	-23.	24.0	-34.
27.0	-43.	14.0	-31.	6.5	-1052.	8.0	-1028.	17.1	-828.	23.2	-29.	24.0	-35.	27.0	-44.
30.0	-47.	16.0	-34.	7.0	-1053.	8.5	-1030.	17.3	-921.	23.5	-60.	26.0	-46.	30.0	-54.
0.0	0.	18.0	-37.	7.5	-1055.	9.0	-1031.	17.5	-952.	23.7	-88.	28.0	-60.	0.0	0.
		20.0	-39.	8.0	-1055.	10.0	-1032.	17.7	-949.	23.9	-126.	30.0	-73.	T = 120.4	
		22.0	-42.	8.5	-1056.	11.0	-1034.	18.0	-921.	24.1	-154.	0.0	-1.	H	Δℓ/ℓ
		24.0	-45.	9.0	-1056.	12.0	-1035.	18.5	-859.	24.3	-186.			0.0	0.
		26.0	-48.	10.0	-1058.	14.0	-1039.	19.0	-855.	24.5	-214.			2.0	0.
		28.0	-5.	12.0	-1061.	16.0	-1044.	19.5	-862.	25.0	-243.			4.0	0.
		30.7	-55.	14.0	-1064.	18.0	-1047.	20.0	-869.	25.5	-244.			6.0	0.
		0.0	2.	16.0	-1068.	21.0	-1054.	20.5	-874.	26.0	-253.			8.0	-0.
				18.0	-1072.	24.0	-1062.	21.0	-879.	26.5	-264.			10.0	-1.
				21.0	-1077.	27.0	-1068.	22.0	-889.	27.0	-275.			12.0	-2.
				24.0	-1082.	30.7	-1075.	23.0	-898.	28.0	-297.			14.0	-3.
				27.0	-1088.	30.7	-1069.	24.0	-906.	29.0	-316.			16.0	-4.
				30.0	-1093.	0.0	-84.	26.0	-926.	30.0	-337.			18.0	-5.
				30.7	-1094.			28.0	-942.	0.0	-1.			21.0	-7.
				0.0	44.			30.0	-959.					24.0	-9.
								0.0	-60.					26.0	-11.
														28.0	-12.
														30.0	-14.
														0.0	2.

Er-- b-AXIS STRAIN VERSUS FIELD APPLIED ALONG c-AXIS

T = 10.0		T = 15.2		T = 20.6		T = 29.0		T = 50.2		T = 64.8		T = 80.7		T = 91.0	
H	Δℓ/ℓ	H	Δℓ/ℓ	H	Δℓ/ℓ	H	Δℓ/ℓ	H	Δℓ/ℓ	H	Δℓ/ℓ	H	Δℓ/ℓ	H	Δℓ/ℓ
0.0	0.	0.0	0.	0.0	0.	0.0	0.	0.0	0.	0.0	0.	0.0	0.	0.0	0.
3.0	-2.	3.0	-3.	1.0	0.	2.0	5.	3.0	-3.	3.0	-0.	3.0	0.	3.0	-0.
6.0	-13.	6.0	-15.	1.5	24.	3.0	6.	6.0	-15.	6.0	-1.	6.0	0.	6.0	-2.
9.0	-18.	9.0	-21.	1.8	14.	4.0	8.	9.0	-19.	9.0	-4.	9.0	-1.	9.0	-5.
12.0	-21.	12.0	-25.	2.0	-3.	4.5	11.	12.0	-19.	12.0	-6.	12.0	-1.	12.0	-9.
15.0	-24.	15.0	-28.	2.3	-96.	5.0	20.	15.0	-21.	15.0	-11.	15.0	-1.	15.0	-14.
18.0	-28.	18.0	-32.	2.5	-190.	5.5	29.	17.0	-35.	17.0	-14.	18.0	-9.	18.0	-19.
21.0	-31.	21.0	-37.	2.8	-963.	5.8	-92.	17.3	-122.	18.0	-17.	20.0	-16.	21.0	-27.
24.0	-34.	24.0	-40.	3.0	-1010.	6.0	-202.	17.5	-237.	20.0	-20.	22.0	-27.	24.0	-35.
27.0	-38.	27.0	-44.	3.3	-1049.	6.3	-885.	17.7	-510.	22.0	-25.	24.0	-37.	27.0	-46.
30.0	-41.	30.0	-49.	3.5	-1069.	6.5	-987.	18.0	-899.	23.0	-29.	26.0	-49.	30.0	-57.
0.0	1.	0.0	2.	3.8	-1075.	6.8	-1036.	18.3	-926.	23.5	-71.	28.0	-62.	0.0	1.
				4.0	-1064.	7.0	-1051.	18.5	-917.	23.8	-126.	30.0	-77.	T = 120.7	
				4.3	-1048.	7.5	-1015.	18.7	-899.	24.0	-172.	0.0	0.	H	Δℓ/ℓ
				4.5	-1040.	8.0	-991.	19.0	-871.	24.3	-222.			0.0	0.
				5.0	-1033.	9.0	-994.	19.5	-862.	24.5	-253.			3.0	0.
				6.0	-1036.	10.0	-999.	20.0	-931.	24.8	-278.			6.0	-0.
				7.0	-1038.	12.0	-1004.	20.5	-936.	25.0	-283.			9.0	-1.
				8.0	-1040.	14.0	-1010.	21.0	-942.	25.5	-285.			12.0	-2.
				10.0	-1044.	16.0	-1016.	22.0	-951.	26.0	-294.			15.0	-4.
				12.0	-1048.	18.0	-1023.	23.0	-959.	26.5	-311.			18.0	-5.
				14.0	-1052.	21.0	-1031.	24.0	-968.	27.0	-322.			21.0	-8.
				16.0	-1055.	24.0	-1038.	26.0	-984.	28.0	-348.			24.0	-10.
				18.0	-1059.	27.0	-1046.	28.0	-998.	29.0	-374.			27.0	-13.
				21.0	-1068.	30.0	-1055.	30.0	-1015.	30.0	-403.			30.0	-16.
				24.0	-1073.	0.0	-57.	0.0	-95.	0.0	-14.			0.0	1.
				27.0	-1078.										
				30.0	-1083.										
				0.0	5.										

Figure 58. Er a- and b-axis strain (in x 10^{-6}/in) versus field, H, applied along c axis.

Er-- c-AXIS STRAIN VERSUS FIELD APPLIED ALONG c-AXIS

T = 11.1		T = 15.2		T = 20.4		T = 29.1		T = 49.8		T = 65.4		T = 78.9		T = 89.2	
H	Δℓ/ℓ	H	Δℓ/ℓ	H	Δℓ/ℓ	H	Δℓ/ℓ	H	Δℓ/ℓ	H	Δℓ/ℓ	H	Δℓ/ℓ	H	Δℓ/ℓ
0.0	0.	0.0	0.	0.0	0.	0.0	0.	0.0	0.	0.0	0.	0.0	0.	0.0	0.
2.0	2.	2.0	8.	1.0	1.	1.0	-4.	2.0	11.	2.0	1.	2.0	0.	2.0	1.
4.0	8.	4.0	18.	1.5	2.	1.5	-8.	3.0	12.	4.0	1.	4.0	0.	4.0	4.
6.0	23.	6.0	38.	1.7	11.	2.0	-12.	4.0	12.	6.0	2.	6.0	-1.	6.0	9.
8.0	32.	8.0	50.	1.9	52.	2.5	-19.	5.0	11.	8.0	2.	8.0	-2.	8.0	16.
10.0	41.	10.0	58.	2.1	2672.	3.0	-24.	6.0	9.	10.0	4.	10.0	-2.	10.0	24.
12.0	50.	12.0	68.	2.3	3021.	3.5	-33.	7.0	7.	12.0	10.	12.0	-2.	12.0	34.
14.0	60.	14.0	78.	2.5	3232.	4.0	-43.	8.0	4.	14.0	19.	14.0	-2.	15.0	53.
16.0	68.	16.0	88.	2.7	3507.	4.5	-56.	9.0	1.	16.0	31.	16.0	-2.	18.0	75.
18.0	77.	18.0	98.	2.9	3660.	5.0	-66.	10.0	-1.	18.0	36.	18.0	-2.	21.0	103.
20.0	87.	21.0	114.	3.1	3807.	5.3	20.	11.0	-3.	19.0	37.	20.0	0.	23.0	124.
22.0	96.	24.0	128.	3.3	3897.	5.5	1325.	12.0	-6.	20.0	39.	21.0	7.	25.0	146.
24.0	106.	27.0	144.	3.5	3573.	5.7	1723.	14.0	-10.	21.0	40.	22.0	16.	27.0	170.
26.0	116.	30.0	159.	3.7	3518.	6.0	2137.	16.0	-12.	22.0	42.	22.5	27.	29.0	196.
28.0	125.	0.0	16.	4.0	3341.	6.5	2705.	17.0	-11.	23.0	45.	23.0	37.	30.0	211.
30.7	138.			4.5	3322.	7.0	2869.	17.7	5.	24.0	48.	23.5	47.	0.0	3.
0.0	11.			5.0	3326.	7.5	2542.	18.0	2520.	25.0	143.	24.0	58.		
				5.5	3322.	8.0	2576.	18.5	3086.	25.3	379.	24.5	69.	T = 119.1	
				6.0	3328.	8.5	2589.	19.0	2770.	25.6	529.	25.0	81.	H	Δℓ/ℓ
				7.0	3335.	9.0	2594.	19.5	2643.	26.0	747.	25.5	93.	0.0	0.
				8.0	3342.	10.0	2607.	20.0	2656.	26.5	884.	26.0	106.	2.0	1.
				10.0	3353.	11.0	2617.	21.0	2692.	27.0	940.	26.5	117.	4.0	1.
				12.0	3365.	12.0	2625.	22.0	2722.	27.5	978.	27.0	130.	6.0	3.
				14.0	3377.	14.0	2641.	24.0	2779.	28.0	1012.	28.0	155.	8.0	5.
				16.0	3388.	16.0	2661.	26.0	2831.	29.0	1077.	29.0	182.	10.0	7.
				18.0	3400.	18.0	2674.	28.0	2880.	30.0	1141.	30.0	210.	12.0	11.
				21.0	3418.	21.0	2700.	30.0	2930.	0.0	3.	0.0	-2.	14.0	14.
				24.0	3436.	24.0	2726.	0.0	111.					16.0	18.
				27.0	3454.	27.0	2751.							18.0	22.
				30.0	3472.	30.0	2775.							21.0	30.
				0.0	-105.	0.0	-17.							24.0	40.
														27.0	50.
														30.0	62.
														0.0	0.

Er-- c-AXIS STRAIN VERSUS FIELD APPLIED ALONG b-AXIS

T = 4.9		T = 10.7		T = 15.2		T = 20.4		T = 29.4		T = 50.8		T = 65.8		T = 78.9	
H	Δℓ/ℓ	H	Δℓ/ℓ	H	Δℓ/ℓ	H	Δℓ/ℓ	H	Δℓ/ℓ	H	Δℓ/ℓ	H	Δℓ/ℓ	H	Δℓ/ℓ
0.0	0.	0.0	0.	0.0	0.	0.0	0.	0.0	0.	0.0	0.	0.0	0.	0.0	0.
2.0	-4.	2.0	1.	2.0	0.	2.0	-3.	2.0	-3.	2.0	1.	2.0	1.	2.0	1.
4.0	-2.	4.0	2.	4.0	1.	4.0	1.	4.0	3.	4.0	3.	4.0	3.	4.0	2.
6.0	-1.	6.0	5.	6.0	1.	6.0	7.	6.0	12.	6.0	8.	6.0	7.	6.0	5.
8.0	-0.	8.0	6.	8.0	1.	8.0	14.	8.0	20.	8.0	15.	8.0	13.	8.0	9.
10.0	-2.	10.0	7.	10.0	-1.	10.0	23.	10.0	26.	10.0	23.	10.0	21.	10.0	15.
12.0	-6.	12.0	5.	12.0	-5.	12.0	34.	14.0	45.	12.0	33.	12.0	30.	12.0	21.
13.0	-10.	14.0	0.	14.0	-9.	14.0	47.	16.0	58.	14.0	44.	14.0	41.	14.0	29.
14.0	-16.	16.0	-8.	16.0	-16.	16.0	81.	18.0	69.	16.0	59.	16.0	53.	16.0	37.
15.0	-23.	17.0	-10.	18.0	-18.	19.0	92.	21.0	93.	18.0	74.	18.0	67.	18.0	47.
16.0	-31.	18.0	-9.	18.5	-10.	20.0	102.	24.0	115.	20.0	92.	20.0	84.	20.0	59.
17.0	-36.	18.3	-3.	18.7	20.	21.0	115.	27.0	141.	22.0	111.	22.0	101.	22.0	71.
18.0	-39.	18.5	20.	18.9	101.	22.0	128.	30.0	169.	24.0	133.	24.0	120.	24.0	84.
18.5	-34.	18.7	68.	19.1	215.	23.0	143.	30.7	177.	27.0	166.	26.0	140.	25.0	91.
18.7	-8.	18.9	141.	19.3	480.	24.0	158.	0.0	-72.	30.0	186.	28.0	163.	26.0	98.
18.9	65.	19.1	259.	19.5	589.	25.0	177.			0.0	-1.	30.0	185.	27.0	106.
19.1	148.	19.3	474.	19.7	621.	26.0	194.					0.0	-4.	28.0	114.
19.3	260.	19.5	638.	19.9	640.	27.0	213.							29.0	122.
19.5	463.	19.7	672.	20.1	654.	28.0	234.	T = 89.5		T = 119.1		T = 150.4		30.0	131.
19.7	565.	19.9	691.	20.5	669.	29.0	275.	H	Δℓ/ℓ	H	Δℓ/ℓ	H	Δℓ/ℓ	30.7	137.
19.9	608.	20.1	704.	21.0	683.	30.0	1260.	0.0	0.	0.0	0.	0.0	0.	0.0	-2.
20.1	635.	20.3	718.	22.0	708.	30.2	1725.	2.0	1.	2.0	0.	3.0	0.		
20.3	626.	20.5	726.	24.0	759.	30.4	2107.	4.0	2.	4.0	1.	6.0	0.		
20.5	639.	21.0	744.	26.0	810.	30.6	2439.	6.0	5.	6.0	3.	9.0	-0.		
21.0	660.	22.0	768.	28.0	857.	30.7	2577.	8.0	8.	8.0	4.	12.0	-1.		
22.0	669.	23.0	792.	30.0	903.	0.0	113.	10.0	13.	10.0	7.	15.0	-2.		
23.0	693.	24.0	814.	0.0	-24.			12.0	18.	12.0	9.	18.0	-2.		
24.0	715.	25.0	838.					15.0	27.	15.0	14.	21.0	-3.		
26.0	743.	26.0	858.					18.0	40.	18.0	20.	24.0	-4.		
28.0	780.	28.0	901.					21.0	54.	21.0	27.	27.0	-5.		
30.0	820.	30.0	942.					24.0	71.	24.0	34.	30.0	-7.		
0.0	-55.	0.0	-3.					27.0	90.	27.0	43.	0.0	0.		
								30.0	111.	30.0	53.				
								0.0	0.	0.0	-1.				

Figure 59. Er c-axis strain (in x 10^{-6}/in) versus field, H, applied along c and b axes of a-c and b-c planes respectively.

Er-- a- AXIS STRAIN VERSUS FIELD APPLIED ALONG a-AXIS

T = 10.6		T = 15.0		T = 20.4		T = 49.0		T = 64.9		T = 79.6		T = 90.2		T = 120.4	
H	Δℓ/ℓ	H	Δℓ/ℓ	H	Δℓ/ℓ	H	Δℓ/ℓ	H	Δℓ/ℓ	H	Δℓ/ℓ	H	Δℓ/ℓ	H	Δℓ/ℓ
0.0	0.	0.0	0.	0.0	0.	0.0	0.	0.0	0.	0.0	0.	0.0	0.	0.0	0.
2.0	0.	1.0	0.	1.0	5.	2.0	4.	2.0	0.	2.0	0.	2.0	0.	2.0	0.
4.0	0.	1.5	0.	2.0	22.	4.0	15.	4.0	-3.	4.0	-1.	4.0	-1.	4.0	-0.
6.0	-1.	2.0	0.	3.0	27.	6.0	26.	6.0	-6.	6.0	-3.	6.0	-2.	6.0	-1.
8.0	-2.	3.0	0.	4.0	28.	8.0	28.	8.0	-9.	8.0	-5.	8.0	-5.	8.0	-2.
10.0	-3.	4.0	-1.	5.0	28.	10.0	26.	10.0	-14.	10.0	-8.	10.0	-7.	10.0	-3.
12.0	-2.	5.0	-1.	6.0	28.	12.0	20.	12.0	-19.	12.0	-12.	12.0	-10.	12.0	-5.
14.0	-1.	6.0	-1.	8.0	28.	14.0	13.	14.0	-25.	14.0	-16.	14.0	-13.	14.0	-6.
16.0	-1.	7.0	-2.	10.0	26.	16.0	4.	16.0	-32.	16.0	-21.	16.0	-17.	16.0	-8.
17.0	-5.	8.0	-3.	12.0	21.	18.0	-5.	18.0	-41.	18.0	-26.	18.0	-21.	18.0	-10.
17.5	-19.	9.0	-3.	14.0	16.	20.0	-16.	20.0	-90.	20.0	-32.	20.0	-26.	20.0	-12.
17.7	-42.	10.0	-3.	16.0	12.	22.0	-29.	22.0	-60.	22.0	-39.	22.0	-31.	22.0	-14.
17.9	-87.	12.0	-3.	18.0	7.	24.0	-42.	24.0	-71.	24.0	-46.	24.0	-37.	24.0	-17.
18.1	-130.	14.0	-2.	21.0	-1.	26.0	-59.	26.0	-83.	26.0	-54.	26.0	-43.	26.0	-20.
18.3	-167.	15.0	-1.	24.0	-12.	28.0	-77.	28.0	-95.	28.0	-62.	28.0	-51.	28.0	-23.
18.5	-197.	16.5	-1.	27.0	-23.	30.0	-99.	30.0	-109.	30.0	-72.	30.0	-58.	30.0	-26.
18.7	-229.	17.0	-3.	28.0	-28.	0.0	34.	0.0	-4.	0.0	0.	0.0	-2.	0.0	1.
19.0	-266.	17.5	-10.	29.0	-33.										
19.5	-275.	17.8	-30.	29.5	-37.										
20.0	-272.	18.0	-60.	30.0	-45.										
20.5	-270.	18.3	-116.	30.0	-89.										
21.0	-268.	18.5	-174.	30.3	-132.										
22.0	-266.	18.8	-213.	30.7	-215.										
24.0	-268.	19.0	-234.	0.0	16.										
26.0	-266.	19.5	-248.												
28.0	-274.	20.0	-247.												
30.0	-277.	20.5	-245.												
0.0	-3.	21.0	-243.												
		22.0	-244.												
		23.0	-246.												
		24.0	-247.												
		25.0	-248.												
		26.0	-248.												
		27.0	-249.												
		28.0	-252.												
		29.0	-256.												
		30.0	-258.												
		30.7	-259.												
		0.0	-7.												

Er-- b-AXIS STRAIN VERSUS FIELD APPLIED ALONG a-AXIS

T = 9.9		T = 15.2		T = 20.3		T = 29.0		T = 47.4		T = 65.1		T = 79.0		T = 89.8	
H	Δℓ/ℓ	H	Δℓ/ℓ	H	Δℓ/ℓ	H	Δℓ/ℓ	H	Δℓ/ℓ	H	Δℓ/ℓ	H	Δℓ/ℓ	H	Δℓ/ℓ
0.0	0.	0.0	0.	0.0	0.	0.0	0.	0.0	0.	0.0	0.	0.0	0.	0.0	0.
3.0	0.	2.0	1.	3.0	-22.	2.0	-11.	2.0	-12.	3.0	-1.	3.0	0.	3.0	0.
6.0	-1.	4.0	1.	6.0	-23.	4.0	-56.	4.0	-47.	6.0	-2.	6.0	0.	6.0	-0.
9.0	-2.	6.0	-1.	9.0	-21.	6.0	-99.	6.0	-79.	9.0	-3.	9.0	-1.	9.0	-1.
12.0	-2.	8.0	-2.	12.0	-23.	8.0	-115.	8.0	-90.	12.0	-4.	12.0	-2.	12.0	-2.
15.0	-3.	10.0	-2.	15.0	-42.	10.0	-125.	9.0	-92.	15.0	-6.	15.0	-3.	15.0	-3.
18.0	-16.	12.0	-2.	16.0	-49.	12.0	-139.	10.0	-93.	18.0	-9.	18.0	-5.	18.0	-5.
18.3	-49.	14.0	-3.	17.0	-56.	14.0	-154.	11.0	-94.	21.0	-12.	21.0	-6.	21.0	-7.
18.5	-106.	16.0	-3.	18.0	-64.	16.0	-164.	12.0	-95.	24.0	-15.	24.0	-8.	24.0	-8.
18.7	-162.	17.0	-3.	20.0	-80.	18.0	-174.	14.0	-95.	27.0	-19.	27.0	-11.	27.0	-11.
18.9	-193.	18.0	-6.	22.0	-95.	20.0	-183.	16.0	-94.	30.0	-23.	30.0	-14.	30.0	-13.
19.1	-204.	18.3	-13.	24.0	-111.	22.0	-192.	18.0	-92.			0.0	0.	0.0	0.
19.3	-211.	18.5	-45.	26.0	-127.	24.0	-201.	20.0	-88.						
19.5	-216.	18.7	-112.	28.0	-144.	26.0	-210.	22.0	-80.					T = 119.1	
20.0	-224.	18.9	-159.	29.0	-150.	28.0	-218.	24.0	-65.					H	Δℓ/ℓ
21.0	-236.	19.1	-184.	29.8	-158.	30.0	-226.	26.0	-46.					0.0	0.
22.0	-247.	19.3	-193.	30.0	-162.	30.0	-222.	28.0	-24.					3.0	0.
24.0	-272.	19.5	-201.	30.2	-169.	0.0	-5.	30.0	-1.					6.0	0.
26.0	-295.	19.7	-205.	30.4	-178.			0.0	-11.					9.0	-1.
28.0	-319.	20.0	-210.	30.6	-196.									12.0	-1.
30.0	-344.	21.0	-223.	30.7	-213.									15.0	-2.
0.0	3.	22.0	-236.	0.0	14.									18.0	-2.
		23.0	-251.											21.0	-3.
		24.0	-264.											24.0	-4.
		26.0	-291.											27.0	-6.
		28.0	-318.											30.0	-7.
		30.0	-345.												
		0.0	6.												

Figure 60. Er a- and b-axis strain (in x 10^{-6}/in) versus field, H, applied along the a axis of the a-c and a-b plane specimens respectively.

Er-- b-AXIS STRAIN VERSUS FIELD APPLIED ALONG b-AXIS

T = 4.6		T = 9.9		T = 15.2		T = 20.4		T = 29.0		T = 47.3		T = 64.6		T = 79.3	
H	Δℓ/ℓ	H	Δℓ/ℓ	H	Δℓ/ℓ	H	Δℓ/ℓ	H	Δℓ/ℓ	H	Δℓ/ℓ	H	Δℓ/ℓ	H	Δℓ/ℓ
0.0	0.	0.0	0.	0.0	0.	0.0	0.	0.0	0.	0.0	0.	0.0	0.	0.0	0.
2.0	-7.	3.0	0.	2.0	0.	2.0	40.	2.0	21.	2.0	14.	2.0	-0.	3.0	-1.
4.0	-6.	6.0	0.	4.0	0.	3.0	56.	4.0	92.	4.0	48.	4.0	-2.	6.0	-3.
6.0	-6.	9.0	-1.	6.0	-1.	4.0	62.	6.0	144.	5.0	64.	6.0	-4.	9.0	-7.
8.0	-4.	12.0	-0.	8.0	-2.	5.0	62.	8.0	161.	6.0	72.	8.0	-7.	12.0	-12.
10.0	-5.	15.0	-0.	10.0	-4.	6.0	61.	10.0	155.	7.0	75.	10.0	-12.	15.0	-18.
12.0	-3.	17.0	-2.	12.0	-5.	7.0	62.	12.0	148.	8.0	75.	12.0	-16.	18.0	-25.
14.0	-1.	17.5	-3.	14.0	-5.	8.0	60.	14.0	138.	10.0	71.	14.0	-22.	21.0	-35.
16.0	-0.	18.0	-8.	16.0	-7.	9.0	59.	16.0	126.	12.0	65.	16.0	-29.	24.0	-45.
18.0	-4.	18.3	-21.	18.0	-12.	10.0	58.	18.0	113.	14.0	58.	18.0	-37.	27.0	-56.
18.3	-10.	18.5	-53.	18.3	-16.	12.0	55.	20.0	96.	16.0	86.	20.0	-45.	30.0	-70.
18.5	-35.	18.7	-107.	18.5	-28.	14.0	48.	22.0	80.	18.0	39.	22.0	-54.		
18.7	-87.	18.9	-153.	18.7	-74.	16.0	42.	24.0	62.	20.0	27.	24.0	-65.		
18.9	-128.	19.1	-167.	18.9	-118.	18.0	35.	26.0	41.	22.0	15.	26.0	-76.		
19.1	-160.	19.3	-170.	19.1	-169.	20.0	25.	28.0	19.	24.0	6.	28.0	-88.		
19.3	-167.	19.5	-173.	19.3	-177.	22.0	13.	30.0	-3.	26.0	-5.	30.0	-100.		
19.5	-170.	20.0	-177.	19.5	-181.	24.0	1.	0.0	25.	28.0	-16.	0.0	0.		
20.0	-174.	22.0	-180.	20.0	-186.	26.0	-13.			0.0	10.				
21.0	-177.	24.0	-180.	20.5	-189.	28.0	-28.								
22.0	-177.	26.0	-179.	21.0	-193.	30.0	-86.								
24.0	-175.	28.0	-178.	22.0	-195.	30.2	-160.								
26.0	-173.	30.0	-177.	23.0	-197.	30.4	-222.								
28.0	-170.	0.0	0.	24.0	-199.	30.6	-677.								
30.0	-167.			26.0	-203.	30.7	-913.								
0.0	2.			28.0	-206.	30.7	-536.								
				30.0	-209.	0.0	-36.								
				0.0	2.										

Er-- c-AXIS STRAIN VERSUS FIELD APPLIED ALONG a-AXIS

T = 89.8		T = 119.4		T = 150.2		T = 10.5		T = 14.2		T = 20.5		T = 29.0	
H	Δℓ/ℓ	H	Δℓ/ℓ	H	Δℓ/ℓ	H	Δℓ/ℓ	H	Δℓ/ℓ	H	Δℓ/ℓ	H	Δℓ/ℓ
0.0	0.	0.0	0.	0.0	0.	0.0	0.	0.0	0.	0.0	0.	0.0	0.
3.0	-0.	3.0	-0.	3.0	-0.	3.0	2.	3.0	3.	3.0	-9.	3.0	-5.
6.0	-2.	6.0	-1.	6.0	-1.	6.0	7.	6.0	8.	6.0	-1.	6.0	3.
9.0	-5.	9.0	-3.	9.0	-2.	9.0	11.	9.0	15.	9.0	11.	9.0	14.
12.0	-9.	12.0	-5.	12.0	-3.	12.0	13.	12.0	20.	12.0	27.	12.0	30.
15.0	-14.	15.0	-7.	15.0	-4.	15.0	9.	15.0	21.	15.0	47.	15.0	53.
18.0	-20.	18.0	-10.	18.0	-6.	17.0	9.	17.0	21.	18.0	75.	18.0	79.
21.0	-27.	21.0	-13.	21.0	-8.	18.0	17.	18.0	28.	21.0	110.	21.0	111.
24.0	-35.	24.0	-17.	24.0	-10.	18.3	44.	18.3	50.	24.0	154.	24.0	149.
27.0	-44.	27.0	-22.	27.0	-12.	18.5	91.	18.5	88.	27.0	213.	27.0	192.
30.0	-55.	30.0	-27.	30.0	-15.	18.7	151.	18.7	139.	28.0	249.	30.0	241.
0.0	0.	0.0	0.	0.0	0.	19.0	306.	19.0	311.	29.0	300.	0.0	-0.
						19.3	578.	19.3	565.	29.3	373.		
						19.5	652.	19.5	633.	29.5	419.		
						19.7	714.	19.7	674.	29.8	904.		
						20.0	747.	20.0	724.	30.0	1446.		
						21.0	798.	21.0	771.	30.2	1739.		
						22.0	826.	22.0	799.	30.5	2680.		
						23.0	852.	24.0	852.	30.7	3036.		
						24.0	877.	26.0	906.	0.0	-7.		
						26.0	925.	28.0	948.				
						28.0	972.	30.0	997.				
						30.0	1018.	0.0	-4.				
						0.0	0.						

Figure 61. Er b- and c-axis strain (in x 10^{-6}/in) versus field, H. Specimens were the a-b and a-c planes respectively.

Er-- b-AXIS STRAIN VERSUS ANGLE OF APPLIED FIELD IN a-b PLANE RELATIVE TO a-AXIS

T = 4.6		T = 9.9		T = 15.2		T = 20.4		T = 29.0		*T = 47.5		T = 47.4		T = 64.8	
θ	Δℓ/ℓ	θ	Δℓ/ℓ	θ	Δℓ/ℓ	θ	Δℓ/ℓ	θ	Δℓ/ℓ	θ	Δℓ/ℓ	θ	Δℓ/ℓ	θ	Δℓ/ℓ
0.0	0.	0.0	0.	0.0	0.	90.0	-302.	0.0	0.	0.0	0.	0.0	0.	0.0	0.
60.0	140.	60.0	135.	10.0	2.	0.0	0.	10.0	6.	10.0	4.	10.0	-0.	60.0	-61.
90.0	179.	90.0	170.	20.0	11.	10.0	0.	20.0	31.	20.0	17.	20.0	-1.	90.0	-80.
0.0	1.	0.0	0.	25.0	19.	20.0	-46.	30.0	103.	30.0	36.	30.0	-4.	0.0	-1.
10.0	3.	10.0	3.	30.0	30.	25.0	-190.	40.0	178.	40.0	61.	40.0	-7.	10.0	-4.
20.0	15.	20.0	15.	35.0	42.	30.0	-294.	50.0	192.	50.0	86.	50.0	-13.	20.0	-11.
30.0	38.	30.0	38.	40.0	56.	35.0	-286.	60.0	190.	60.0	111.	60.0	-20.	30.0	-23.
40.0	70.	40.0	67.	50.0	87.	40.0	-277.	70.0	189.	70.0	130.	70.0	-26.	40.0	-35.
50.0	108.	50.0	102.	60.0	113.	50.0	-225.	80.0	197.	80.0	143.	80.0	-30.	50.0	-49.
60.0	143.	60.0	135.	70.0	130.	60.0	-140.	90.0	216.	90.0	148.	90.0	-32.	60.0	-62.
70.0	165.	70.0	156.	80.0	138.	70.0	-120.	100.0	194.	100.0	144.	100.0	-30.	70.0	-73.
80.0	177.	80.0	167.	90.0	139.	80.0	-130.	110.0	180.	110.0	130.	110.0	-25.	80.0	-79.
90.0	181.	90.0	170.	100.0	136.	90.0	-247.	120.0	179.	120.0	110.	120.0	-18.	90.0	-82.
100.0	176.	100.0	166.	110.0	127.	95.0	-257.	130.0	182.	130.0	85.	130.0	-11.	100.0	-79.
110.0	163.	110.0	154.	120.0	112.	100.0	-260.	140.0	174.	140.0	60.	140.0	-4.	110.0	-73.
120.0	141.	120.0	133.	130.0	88.	110.0	-239.	150.0	121.	150.0	35.	150.0	-0.	120.0	-62.
130.0	110.	130.0	103.	140.0	59.	120.0	-173.	160.0	42.	160.0	16.	160.0	3.	130.0	-49.
140.0	71.	140.0	66.	150.0	30.	130.0	-163.	170.0	13.	170.0	3.	170.0	4.	140.0	-35.
150.0	37.	150.0	34.	160.0	11.	140.0	-200.	180.0	5.	180.0	-1.	180.0	5.	150.0	-22.
160.0	14.	160.0	12.	170.0	2.	150.0	-325.	0.0	5.	90.0	148.	90.0	-31.	160.0	-12.
170.0	1.	170.0	1.	180.0	1.	160.0	-358.			60.0	110.	0.0	6.	170.0	-5.
180.0	1.	180.0	2.	90.0	140.	170.0	-342.			0.0	-0.	60.0	-18.	180.0	-3.
90.0	180.	90.0	171.	60.0	117.	180.0	-273.					90.0	-31.	90.0	-82.
0.0	2.	0.0	2.	0.0	2.	90.0	-185.					0.0	7.	0.0	-2.
				60.0	115.	0.0	78.								
				90.0	141.										
				0.0	2.										

T = 79.0		T = 89.8		T = 119.2		T = 150.0	
θ	Δℓ/ℓ	θ	Δℓ/ℓ	θ	Δℓ/ℓ	θ	Δℓ/ℓ
0.0	0.	0.0	0.	0.0	0.	0.0	0.
10.0	-2.	60.0	-31.	10.0	-0.	10.0	0.
20.0	-6.	90.0	-41.	20.0	-2.	20.0	-1.
30.0	-14.	0.0	0.	30.0	-5.	30.0	-3.
40.0	-23.	10.0	-1.	40.0	-8.	40.0	-5.
50.0	-23.	20.0	-5.	50.0	-12.	50.0	-7.
60.0	-32.	30.0	-10.	60.0	-15.	60.0	-8.
70.0	-48.	40.0	-17.	70.0	-17.	70.0	-10.
80.0	-53.	50.0	-24.	80.0	-19.	80.0	-11.
90.0	-54.	60.0	-31.	90.0	-19.	90.0	-11.
100.0	-52.	70.0	-37.	100.0	-19.	100.0	-10.
110.0	-47.	80.0	-40.	110.0	-17.	110.0	-9.
120.0	-40.	90.0	-41.	120.0	-14.	120.0	-8.
130.0	-31.	100.0	-40.	130.0	-11.	130.0	-6.
140.0	-22.	110.0	-36.	140.0	-7.	140.0	-4.
150.0	-13.	120.0	-31.	150.0	-4.	150.0	-2.
160.0	-6.	130.0	-24.	160.0	-1.	160.0	-1.
170.0	-1.	140.0	-17.	170.0	0.	170.0	1.
180.0	0.	150.0	-10.	180.0	1.	180.0	1.
90.0	-54.	160.0	-5.	90.0	-19.	90.0	-11.
60.0	-41.	170.0	-1.	60.0	-14.	60.0	-8.
0.0	0.	180.0	0.	0.0	1.	0.0	1.
60.0	-40.	90.0	-41.	60.0	-14.		
90.0	-54.	60.0	-31.	90.0	-19.		
0.0	1.	0.0	0.	0.0	1.		

Figure 62. Er b-axis strain (in x 10^{-6}/in) versus angle of applied field, θ, relative to a axis. The 30 kOe field was applied in the basal plane.

Tb-- STRAIN VERSUS TEMPERATURE

H APPLIED ALONG b-AXIS

a-Axis H=0		a-Axis H=30		b-Axis H=0		b-Axis H=30		c-Axis H=0		c-Axis H=30	
T	Δℓ/ℓ	T	Δℓ/ℓ	T	Δℓ/ℓ	T	Δℓ/ℓ	T	Δℓ/ℓ	T	Δℓ/ℓ
300.0	4.	291.4	-94.	300.0	0.	300.1	0.	364.6	563.	350.0	462.
239.3	-320.	280.4	-184.	296.7	-25.	300.1	10.	351.2	463.	350.0	493.
232.9	-377.	272.5	-266.	289.5	-57.	296.8	-5.	350.0	456.	340.7	430.
229.1	-447.	259.2	-466.	277.8	-118.	280.8	-70.	338.2	368.	329.6	340.
224.8	-554.	259.0	-485.	258.0	-215.	271.3	-108.	327.4	278.	318.9	259.
221.4	-643.	266.1	-363.	251.0	-255.	265.6	-128.	316.5	170.	297.7	88.
219.4	-772.	252.0	-652.	242.7	-309.	258.0	-150.	303.0	29.	280.1	44.
216.8	-867.	245.5	-851.	238.3	-343.	249.7	-157.	290.5	-95.	271.9	44.
213.6	-966.	240.8	-1014.	234.3	-384.	242.9	-142.	289.7	-102.	267.8	77.
210.4	-1051.	235.9	-1196.	232.3	-476.	233.5	-85.	273.3	-242.	260.7	176.
205.9	-1174.	232.4	-1322.	226.6	-543.	224.3	8.	258.0	-335.	255.8	281.
202.4	-1261.	226.0	-1555.	222.0	-668.	211.5	181.	252.3	-358.	251.3	434.
197.6	-1370.	217.6	-1851.	219.7	-727.	205.0	281.	248.5	-360.	234.9	1182.
214.4	-985.	217.0	-1869.	217.7	-751.	195.9	428.	238.6	-328.	227.7	1540.
217.8	-884.	211.5	-2054.	215.0	-774.	179.6	698.	211.1	1717.	213.1	2115.
219.2	-832.	210.8	-2076.	211.2	-794.	163.9	985.	222.7	582.	200.8	2427.
222.1	-636.	201.8	-2366.	204.5	-815.	147.2	1272.	225.0	346.	190.6	2595.
225.3	-550.	192.6	-2657.	195.0	-814.	132.5	1524.	228.0	-13.	180.7	2696.
229.7	-432.	192.2	-2671.	185.0	-796.	123.2	1678.	230.0	-155.	155.2	2746.
235.0	-358.	182.9	-2948.	175.0	-773.	109.1	1927.	233.0	-252.	145.4	2710.
242.2	-301.	173.4	-3226.	160.0	-732.	95.0	2188.	235.8	-301.	129.9	2614.
244.8	-282.	163.4	-3522.	136.8	-669.	79.3	2404.	244.1	-359.	112.7	2472.
251.4	-240.	154.3	-3790.	123.3	-647.	65.0	2584.	254.9	-349.	93.7	2284.
258.7	-199.	145.8	-4038.	108.0	-666.	50.0	2764.	268.1	-280.	80.6	2154.
264.1	-170.	135.4	-4358.	92.7	-672.	35.0	2775.	280.4	-186.	79.3	2141.
271.6	-132.	125.1	-4672.	74.7	-684.	20.5	2782.	291.5	-85.	62.3	1945.
277.6	-102.	109.6	-5125.	63.4	-752.			284.6	-150.	55.7	1890.
284.8	-69.	99.9	-5264.	59.0	-765.	79.1	2406.	296.0	-41.	50.0	1811.
290.1	-44.	119.8	-4863.			70.6	2527.	306.8	69.	43.0	1759.
295.8	-19.	120.4	-4845.	300.0	0.	60.5	2654.	311.8	126.	34.4	1707.
297.8	-10.	115.3	-4995.	171.6	-720.	49.8	2777.	323.1	233.	26.0	1675.
300.0	0.	98.4	-5492.	167.7	-708.	39.2	2869.	335.1	356.	17.4	1660.
307.3	31.	91.8	-5686.	151.6	-657.			350.0	483.	10.0	1662.
313.6	59.	111.0	-5123.	132.7	-609.	359.8	220.			5.1	1684.
320.4	87.	112.2	-5090.	121.8	-586.	359.8	223.	239.4	-403.	6.8	1673.
326.9	119.	105.7	-5279.	106.6	-535.	350.2	203.	229.5	-167.	8.6	1665.
331.9	146.	85.2	-5888.	94.2	-518.	340.8	174.	229.2	-161.	13.3	1659.
335.8	166.	79.6	-6058.	76.6	-525.	327.0	96.	229.1	-132.	21.0	1666.
340.0	186.	71.4	-6300.	64.2	-537.	315.6	41.	228.0	-13.	5.0	1685.
346.4	221.	64.0	-6485.	301.2	4.	302.0	7.	225.0	332.	28.1	1684.
350.0	238.	63.5	-6495.	300.5	1.	287.8	-47.	224.0	433.	49.7	1818.
		76.4	-6152.	284.6	-73.	272.9	-89.	223.0	527.	165.0	2739.
225.7	-531.	54.8	-6754.	275.3	-118.	256.9	-131.	222.0	622.	164.2	2740.
225.2	-542.	52.1	-6821.	266.6	-159.	246.8	-131.	221.9	633.	174.9	2718.
225.1	-547.	51.7	-6836.	263.7	-175.	237.0	-92.	221.8	642.	221.6	1778.
224.8	-553.	41.1	-7065.	244.1	-292.	216.0	123.	221.7	652.	220.0	1859.
224.5	-559.	40.7	-7080.	237.0	-346.	206.7	250.	221.6	661.		
224.1	-569.	33.9	-7189.	220.7	-699.	182.6	643.	221.5	672.		
223.5	-585.	32.2	-7212.	202.4	-795.	172.1	820.	221.4	681.		
223.1	-596.	24.3	-7301.	195.7	-789.	156.8	1109.	221.3	691.		
222.6	-607.	22.4	-7323.	185.0	-767.	138.3	1433.	221.2	702.		
222.1	-615.	16.8	-7362.			126.2	1638.	221.1	711.		
222.0	-623.	11.6	-7380.	358.6	247.	105.7	2008.	221.0	721.		
221.8	-629.	7.5	-7381.	348.5	224.	88.0	2215.	220.8	742.		
221.6	-635.	5.2	-7369.	339.3	195.			220.6	763.		
221.4	-640.	5.1	-7374.	326.7	142.	44.4	2796.	220.4	785.		
221.3	-644.	4.7	-7371.	315.5	81.	32.6	2894.	220.2	808.		
221.2	-648.	3.3	-7362.	303.9	15.	9.5	2951.	220.0	830.		
221.1	-651.			287.7	-53.	5.3	2981.	219.8	854.		
221.0	-655.	300.0	0.			6.9	2990.	219.6	878.		
220.9	-659.	299.9	-48.			9.6	2979.	219.4	901.		
220.8	-664.	305.4	-16.			15.1	2974.	219.2	925.		
220.7	-669.	306.7	-10.			25.0	2959.	219.0	951.		
220.6	-674.	314.3	31.			36.1	2905.	217.1	1206.		
220.5	-681.	319.6	59.			37.4	2894.	215.9	1317.		
220.4	-688.	324.8	84.			49.2	2774.	209.9	1682.		
220.3	-697.	329.9	108.			60.0	2632.	207.0	1820.		
220.2	-705.	334.8	133.					203.2	1977.		
220.1	-715.	340.7	160.					197.8	2165.		
220.0	-722.	345.6	183.								
219.9	-732.	350.4	208.								
219.8	-740.										
219.7	-747.										
219.6	-754.										
219.5	-759.										
219.4	-765.										
219.3	-771.										
219.2	-775.										
219.1	-780.										
219.0	-784.										
218.9	-788.										
218.8	-792.										
218.6	-799.										
218.4	-806.										
218.2	-813.										
217.9	-824.										
217.5	-837.										
217.0	-853.										

Figure 63. Tb a-, b-, and c-axis strain (in x 10^{-6}/in) as a function of temperature in zero field and in a 30 kOe field applied along the b axis. The horizontal lines separate data runs.

Tb-- a-AXIS STRAIN VERSUS FIELD APPLIED b-AXIS

T = 20.5		T = 60.3		T = 79.6		T = 99.3		T = 120.2		T = 140.0		T = 160.4		T = 179.6	
H	Δℓ/ℓ	H	Δℓ/ℓ	H	Δℓ/ℓ	H	Δℓ/ℓ	H	Δℓ/ℓ	H	Δℓ/ℓ	H	Δℓ/ℓ	H	Δℓ/ℓ
0.0	0.	0.0	0.	0.0	0.	0.0	0.	0.0	0.	0.0	0.	0.0	0.	0.0	0.
0.5	89.	0.5	19.	0.5	28.	0.5	-1.	0.5	0.	0.5	15.	0.5	-25.	0.5	-8.
1.0	84.	1.0	14.	1.0	17.	1.0	-10.	1.0	-17.	1.0	-2.	1.0	-43.	1.0	-28.
1.5	64.	1.5	-22.	1.5	-71.	1.5	-52.	1.5	-57.	1.5	-42.	1.5	-92.	1.5	-92.
2.0	19.	2.0	-97.	2.0	-98.	2.0	-135.	2.0	-138.	2.0	-124.	2.0	-184.	2.0	-205.
2.5	-65.	2.5	-224.	2.5	-230.	2.5	-281.	2.5	-295.	2.5	-290.	2.5	-365.	2.5	-384.
3.0	-206.	3.0	-428.	3.0	-437.	3.0	-496.	3.0	-527.	3.0	-535.	3.0	-609.	3.0	-589.
3.5	-432.	3.5	-706.	3.5	-734.	3.5	-800.	3.5	-857.	3.5	-839.	3.5	-873.	3.5	-752.
4.0	-728.	4.0	-1083.	4.0	-1144.	4.0	-1194.	4.0	-1240.	4.0	-1170.	4.0	-1087.	4.0	-889.
4.5	-1149.	4.5	-1656.	4.5	-1717.	4.5	-1741.	4.5	-1717.	4.5	-1470.	4.5	-1212.	4.5	-942.
5.0	-1740.	5.0	-2347.	5.0	-2367.	5.0	-2289.	5.0	-1964.	5.0	-1562.	5.0	-1248.	5.0	-971.
5.5	-2343.	5.5	-2959.	5.5	-2785.	5.5	-2478.	5.5	-2037.	5.5	-1592.	5.5	-1270.	6.0	-1009.
6.0	-2540.	6.0	-3162.	6.0	-2896.	6.0	-2530.	6.0	-2056.	6.0	-1606.	6.0	-1288.	7.0	-1033.
6.5	-2603.	6.5	-3229.	6.5	-2935.	6.5	-2549.	6.5	-2070.	7.0	-1634.	7.0	-1313.	8.0	-1052.
7.0	-2632.	7.0	-3259.	7.0	-2952.	7.0	-2561.	7.0	-2082.	8.0	-1653.	8.0	-1333.	9.0	-1069.
8.0	-2657.	8.0	-3290.	8.0	-2975.	8.0	-2579.	8.0	-2101.	9.0	-1668.	9.0	-1349.	10.0	-1083.
9.0	-2666.	9.0	-3309.	9.0	-2989.	9.0	-2593.	9.0	-2116.	10.0	-1681.	10.0	-1363.	11.0	-1097.
10.0	-2676.	10.0	-3321.	10.0	-3000.	10.0	-2604.	10.0	-2127.	11.0	-1693.	11.0	-1375.	12.0	-1110.
11.0	-2684.	12.0	-3335.	11.0	-3008.	11.0	-2608.	11.0	-2138.	12.0	-1704.	12.0	-1387.	14.0	-1133.
12.0	-2688.	14.0	-3342.	12.0	-3013.	12.0	-2616.	12.0	-2148.	14.0	-1724.	14.0	-1408.	16.0	-1155.
14.0	-2693.	16.0	-3350.	14.0	-3024.	14.0	-2631.	14.0	-2161.	16.0	-1743.	16.0	-1427.	18.0	-1175.
16.0	-2696.	18.0	-3359.	16.0	-3035.	16.0	-2646.	16.0	-2178.	18.0	-1759.	18.0	-1446.	21.0	-1201.
18.0	-2701.	21.0	-3370.	18.0	-3046.	18.0	-2659.	18.0	-2193.	21.0	-1782.	21.0	-1470.	24.0	-1226.
21.0	-2706.	24.0	-3381.	21.0	-3061.	21.0	-2677.	21.0	-2214.	24.0	-1803.	24.0	-1493.	27.0	-1251.
24.0	-2713.	27.0	-3391.	24.0	-3075.	24.0	-2694.	24.0	-2233.	27.0	-1824.	27.0	-1514.	30.0	-1275.
27.0	-2718.	30.0	-3400.	27.0	-3088.	27.0	-2710.	27.0	-2252.	30.0	-1842.	30.0	-1534.	0.0	-302.
30.0	-2723.	0.0	-845.	30.0	-3100.	30.0	-2726.	30.0	-2269.	0.0	-439.	0.0	-381.		
0.0	33.			0.0	-787.	0.0	-637.	0.0	-550.						

T = 199.0		T = 214.7		T = 225.4		T = 232.4		T = 240.3		T = 250.5		T = 259.7		T = 280.0	
H	Δℓ/ℓ	H	Δℓ/ℓ	H	Δℓ/ℓ	H	Δℓ/ℓ	H	Δℓ/ℓ	H	Δℓ/ℓ	H	Δℓ/ℓ	H	Δℓ/ℓ
0.0	0.	0.0	0.	0.0	0.	0.0	0.	0.0	0.	0.0	0.	0.0	0.	0.0	0.
0.5	-10.	0.5	-62.	0.5	-33.	0.5	-6.	1.0	-4.	1.0	-1.	1.0	-0.	1.0	0.
1.0	-39.	1.0	-87.	1.0	-101.	1.0	-24.	2.0	-15.	1.5	-3.	2.0	-1.	2.0	-0.
1.5	-115.	1.5	-150.	1.5	-192.	1.5	-50.	3.0	-33.	2.0	-4.	3.0	-4.	3.0	-1.
2.0	-235.	2.0	-238.	2.0	-281.	2.0	-81.	4.0	-57.	3.0	-10.	4.0	-7.	4.0	-2.
2.5	-375.	2.5	-338.	2.5	-352.	2.5	-114.	5.0	-84.	4.0	-16.	5.0	-11.	5.0	-3.
3.0	-488.	3.0	-441.	3.0	-393.	3.0	-150.	6.0	-114.	5.0	-25.	6.0	-16.	6.0	-5.
3.5	-604.	3.5	-495.	3.5	-428.	3.5	-184.	7.0	-147.	6.0	-35.	7.0	-22.	8.0	-9.
4.0	-665.	4.0	-527.	4.0	-456.	4.0	-216.	8.0	-180.	7.0	-47.	8.0	-28.	10.0	-14.
4.5	-698.	5.0	-550.	4.5	-483.	4.5	-249.	9.0	-215.	8.0	-61.	9.0	-36.	12.0	-21.
5.0	-720.	5.5	-582.	5.0	-505.	5.0	-274.	10.0	-247.	9.0	-76.	10.0	-44.	14.0	-28.
5.5	-738.	6.0	-598.	6.0	-544.	6.0	-328.	11.0	-280.	10.0	-92.	11.0	-52.	16.0	-36.
6.0	-753.	7.0	-626.	7.0	-582.	7.0	-376.	12.0	-312.	12.0	-125.	12.0	-62.	18.0	-46.
7.0	-777.	8.0	-649.	8.0	-618.	8.0	-422.	14.0	-373.	14.0	-161.	14.0	-82.	20.0	-56.
8.0	-798.	9.0	-673.	9.0	-651.	9.0	-465.	16.0	-431.	16.0	-201.	16.0	-105.	22.0	-67.
9.0	-818.	10.0	-693.	10.0	-678.	10.0	-498.	18.0	-487.	18.0	-242.	18.0	-129.	24.0	-79.
10.0	-836.	11.0	-713.	12.0	-733.	12.0	-567.	21.0	-561.	21.0	-303.	20.0	-155.	27.0	-99.
12.0	-867.	12.0	-732.	14.0	-780.	14.0	-628.	24.0	-627.	24.0	-363.	22.0	-182.	30.0	-120.
14.0	-896.	14.0	-770.	16.0	-823.	16.0	-682.	27.0	-691.	27.0	-422.	24.0	-210.	0.0	1.
16.0	-923.	16.0	-802.	18.0	-865.	18.0	-733.	30.0	-747.	30.0	-479.	27.0	-253.		
18.0	-950.	18.0	-833.	21.0	-920.	21.0	-802.			0.0	-4.	30.0	-297.		
21.0	-982.	21.0	-874.	24.0	-971.	24.0	-863.					0.0	2.		
24.0	-1014.	24.0	-912.	27.0	-1022.	27.0	-919.								
27.0	-1045.	27.0	-952.	30.0	-1068.	30.0	-969.								
30.0	-1076.	30.0	-990.	0.0	-7.	0.0	-4.								
0.0	-233.	30.0	-994.												
		0.0	-99.												

Figure 64. Tb a-axis strain (in x 10^{-6}/in) versus field, H, applied along the b axis.

Tb-- b-AXIS STRAIN VERSUS FIELD APPLIED ALONG b-AXIS

T = 20.5		T = 62.5		T = 78.7		T = 99.5		T = 120.3		T = 139.6		T = 160.4		T = 180.8	
H	Δℓ/ℓ	H	Δℓ /ℓ	H	Δℓ/ℓ	H	Δℓ/ℓ	H	Δℓ/ℓ	H	Δℓ/ℓ	H	Δℓ/ℓ	H	Δℓ /ℓ
0.0	0.	0.0	0.	0.0	0.	0.0	0.	0.0	0.	0.0	0.	0.0	0.	0.0	0.
0.5	-5.	0.5	-5.	0.5	-9.	0.5	0.	0.5	0.	0.5	19.	0.5	36.	0.5	11.
1.0	31.	1.0	39.	1.0	28.	1.0	47.	1.0	21.	1.0	61.	1.0	82.	1.0	63.
1.5	90.	1.5	113.	1.5	103.	1.5	128.	1.5	121.	1.5	156.	1.5	177.	1.5	164.
2.0	183.	2.0	233.	2.0	215.	2.0	259.	2.0	273.	2.0	306.	2.0	359.	2.0	341.
2.5	353.	2.5	429.	2.5	467.	2.5	480.	2.5	533.	2.5	569.	2.5	647.	2.5	600.
3.0	594.	3.0	731.	3.0	800.	3.0	800.	3.0	903.	3.0	917.	3.0	994.	3.0	856.
3.5	994.	3.5	1152.	3.5	1254.	3.5	1250.	3.5	1367.	3.5	1303.	3.5	1328.	3.5	1060.
4.0	1486.	4.0	1665.	4.0	1808.	4.0	1728.	4.0	1846.	4.0	1629.	4.0	1584.	4.0	1207.
4.5	2143.	4.5	2311.	4.5	2397.	4.5	2244.	4.5	2293.	4.5	1891.	4.5	1740.	4.5	1267.
5.0	2935.	4.7	2553.	5.0	2975.	5.0	2653.	5.0	2604.	5.0	1986.	5.0	1788.	5.0	1294.
5.5	3588.	5.0	2965.	5.5	3293.	5.5	2780.	5.5	2657.	5.5	2015.	5.5	1813.	5.5	1311.
6.0	3866.	5.3	3298.	6.0	3323.	6.0	2793.	6.0	2678.	6.0	2033.	6.0	1829.	6.0	1321.
6.5	3897.	5.5	3422.	6.5	3325.	6.5	2805.	7.0	2704.	6.5	2045.	6.5	1839.	6.5	1327.
7.0	3885.	5.8	3509.	7.0	3331.	7.0	2813.	8.0	2714.	7.0	2054.	7.0	1846.	7.0	1333.
7.5	3880.	6.0	3521.	8.0	3337.	7.5	2818.	9.0	2720.	7.5	2060.	8.0	1854.	7.5	1336.
8.0	3879.	6.5	3520.	9.0	3339.	8.0	2821.	10.0	2722.	8.0	2064.	9.0	1861.	8.0	1340.
8.5	3878.	7.0	3521.	10.0	3337.	8.5	2823.	12.0	2726.	9.0	2070.	10.0	1866.	9.0	1348.
9.0	3877.	7.5	3523.	11.0	3334.	9.0	2824.	14.0	2734.	10.0	2074.	12.0	1877.	10.0	1354.
9.5	3874.	8.0	3525.	12.0	3331.	9.5	2824.	17.0	2745.	12.0	2082.	14.0	1889.	12.0	1368.
10.0	3871.	8.5	3525.	13.0	3329.	10.0	2824.	20.0	2755.	14.0	2091.	17.0	1906.	14.0	1381.
10.5	3868.	9.0	3524.	14.0	3329.	11.0	2824.	23.0	2767.	17.0	2103.	20.0	1922.	17.0	1401.
11.0	3865.	9.5	3523.	15.0	3331.	12.0	2824.	26.0	2777.	20.0	2117.	23.0	1939.	20.0	1420.
11.5	3861.	10.0	3522.	16.0	3333.	13.0	2825.	30.0	2791.	23.0	2130.	26.0	1956.	23.0	1439.
12.0	3857.	10.5	3520.	18.0	3338.	14.0	2827.	0.0	972.	26.0	2143.	30.0	1977.	26.0	1457.
12.5	3854.	11.0	3517.	20.0	3342.	15.0	2830.			30.0	2159.	0.0	595.	30.0	1481.
13.0	3851.	12.0	3512.	22.0	3347.	17.0	2836.			0.0	693.			0.0	470.
13.5	3847.	12.5	3513.	24.0	3352.	20.0	2845.								
14.0	3845.	13.0	3511.	26.0	3357.	23.0	2854.								
15.0	3842.	14.0	3509.	28.0	3361.	26.0	2862.								
16.0	3840.	15.0	3509.	30.0	3366.	30.0	2873.								
17.0	3840.	16.0	3510.	0.0	1109.	0.0	863.								
18.0	3840.	17.0	3511.												
19.0	3841.	18.0	3513.												
20.0	3842.	20.0	3517.												
21.0	3844.	22.0	3520.												
23.0	3846.	24.0	3524.												
25.0	3848.	27.0	3530.												
27.0	3850.	30.0	3535.												
29.0	3847.	0.0	1069.												
30.7	3849.														

T = 200.5		T = 215.5		T = 224.5		T = 232.1		T = 240.3		T = 246.5		T = 260.2		T = 279.5	
H	Δℓ/ℓ	H	Δℓ/ℓ	H	Δℓ/ℓ	H	Δℓ /ℓ	H	Δℓ/ℓ	H	Δℓ/ℓ	H	Δℓ /ℓ	H	Δℓ/ℓ
0.0	0.	0.0	0.	0.0	0.	0.0	0.	0.0	0.	0.0	0.	0.0	0.	0.0	0.
0.3	5.	0.5	46.	0.5	12.	1.0	6.	2.0	2.	3.0	4.	2.0	0.	2.0	1.
1.0	68.	1.0	104.	1.0	53.	1.5	12.	3.0	4.	5.0	10.	4.0	1.	4.0	1.
1.5	200.	1.5	218.	1.5	111.	2.0	19.	4.0	7.	7.0	18.	6.0	2.	6.0	1.
2.0	379.	2.0	346.	2.0	176.	2.5	28.	5.0	11.	9.0	27.	8.0	4.	8.0	1.
3.0	728.	2.5	465.	2.5	231.	3.0	38.	6.0	16.	11.0	37.	10.0	5.	10.0	2.
4.0	913.	3.0	566.	3.0	258.	3.5	47.	8.0	30.	13.0	49.	12.0	8.	12.0	2.
5.0	946.	3.5	605.	3.5	275.	4.0	58.	10.0	45.	15.0	62.	15.0	12.	15.0	3.
6.0	959.	4.0	622.	4.0	288.	5.0	76.	12.0	59.	17.0	75.	18.0	17.	18.0	5.
7.0	970.	4.5	633.	5.0	307.	6.0	96.	14.0	74.	19.0	90.	21.0	23.	21.0	7.
8.0	981.	5.0	642.	6.0	328.	7.0	112.	17.0	95.	21.0	103.	24.0	30.	24.0	9.
9.0	991.	6.0	650.	7.0	343.	8.0	129.	20.0	115.	23.0	117.	27.0	38.	27.0	12.
10.0	1000.	7.0	673.	8.0	349.	9.0	145.	23.0	135.	25.0	134.	30.0	47.	30.0	15.
12.0	1017.	8.0	682.	8.0	358.	10.0	159.	26.0	154.	27.0	148.	0.0	1.	0.0	-1.
14.0	1034.	9.0	696.	9.0	367.	11.0	174.	30.0	178.	30.0	172.				
16.0	1050.	10.0	708.	9.0	371.	12.0	186.	0.0	-4.	0.0	0.				
18.0	1066.	12.0	728.	10.0	384.	14.0	212.			10.0	32.				
20.0	1080.	15.0	758.	12.0	399.	16.0	237.			0.0	1.				
23.0	1103.	18.0	786.	12.0	406.	18.0	259.								
26.0	1124.	21.0	812.	14.0	426.	20.0	281.								
30.0	1151.	27.0	860.	17.0	447.	22.0	303.								
0.0	252.	30.0	884.	17.0	456.	25.0	335.								
30.0	1153.	0.0	109.	20.0	486.	30.0	381.								
0.0	255.			23.0	503.	0.0	-3.								
				23.0	513.										
				26.0	543.										
				30.0	566.										
				30.0	576.										
				0.0	-9.										

Figure 65. The b-axis strain (in x 10^{-6}/in) versus field, H, applied along the b axis of the a-b plane specimen.

Tb-- c-AXIS STRAIN VERSUS FIELD APPLIED ALONG b- AXIS

T = 63.6		T = 79.7		T = 99.9		T = 120.8		T = 140.3		T = 159.4		T = 180.0		T = 199.5	
H	Δℓ/ℓ	H	Δℓ/ℓ	H	Δℓ/ℓ	H	Δℓ/ℓ	H	Δℓ/ℓ	H	Δℓ/ℓ	H	Δℓ/ℓ	H	Δℓ/ℓ
0.0	0.	0.0	0.	0.0	0.	0.0	0.	0.0	0.	0.0	0.	0.0	0.	0.0	0.
0.5	1.	0.5	-6.	0.5	-3.	0.5	-1.	0.5	1.	0.5	1.	0.5	1.	0.5	1.
1.0	-3.	1.0	-28.	1.0	-19.	1.0	-16.	1.0	-8.	1.0	-4.	1.0	-7.	1.0	-6.
1.5	-17.	1.5	-64.	1.5	-46.	1.5	-41.	1.5	-28.	1.5	-25.	1.5	-24.	1.5	-23.
2.0	-37.	2.0	-95.	2.0	-76.	2.0	-67.	2.0	-49.	2.0	-59.	2.0	-53.	2.0	-47.
2.5	-63.	2.5	-138.	2.5	-124.	2.5	-109.	2.5	-88.	2.5	-102.	2.5	-87.	2.5	-72.
3.0	-124.	3.0	-189.	3.0	-173.	3.0	-139.	3.0	-123.	3.0	-136.	3.0	-116.	3.0	-65.
3.5	-185.	3.5	-215.	3.5	-200.	3.5	-151.	3.5	-154.	3.5	-167.	3.5	-113.	3.5	-40.
4.0	-239.	4.0	-247.	4.0	-223.	4.0	-178.	4.0	-182.	4.0	-164.	4.0	-91.	4.0	-26.
4.5	-275.	4.5	-267.	4.5	-253.	4.5	-202.	4.5	-173.	4.5	-144.	4.5	-77.	4.5	-15.
5.0	-303.	5.0	-288.	5.0	-266.	5.0	-208.	5.0	-159.	5.0	-131.	5.0	-68.	5.0	-8.
5.5	-300.	5.5	-304.	5.5	-255.	5.5	-192.	5.5	-150.	5.5	-123.	5.5	-62.	6.0	6.
6.0	-305.	6.0	-290.	6.0	-238.	6.0	-181.	6.0	-145.	6.0	-118.	6.0	-57.	7.0	20.
6.5	-297.	6.5	-270.	6.5	-228.	6.5	-175.	6.5	-142.	7.0	-111.	7.0	-49.	8.0	32.
7.0	-288.	7.0	-258.	7.0	-221.	7.0	-170.	7.0	-140.	8.0	-107.	8.0	-43.	10.0	55.
7.5	-280.	7.5	-249.	7.5	-222.	8.0	-166.	8.0	-136.	9.0	-104.	9.0	-37.	12.0	78.
8.0	-275.	8.0	-244.	8.0	-220.	9.0	-164.	9.0	-134.	10.0	-101.	10.0	-32.	14.0	101.
9.0	-271.	9.0	-240.	9.0	-217.	10.0	-163.	10.0	-133.	12.0	-96.	12.0	-21.	17.0	131.
10.0	-269.	10.0	-238.	10.0	-216.	12.0	-161.	11.0	-132.	15.0	-89.	14.0	-12.	18.0	141.
11.0	-268.	12.0	-237.	11.0	-216.	14.0	-160.	12.0	-130.	18.0	-83.	16.0	-2.	21.0	171.
12.0	-268.	14.0	-238.	12.0	-215.	16.0	-159.	14.0	-128.	21.0	-76.	18.0	7.	24.0	198.
14.0	-268.	16.0	-239.	14.0	-215.	18.0	-158.	16.0	-126.	24.0	-70.	21.0	20.	27.0	223.
16.0	-269.	18.0	-240.	16.0	-215.	21.0	-157.	18.0	-124.	27.0	-64.	24.0	33.	30.0	248.
18.0	-268.	21.0	-240.	18.0	-215.	24.0	-155.	21.0	-120.	30.0	-59.	27.0	45.	0.0	-10.
21.0	-268.	24.0	-240.	21.0	-214.	27.0	-154.	24.0	-117.	0.0	-50.	30.0	57.		
24.0	-267.	27.0	-240.	24.0	-214.	30.0	-152.	27.0	-114.			0.0	-32.		
27.0	-267.	30.0	-240.	27.0	-213.	0.0	-142.	30.0	-110.						
30.0	-266.	0.0	-177.	30.0	-212.			0.0	-91.						
0.0	-98.			0.0	-153.										

T = 215.9		T = 218.3		T = 221.2		T = 224.3		T = 229.7		T = 232.8		T = 240.4		T = 248.5	
H	Δℓ/ℓ	H	Δℓ/ℓ	H	Δℓ/ℓ	H	Δℓ/ℓ	H	Δℓ/ℓ	H	Δℓ/ℓ	H	Δℓ/ℓ	H	Δℓ/ℓ
0.0	0.	0.0	0.	0.0	0.	0.0	0.	0.0	0.	0.0	0.	0.0	0.	0.0	0.
0.5	9.	0.5	-3.	0.5	1.	0.5	13.	1.0	49.	1.0	23.	0.5	1.	1.0	2.
1.0	11.	1.0	7.	1.0	88.	1.0	59.	1.5	96.	1.5	50.	1.0	4.	1.5	4.
1.5	3.	1.5	31.	1.5	170.	2.0	193.	2.0	142.	2.0	81.	2.0	19.	2.0	7.
2.0	-1.	2.0	50.	2.0	222.	3.0	285.	2.5	196.	2.5	117.	3.0	42.	2.5	11.
2.5	30.	2.5	81.	2.5	259.	4.0	359.	3.0	243.	3.0	159.	4.0	75.	3.0	15.
3.0	59.	3.0	108.	3.0	293.	5.0	422.	3.5	285.	3.5	196.	5.0	112.	4.0	26.
3.5	84.	3.5	131.	3.5	322.	6.0	483.	4.0	326.	4.0	234.	6.0	156.	5.0	41.
4.0	105.	4.0	152.	4.0	349.	7.0	537.	4.5	362.	4.5	267.	8.0	256.	6.0	58.
5.0	139.	4.5	172.	4.5	374.	8.0	583.	5.0	396.	5.0	299.	10.0	361.	7.0	78.
6.0	173.	5.0	191.	5.0	396.	10.0	667.	5.5	428.	5.5	334.	12.0	464.	8.0	99.
7.0	204.	5.5	210.	5.5	420.	12.0	743.	6.0	459.	6.0	367.	14.0	569.	9.0	123.
8.0	233.	6.0	228.	6.0	442.	14.0	816.	7.0	515.	7.0	426.	17.0	718.	10.0	147.
10.0	287.	7.0	262.	6.5	463.	16.0	877.	8.0	564.	8.0	482.	20.0	857.	11.0	172.
12.0	336.	8.0	294.	7.0	484.	18.0	933.	9.0	610.	9.0	533.	23.0	977.	12.0	200.
14.0	380.	9.0	326.	7.5	504.	21.0	1012.	10.0	652.	10.0	581.	26.0	1088.	13.0	226.
17.0	442.	10.0	356.	8.0	523.	24.0	1084.	11.0	691.	11.0	626.	30.0	1222.	14.0	253.
20.0	498.	11.0	384.	9.0	558.	27.0	1152.	12.0	728.	12.0	669.	0.0	-1.	15.0	281.
23.0	550.	12.0	412.	10.0	592.	30.0	1214.	13.0	765.	13.0	708.			16.0	309.
26.0	599.	14.0	462.	11.0	624.	0.0	35.	14.0	796.	14.0	746.	T = 279.2		17.0	338.
30.0	660.	16.0	511.	12.0	656.			16.0	856.	15.0	780.			18.0	366.
0.0	31.	18.0	555.	13.0	685.	T = 259.8		18.0	911.	16.0	816.	0.0	0.	19.0	396.
		21.0	616.	14.0	714.			20.0	963.	17.0	846.	3.0	2.	20.0	424.
		24.0	674.	16.0	768.	0.0	0.	22.0	1010.	18.0	876.	5.0	7.	21.0	453.
		27.0	727.	18.0	817.	1.0	1.	24.0	1055.	19.0	907.	7.0	14.	22.0	480.
		30.0	778.	21.0	888.	2.0	2.	26.0	1096.	20.0	935.	9.0	23.	23.0	511.
		0.0	-4.	24.0	952.	3.0	7.	28.0	1136.	21.0	963.	11.0	34.	24.0	538.
				27.0	1010.	4.0	12.	30.0	1173.	22.0	989.	13.0	47.	25.0	565.
				30.0	1066.	5.0	19.	0.0	-42.	24.0	1039.	15.0	62.	26.0	592.
				0.0	4.	6.0	27.			26.0	1085.	17.0	78.	27.0	619.
						8.0	48.			28.0	1129.	19.0	96.	28.0	645.
						10.0	74.			30.0	1170.	21.0	117.	29.0	672.
						12.0	106.			0.0	-19.	23.0	138.	30.0	697.
						14.0	141.					25.0	161.	0.0	-17.
						16.0	180.					27.0	185.		
						18.0	222.					30.0	225.		
						21.0	290.					0.0	0.		
						24.0	364.								
						27.0	442.								
						30.0	522.								
						0.0	-1.								

Figure 66. Tb c-axis strain (in x 10^{-6}/in) versus field, H, applied along the b axis.

Tb-- a-AXIS STRAIN VERSUS ANGLE OF APPLIED FIELD IN a-b PLANE RELATIVE TO b-AXIS

T = 10.2		T = 20.6		T = 39.5		T = 63.1		T = 79.1		T = 99.8		T = 118.8		T = 140.6	
θ	Δℓ/ℓ	θ	Δℓ/ℓ	θ	Δℓ/ℓ	θ	Δℓ/ℓ	θ	Δℓ/ℓ	θ	Δℓ/ℓ	θ	Δℓ/ℓ	θ	Δℓ/ℓ
0.0	0.	0.0	0.	0.0	0.	0.0	0.	0.0	-112.	0.0	0.	0.0	0.	0.0	0.
60.0	7907.	60.0	7953.	60.0	7629.	60.0	7028.	10.0	70.	60.0	5725.	60.0	5042.	60.0	4223.
90.0	8508.	90.0	8563.	90.0	8314.	90.0	7841.	20.0	766.	90.0	6663.	90.0	5962.	90.0	5128.
0.0	20.	0.0	62.	0.0	21.	0.0	16.	25.0	1477.	0.0	8.	0.0	11.	0.0	6.
10.0	168.	10.0	215.	10.0	181.	10.0	189.	30.0	2664.	10.0	213.	10.0	224.	10.0	196.
20.0	731.	20.0	785.	20.0	772.	20.0	839.	35.0	3973.	20.0	931.	20.0	890.	20.0	768.
25.0	1308.	25.0	1370.	25.0	1383.	25.0	1534.	40.0	4833.	25.0	1564.	25.0	1428.	25.0	1196.
28.0	2020.	28.0	2120.	28.0	2199.	28.0	2350.	50.0	5820.	30.0	2447.	30.0	2101.	30.0	1693.
30.0	3649.	30.0	3627.	30.0	3411.	30.0	3204.	60.0	6433.	35.0	3317.	35.0	2788.	35.0	2210.
32.0	5585.	32.0	5523.	32.0	5020.	32.0	3963.	70.0	6855.	40.0	4078.	40.0	3400.	40.0	2710.
35.0	6319.	35.0	6287.	35.0	5840.	35.0	4864.	80.0	7178.	50.0	5070.	50.0	4360.	50.0	3568.
40.0	6867.	40.0	6889.	40.0	6491.	40.0	5665.	90.0	7362.	60.0	5731.	60.0	5041.	60.0	4237.
50.0	7510.	50.0	7551.	50.0	7200.	50.0	6506.	100.0	7083.	70.0	6184.	70.0	5528.	70.0	4714.
60.0	7913.	60.0	7958.	60.0	7635.	60.0	7026.	110.0	6709.	80.0	6523.	80.0	5865.	80.0	5028.
70.0	8177.	70.0	8226.	70.0	7927.	70.0	7381.	120.0	6278.	90.0	6661.	90.0	5984.	90.0	5127.
80.0	8365.	80.0	8417.	80.0	8140.	80.0	7658.	130.0	5715.	100.0	6437.	100.0	5796.	100.0	4976.
90.0	8508.	90.0	8562.	90.0	8314.	90.0	7842.	140.0	4817.	110.0	6041.	110.0	5407.	110.0	4613.
100.0	8161.	100.0	8209.	100.0	7952.	100.0	7493.	145.0	4036.	120.0	5552.	120.0	4885.	120.0	4099.
110.0	7933.	110.0	7979.	110.0	7694.	110.0	7163.	150.0	2832.	130.0	4916.	130.0	4215.	130.0	3445.
120.0	7653.	120.0	7691.	120.0	7386.	120.0	6775.	155.0	1331.	140.0	3968.	140.0	3284.	140.0	2613.
130.0	7264.	130.0	7296.	130.0	6957.	130.0	6274.	160.0	879.	145.0	3248.	145.0	2684.	145.0	2115.
140.0	6651.	140.0	6664.	140.0	6292.	140.0	5468.	170.0	179.	150.0	2401.	150.0	2029.	150.0	1615.
145.0	6137.	145.0	6125.	145.0	5692.	145.0	4728.	180.0	0.	155.0	1537.	155.0	1383.	155.0	1139.
150.0	4163.	150.0	4008.	150.0	3836.	150.0	3188.	90.0	7368.	160.0	916.	160.0	879.	160.0	736.
155.0	1274.	155.0	1338.	155.0	1221.	155.0	1511.	0.0	0.	165.0	480.	165.0	473.	165.0	408.
160.0	703.	160.0	765.	160.0	762.	160.0	824.	60.0	6469.	170.0	211.	170.0	224.	170.0	181.
165.0	361.	170.0	227.	165.0	397.	165.0	412.	90.0	7368.	180.0	24.	180.0	38.	180.0	14.
170.0	166.	180.0	87.	170.0	181.	170.0	180.	60.0	6476.			90.0	5985.	0.0	9.
180.0	27.			180.0	40.	180.0	20.	0.0	2.			0.0	34.		
								60.0	6472.						
								90.0	7365.						
								0.0	4.						

T = 150.5		T = 160.4		T = 176.4		T = 200.4		T = 215.5		T = 219.4		T = 224.2		T = 230.2	
θ	Δℓ/ℓ	θ	Δℓ/ℓ	θ	Δℓ/ℓ	θ	Δℓ/ℓ	θ	Δℓ/ℓ	θ	Δℓ/ℓ	θ	Δℓ/ℓ	θ	Δℓ/ℓ
0.0	0.	0.0	0.	0.0	0.	0.0	0.	0.0	0.	0.0	0.	0.0	0.	0.0	0.
10.0	130.	60.0	3538.	10.0	108.	60.0	2125.	60.0	1591.	10.0	51.	10.0	44.	60.0	1061.
20.0	618.	90.0	4370.	20.0	481.	90.0	2705.	90.0	2043.	20.0	222.	20.0	195.	90.0	1375.
25.0	975.	0.0	17.	25.0	739.	0.0	-1.	0.0	-1.	25.0	342.	25.0	296.	0.0	-2.
30.0	1386.	10.0	179.	30.0	1036.	10.0	99.	10.0	72.	30.0	476.	30.0	417.	10.0	46.
35.0	1821.	20.0	655.	35.0	1354.	20.0	370.	20.0	271.	35.0	621.	35.0	544.	20.0	177.
40.0	2267.	25.0	992.	40.0	1679.	25.0	559.	25.0	411.	40.0	776.	40.0	680.	30.0	374.
50.0	3097.	30.0	1380.	50.0	2331.	30.0	776.	30.0	571.	50.0	1098.	50.0	963.	40.0	601.
60.0	3762.	35.0	1780.	60.0	2893.	35.0	1007.	35.0	739.	60.0	1398.	60.0	1227.	50.0	841.
70.0	4233.	40.0	2194.	70.0	3303.	40.0	1248.	40.0	919.	70.0	1631.	70.0	1437.	60.0	1060.
80.0	4559.	50.0	2938.	80.0	3583.	50.0	1711.	50.0	1271.	80.0	1789.	80.0	1577.	70.0	1232.
90.0	4683.	60.0	3549.	90.0	3685.	60.0	2128.	60.0	1591.	90.0	1847.	90.0	1629.	80.0	1342.
100.0	4572.	70.0	3988.	100.0	3600.	70.0	2445.	70.0	1839.	100.0	1803.	100.0	1591.	90.0	1375.
110.0	4251.	80.0	4284.	110.0	3331.	80.0	2645.	80.0	1995.	110.0	1655.	110.0	1460.	100.0	1331.
120.0	3791.	90.0	4370.	120.0	2939.	90.0	2706.	90.0	2043.	120.0	1436.	120.0	1260.	110.0	1211.
130.0	3210.	100.0	4241.	130.0	2444.	100.0	2622.	100.0	1978.	130.0	1162.	130.0	1021.	120.0	1029.
140.0	2460.	110.0	3915.	140.0	1826.	110.0	2401.	110.0	1806.	140.0	842.	140.0	739.	130.0	813.
145.0	2011.	120.0	3438.	150.0	1172.	120.0	2068.	120.0	1543.	150.0	524.	150.0	459.	140.0	576.
150.0	1579.	130.0	2843.	160.0	591.	130.0	1650.	130.0	1227.	160.0	257.	160.0	225.	150.0	346.
155.0	1141.	140.0	2105.	170.0	180.	140.0	1190.	140.0	876.	170.0	74.	170.0	64.	160.0	162.
160.0	771.	145.0	1697.	180.0	16.	145.0	943.	145.0	696.	180.0	-1.	180.0	1.	170.0	40.
170.0	216.	150.0	1311.	150.0	1158.	150.0	721.	150.0	529.	150.0	519.	150.0	454.	180.0	0.
180.0	0.	155.0	932.	90.0	3690.	155.0	511.	155.0	376.	90.0	1848.	90.0	1630.		
150.0	1565.	160.0	614.	60.0	2895.	160.0	337.	160.0	249.	60.0	1400.	60.0	1234.		
90.0	4683.	165.0	352.	0.0	13.	170.0	78.	165.0	140.	0.0	-1.	0.0	0.		
60.0	3762.	170.0	165.			180.0	-3.	170.0	61.						
0.0	-7.	180.0	24.			90.0	2708.	180.0	0.						
		90.0	4373.			0.0	-4.								
		0.0	19.												

Figure 67. Tb a-axis strain (in x 10^{-6}/in) versus angle of applied field, θ, relative to b axis. The 30 kOe field was applied in the basal plane.

Tb-- b-AXIS STRAIN VERSUS ANGLE OF APPLIED FIELD IN a-b PLANE RELATIVE TO b-AXIS

T = 5.3		T = 20.5		T = 40.2		T = 60.7		T = 79.5		T = 99.9		T = 121.2		T = 139.8	
θ	Δℓ/ℓ	θ	Δℓ/ℓ	θ	Δℓ/ℓ	θ	Δℓ/ℓ	θ	Δℓ/ℓ	θ	Δℓ/ℓ	θ	Δℓ/ℓ	θ	Δℓ/ℓ
0.0	34.	0.0	1.	0.0	0.	0.0	0.	0.0	0.	0.0	0.	0.0	0.	0.0	0.
60.0	-7437.	10.0	-101.	60.0	-7155.	60.0	-6744.	60.0	-6208.	60.0	-5490.	60.0	-4745.	60.0	-4110.
90.0	-7873.	60.0	-7482.	90.0	-7669.	90.0	-7406.	90.0	-6978.	90.0	-6394.	0.0	-25.	90.0	-5034.
0.0	0.	90.0	-7932.	60.0	-7195.	60.0	-6774.	60.0	-6187.	60.0	-5481.	10.0	-184.	60.0	-4109.
10.0	-104.	0.0	0.	0.0	23.	0.0	-9.	0.0	-27.	0.0	-18.	20.0	-772.	0.0	-3.
20.0	-474.	10.0	-95.	60.0	-7150.	10.0	-149.	10.0	-159.	10.0	-191.	30.0	-1824.	10.0	-171.
25.0	-865.	20.0	-500.	90.0	-7666.	20.0	-668.	20.0	-702.	20.0	-815.	40.0	-3046.	20.0	-702.
30.0	-1883.	25.0	-918.	60.0	-7192.	25.0	-1229.	25.0	-1267.	25.0	-1409.	50.0	-4039.	25.0	-1106.
35.0	-5496.	30.0	-2111.	0.0	16.	28.0	-1892.	30.0	-2315.	30.0	-2214.	60.0	-4756.	30.0	-1590.
40.0	-6246.	35.0	-5486.	10.0	-87.	30.0	-2666.	35.0	-3573.	35.0	-3077.	70.0	-5228.	35.0	-2082.
50.0	-6999.	40.0	-6273.	20.0	-493.	32.0	-3498.	40.0	-4496.	40.0	-3825.	80.0	-5533.	40.0	-2590.
60.0	-7435.	50.0	-7041.	25.0	-910.	35.0	-4471.	50.0	-5546.	50.0	-4832.	90.0	-5667.	50.0	-3450.
70.0	-7726.	60.0	-7488.	30.0	-1896.	40.0	-5336.	60.0	-6187.	60.0	-5485.	100.0	-5578.	60.0	-4117.
80.0	-7873.	70.0	-7760.	35.0	-4830.	50.0	-6220.	70.0	-6586.	70.0	-5935.	110.0	-5282.	70.0	-4592.
90.0	-7853.	80.0	-7920.	40.0	-5770.	60.0	-6743.	80.0	-6848.	80.0	-6246.	120.0	-4836.	80.0	-4909.
100.0	-7838.	90.0	-7932.	50.0	-6657.	70.0	-7083.	90.0	-6959.	90.0	-6387.	130.0	-4221.	90.0	-5030.
110.0	-7706.	100.0	-7901.	60.0	-7158.	80.0	-7305.	100.0	-6868.	100.0	-6271.	140.0	-3332.	100.0	-4928.
120.0	-7455.	110.0	-7762.	70.0	-7456.	90.0	-7402.	110.0	-6613.	110.0	-5960.	150.0	-2135.	110.0	-4620.
130.0	-7060.	120.0	-7503.	80.0	-7638.	100.0	-7309.	120.0	-6227.	120.0	-5507.	160.0	-1005.	120.0	-4136.
140.0	-6411.	130.0	-7099.	90.0	-7669.	110.0	-7088.	130.0	-5696.	130.0	-4868.	170.0	-340.	130.0	-3485.
145.0	-5829.	140.0	-6436.	100.0	-7638.	120.0	-6748.	140.0	-4816.	140.0	-3892.	180.0	-98.	140.0	-2617.
150.0	-4152.	145.0	-5833.	110.0	-7471.	130.0	-6251.	150.0	-2947.	145.0	-3148.	120.0	-4831.	145.0	-2092.
155.0	-1099.	150.0	-4222.	120.0	-7198.	140.0	-5439.	160.0	-943.	150.0	-2296.	90.0	-5715.	150.0	-1590.
160.0	-590.	160.0	-620.	130.0	-6793.	145.0	-4684.	170.0	-263.	155.0	-1458.	60.0	-4845.	155.0	-1103.
165.0	-295.	165.0	-323.	140.0	-6125.	150.0	-3160.	180.0	-56.	160.0	-871.	0.0	-88.	160.0	-710.
170.0	-116.	170.0	-136.	145.0	-5549.	155.0	-1434.	90.0	-6964.	170.0	-210.	60.0	-4787.	165.0	-393.
180.0	21.	180.0	12.	150.0	-4381.	160.0	-778.	60.0	-6062.	180.0	-21.	0.0	-88.	170.0	-173.
		90.0	-7875.	155.0	-1469.	165.0	-414.	0.0	-52.	90.0	-6377.			180.0	-3.
		60.0	-7560.	160.0	-779.	170.0	-193.			0.0	-27.			90.0	-5029.
		0.0	-3.	170.0	-198.	180.0	-29.							60.0	-4127.
				180.0	-22.	90.0	-7379.							0.0	-3.
				90.0	-7684.	60.0	-6776.								
				60.0	-7255.	0.0	-35.								
				0.0	-1151.										

T = 150.5		T = 159.5		T = 180.0		T = 199.8		T = 221.4		T = 225.3		T = 230.2		T = 240.2	
θ	Δℓ/ℓ	θ	Δℓ/ℓ	θ	Δℓ/ℓ	θ	Δℓ/ℓ	θ	Δℓ/ℓ	θ	Δℓ/ℓ	θ	Δℓ/ℓ	θ	Δℓ/ℓ
0.0	0.	0.0	0.	0.0	0.	0.0	0.	0.0	0.	0.0	0.	0.0	0.	0.0	0.
10.0	-136.	60.0	-3490.	10.0	-108.	10.0	-79.	10.0	-51.	10.0	-46.	60.0	-1049.	60.0	-706.
20.0	-599.	90.0	-4362.	20.0	-452.	20.0	-332.	20.0	-218.	20.0	-188.	90.0	-1387.	90.0	-940.
25.0	-941.	60.0	-3480.	30.0	-970.	30.0	-699.	30.0	-469.	30.0	-391.	60.0	-1050.	60.0	-705.
30.0	-1332.	0.0	-9.	40.0	-1569.	40.0	-1134.	40.0	-768.	40.0	-632.	0.0	3.	0.0	2.
35.0	-1759.	10.0	-152.	50.0	-2179.	50.0	-1591.	50.0	-1082.	50.0	-894.	10.0	-38.	10.0	-25.
40.0	-2185.	20.0	-600.	60.0	-2723.	60.0	-2006.	60.0	-1380.	60.0	-1133.	20.0	-167.	20.0	-111.
50.0	-2968.	25.0	-923.	70.0	-3115.	70.0	-2314.	70.0	-1610.	70.0	-1319.	30.0	-358.	30.0	-237.
60.0	-3603.	30.0	-1304.	80.0	-3375.	80.0	-2520.	80.0	-1766.	80.0	-1441.	40.0	-580.	40.0	-389.
70.0	-4050.	35.0	-1701.	90.0	-3474.	90.0	-2599.	90.0	-1827.	90.0	-1484.	50.0	-824.	50.0	-553.
80.0	-4366.	40.0	-2110.	100.0	-3405.	100.0	-2542.	100.0	-1787.	100.0	-1446.	60.0	-1051.	60.0	-710.
90.0	-4490.	50.0	-2871.	110.0	-3162.	110.0	-2343.	110.0	-1645.	110.0	-1321.	70.0	-1226.	70.0	-831.
100.0	-4402.	60.0	-3490.	120.0	-2777.	120.0	-2039.	120.0	-1422.	120.0	-1134.	80.0	-1344.	80.0	-914.
110.0	-4112.	70.0	-3948.	130.0	-2286.	130.0	-1645.	130.0	-1148.	130.0	-903.	90.0	-1388.	90.0	-945.
120.0	-3672.	80.0	-4247.	140.0	-1693.	140.0	-1189.	140.0	-830.	140.0	-642.	100.0	-1353.	100.0	-921.
130.0	-3076.	90.0	-4356.	150.0	-1054.	150.0	-727.	150.0	-514.	150.0	-388.	110.0	-1241.	110.0	-842.
140.0	-2286.	100.0	-4257.	160.0	-514.	160.0	-341.	160.0	-247.	160.0	-181.	120.0	-1065.	120.0	-721.
145.0	-1820.	110.0	-3973.	170.0	-149.	170.0	-90.	170.0	-66.	170.0	-46.	130.0	-851.	130.0	-575.
150.0	-1387.	120.0	-3516.	180.0	0.	180.0	-6.	180.0	5.	180.0	-1.	140.0	-606.	140.0	-410.
155.0	-968.	130.0	-2908.	120.0	-2784.	150.0	-724.	90.0	-1840.	150.0	-387.	150.0	-369.	150.0	-246.
160.0	-622.	140.0	-2155.	90.0	-3483.	90.0	-2606.	60.0	-1402.	90.0	-1486.	160.0	-173.	160.0	-114.
170.0	-159.	145.0	-1715.	60.0	-2748.	30.0	-707.	0.0	9.	60.0	-1135.	170.0	-41.	170.0	-24.
180.0	-8.	150.0	-1321.	0.0	8.	0.0	-3.	60.0	-1400.	0.0	1.	180.0	8.	180.0	8.
150.0	-1389.	155.0	-940.	60.0	-2723.			90.0	-1846.			90.0	-1390.	90.0	-947.
90.0	-4498.	160.0	-615.	0.0	8.			60.0	-1402.			60.0	-1053.	60.0	-713.
60.0	-3603.	170.0	-164.					0.0	11.			0.0	10.	0.0	8.
0.0	2.	180.0	-13.												
		90.0	-4351.												
		0.0	-17.												

Figure 68. Tb b-axis strain (in x 10^{-6}/in) versus angle of applied field, θ, relative to b axis. The 30 kOe field was applied in the basal plane.

Tb-- b-AXIS STRAIN VERSUS ANGLE OF APPLIED FIELD IN a-b PLANE RELATIVE TO b-AXIS (CON'D)

T = 249.7		T = 260.0		T = 270.0		T = 280.7		T = 299.5		T = 320.0		T = 338.5	
θ	Δℓ/ℓ	θ	Δℓ/ℓ	θ	Δℓ/ℓ	θ	Δℓ/ℓ	θ	Δℓ/ℓ	θ	Δℓ/ℓ	θ	Δℓ/ℓ
0.0	0.	0.0	0.	0.0	0.	0.0	0.	0.0	0.	0.0	0.	0.0	0.
10.0	-17.	10.0	-9.	60.0	-158.	10.0	-4.	10.0	-2.	10.0	-1.	60.0	-20.
20.0	-71.	20.0	-40.	90.0	-212.	20.0	-16.	20.0	-8.	20.0	-4.	0.0	0.
30.0	-152.	30.0	-85.	60.0	-159.	30.0	-34.	30.0	-18.	30.0	-10.	0.0	-1.
40.0	-248.	40.0	-140.	0.0	0.	40.0	-56.	40.0	-29.	40.0	-17.	10.0	-2.
50.0	-352.	50.0	-199.	10.0	-6.	50.0	-80.	50.0	-41.	50.0	-23.	20.0	-4.
60.0	-452.	60.0	-257.	20.0	-25.	60.0	-102.	60.0	-53.	60.0	-31.	30.0	-7.
70.0	-529.	70.0	-301.	30.0	-54.	70.0	-120.	70.0	-63.	70.0	-36.	40.0	-11.
80.0	-581.	80.0	-332.	40.0	-87.	80.0	-132.	80.0	-69.	80.0	-40.	50.0	-16.
90.0	-601.	90.0	-343.	50.0	-124.	90.0	-137.	90.0	-72.	90.0	-41.	60.0	-20.
100.0	-585.	100.0	-335.	60.0	-159.	100.0	-134.	100.0	-70.	100.0	-40.	70.0	-24.
110.0	-535.	110.0	-306.	70.0	-187.	110.0	-123.	110.0	-64.	110.0	-36.	80.0	-26.
120.0	-458.	120.0	-262.	80.0	-206.	120.0	-105.	120.0	-55.	120.0	-31.	90.0	-27.
130.0	-365.	130.0	-209.	90.0	-212.	130.0	-84.	130.0	-44.	130.0	-24.	100.0	-26.
140.0	-262.	140.0	-149.	100.0	-206.	140.0	-61.	140.0	-31.	140.0	-18.	110.0	-24.
150.0	-161.	150.0	-91.	110.0	-188.	150.0	-38.	150.0	-18.	150.0	-10.	120.0	-20.
160.0	-79.	160.0	-45.	120.0	-161.	160.0	-18.	160.0	-9.	160.0	-4.	130.0	-16.
170.0	-25.	170.0	-13.	130.0	-127.	170.0	-6.	170.0	-2.	170.0	-1.	140.0	-11.
180.0	-5.	180.0	0.	140.0	-90.	180.0	-1.	180.0	1.	180.0	1.	150.0	-6.
		120.0	-264.	150.0	-55.	120.0	-107.	120.0	-55.	120.0	-31.	160.0	-3.
		90.0	-344.	160.0	-27.	90.0	-138.	90.0	-71.	90.0	25.	170.0	-0.
		60.0	-257.	170.0	-8.	60.0	-105.	60.0	-53.	60.0	-30.	180.0	1.
		0.0	-1.	180.0	-1.	0.0	-1.	0.0	1.	0.0	1.	120.0	-20.
				90.0	-212.							90.0	-26.
				0.0	-1.							60.0	-19.
												0.0	1.
												60.0	-19.
												0.0	1.

Figure 69. Tb b-axis strain (in x 10^{-6}/in) versus angle of applied field, θ, relative to b axis. The 30 kOe field was applied in the basal plane.

Table 7. Magnetic field dependence of constants A and C for Tb

Gage parallel to b axis				Gage parallel to a axis			
T °K	H kOe	C μ in/in	A μ in/in	T °K	H kOe	C μ in/in	A μ in/in
240.6	5	45.7	-	61.1	24	3887.	1484.
	10	141.9	-		26	3885.	1482.
	15	234.7	-		28	3883.	1497.
	20	315.9	1.3		30	3880.	1497.
	25	387.8	3.2				
	30	451.9	4.3				
				68.0	24	3787.	1367.
					26	3786.	1377.
260.0	5	6.6	-		28	3786.	1384.
	10	24.4	-		30	3786.	1394.
	15	42.5	-				
	20	87.0	-				
	25	126.6	-	79.7	24	3610.	1182.
	30	169.4	-		26	3608.	1201.
					28	3610.	1208.
					30	3611.	1207.
269.2	5	3.7	-				
	10	13.6	-				
	15	30.9	-	99.7	24	3272.	904.
	20	53.5	-		26	3276.	906.
	25	80.7	-		28	3280.	923.
	30	111.6	-		30	3284.	930.
280.2	5	2.5	-				
	10	8.2	-	120.5	24	2897.	643.
	15	18.2	-		26	2906.	658.
	20	31.7	-		28	2914.	664.
	25	48.7	-		30	2921.	662.
	30	68.4	-				
				139.7	24	2526	455.
290.5	5	1.6	-		26	2539.	465.
	10	5.3	-		28	2548.	467.
	15	12.0	-		30	2556.	473.
	20	20.8	-				
	25	33.0	-				
	30	47.0	-	160.0	24	2131.	310.

Table 7 (Continued)

Gage parallel to b axis				Gage parallel to a axis			
T °K	H kOe	C μ in/in	A μ in/in	T °K	H kOe	C μ in/in	A μ in/in
					26	2145.	315.
					28	2156.	321.
300.6	5	0.9	-		30	2167.	322.
	10	3.9	-				
	15	8.8	-				
	20	15.3	-	179.1	24	1745.	194.
	25	24.2	-		26	1760.	203.
	30	34.7	-		28	1773.	202.
					30	1785.	209.
				200.2	24	1300.	106.
					26	1319.	110.
					28	1336.	114.
					30	1352.	114.
				219.7	24	858.	44.
					26	880.	54.
					28	902.	53.
					30	924.	52.
				238.8	24	401.	33.
					26	443.	13.
					28	471.	16.
					30	498.	71.